Design, synthesis and biological characterization of isoform selective histone deacetylase (HDAC) inhibitors

THESIS

Submitted in partial fulfilment

of the requirements for the degree of

DOCTOR OF PHILOSOPHY

by

TRIVEDI PRAKRUTI HARSHVARDHANBHAI

ID No. 2013PHXF0415H

Under the supervision of

Dr. BALARAM GHOSH

BITS Pilani

Pilani | Dubai | Goa | Hyderabad

BIRLA INSTITUTE OF TECHNOLOGY AND SCIENCE, PILANI

2018

Design, Synthesis and Biological Characterization of Isoform Selective Histone Deacetylase (HDAC) Inhibitors

THESIS

Submitted in partial fulfilment

of the requirements for the degree of

DOCTOR OF PHILOSOPHY

by

TRIVEDI PRAKRUTI HARSHVARDHANBHAI

ID No. 2013PHXF0415H

Under the supervision of

Dr. BALARAM GHOSH

BITS Pilani

Pilani | Dubai | Goa | Hyderabad

BIRLA INSTITUTE OF TECHNOLOGY AND SCIENCE, PILANI

2018

BIRLA INSTITUTE OF TECHNOLOGY AND SCIENCE, PILANI

CERTIFICATE

This is to certify that the thesis entitled "**Design, Synthesis and Biological Characterization of Isoform Selective Histone Deacetylase (HDAC) Inhibitors**" and submitted by **TRIVEDI PRAKRUTI HARSHVARDHANBHAI** ID No. **2013PHXF0415H** for award of Ph.D. of the Institute embodies original work done by her under my supervision.

Signature of the Supervisor:

Name in capital letters: **BALARAM GHOSH**

Designation : **Assistant Professor**

Date:

I would like to dedicate this thesis to my beloved parents

Mr. Harshvardhan Trivedi

and

Mrs. Kusum Trivedi

ACKNOWLEDGEMENT

This dissertation would not have been possible without the guidance and the help of several individuals who in one way or another contributed and extended their valuable assistance in the preparation and completion of this study.

First and foremost, my utmost gratitude to my esteemed research guide Dr. Balaram Ghosh, Assistant Professor, Department of Pharmacy, BITS Pilani, Hyderabad Campus whose sincerity and encouragement I will never forget. His wide knowledge, experience and logical way of thinking have been of great value for me. His understanding, encouraging and personal guidance have provided a good basis for the present thesis. His extensive discussions around my work and interesting explorations in operations have been very helpful for this study.

I wish to express my sincere thanks to Prof. P. Yogeeswari, Department of Pharmacy, BITS Pilani Hyderabad who kindly agreed to serve as a Doctoral Advisory Committee (DAC) member and for her suggestions and valuable time to review my dissertation report.

I am heartily grateful to Prof. Swati Biswas, Department of Pharmacy, BITS Pilani Hyderabad who acted as Doctoral Advisory Committee (DAC) member, for her detailed and constructive discussions and suggestions whenever I needed, and for her continuous support throughout this work.

I would like to thank Head of the department (HOD), faculty members and staff of the department of Pharmacy for their kind support and help.

I express my sincere thanks to the Vice Chancellor, BITS Pilani, Director, Prof. G. Sunder, BITS Pilani, Hyderabad Campus, Dean, General Administration, Dean and Associate Dean, Academic Research Division (Ph.D. Programme) BITS-Pilani, Hyderabad, for providing excellent working facilities and academic environment.

I gratefully acknowledge Council of Scientific and Industrial Research (CSIR), Government of India, New Delhi for financial assistance in the form of senior research fellowship (SRF). I

acknowledge BITS-Pilani, Hyderabad for providing institute fellowship for my research work.

I sincerely admire the contribution of all my lab mates Yamini, Ganesh, Dr. Omkara, Vishnu Kiran, Preeti, Himanshu, Anusha and Soniya.

My heartily thanks to my friends Smruti, Shubham, Priyanka, Kirti, Pragya, Dr. Yadagiri and Mr. Uday for their support and help during this work.

I owe my loving thanks to my parents, my parents in law and other family members for their encouragement and understanding. My special gratitude is to my husband, Bhagirath for his constant encouragement, support and love throughout the journey.

Last but not the least, the omnipresent God, for giving me the strength to undertake this research task and making my destiny to reach this milestone.

Prakruti Trivedi

ABSTRACT

Histone deacetylases (HDACs) have been found as a potential target for anticancer therapy. A number of HDAC inhibitors have been used pre-clinically and clinically as anticancer agents. Structural modifications of prototype HDAC inhibitors with different chemical moiety enhance efficiency and selectivity of compounds. With this approach, we have designed and synthesized three series of compounds and evaluated their HDAC inhibition efficiency and anticancer activity.

First, we have designed and synthesized compound **12a** by combining the scaffolds of **CI-994** and **BG45.** Moreover, the structure of compound **12a** was optimized and a series of 2-aminobenzamide derivatives were synthesized further. These compounds were tested for their HDAC inhibitory activity and found to be efficient HDAC inhibitors. Compound **26c** showed around 12-fold HDAC3 selectivity over pan HDACs, more than the prototype HDAC3 inhibitor **BG-45**. Most of these compounds exhibited antiproliferative activity in both B16F10 and HeLa cell lines. Particularly, compound **26c** exhibited better antitumor efficacy in the cell lines compared to both prototype inhibitors **CI-994** and **BG45.** It was also found to promote apoptosis as well as induced significant cell growth arrest in the G2/M phase of cell cycle in B16F10 melanoma cells.

Second, we have modified the structure of hydroxamate drug **SAHA** by incorporating piperidine and piperazine moiety with alkyl side chain in linker region. These derivatives were further modified in cap region with different hydrophobic and bulky groups and a series of derivatives were synthesized. These compounds were screened for their HDAC

inhibitory activity using HeLa nuclear extract and found to be efficient HDAC inhibitors. Further they were tested on human recombinant HDAC3 and human recombinant HDAC8 and they exhibited efficient inhibition of HDAC8 while minimum inhibition of HDAC3. These compounds were found to show potent anticancer activity on B16F10, HeLa, A-549, MCF-7 and Jurkat E6 cells. Promising three compounds **5e, 16c** and **16d** increased Caspase3/7 activity in Jurkat E6 cells.

Third, we have designed and synthesized a series of compounds having aliphatic side chain as linker with a hanging aliphatic moiety between the hydroxamate (ZBG) and cap region. These compounds were screened for their HDAC inhibition activity using HeLa nuclear extract, human recombinant HDAC3 and human recombinant HDAC8. All target compounds inhibited HDAC8 with highest efficiency, while negligible inhibition of HDAC3. With HDAC8 selectivity, these compounds exhibited promising antiproliferative activity in B16F10, A-549 and Jurkat E6 cells. Compound **7d** and **7i** induced cell cycle arrest in G2/M phase in B16F10 cells.

This work may provide significant insight regarding structural information to design newer small molecule selective as HDAC3 or HDAC8 inhibitors to fight against the target specific malignancies in future.

TABLE OF CONTENTS

LIST OF TABLES

LIST OF FIGURES

LIST OF ABBREVIATIONS

µg	Microgram
µL	Microlitre
µM	Micromolar
^{1}H NMR	Proton Nuclear Magnetic Resonance
A549	Human alveolar adenocarcinoma cell
ADP	Adenine diphosphate
B16F10	Murine melanoma cells
$CDCl_3$	Deuterated chloroform
Ch.	Chapter
CTCL	Cutaneous T-cell lymphoma
DCM	Dichloromethane
DFT	Density functional theory
DMAP	4-Dimethylaminopyridine
DMEM	Dulbecco's modified Eagle's media
DMF	Dimethylformamide
DMSO	Dimethyl sulphoxide
DMSO-d6	Deuterated dimethyl sulphoxide
DNA	Deoxyribonucleic acid
EDC	1-Ethyl-3-(3-dimethylaminopropyl)carbodiimide
ESI	Electron spray ionization
ESI	Electron spray ionization
EtOAc	Ethyl acetate

FITC	Fluorescein isothiocyanate
HCl	Hydrochloric acid
HDAC	Histone deacetylase
HDACi	Histone deacetylase inhibitors
HeLa	Human cervical cancer cell line
HOMO	Highest energy occupied molecular orbital
HPLC	High performance liquid chromatography
IC_{50}	Half maximal inhibitory concentration
LC-MS	Liquid chromatography–mass spectrometry
LUMO	Lowest energy unoccupied molecular orbital
MCF-7	Human breast cancer cell line
mg	Milligram
min	Minute
mL	Millilitre
mm	Millimetre
mmol	Millimole
MS	Mass spectroscopy
MTT	3-(4,5-dimethylthiazol-2-yl)-2,5-di-phenyltetrazolium bromide
Na_2SO_4	Sodium sulphate
$NaHCO_3$	Sodium bicarbonate
NCOR1	Nuclear receptor corepressor 1
NMR	Nuclear magnetic resonance
^oC	Degree centigrade
PBS	Phosphate buffered saline
PI	Propidium iodide

ppm	Parts per million
PTCL	Peripheral T-cell lymphoma
RNA	Ribonucleic acid
Rt	Retention time
RT	Room temperature
SAHA	Suberoylanilide hydroxamic acid
SIRT	Sirtuin
t-Boc	tert-Butyloxycarbonyl protecting group
THF	Tetrahydrofuran
TLC	Thin layer chromatography
TNF-α	Tumor necrosis factor- alpha
TSA	Trichostatin A
USFDA	US food and drug administrations
ZBG	Zinc binding group

Chapter 1

Introduction

1.1. Epigenetic modifications

Epigenetic modifications are changes to DNA or nucleosome which do not change the sequence of nucleotides, but redesign the transcription of genes. These changes do not involve changes to the DNA sequence, but do post translational modifications which ultimately affect how cells interprete the genes (Portela and Esteller 2010). Epigenetic changes are natural but can also be affected by some factors like age, lifestyle, environment and disease state (Jirtle and Skinner 2007). These modifications leads to chromatin remodeling, altered gene expression and modifies cellular phenotype without changing genotype (Egger et al. 2004; Holliday 2006).

The epigenetic modifications are series of chemical changes that occur on DNA or specific amino acids of histone proteins around which DNA is wrapped. The most widely studied DNA modification is DNA methyaltion, catalyzed by the enzymes DNA methyl transferases (Baylin and Jones 2011). The most diverse modifications are those that take place on histone proteins. The amino-terminal tail of histone protein can undergo acetylation, phosphorylation, methylation, ubiquitylation, ADP ribosylation, sumoylation, deimination, proline isomerization, crotonylation, hydroxylation and *O*-GlcNAcylation (Berger 2007; Kouzarides 2007). Apart from these modification, structure and function of chromatin are regulated by chromatin remodelling complexes, non-coding RNAs and mutations in histone proteins themselves (Dawson and Kouzarides 2012).

1.2. Chromatin structure and modifications

Inside cell nucleus, DNA is found within nucleosomes, which comprise of nucleotide base pairs enveloped around histone protein octamer (Bannister and Kouzarides 2011; Kouzarides 2007). Each nucleosome is composed of an octamer of four histones namely H3,

H4, H2A, and H2B. DNA is folded around these four histones and H1 histone is associated with chromatin packaging (Grant 2001; Mersfelder and Parthun 2006). Nucleosomes involved in replication and repair and compose chromatin in accordance with other proteases and nucleases (non-histone proteins). There are two main states of chromatin, active (euchromatin) and inactive (heterochromatin). Heterochromatin is inactive state in which chromatin is tightly packed state and restricts the entry of RNA polymerase II to DNA and hence repressing gene transcription. Contrarily, euchromatin is loose and allows entry of RNA polymerase II and other transcriptional proteins, increases gene expression. The transition between euchromatin and heterochromatin can be induced through epigenetic modifications (Campos and Reinberg 2009).

Histone acetylation process catalyzed by histone acetyl transferases (HAT) where acetyl group from acetyl-coenzyme A gets transferred to the ε-NH+ group of lysine residues. In reverse, histone deacetylation causes the transfer of acetyl groups from histones to coenzyme A, catalyzed by histone deacetylases (HDACs). Histone acetylation neutralizes the positive charge of the histone amino terminal tail and hence reduces its attraction to the negatively charged phosphate backbone of DNA, hence loosening the nucleosome. These changes allow access of additional transcriptional proteins and enzymes which ultimately increases gene transcription. In reverse histone deacetylation increases wrapping of histone tails to DNA and decreases transcription factor to activate gene expression (Figure 1.1) (Felsenfeld and Groudine 2003).

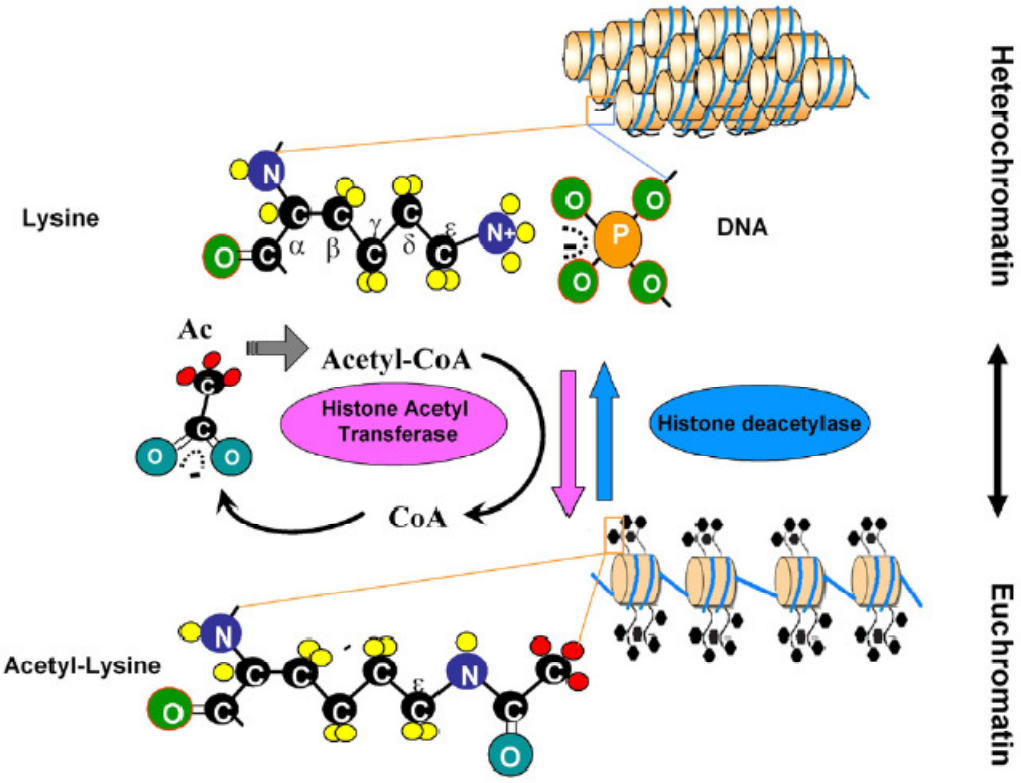

Figure 1.1. Histone acetylation process and change in chromatin states from heterochromatin to euchromatin. The figure explains the molecular structure of deacetylated and acetylated lysine and charge neutralization which is responsible for the interaction of histones with DNA. Reproduced from (Khan and Khan 2010).

1.3. Histone deacetylases (HDACs)

Histone Deacetylases (HDACs) are a family of enzymes which deacetylate lysine residue of core histone and other cellular proteins results in chromatin condensation and transcriptional repression (Lu 2013). Till date 18 HDACs are identified. Based on their size, number of active sites, cellular localization and homology to yeast HDAC protein, they are divided into four classes (Gregoretti et al. 2004). Class I comprises of HDAC1, HDAC2, HDAC3 and HDAC8. Class II contains six HDAC proteins which are further classified into two subclasses. Class IIa contains HDAC4, HDAC5, HDAC7, and HDAC9. These isoforms

contain a single catalytic active site. Class IIb comprises of HDAC6 and HDAC10, having two catalytic active sites. Class IV HDACs has only one member HDAC11. Class I, II, and IV HDAC proteins called as classical HDACs and their catalytic activity depend on metal ion (Zn^{+2} ion) presents at active site. Class III HDAC proteins, called as sirtuins (SIRT1-7), which operate by a NAD+-dependent mechanism unrelated to the classical HDAC proteins (Finnin et al. 1999). Class I and II HDACs are more expressive in mammals, among them class I HDACs have wide spread tissue distribution while class II HDACs have high expression in muscle and brain (Sterner and Berger 2000).

1.4. Histone deacetylases and cancer

Aberrant expression or mutation of several histone deacetylases (HDACs) have been seen in cancer; rendering them as potential targets for cancer treatment. It has been reported certainly that cancer cells undergo a loss of acetylation of histone H4 at lysine 16 which indicates that HDAC activity is crucial in establishing the tumor phenotype (Fraga et al. 2005). In cancer pathological situations where classical HDACs are overexpressed, histone deacetylase inhibitors (HDIs) showed potential as cancer therapeutic agents. Moreover, it needs to remember that the role of HDACs in cancer can be due to mechanisms other than overexpression. HDACs can be aberrantly recruited to target genes via their interaction with fusion proteins for example certain leukemias.

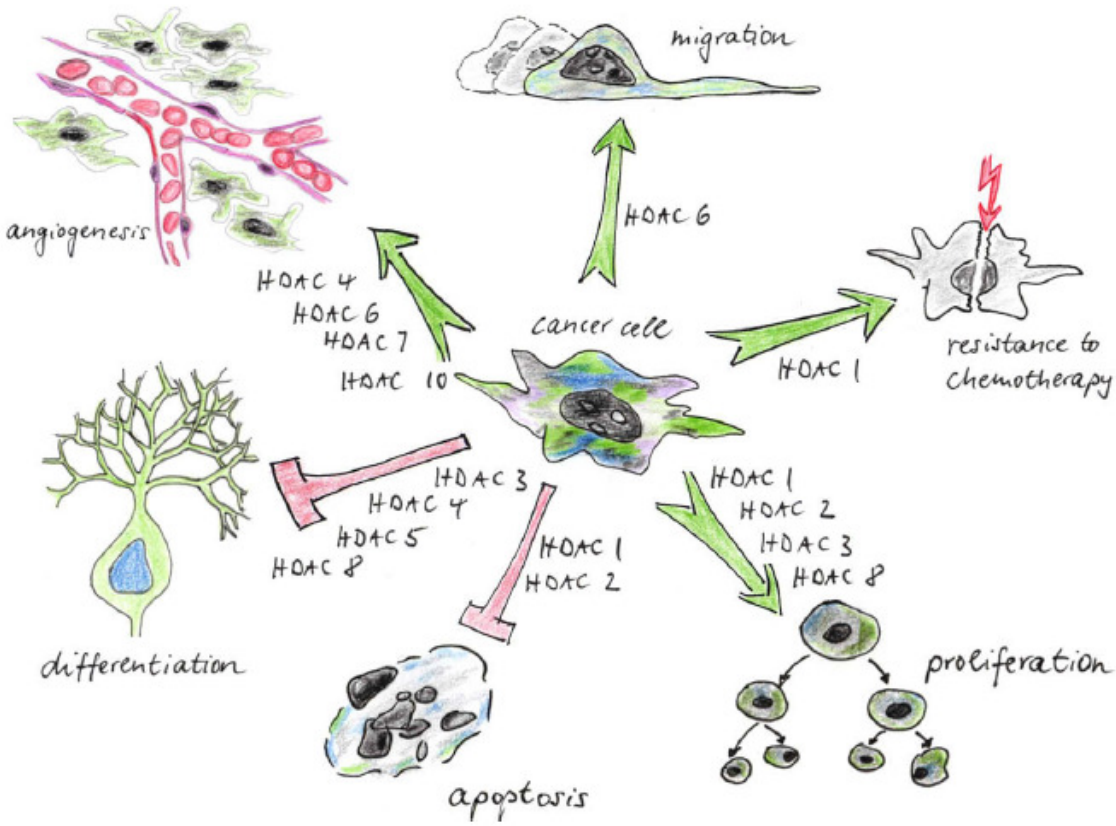

Figure 1.2. HDAC isoforms control hallmarks of cancer cell biology. Reproduced from (Witt et al. 2009).

1.4.1. Class I HDACs

Class I HDAC family members are deregulated in many cancers. Analysis of cancer samples of patients showed overexpression of HDAC1 in breast, gastric, pancreatic, lung, hepatocellular and prostate carcinomas (Jae-Hoon Choi et al. 2001; Jung Hye Choi et al. 2010; Minamiya et al. 2011; Zhenhuan Zhang et al. 2005). Overexpression of HDAC1,2 and 3 have also been reported in colorectal, gastric and renal cell cancer as well as in classical Hodgkin's lymphoma (Adams et al. 2010; Fritzsche et al. 2008; Weichert et al. 2008). In a study analyzing breast tumors, HDAC1 and HDAC3 expression found to

correlate with progesterone and estrogen receptor expression (Krusche et al. 2005). HDAC2 was found to contribute more to the pathogenesis of the disease as well as its aberrant expression was found in lung cancer (Pacheco and Nielsen 2012), (Jung et al. 2012). All together, these studies reveal that overexpression of class I HDACs associated with cancer progression. Overexpression of another Class I family member HDAC8 have been reported in childhood neuroblastoma and found to be cancer-type specific (Oehme et al. 2009).

Class II HDACs

1.4.1.1. Class IIa HDACs

Class I HDACs were found to show potential contribution in cancer pathogenesis. However, in past few years cancer has started to be linked with Class II HDACs also. Overexpression of HDAC4 with HDAc9 and SIRT5 was observed in patients with Waldenstrom's macroglobulinemia (Sun et al. 2011). HDAC4 expression was also found to be upregulated in breast cancer samples (Özdağ et al. 2006). However, dysfunction and downregulation of HDAC4 are associated with cancer development. HDAC5 and HDAC9 found to be critical markers for medulloblastoma. Both of these HDACs are overrexpressed in high-risk medulloblastoma patients, indicating its role in this diseases (Milde et al. 2010). Aberrant expression of HDAC5 along with HDAC3 was observed in hepatocellular carcinoma (HCC). Increased levels of HDAC7 have been reported in pancreatic cancer patients (Ouaïssi et al. 2008; Weichert 2009). High level of HDAC7 and HDAC9 have been reported in children with acute lymphoblastic leukemia (ALL) with poor prognosis (Moreno et al. 2010). Significant downregulated of HDAC7 has been reported in myeloproliferative neoplasms (Skov et al. 2012). HDAC9 has been reported to be overexpressed in cervical cancer (Y. W. CHOI et al. 2007). Increased level of HDAC9 is also associated with poor

survival in medulloblastoma patients (Milde et al. 2010) and in childhood acute lymphoblastic leukemia (ALL) patients (Moreno et al. 2010).

1.4.1.2. Class IIb HDACs

Increased HDAC6 expression has been linked with tumorigenesis (Lee et al., 2008; Sakuma et al., 2006). Significantly higher expression of HDAC6 was found in oral squamous cell (Sakuma et al. 2006). While in breast cancer, HDAC6 expression was associated with better survival and was higher in small tumors, low histologic grade, and in estrogen and progesterone receptor-positive tumors. High levels of HDAC6 mRNA tended to be more responsive to endocrine treatment than those with low levels. HDAC6 may thus serve as a predictive indicator of responsiveness to endocrine treatment and also as a prognostic indicator for breast cancer progression (Zhenhuan Zhang et al. 2004). However, in another study analyzing breast cancer tissues, HDAC6 protein expression revealed no significant prognostic differences based on its expression (Saji et al. 2005).

1.4.2. Class III HDACs-sirtuins

In recent years growing evidence has also linked sirtuins to cancer. However, as is the case for other HDACs, sirtuins seem to play both a pro-oncogenic as well as a tumor suppressor role in cancer. Similarly to classical HDACs, aberrant expression of several sirtuins is found in many types of cancer. For example, SIRT1 is upregulated in acute myeloid leukemia (AML), prostate cancer and non-melanoma skin cancer (Bradbury et al. 2005; Hida et al. 2007; Huffman et al. 2007), whereas it has been downregulated in colon tumors (Özdağ et al. 2006). SIRT3 and SIRT7 are upregulated in breast cancer (Ashraf et al. 2006). In contrast, SIRT2 is downregulated in gliomas and gastric carcinoma (Hiratsuka et al. 2003). Altered expression of SIRT5 and SIRT6 in cancer has not been reported so far.

1.4.3. Class IV HDACs

Very few studies have reported a potential role for HDAC11 in cancer. HDAC11 has been found to be involved in Hodgkin lymphoma (HL). Small interfering RNAs (siRNAs) that selectively inhibit HDAC11 expression induced apoptosis in HL cell lines and boost the production of tumor necrosis-a (TNFα) and IL-17 in the supernatants of HL cells (Buglio et al. 2011). Aberrant expression of HDAC11 has been reported in other hematopoietic cell malignancies.

1.5. Histone deacetylase inhibitors (HDACi) as anticancer agents

HDAC inhibitors (HDACis) were found to be effective in cancer pathological conditions and subsequently emerged as promising cancer therapeutic agents. HDAC inhibitors have the potential to disrupt multiple signaling pathways to inhibit tumor growth and induce apoptosis. HDAC inhibitors not only target histones but also targets non histone proteins and influence a variety of processes such as cell cycle arrest, angiogenesis, immune modulation and apoptosis (J. E. Bolden et al. 2006; Fraga et al. 2005; Peng and Seto 2011).Several nonhistone proteins have been identified as HDAC substrates with diverse biological functions are, transcription factors (E2F, p53, c-Myc, NF-κB), hypoxia-inducible factor 1 alpha (HIF-1α), estrogen receptor (ER α), androgen receptor (AR), MyoD, Chaperons (HSP90), signaling mediators (Stat3, Smad7), DNA repair proteins (Ku70), α-tubulin, β-catenin, retinoblastoma protein (pRb) and many others (Kim and Bae 2011; Singh et al. 2010).

1.5.1. FDA approved HDAC inhibitors

Till today, four HDAC inhibitors have been approved for cancer therapy by the US Food and Drug Administration (FDA). The first drug, Vorinostat (SAHA, Zolinza), developed by

Merck & Co. Inc. was approved in October 2006 for treatment of cutaneous T-Cell Lymphoma (CTCL). The second drug, Romidepsin (Istodax, FK228, FR901228, depsipeptide), developed by Gloucester Pharmaceuticals (acquired by Celgene in 2009) was approved in 2009, also for the treatment of T-cell lymphoma. Romidepsin is a natural product isolated from the cultures of *Chromobacterium violaceum*, a Gram negative bacterium isolated from a Japanese soil sample (Ueda et al. 1994). In June 2011, romidepsin was also approved for peripheral T-cell lymphoma (PTCL). The third drug, belinostat (Beleodaq, PXD-101), developed by Spectrum Pharmaceuticals was approved on July 3, 2014 for the treatment of patients with relapsed or refractory peripheral T-cell lymphoma (PTCL) (Food and Administration 2014). The fourth drug, Panabinostat (Farydak, LBH589), developed by Novartis Pharmaceutical Company was approved in 2015 for treatment of multiple myeloma (Fenichel 2015).

1.5.2. Classes of HDAC inhibitors:

HDAC inhibitors are divided in four classes according to their chemical structure.

1. Hydroxamates: vorinostat (SAHA), belinostat, panabinostat, abexinostat, givinostat,etc.
2. Benzamides: entinostat, mocetinostat, chidamide, tacedinaline (CI-994)
3. Short chain fatty acids: Valproic acid, phenyl butyrate
4. Cyclic peptides: romidepsin
5. HDAC inhibitors derived from natural source: trichostatin A, apicidin, largazole,etc.

Structures of representative HDAC inhibitors are represented in Figure 1.3.

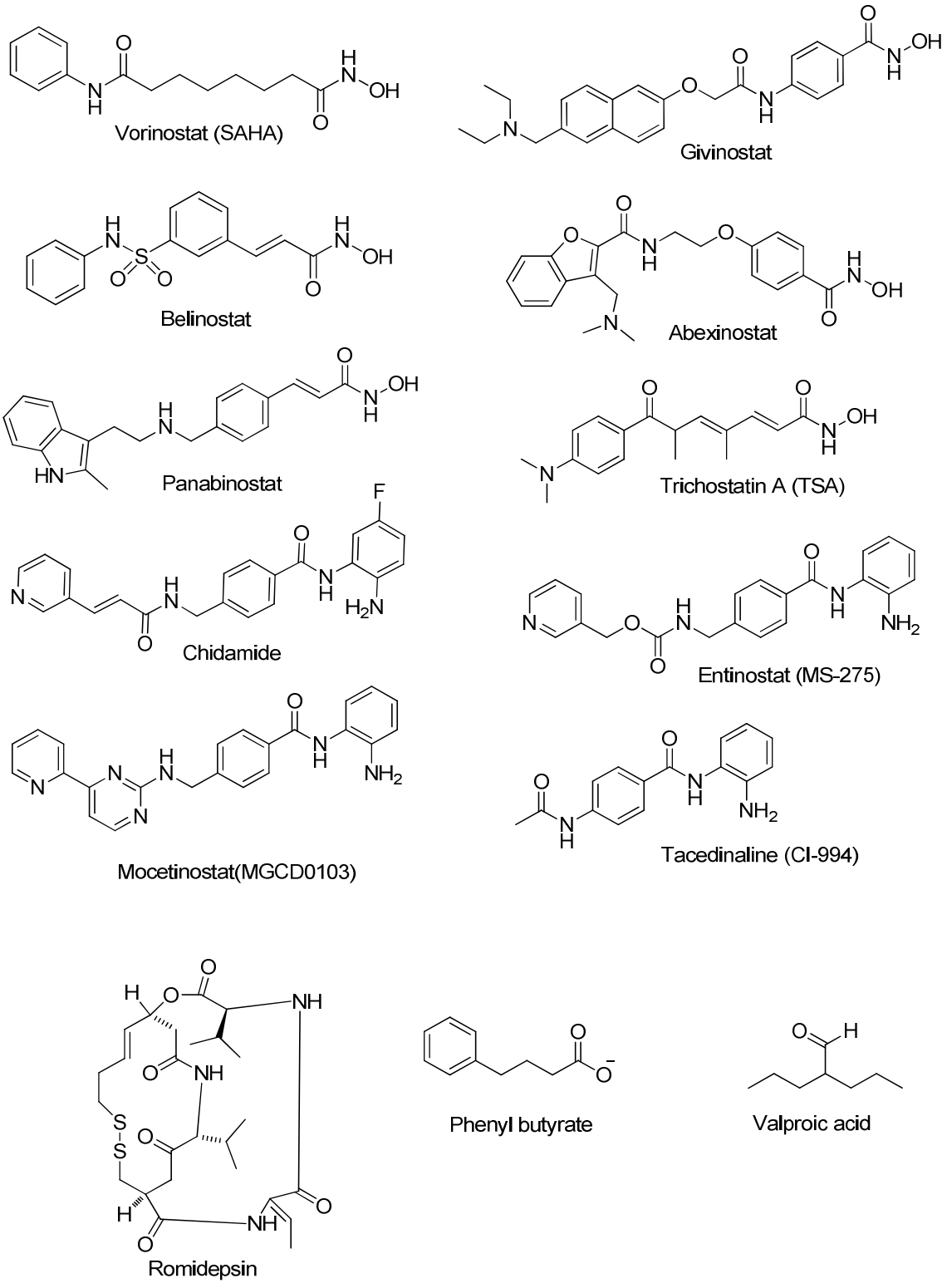

Figure 1.3. HDAC inhibitors; clinically approved and in clinical trials

1.5.3. Mechanism of action of HDAC inhibitors

The mechanism for antiproliferative effect of HDAC inhibitors is clearly associated with inhibition of HDAC activity and increased level of histone acetylation. However, this is not the only effect that can confer their activity (Schrump et al. 2008; Siu et al. 2008). HDACs not only act on histones and modify it, but also have many different cellular substrates and target proteins, including proteins that are involved in tumor progression, cell cycle control, apoptosis, angiogenesis and cell invasion. Thus HDAC inhibitors exert multiple cellular effects and the mechanism of action includes cell cycle arrest, activation of apoptotic pathway, induction of autophagy, reactive oxygen species generation, and angiogenesis. The main cause of cell death by HDAC inhibitors is induction of apoptosis, which occurs through intrinsic (mitochondrial) or extrinsic (death receptor) pathways, both of which lead to caspase activation and cell death. Extrinsic pathway is initiated by binding of ligands, such as Fas ligand (FasL), tumor necrosis factor (TNF) and TNF-related apoptosis-inducing ligand (TRAIL) to their respective cell surface death receptors (DR), whereas intrinsic pathways are activated by disruption of mitochondrial membranes by cellular stresses such as chemotherapy, ionizing radiation, and withdrawal of growth factors (Johnstone et al. 2002).

Vorinostat treatment induced transcription of BH3-only pro-apoptotic protein encoding genes (Bad, Bim, Bix, Noxa), the multi-domain pro-apoptotic gene BAK1 and genes encoding death effector components downstream of mitochondrial damage (Diablo, Apaf1, Casp9, HtrA2 and CytC) in transformed fibroblasts (J. Bolden et al. 2013). Besides, the pro-survival genes, such as Bcl2A1, Bcl2L1 (encoding Bcl-xL) and Bcl2L2 (encoding Bcl-w), were concomitantly repressed in these cells. HDAC inhibitors upregulated the expression of

pro-apoptotic proteins Bmf, Bid, and Bim that belong to the Bcl2 family, and down regulated the expression of the anti-apoptotic proteins of the Bcl2 family such as Bcl2 and Bcl-xL (J. E. Bolden et al. 2006).

HDAC inhibitors can also induce cell cycle arrest at G1/S or G2/M transition, leading to differentiation and/or apoptosis. HDAC inhibitor mediated increase in CDK inhibitor p21WAF1/CIP1 expression leads to cell cycle arrest at G1/S (Zhihua Zhang et al. 2013). Silencing of HDAC3 has been found to induce the expression of p21WAF1/CIP1 and cell cycle arrest in the G2/M phase in colon cancer cells (Wilson et al. 2006). SAHA was found to promote cell cycle arrest at G1/S and G2/M and subsequent apoptosis of leukemic K562, HL60 and THP1 cells (Silva et al. 2013).

HDAC inhibitors indirectly damage DNA by inducing changes in chromatin conformation upon histone acetylation that might expose the DNA to UV rays, ionizing radiation, ROS and chemotherapeutic genotoxic chemicals. This complex biochemical reaction can eventually lead to double strand breaks (DSBs) in DNA. Vorinostat was shown to induce DSBs in normal (HFS) and cancer (LNCaP, A549) cells, which can be repaired by normal cells but not transformed cells (Lee et al. 2010). HDACi can also downregulate the levels of DNA repair proteins, such as Ku70 and Ku86 that are involved in NHEJ pathway as well as suppressed gene expression of DNA repair proteins like RAD51, BRCA1 and BRCA2 (Adimoolam et al. 2007; Chen et al. 2007; Munshi et al. 2005)

Another responsible factor causing cell death and DNA damage by HDAC inhibitor is generation of reactive oxygen species. Free radical scavengers like N-acetylcysteine reduce ROS generation which in turn abrogates HDACi mediated cell death (Lee et al. 2010;

Rosato et al. 2003). HDACi increase ROS production through downregulation of thioredoxin (Trx), a thiol reductase that acts as a scavenger of ROS, and through upregulation of thioredoxin binding protein-2 (TBP-2), a protein that binds to Trx and blocks its reducing activity (Marks 2006). Vorinostat treatment induced TBP-2 expression followed by suppression of Trx expression (Butler et al. 2002). Together, these mechanisms by which HDAC inhibitors act upon cancer cell survival and death are depicted in Figure 1.4.

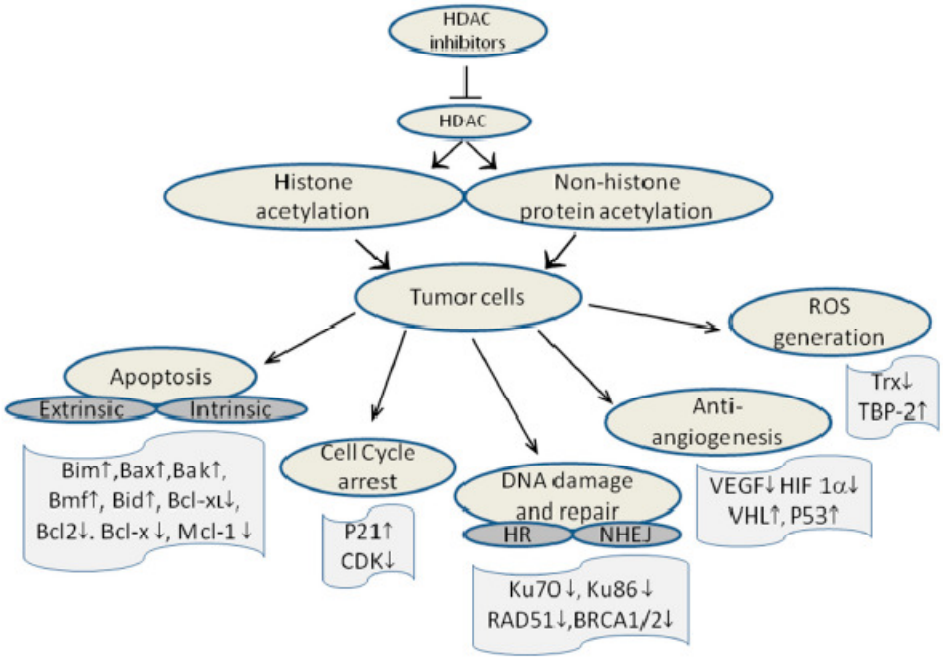

Figure 1.4. Multiple anti-tumor pathways activated by HDACi. Extrinsic and intrinsic refer to two apoptosis pathways, and HR and NHEJ refer to two DBS repair pathways. Reproduced from (Mottamal et al. 2015).

1.5.4. Basic Structure of Zinc Binding HDAC Inhibitors

HDAC inhibitors acting through zing binding mechanism have general pharmacophore model (Figure 1.5). This model consists three distinct region: (1) cap group or a surface recognition unit, usually a hydrophobic and aromatic group, which interacts with the entrance of the active site pocket (2) zinc binding domain (ZBD), which chelates zinc ion in the active site which is responsible for catalytic function of enzyme; and (3) linker region that connects the cap group to the ZBD (Gupta et al. 2012; Miller et al. 2003).

X-ray crystal structure analysis of SAHA bound in the active site of a bacterial homologue of class I HDAC proteins (HDLP) confirms that the hydroxamic acid (ZBG) coordinates to the catalytic metal atom (zinc) at the bottom of the active site, the anilide capping group interacts with the amino acids the residues at the entrance of active site and the linker lies in a confined hydrophobic channel that appropriately positions the metal-binding moiety and capping group for interactions in the active site (Finnin et al. 1999; Somoza et al. 2004).

Figure 1.5. General pharmacophore model of HDAC inhibitors

1.5.5. Toxicity in Clinical Trials of HDAC inhibitors

Toxicities were observed during clinical trial of HDAC inhibitors. The most common adverse events observed with the use of HDAC inhibitors were thrombocytopenia, neutropenia, anemia, fatigue and diarrhea (Coiffier et al. 2012; Mackay et al. 2010; Morita et al. 2012; Pili et al. 2012; Younes et al. 2011; Zorzi et al. 2013). In few cases it was

noticed that HDAC-induced thrombocytopenia was reversible upon withdrawal of the drug (Bishton et al. 2011). Some other side effects like nausea, vomiting, anorexia, constipation and dehydration were also seen in patients under treatment with HDAC inhibitors. Deaths have been reported in clinical studies involving HDAC inhibitors like vorinostat (Kelly et al. 2003), givinostat (Galli et al. 2010), moceinostat (Younes et al. 2011) and many other HDAC inhibitors. Thus more studies are needed to determine the toxicity of HDAC inhibitors before a clinical trial can be done, to minimize the cytotoxic effects in patients.

1.5.6. Isoform selective HDAC inhibitors

The majority of HDAC inhibitors approved or in clinical trials inhibit all HDAC isoforms called as pan inhibitors. Pan-HDAC inhibitors display a wide spectrum of toxicities ranging from fatigue, nausea and vomiting to thrombocytopenia, neutropenia and some cardiac toxicity. These compounds inhibit several HDAC isoforms and multiple cellular processes that depend on protein acetylation. The administration of single drug can result in large global changes in cellular pathways that may affect normal physiological function rather than only desired cancer cell (Li et al. 2004).

Selective HDAC inhibitors, which can be isoform selective or class-selective, would be ideal chemical tools to explain functions of individual HDAC isoform. Specifically, selective HDAC inhibitors would help in defining the molecular mechanism connecting HDAC activity to cancer formation (Fischer et al. 2010). Moreover, class-selective or isoform selective HDAC inhibitor might provide a more effective chemotherapy compared to pan-inhibitors (Bieliauskas and Pflum 2008).

Despite therapeutic advantage of selective HDAC inhibitors, their design has been challenging. The high sequence similarity within the active sites of the isoforms makes inhibitor design problematic (Finnin et al. 1999). In addition, minute differences among the active sites of each human isoform are not well characterized because of limited crystallographic analysis (Haggarty et al. 2003).

There are still relatively few isoform-specific HDAC inhibitors available, but compounds with proposed selectivity for HDAC3, HDAC6 and HDAC8 (based on assays using recombinant purified proteins) have been developed (Table1.1).

Table 1.1. Isoform selective HDAC inhibitors

HDAC inhibitor	HDAC isoform selectivity	Development status	Target disease
Compound 60	HDAC1 and 2	Preclinical	Neurology
MRLB-223	HDAC1 and 2	Preclinical	Cancer
RG2833	HDAC3	Phase I trial	Friedreich's ataxia
RGFP966	HDAC3	Preclinical	Cancer, neurology
BG45	HDAC3	Preclinical	Cancer
Rocilinostat (ACY-1215)	HDAC6	Phase IIa trial	Cancer
Tubacin	HDAC6	Preclinical	Cancer
Tubastatin A	HDAC6	Preclinical	Inflamation, neurodegenaration
HPOB	HDAC6	Preclinical	Cancer
C1A	HDAC6	Preclinical	Cancer

PCI-34051	HDAC8	Preclinical	Cancer
C148	HDAC8	Preclinical	Cancer

1.6. Objectives

Histone deacetylase inhibitors are emerging as potential anticancer therapeutics. Majority of the HDAC inhibitors which are clinically approved and in clinical trial are Pan HDAC inhibitors. In recent research is focused on development of isoform selective HDAC inhibitors. Few isoform specific inhibitors are in preclinical or clinical stage.

Our objective is to design and synthesize novel compounds with increased selectivity towards specific HDAC isoform with improved anticancer potential. In this study, we have designed and synthesized various molecules by modification of cap, linker region of prototype HDAC inhibitors and characterized them for their selective HDAC inhibition efficiency as well as anticancer activity.

Objective 1: To develop 2-aminobenzamides as selective HDAC3 inhibitors with promising anticancer effects

Specific aims:

(i) To design and synthesis a series of novel 2-aminobenzamides.

(ii) To characterize them by ^{1}H NMR, ^{13}C NMR and LC/MS.

(iii) To evaluate their HDAC inhibition efficiency using HeLa nuclear extract and human recombinant HDAC3 enzyme.

(iv) To evaluate their anticancer potential *in vitro* by various studies using different cancer cell lines.

Objective 2: To develop novel hydroxamates with piperidine and piperazine linker as HDAC inhibitors

Specific aims:

(i) To design and synthesis a series of novel hydroxamates with alkyl chain attached with piperidine and piperazine moiety as linker

(ii) To characterize them by ^{1}H NMR, ^{13}C NMR and LC/MS.

(iii) To evaluate their HDAC inhibition efficiency using HeLa nuclear extract and human recombinant HDAC3 enzyme and human recombinant HDAC8 enzyme.

(iv) To evaluate their anticancer activity *in vitro* using different cell line

Objective 3: To develop novel hydroxamates as selective HDAC8 inhibitors

Specific aims:

(i) To design and synthesis a series of novel hydroxamates.

(ii) To characterize them by ^{1}H NMR, ^{13}C NMR and LC/MS.

(iii) To evaluate their HDAC inhibition efficiency using HeLa nuclear extract and human recombinant HDAC3 enzyme and human recombinant HDAC8 enzyme.

(iv) To evaluate their anticancer activity *in vitro* using different cell line

Chapter 2

Design, synthesis and biological screening of 2-aminobenzamides as selective HDAC3 inhibitors with promising anticancer effects

2.1. Introduction

Cancer is one of the major causes of death worldwide. Even though progress has been made in prevention and treatment of cancer, still cancer burden is increasing globally (Fitzmaurice et al. 2015). In past few years, deacetylation of histone has been considered as a promising target for anticancer therapy. Histone deacetylases (HDACs) are a family of enzymes which deacetylate the lysine residue of core histone and other cellular proteins and subsequently results in chromatin condensation and transcriptional repression (Kouzarides 2007; Rosato and Grant 2005; Xu et al. 2007). These epigenetic alterations by HDACs are involved in suppressing the gene transcription and finally lead to the silencing of tumor suppressor genes. Abnormal expression of various HDACs has been reported in many cancer cell lines and tumor tissues (Mottamal et al. 2015). HDAC inhibitors cause tumor cell death by inducing apoptosis, cell cycle arrest, senescence, differentiation, autophagy, etc. Therefore, HDAC inhibition has emerged as a potential anticancer target (Amin et al. 2017a, 2017b; Frew et al. 2009; Witt et al. 2009).

Since past few years, a number of HDAC inhibitors have been studied clinically and pre-clinically for various cancers (**Figure 2.2**). Four of them are approved by USFDA for clinical use. Vorinostat (SAHA) has been approved for the treatment of cutaneous T-cell lymphoma, whereas romidepsin is approved for cutaneous T-cell lymphoma as well as peripheral T-cell lymphoma (PTCL). Again, belinostat is utilized for peripheral T-cell lymphoma and panobinostat is approved for multiple myeloma. Chidamide has been approved for peripheral T-cell lymphoma in China (Suresh et al. 2017). Many other promising HDAC inhibitors such as entinostat (MS-275), mocetinostat (MGCD-0103), tacedinaline (CI-994) are now in clinical trials for the treatment of different types of cancers (Campas-Moya 2009; Maiso et al. 2006; Mann et al. 2007; O'Connor

et al. 2015; Xie et al. 2017). Generally, HDAC inhibitors have a common pharmacophore model (**Figure 2.1**) which includes three regions, i.e., one cap group or surface recognition domain, a linker function and a zinc binding group (ZBG) (Amin et al. 2018a).

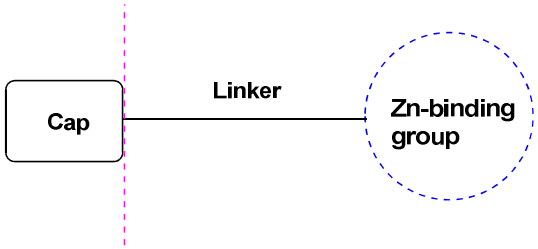

Figure 2.1. General pharmacophore model for HDAC inhibitors

The first generation HDAC inhibitors (such as vorinostat, romidepsin, belinostat and panobinostat) containing hydroxamate function as ZBG having pan HDAC inhibitory effects are found to be effective anticancer agents (**Figure 2.2**).

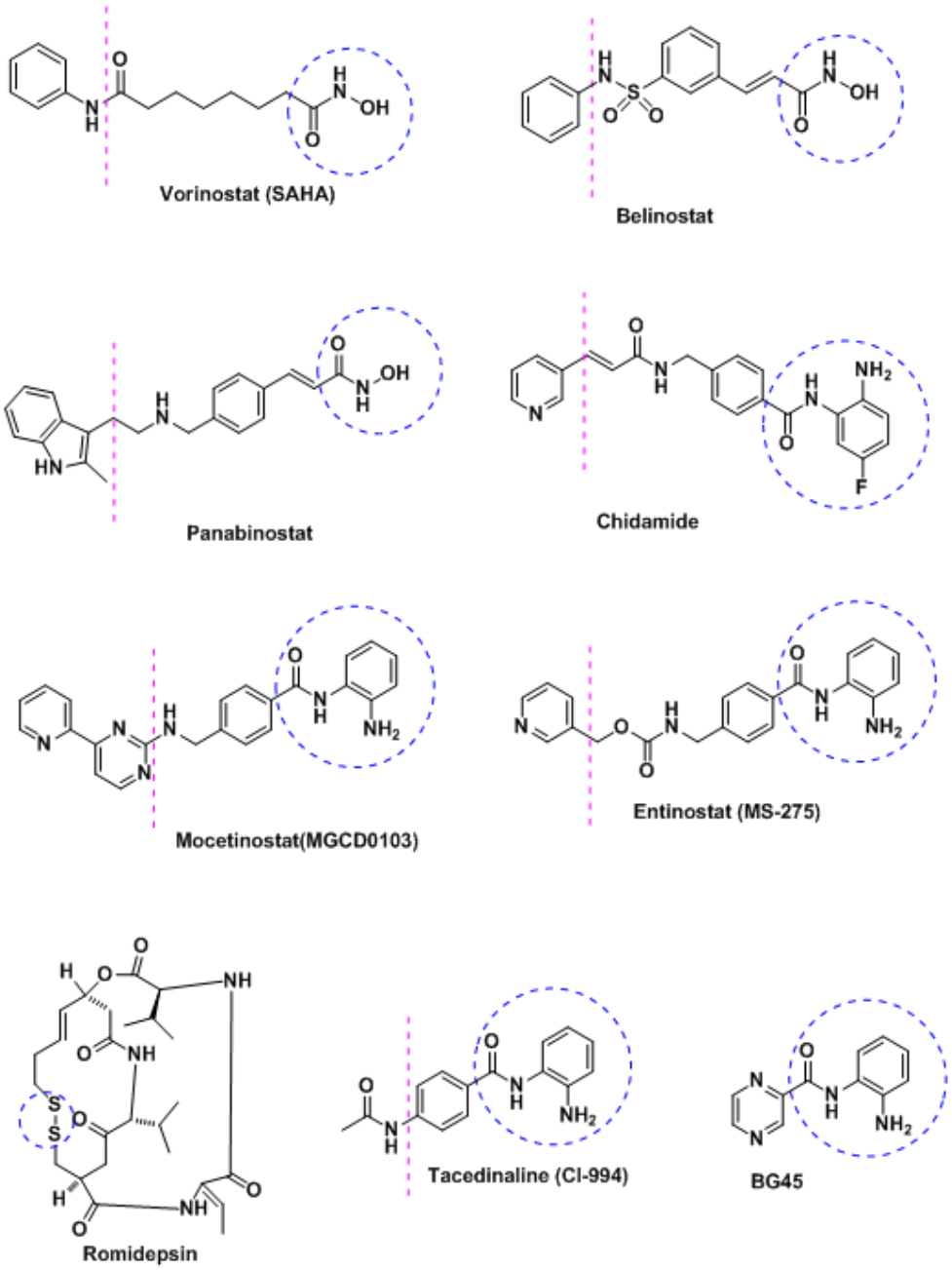

Figure 2.2. Potential HDAC inhibitors [clinically approved and in clinical trials]

Among different HDACs, histone deacetylase 3 (HDAC3) has been found to play pivotal roles in the cancer cell proliferation, migration and apoptosis (Li et al. 2014) along with DNA repair, genome stabilization and maintaining structural integrity of chromatin as well as histone deacetylation mechanisms during cell cycle progression and apoptosis (Bhaskara et al. 2008; Bhaskara et al. 2010; Bose et al. 2014). Overexpression of HDAC3 has been attributed in numerous cancers such as breast cancer (Hanigan et al. 2017; Huang et al. 2016), lung cancer (Chen et al. 2013), liver cancer (Liu et al. 2013), colon cancer (Wilson et al. 2006), leukemia (Zhang et al. 2016), multiple myeloma (Harada et al. 2017), lymphoma (Jiang et al. 2017), melanoma (Shan et al. 2014) and glioma (Libý et al. 2006). Therefore, inhibitors targeted to HDAC3 may be considered as a useful tool to combat various malignancies.

In recent scenario to achieve increased selectivity and specificity, other ZBGs (such as benzamides, thiols, sulphamides) have been taken into consideration (Gupta et al. 2012). In general, benzamides are found to inhibit class I HDACs (namely entinostat, mocetinostat and **CI-994**) (Loprevite et al. 2005; Ryan et al. 2005). Modifications of the cap region having supremacy to target selective HDAC as it not only binds to the enzyme surface but also forms complexes present nearby. These could help to design the selective HDAC inhibitors (Falkenberg and Johnstone 2014; Salisbury and Cravatt 2007). Compounds possessing 2-aminobenzamide moiety as zinc binding group (ZBG) has already been proven to execute selectivity towards HDAC3 with promising anticancer properties (Hsieh et al. 2017; Marson et al. 2013; Marson et al. 2015). Depending on some crucial observations obtained by our recent molecular modeling study (Amin et al. 2018b) on selective HDAC3 inhibitors, newer HDAC3 inhibitors are designed in the present work. These observations for designing newer HDAC3 inhibitors are furnished below:

1. The free amino group of benzamide moiety may serve as hydrogen bonding interaction. Therefore, no substitution was made here.
2. Hydrophobicity of the phenyl group is crucial for HDAC3 inhibition. Not only that, no bulky steric and hydrophobic substitution at 5^{th} position of the phenyl group of benzamide moiety was considered for designing HDAC3 inhibitor as it was unfavorable for HDAC3 inhibition.
3. Smaller electron-withdrawing substituents (such as fluoro) at the *para* position of the benzamide moiety was considered for designing newer HDAC3 inhibitors as it may favor HDAC3 selectivity.
4. Carboxamide function attached to the benzamide scaffold was kept intact as the carbonyl group is necessary for hydrogen bonding and amide group coordinated to the catalytic Zn^{2+} ion.
5. Steric and hydrophobic aryl linker function was taken into consideration.
6. Smaller aryl cap group was taken into account.

BG45, a benzamide-based class I HDAC inhibitor with preferential selectivity towards HDAC3 showed a significant inhibition of cellular proliferation in multiple myeloma *in vitro*. Moreover, it was also found to be effective *in vivo* in arresting tumor growth as evidenced in the murine xenograft model of multiple myeloma (Minami et al. 2014). In the present study, we have designed and synthesized a series of novel benzamides by modifying the cap region of **BG45** in order to increase selectivity and efficacy towards HDAC3. These novel compounds were screened for their potency and selectivity for the enzyme in the *in vitro* enzyme inhibition assay and for their anti-proliferative efficiency on different cancer cell lines.

2.2. Results and Discussion

2.2.1. Designing of benzamide-based HDAC3 inhibitors

Taking into account the density functional theory (DFT)-energy minimized electrostatic potential maps of **BG45** and **CI-994** (both are prototype isoform-selective HDAC inhibitors), it is observed that there is only a slight difference between them (**Figure 2.3**).

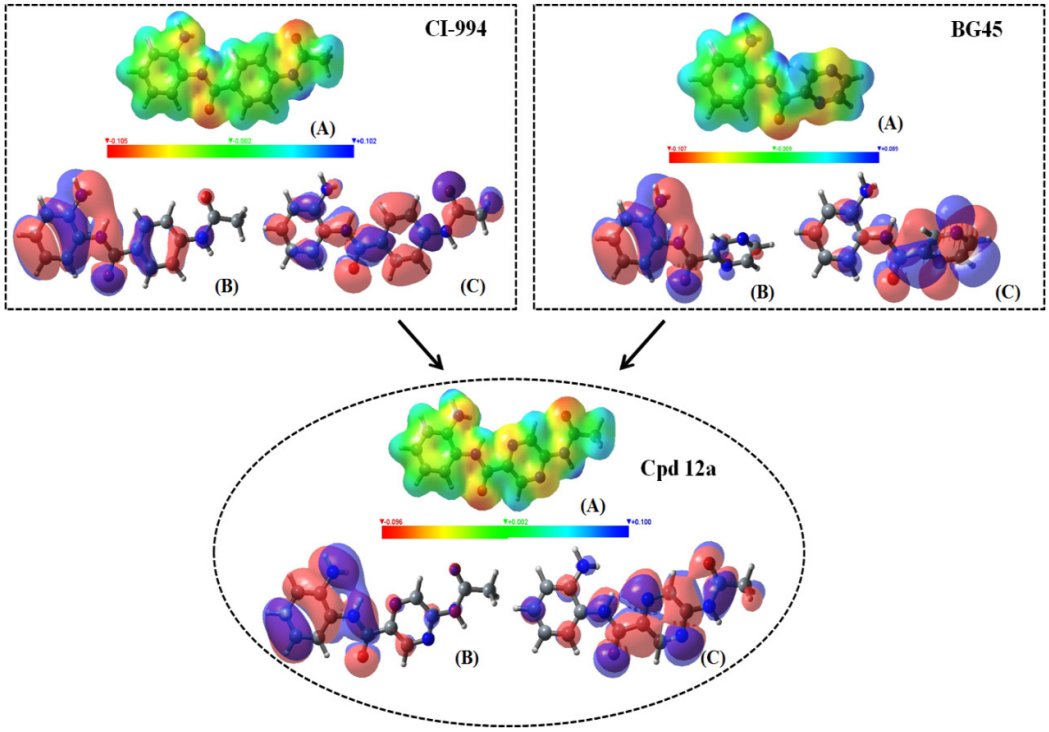

Figure 2.3. Designing of the initial hit molecule compound **12a** combining the structures of **CI-994** and **BG45** [(A): Electrostatic potential map; (B): HOMO orbital electron density map; (C): LUMO orbital electron density map].

Comparing their activities, it is observed that both of these molecules exhibit similar efficacy in HDAC3 inhibition. However, **BG45** is smaller in size or shorter in length compared to **CI-994**. Therefore, it may be inferred that as both of these molecules comprise the carboxybenzamide moiety, the pyrazine scaffold obviously possesses a positive influence on HDAC isoform selectivity. Comparing their electrostatic potential

maps, it may be assumed that due to the higher electron-rich region (yellow) imparted by both the nitrogen atoms of the pyrazine ring (**Figure3**), **BG45** produces more HDAC3 inhibition compared to **CI-994**. Therefore, the phenyl ring of **CI-994** has been replaced with that pyrazine scaffold in compound **12a** to judge whether the activity will increase or not. Interestingly, it displays both the features of **BG45** and **CI-994** (**Figure 2.4**).

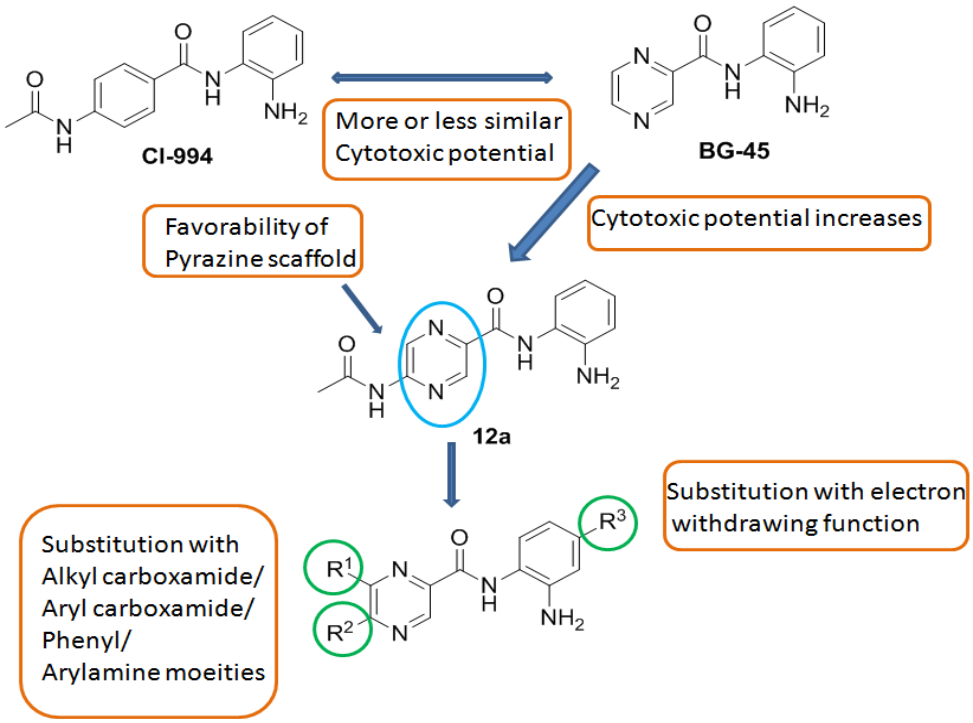

Figure 2.4. Designing of **BG45**-derived compounds

Nevertheless, the electrostatic potential map reveals that compound **12a** consists of more electronegative regions (yellow) compared to both **BG45** and **CI-994** (**Figure 2.3**). Moreover, the HOMO-LUMO electron density maps of both **BG45** and compound **12a** suggest that both the HOMO and LUMO orbitals are located terminally and the LUMO orbitals of both these compounds comprise the overlapping feature of both the nucleophilic (blue) and electrophilic (red) regions at the pyrazine ring system (**Figure 2.3**). It clearly implies the ability of the pyrazine ring to involve charge transfer

mechanisms or π-π interaction. Interestingly, it has been found that compound **12a** results in better efficacy regarding both HDAC3 inhibition as well as cellular toxicity which strongly implicated the importance of pyrazine scaffold in the molecular structure for exerting better efficacy.

Considering compound **12a** as an initial hit molecule, newer molecules have been designed and synthesized by substitution at the *para* position of the benzamide moiety with small electron-withdrawing substituents (namely fluorine) as well as by substitution with alkyl carboxamide / aryl carboxamide/ phenyl/ aryl amine functions at the pyrazine scaffold (**Figure 2.4**).

As **CI-994** contains -$NHCOCH_3$ group, initially it was tried in both these positions (R^1 and R^2). Then, the effect of NHCOPh was taken into consideration whether bulkier substitution was better or not. Finally, phenyl, aminophenyl and aminobenzyl substitutions were tried at these R^1 and R^2 positions to judge or compare their efficacy with respect to the earlier ones. As there is no compounds of such type reported earlier combining scaffolds of these two prototype compounds (**CI-994** and **BG-45**), these groups (alkyl carboxamide / aryl carboxamide/ phenyl/ aryl amine functions) were chosen particularly at these R^1 and R^2 positions to get an initial idea that which type of substituents was preferable at these positions to synthesize newer better active molecules in future.

2.2.2. Chemistry

Scheme 2.1 outlines the synthesis of an intermediate; *tert*-butyl (2-aminophenyl) carbamate (**2**). Here *o*-phenylenediamine (**1**) was protected at one amino group using di-*tert*-butyl dicarbonate.

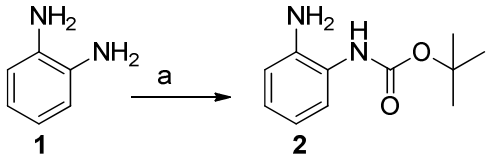

Scheme 2.1. *Reagent and conditions*: (a) di-tert-butyl dicarbonate, triethylamine, ethanol, RT, 5h.

Scheme 2.2 represents the synthesis of an intermediate *tert*-butyl (2-amino-5-fluorophenyl) carbamate (**6**). The reaction started with boc protection of 5-fluro-2-nitroaniline (**3**) which yielded the compound (**4**) with diprotection at the amino group. This compound (**4**) was selectively deprotected with controlled condition using trifluoroacetic acid gave monoprotected amino group (**5**) (Reis et al. 2016). Compound **5** upon catalytic hydrogenation with Pd/C produced compound **6** which was further utilized as an intermediate for synthesis of the final compounds.

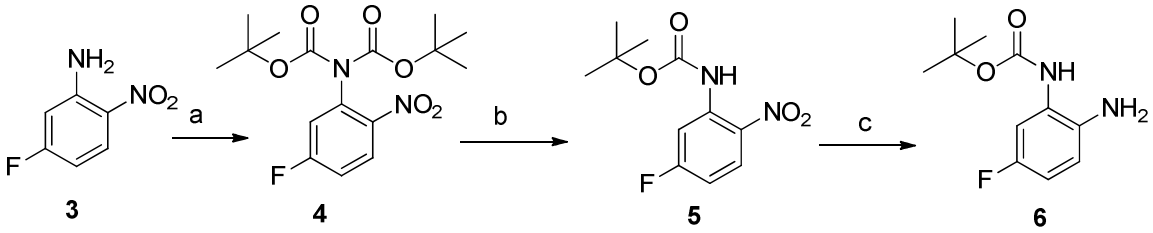

Scheme 2.2. *Reagent and conditions*: (a) di-tert-butyl-dicarbonate, DMAP, 2-methyl THF, RT, 12h (b) trifluoroacetic acid(3%), DCM, RT, 2 h (c) Pd/C, H_2balloon, Methanol, RT, 4h

Scheme 2.3 illustrates the synthetic route of final molecules (compound **12a**, **12b**, **12c** and**12d**). Here, methyl 5-(chloropyrazine)-2-carboxylate (**7**) was first converted to methyl 5-(aminopyrazine)-2-carboxylate (**8**) using sodium azide and triphenylphosphene (Kandalkar et al. 2013). Here, substituted chloropyrazine got converted to substituted azidopyrazine using sodium azide which also isomerizes to its

tetrazolo form *in situ*. The azidopyrazine forms iminophosphorane in the presence of triphenylphosphene which gets hydrolyzed to amine under acidic condition, a typical Staudinger reaction (Staudinger and Meyer 1919). *N*-acetylation of methyl 5-(aminopyrazine)-2-carboxylate (**8**) yielded compound **9a** while *N*-benzoylation produced compound **9b**. These intermediates were hydrolyzed to their acid derivatives compound **10a** and compound **10b**, and were coupled with **2** and **6** to get **11a**, **11b**, **11c** and **11d**. Deprotection of the compounds afforded final compounds **12a**, **12b**, **12c**, **12d**.

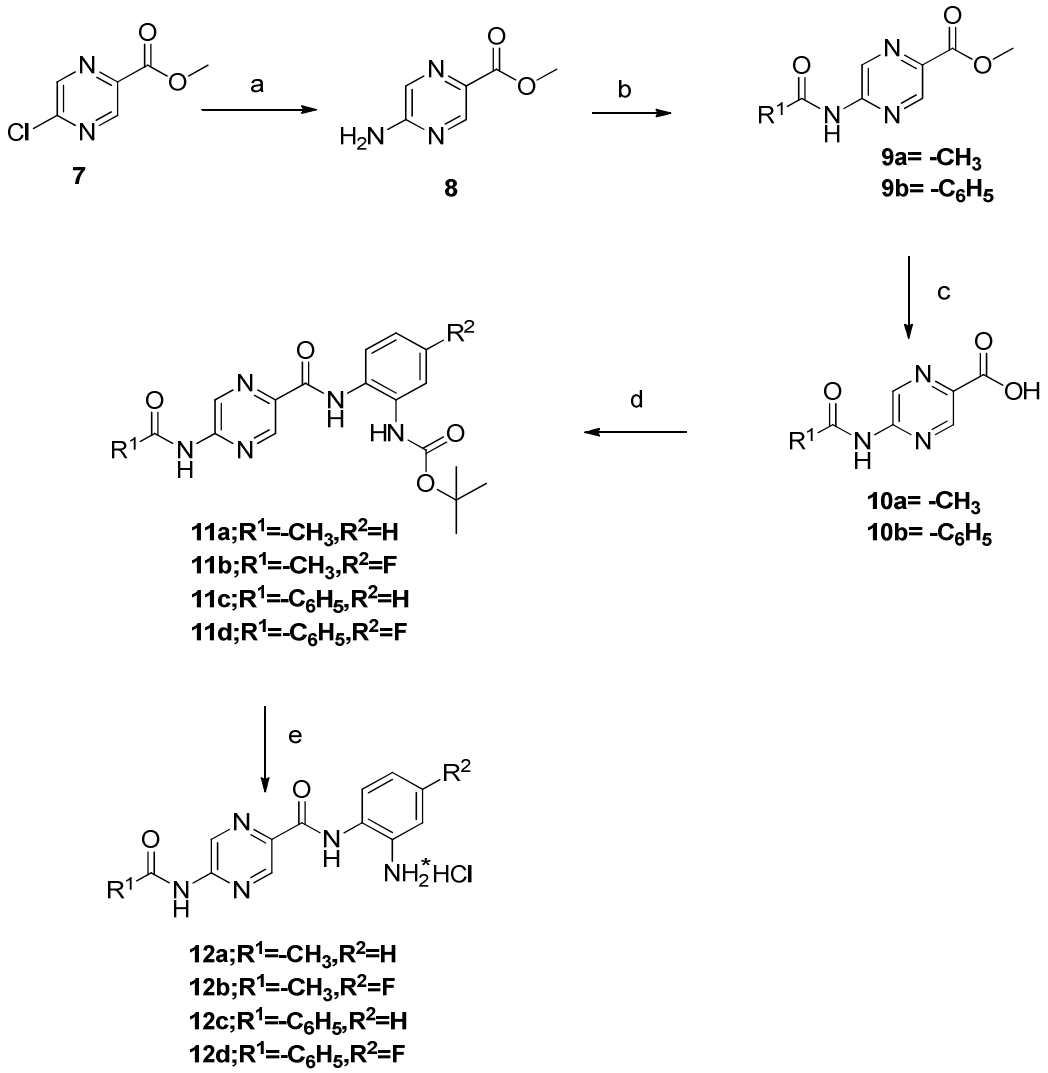

Scheme 2.3. *Reagent and conditions*: (a) i. sodium azide, triphenylphosphene, dimethyl sulphoxide, 120°C, 4h ii. 1N HCl, 120°C, 2h iii. $NaHCO_3$ (b) i. acetic anhydride, 90°C,

2h ii. benzoyl chloride, sodium hydride, DMF, 0°C, 5 h (c) lithium hydroxide, THF:water (3:1), RT, 3h (d) compd. **2** or compd. **6**, EDC, DMAP, DCM:pyridine (1:1), RT, 12h (e) 4M HCl in dioxane, DCM, 0°C, 2h.

Scheme 2.4 discusses the synthesis of target molecules**18a** and **18b** which mimics scheme 3 in mechanisms with difference of methyl 6-(chloropyrazine)-2-carboxylate (**13**) instead of methyl 5-(chloropyrazine)-2-carboxylate (**7**).

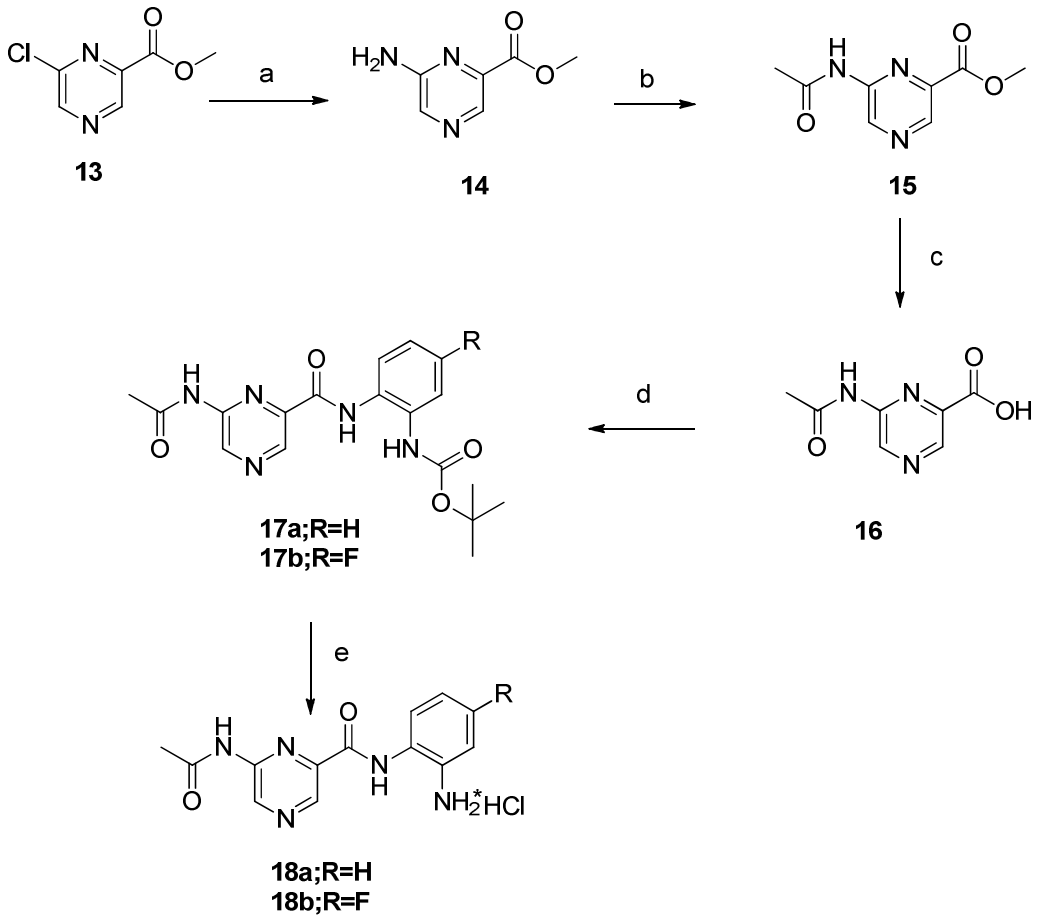

Scheme 2.4. *Reagent and conditions*: (a) i. sodium azide, triphenylphosphene, dimethyl sulphoxide, 120°C, 4h ii. 1N HCl, 120°C, 2h, iii. $NaHCO_3$ (b) acetic anhydride, 90°C, 2h (c) lithium hydroxide, THF:water (3:1), RT, 3h (d) compounds **2** or **6**, EDC, DMAP, DCM:pyridine (1:1),RT, 12h (e) 4M HCl in dioxane, DCM, 0°C, 2h

Scheme 2.5 shows the synthesis of target molecules **22a** and **22b**. The first reaction describes Suzuki coupling where methyl 5-(chloropyrazine)-2-carboxylate (**7**) was reacted with phenyl boronic acid in presence of bis(triphenylphosphine)palladium(II)dichloride as a catalyst and potassium carbonate using 1,4-dioxane solvent to get compound **19**. This compound (**19**) on alkaline hydrolysis formed its acid derivative **20**. This was coupled with intermediates **2** and **6** by EDC catalyzed acid-amine coupling to get **21a** and **21b** which upon boc deprotection by acid made final products **22a** and **22b** respectively.

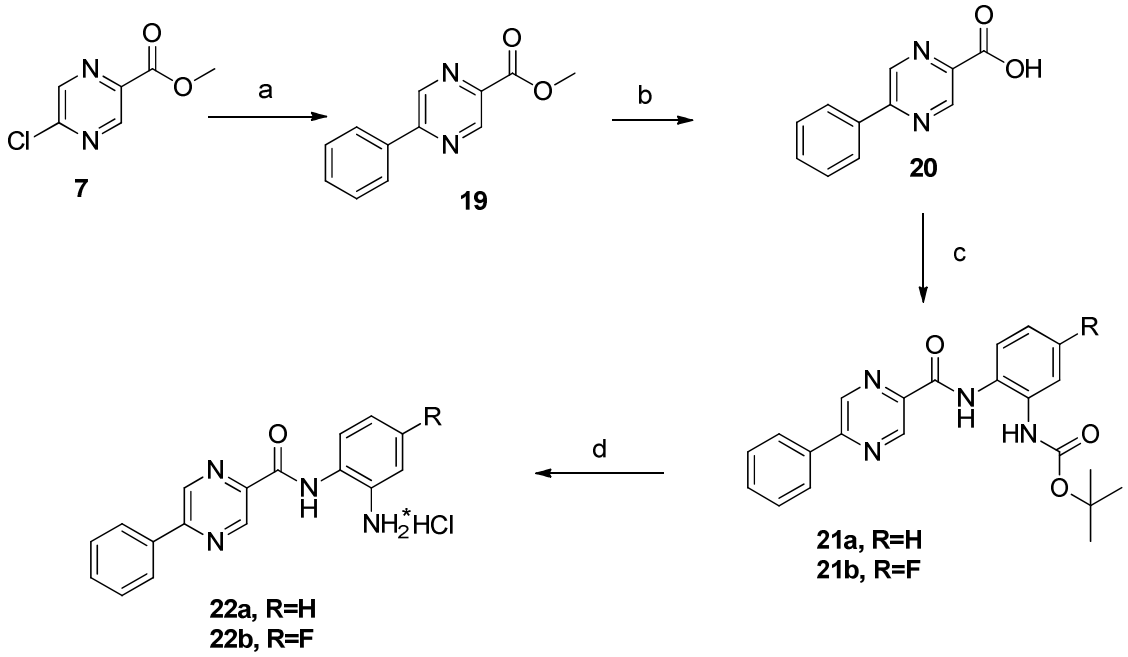

Scheme 2.5. *Reagent and conditions*: (a) phenyl boronic acid, bis (triphenylphosphine) palladium(II) dichloride, potassium carbonate, 1,4-dioxane, 100^{o}C, 12h (b) lithium hydroxide, THF: Water (3:1), RT, 3h (c) 2 or 6, EDC, DMAP, DCM:pyridine (1:1), RT, 12h (d) 4M HCl in dioxane, DCM, 0^{o}C, 2h.

Scheme 2.6 depicts synthesis of target molecules **26a**, **26b**, **26c** and **26d.** Methyl 5-(chloro pyrazine)-2-carboxylate (**7**) was reacted with aniline or benzylamine in

presence of *p*-toluene sulphonic acid and respective amines (compound **23a**, **23b**) were prepared. These compounds on alkaline hydrolysis formed respective acids (compound **24a**, **24b**). These were coupled with intermediate compounds **2** and **6** by EDC catalyzed acid-amine coupling to get compounds **25a**, **25b**, **25c**, **25d** which upon deprotection by acid made final products **26a**, **26b**, **26c** and **26d**.

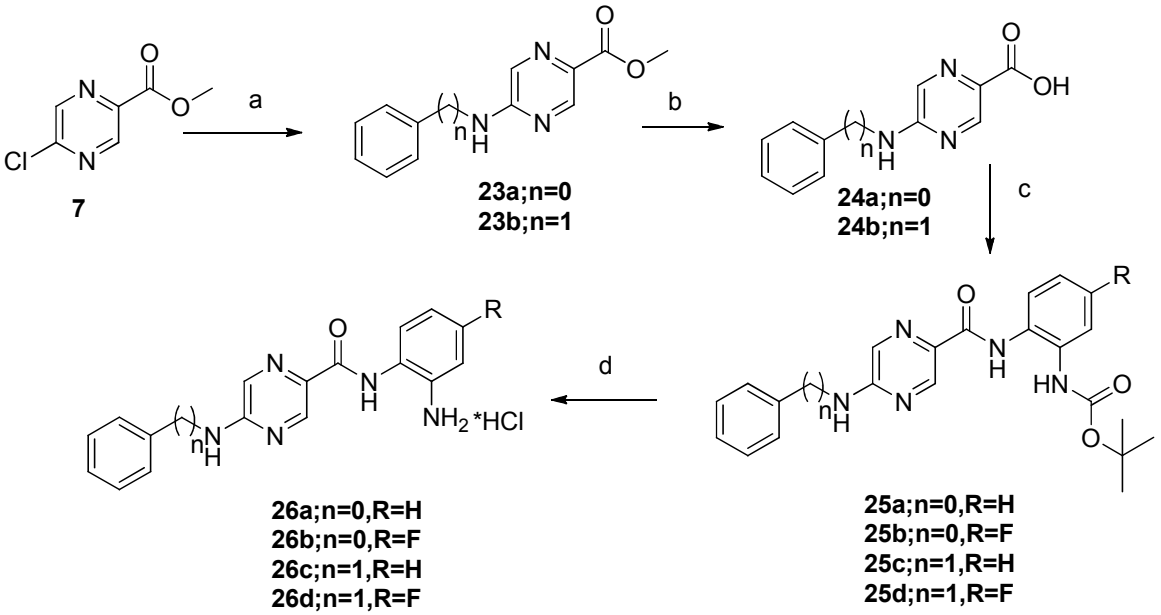

Scheme 2.6. *Reagent and conditions* (a) aniline (n=0) or benzylamine (n=1), p-toluenesulphonic acid, 1,4-dioxane, 100^{o}C,12h (b) lithium hydroxide, THF:water (3:1), RT, 3h (c) compound **2** or compound **6**, EDC, DMAP, DCM:pyridine (1:1), RT, 12h (d) 4M HCl in dioxane, DCM, 0^{o}C, 2h.

Purity of these final compounds was evaluated using ^{1}H NMR, ^{13}C NMR and LC-MS analysis. Spectral data of these final compounds are provided in the previous section.

2.2.3. Pan HDAC inhibition assay using HeLa nuclear extract

The target compounds were screened for their HDAC inhibitory activity using *color de lys*® HDAC assay kit (BML-AK501, ENZO life sciences). **CI-994** and **BG45** are used as positive control for the assay. HeLa nuclear extract (expresses HDAC1 and HDAC2

dominantly) (Serebryannyy et al. 2016) was used as a source of HDAC activity. The results are summarized in **Table 2.1**.

All compounds were found to exhibit HDAC enzyme inhibition at 5µM in duplicate. Compounds **26b**, **26c** and **26d** demonstrated an increased HDAC inhibition compared to **CI-994** and **BG45**. These compounds were screened for determination of IC_{50} of enzyme inhibition along with **CI-994** and **BG45.** Compound **26b**, **26c** and **26d** (IC_{50}= 1.972, 2.869 and 3.072µM, respectively) showed more promising HDAC inhibitory efficacy compared to **CI-994** (IC_{50}= 5.369 µM) and **BG-45** (IC_{50}= 5.506 µM) (**Table 2.2**) and **(Figure 2.5 A and B**).

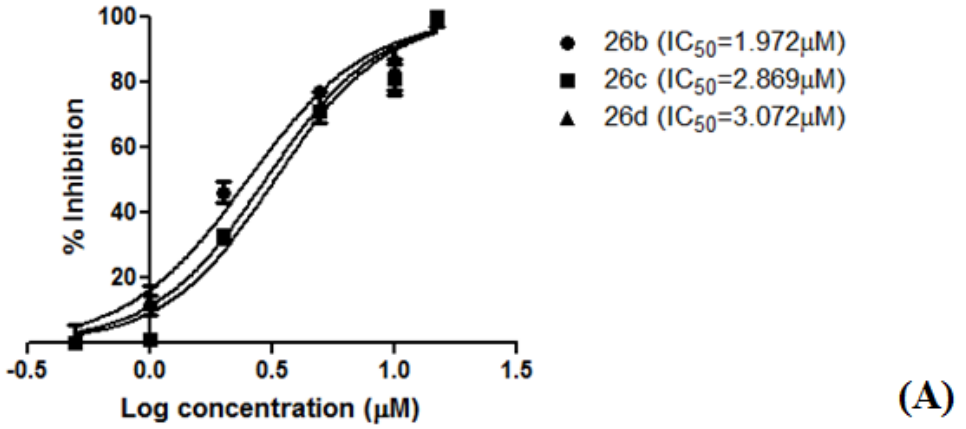

(A)

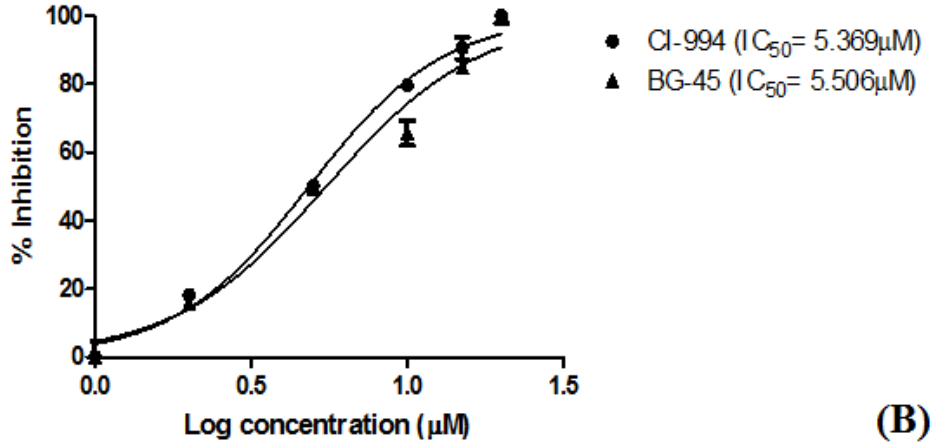

(B)

Figure 2.5. IC_{50} determination of HDAC enzyme inhibition using HeLa nuclear extract for compound **26b, 26c** and **26d** [A] and **BG-45** and **CI-994** [B]. The data represents mean± SD (n=2).

2.2.4. HDAC3 inhibition assay using recombinant HDAC3/NCOR1

Target compounds were evaluated for their inhibition potency towards HDAC3 enzyme using HDAC3/NCOR1 fluorometric drug discovery kit (BML-AK531, ENZO life sciences). All these compounds showed more inhibition of HDAC3 activity compared to nuclear extract (**Table 2.1**). For better understanding, the most potent HDAC3 inhibitor compounds **26b**, **26c** and **26d** (67.48%, 62.24% and 59.04% respectively with 1μM compound concentration in duplicate) were further evaluated for their IC_{50} values along with **CI-994** and **BG45** as positive control (**Table 2.2**, **Figure 2.6 A and B).** Compound **26b, 26c, 26d**, **BG-45** and **CI-994** were evaluated for IC_{50} determination. It was observed that the selected compounds were more effective than **CI-994** and **BG-45**. Compound **26c** appeared to be as a lead in the series having the highest HDAC3 inhibition (IC_{50} = 0.245μM) with ~12 fold HDAC3 selectivity over Pan HDACs.

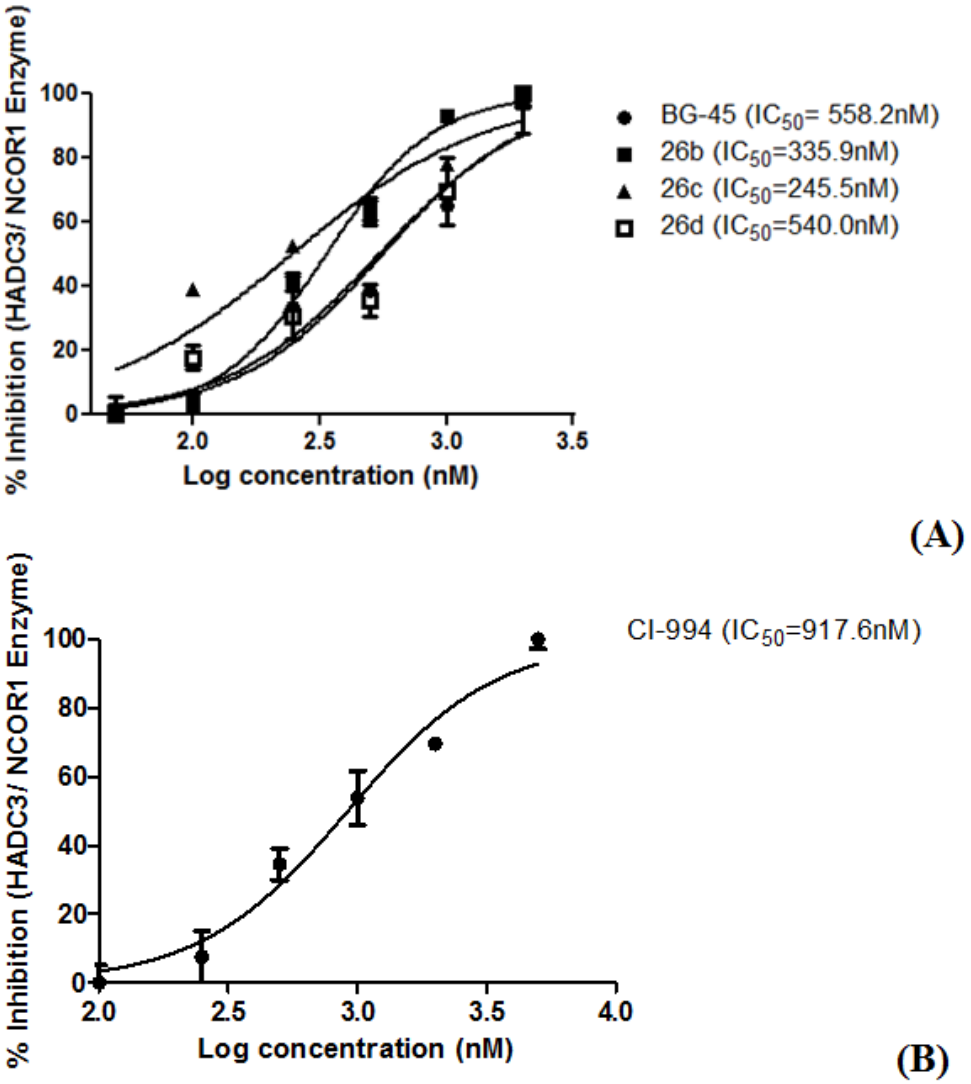

Figure 2.6. IC_{50} determination of HDAC3 enzyme inhibition using recombinant HDAC3/NCOR1 complex for compound **26b, 26c** and **26d** and **BG-45** [A] and **CI-994** [B]. The data represents mean± SD (n=2).

Table 2.1. HDAC inhibitory data of target compounds

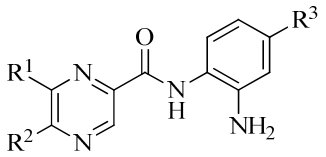

Cpd[a]	R^1	R^2	R^3	% inhibition in HeLa nuclear extract (at 5 µM)	% inhibition in HDAC3 assay (at 1 µM)
12a	H	$CONHCH_3$	H	59.6	43.54
12b	H	$CONHCH_3$	F	64.1	39.04
12c	H	NHCOPh	H	57.1	44.70
12d	H	NHCOPh	F	57.6	28.60
18a	$CONHCH_3$	H	H	48.6	29.27
18b	$CONHCH_3$	H	F	50.4	38.70
22a	H	Ph	H	35.47	32.11
22b	H	Ph	F	29.27	22.24
26a	H	NHPh	H	63.9	40.24
26b	H	NHPh	F	71.5	67.48
26c	H	NHBnz	H	65.6	62.24
26d	H	NHBnz	F	65.0	59.04
CI-994	--	--	--	53.8	53.65
BG45	H	H	H	55.4	57.97

[a] Compound number

Table 2.2. IC_{50} values of promising compounds and their selectivity profile

Cpd[a]	**IC_{50} (µM)**		**Selectivity for HDAC3 (Pan HDAC/HDAC3)**
	HeLa nuclear extract (Pan HDAC inhibition)	**HDAC3**	
26b	1.972	0.335	5.87
26c	2.869	0.245	11.68
26d	3.072	0.540	5.68
CI-994	5.369	0.917	5.85
BG45	5.506	0.558	9.87

[a] Compound number

2.2.5. Antiproliferative assay using cancer cell lines

Cytotoxicity studies were performed on two different cell lines, i.e., B16F10 (murine melanoma cell line) and HeLa (Human cervical cancer cell line) by MTT assay method. All the synthesized compounds were evaluated at two different concentrations (100 µM and 10 µM) in triplicate. **CI-994** and **BG45** were taken as the standard reference

compounds in the assay (**Figure 2.7).** From the assay results, it was observed that majority of the compounds displayed good cytotoxicity on both the cell lines. Compounds **12a, 22a, 26a**, **26c** and **26d** were found to be more promising and these were further subjected to evaluate for their 50% inhibitory concentration (IC_{50}) with a wider of concentrations. The cell viability after 72 hours of treatment was measured by MTT assay (**Figure 2.8**). Most of the selected compounds exhibited better cytotoxicity compared to **CI-994** and **BG45**. Interestingly compound **12a** containing the molecular structural information of both **BG45** and **CI-994** exhibited similar efficacy compared to **CI-994** but more efficacious than **BG45** in both the B16F10 and HeLa cell lines (**Figure 2.8**). Compound **26c** (IC_{50} of 5.33 µM in B16F10 cells and 3.99 µM in HeLa cells) and compound **26d** (IC_{50} of 6.00 µM in B16F10 cells and 5.80 µM in HeLa cells) were found to be the most potent among these compounds and therefore, these compounds (compounds **26c** and **26d**) were further carried over for other biological assays.

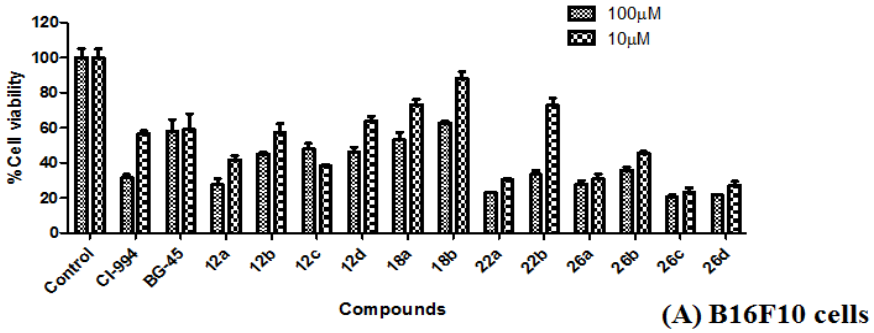

(A) B16F10 cells

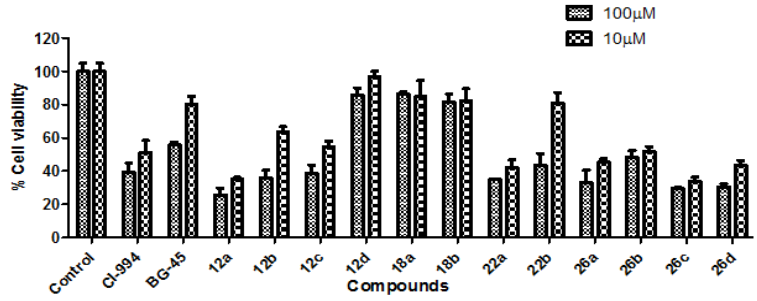

(B) HeLa cells

Figure 2.7. (A) Anticancer activity of novel benzamide derivatives along with CI-994 and BG-45 on B16F10 cells. All compounds were screened at two concentrations 100 μM and 10μM for 72 hours. Cell viability was measured by using *in vitro* MTT assay method. Data represents mean ± SD (n=3). (B) Anticancer activity of novel synthesized compounds, BG-45 and CI-994 on HeLa cells using same procedure as described above.

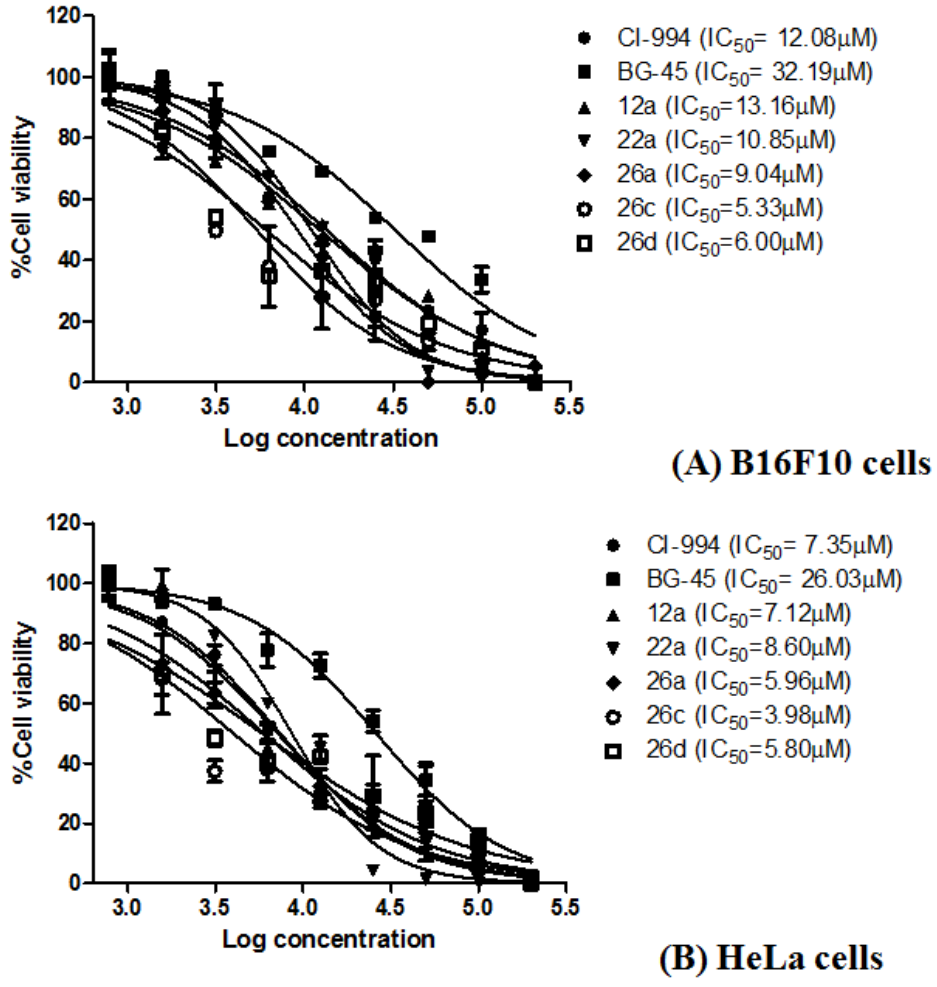

Figure 2.8. Dose response curve and IC_{50} values of promising compounds **12a**, **22a**, **26a**, **26c** and **26d** along with **BG-45** and **CI-994**. All compounds were explored in larger range of nine different concentrations on B16F10 (A) and HeLa (B) cells. Cells were treated with compounds for 72 hours and cell viability was measured by *in vitro* MTT assay method. Data represents mean ± SD (n=2) and plotted in dose response

format. IC_{50} was calculated using nonlinear regression analysis method using Graph Pad Prism5.

2.2.6. Structure activity relationship (SAR) of the synthesized molecules

Some interesting relationship between the structures of the synthesized molecules and their biological activity came out from the study. Incorporating fluoro substitution at the *para* position of the benzamide moiety at compound **12a** resulted in lower Hela nuclear extract inhibition than compound **12b**. However, compound **12b** showed slightly lower HDAC3 inhibition (39.04%) compared to compound **12a** (43.54%). Again, the corresponding methyl carboxamide substitution at R^1 position instead of R^2 position led to a decreased Hela nuclear extract inhibition that strongly suggested that R^2 substituents (such as $CONHCH_3$) were not preferable than the corresponding R^1 substituents (compound **12a** *vs* compound **18a**; compound **12b** *vs* compound **18b**) as far as the HeLa nuclear extract inhibition was concerned. However, $CONHCH_3$ substitution at R^2 position yielded better HDAC3 inhibitors (compound **12a** *vs* compound **18a**; compound **12b** *vs* compound **18b**). Hence, further structural modification was performed at R^2 position to judge the activity trend. Incorporation of phenyl group at the terminal end of amino carbonyl moiety did not improve HeLa nuclear extract inhibition rather showed decrease activity (compound **12a** *vs* compound **12c**; compound **12b** *vs* compound **12d**). However, these compounds also displayed lower (compound **12b** *vs* compound **12d**) or comparable (compound **12a** *vs* compound **12c)** HDAC3 inhibitory activity. Therefore, the carbonyl function has been withdrawn from the next design. Incorporation of bulky phenyl ring at R^2 decreased both the HeLa nuclear extract inhibitory and HDAC3 inhibitory properties (compound **22a** *vs* compound **12a**). The structure was further modified with the introduction of aryl amine function at R^2 position which yielded compounds with comparable HDAC3 inhibitory

efficacy (compound **26a** *vs* compound **12a**). However, both higher HeLa nuclear inhibitory and HDAC3 inhibitory activities were observed for the corresponding *p*-fluoro analogs (compound **26b** *vs* compound **12b**). Additionally, incorporation of a methylene spacer between the aryl (phenyl) and amine nitrogen resulted in both comparable HeLa nuclear inhibition and HDAC3 inhibition (compound **26c** and **26d**). Moreover, it was noticed that for both HeLa nuclear inhibitory activity and HDAC3 inhibitory activity, arylamine groups (NHPh and NHBnz) at R^2 position were better effective than the corresponding phenyl groups (compounds **26a**-**26d** vs compounds **22a**-**22b**). Therefore, it may be assumed that not only the steric or hydrophobic effect at R^2 position (phenyl or benzyl) is necessary but also the presence of associated amino function is crucial for imparting higher inhibitory effects. The overall approach of derivatization of **BG-45** and **CI-994** resulted in the identification of compound **26c** with 11.68-fold HDAC3 selectivity over pan-HDAC (**BG-45**; 9.9-fold and **CI-994**; 5.85-fold). In a nutshell, it may be inferred that aminobenzyl or aminophenyl group at R^2 position is better effective than the phenyl, methylcarboxamido (NHCOMe) or methylaminocarbonyl (CONHMe) functions at the same position.

2.2.7. Apoptosis assay

The extent of apoptosis induced by novel molecules (compounds **26c** and **26d**) was determined by using Annexin V FITC/PI dead cell detection kit using B16F10 cells. HDAC inhibitors induce apoptosis which results in cell death by altering gene expression (Manal et al. 2016). The percentage apoptosis induced by target compounds **26c** and **26d** was investigated in the experiment along with **CI-994** and **BG45** (**Figure 2.9**).

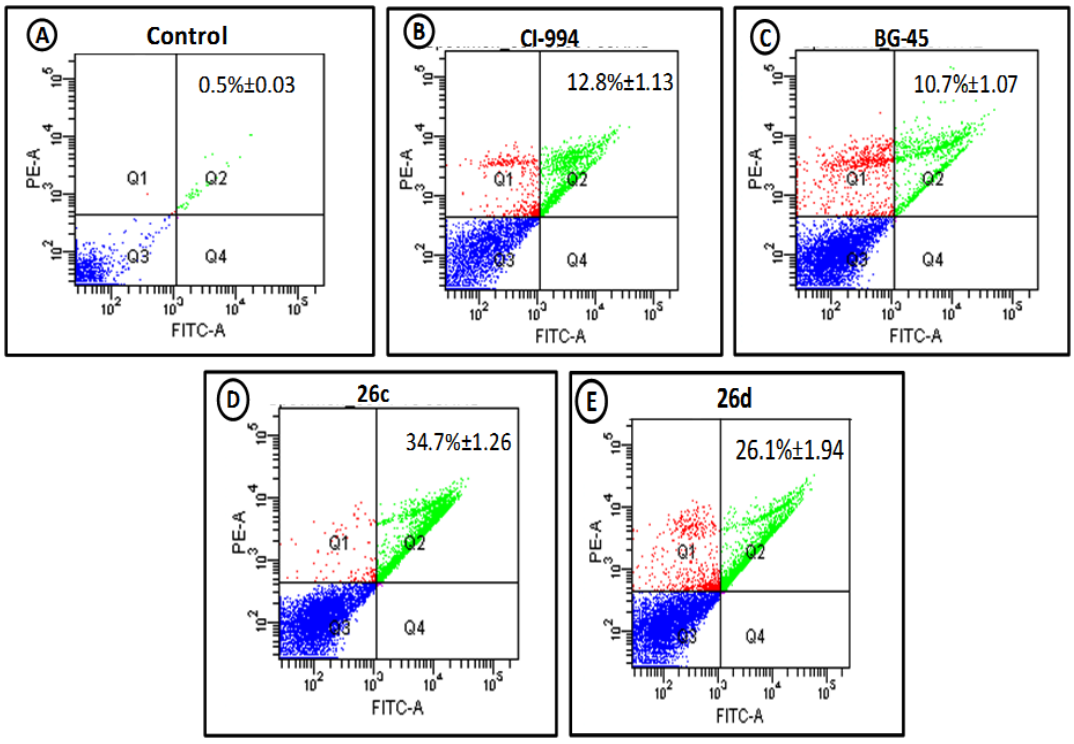

Figure 2.9. Induction of apoptosis in B16F10 cells quantified by Annexin V/PI assay using flow cytometry. (A) **Control** (B) **CI-994** (C) **BG45** (D) **26c** (E) **26d**. [Q2 quadrant depicts late apoptosis and Q4 quadrant shows early apoptosis. X-axis: Annexin-V intensity, Y-axis: propidium iodide intensity.

Results displayed (**Figure 2.9**) that 10.7±1.07% and 12.8±1.07% cells were present in late apoptotic phase (Q2) for **BG45** and **CI-994** respectively. For compound **26d**, 26.1±1.94% cells were present in Q2 quadrant demonstrated more effective while the highest apoptosis was exhibited by compound **26c** showing 34.7±1.26% cells in the late apoptotic phase [Q2]. The experiment proved an enhanced efficacy of the novel synthesized lead derivatives compared to **CI-994** and **BG45**.

2.2.8. Cell cycle analysis

We further investigated the effect of **26c** and **26d** on cell cycle progression in B16F10 cells (**Figure 2.10**). From the result, it was found that compound **26c** and **26d** induced

growth arrest at G2/M phase of cell growth. Compound **26c** induced significant growth arrest around 43.7% in G2/M phase compared to control showing 9.32%, while G0/G1 phase decreased to 11.6% from 74.6%. The similar pattern of growth arrest was found for **26d** and **BG-45** also. While **CI-994** induced cell arrest in G0/G1 phase of cell cycle was 82.3%. These results indicated that compound **26c** might produce anticancer activity with the growth arrests at G2/M phase.

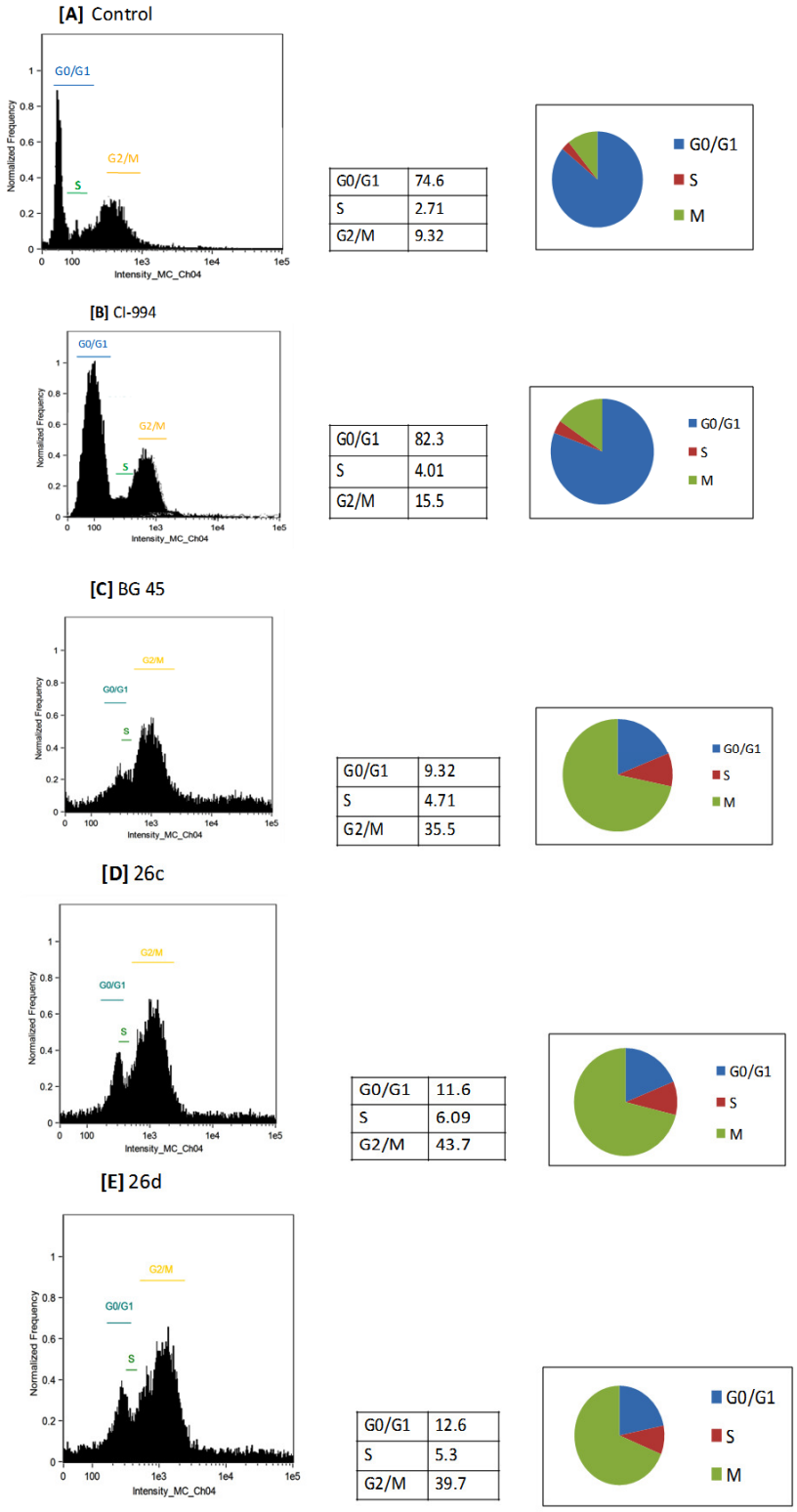

Figure 2.10 Cell cycle arrest induced in B16F10 cells by (A) **control**, (B) **CI-994**, (C) **BG-45**, (D) **26c**, (E) **26d**.

2.3. Experimental

2.3.1. Chemistry

All starting materials and reagents were commercially available and used without further purification. All reactions were monitored by thin layer chromatography (TLC) using precoated plates with silica gel F254 from Merck Millipore Co., USA. ^{1}H and ^{13}C NMR spectrum were recorded in DMSO-d_6 and $CDCl_3$ using Bruker-400 MHz and chemical shifts reported in ppm using tetramethylsilane as internal standard. Mass spectroscopy was performed in LCMS-2020, Schimadzu using ESI mode. The Purity of the compounds were analyzed by Analytical LC/MS. Analysis was performed on a LCMS-8040 equipped with a photodiode array detector using a Shiseido C18 4.6×150 mm, 5µ column at a flow rate of 1 mL/min with isocratic flow (50% A: 50% B for compound **12a, 12b, 18a** and **18b** while for rest of the compounds it was 65%A: 35%B; Solvent A = water, solvent B = methanol).

***tert*-butyl (2-aminophenyl)carbamate (2)**

o-phenylenediamine (5 g, 0.0462 mmol) was dissolved in 20 mL ethanol and triethylamine (7.01 g, 0.0693 mmol) was added. The mixture was stirred in ice bath for 20 minutes. Di-*tert*-butyl dicarbonate (10.09 g, 0.04623 mmol) was mixed with 10 mL of ethanol and added slowly to stirring reaction mixture and stirred for 5 hours at ambient temperature. The solvent was evaporated and the residue was fractioned between ethyl acetate and water. The ethyl acetate layer was evaporated and crude mixture was purified using column chromatography (EtOAc:Hexane;1:9) to give 6.5 g (yield 67.7 %) of **2** as white solid. ^{1}H NMR (400 MHz, DMSO-d_6) δ 8.29 (s, 1H), 7.17 (d, *J* = 7.6 Hz, 1H), 6.83 (t, *J* = 7.6 Hz, 1H), 6.67 (dd, *J*= 7.9, 1.3 Hz, 1H), 6.54 – 6.49 (m, 1H), 4.82 (s, 2H), 1.45 (s, 10H). $C_{11}H_{16}N_2O_2$ [M]: 208.26; MS (ESI) *m/z*: $[M+H]^+$: 209.10 $[M-H]^+$: 207.10

Di boc protection of 5-fluoro 2-nitro aniline as compound 4

5-fluoro-2-nitroaniline (**3**) (4 g, 0.0256 mmol) was dissolved in 2-methyl THF (40 mL) and 4-dimethyl amino pyridine (62 mg, 0.0005 mmol) was added. The reaction mixture was cooled at 0°C, di-tert-butyl dicarbonate (11.18 g, 0.05124 mmol) was added drop wise and stirred at room temperature for 12 hours. Solvent was evaporated and crude was fractioned between water and EtOAc, dried over Na_2SO_4 and concentrated. The crude mixture was purified using column chromatography (EtOAc: Hexane; 0.1:9.9) to yield intermediate **4** as yellow solid 5.2 g (yield 69%).^{1}H NMR (400 MHz, $CDCl_3$) δ 8.15 (dd, *J* = 9.1, 5.5 Hz, 1H), 7.24 – 7.15 (m, 1H), 7.06 (dd, *J* = 8.3, 2.6 Hz, 1H), 1.42 (s, 18H). $C_{16}H_{21}FN_2O_6$ [M]: 356.35; MS (ESI) *m/z*: $[M+Na]^+$: 379.10

***tert*-butyl (5-fluro-2-nitrophenyl) carbamate (5)**

Compound **4** (5 g, 0.0104 mmol) was dissolved in 50 mL of DCM and cooled in an ice bath. Trifluoroacetic acid (1.5mL) was added and stirred for 2 hours. Dichloromethane was evaporated and the mixture was neutralized with sodium bicarbonate solution. Product was extracted in ethyl acetate. Organic layer was concentrated to yield 3.47 g of compound **5** as yellow solid (yield 96.6%). ^{1}H NMR (400 MHz, $CDCl_3$) δ 9.89 (s, 1H), 8.40 (dd, *J* = 11.6, 2.6 Hz, 1H), 8.26 (dd, *J* = 9.4, 5.9 Hz, 1H), 6.78 (m, 1H), 1.55 (s, 9H). $C_{11}H_{13}FN_2O_4$ [M]: 256.23; MS (ESI) *m/z*: $[M-H]^+$: 255.10

***tert*-butyl (2-amino-5-fluorophenyl)carbamate (6)**

Compound **5** (3.4 g, 0.0132 mmol) was mixed with 40 mL methanol and a catalytic amount of 10% Pd/C was added. Hydrogen gas was supplied through hydrogen balloon and the reaction was stirred for 4 hours. The reaction mixture was filtered through the bed of celite® and filtrate was evaporated to get 2.9 g of compound **6** as brown solid. (yield 96.6%). ^{1}H NMR (400 MHz, DMSO-d_6) δ 8.42 (s, 1H), 7.20 (d, *J* = 10.9 Hz,

1H), 6.66 (dd, *J* = 6.9, 1.5 Hz, 2H), 4.78 (s, 2H), 1.47 (s, 10H). $C_{11}H_{15}FN_2O_2$ [M]: 226.25; MS (ESI) *m/z*:: $[M-H]^+$:225.10

methyl 5-aminopyrazine-2-carboxylate (8)

Methyl 5-(chloropyrazine)-2-carboxylate (**7**) (2 g, 0.0115 mmol) was dissolved in 80 mL of DMSO. Sodium azide (3 g, 0.0463 mmol) and triphenylphosphene (4.6 g, 0.1738 mmol) were added and the mixture was refluxed at 120°C for 4 hours. 20 mL of 1N HCl was added and the reaction was continued at 120°C for 2 hours. The mixture was cooled and neutralized by aqueous $NaHCO_3$ solution and product was extracted in ethyl acetate, dried using Na_2SO_4. The ethyl acetate fraction was evaporated and washed with n-pentane to get 0.7 g (yield 39.5%) yellow solid of compound **8**.^{1}H NMR (400 MHz, DMSO-d_6) δ 8.53 (d, *J* = 1.2 Hz, 1H), 7.91 (d, *J* = 1.2 Hz, 1H), 7.39 (s, 2H), 3.79 (s, 3H). $C_6H_7N_3O_2$ [M]: 153.14; MS (ESI) *m/z*: $[M-H]^+$: 152.05

methyl 5-acetamidopyrazine-2-carboxylate (9a)

Methyl 5-aminopyrazine-2-carboxylate (**8**) (0.650 g, 4.2483 mmol) was reacted with excess of acetic anhydride (5mL) and heated at 90°C for 2 hours. The reaction mixture was evaporated and partitioned between saturated $NaHCO_3$ solution and ethyl acetate. Organic layer was evaporated to get 0.345 g of compound **9a** as pale yellow solid (yield 41.6%). ^{1}H NMR (400 MHz, DMSO-d_6) δ 11.29 (s, 1H), 9.41 (d, *J* = 1.4 Hz, 1H), 8.96 (d, *J* = 1.4 Hz, 1H), 2.18 (s, 3H), 1.81 (s, 3H). $C_8H_9N_3O_3$ [M]: 195.18; MS (ESI) *m/z*: $[M+H]^+$: 196.05 $[M-H]^+$, 194.05

methyl 5-benzamidopyrazine-2-carboxylate (9b)

Methyl 5-aminopyrazine-2-carboxylate (**8**) (0.250 g, 1.6339 mmol) was dissolved in 5 mL of DMF. Sodium hydride (0.118 g, 4.9017 mmol) was added to above mixture and stirred in ice bath for 30 minutes. Benzoyl chloride (0.230 g, 1.6339 mmol) was added

and stirred for 12 hours. Reaction mixture was poured in a beaker containing ice and slowly aqueous ammonium chloride solution was added. Product was extracted in ethyl acetate and evaporated ethyl acetate fraction was purified by column chromatography (EtOAc:Hexane; 3:7) to get 0.3 g of compound **9b** as white fluffy solid (yield 70.62%).^{1}H NMR (400 MHz, DMSO-d_6) δ 11.60 (s, 1H), 9.55 (d, *J* = 1.4 Hz, 1H), 9.05 (d, *J* = 1.4 Hz, 1H), 8.09 – 8.05 (m, 2H), 7.66 (t, *J* = 7.4 Hz, 1H), 7.56 (t, *J* = 7.6 Hz, 2H), 3.92 (s, 3H). $C_{13}H_{11}N_3O_3$ [M]: 257.24; MS (ESI) *m/z*: $[M+H]^+$: 258.05 $[M-H]^+$, 256.05

Procedure A. Preparation of 5-acetamidopyrazine-2-carboxylic acid (10a)

Compound **9a** (0.334 g, 1.7641 mmol) was added in THF and stirred for 30 minutes. Lithium hydroxide (0.081 g, 3.5282 mmol) was dissolved in water and added to the above mixture and stirred overnight. It was neutralized with dil. HCl and extracted in ethyl acetate, dried and concentrated to get 0.220 g of 1**0a** as white solid (yield 69%) and it was sufficiently pure to use as a starting material for the successive step. ^{1}H NMR (400 MHz, DMSO-d_6) δ 11.19 (s, 1H), 9.40 (s, 1H), 8.94 (s, 1H), 2.18 (s, 3H). $C_7H_7N_3O_3$ [M]: 181.05; MS (ESI) *m/z*: $[M-H]^+$: 180.05

5-benzamidopyrazine-2-carboxylic acid (10b)

This compound was also prepared by following method A form compound **9b** (0.3 g, 1.1673 mmol) to obtain 0.183 g of pale yellow solid (yield 64.5%). ^{1}H NMR (400 MHz, DMSO-d_6) δ 13.53 (s, 1H), 11.55 (s, 1H), 9.54 (d, *J* = 1.4 Hz, 1H), 9.03 (d, *J* = 1.4 Hz, 1H), 8.10 – 8.05 (m, 2H), 7.68 – 7.63 (m, 1H), 7.56 (t, *J* = 7.6 Hz, 2H). $C_{12}H_9N_3O_3$ [M]: 243.22; MS (ESI) *m/z*: $[M-H]^+$: 242.05

Procedure B. Preparation of *tert*-butyl (2-(5-acetamidopyrazine-2-carboxamido) phenyl) carbamate (11a)

Compound **10a** (0.2 g, 1.0256 mmol) was dissolved in a mixture of DCM: Pyridine (1:1). 1-(3-Dimethylaminopropyl)-3-ethylcarbodiimide hydrochloride (0.294 g, 1.5384 mmol) and catalytic amount of 4-(dimethylamino) pyridine (DMAP) were added to the reaction mixture. *tert*-butyl (2-aminophenyl) carbamate (**2**) (0.234 g, 1.1281 mmol) was added and reaction was flushed with nitrogen gas. The reaction mixture was stirred for 12 hours at room temperature to complete reaction. The solvent was evaporated and product was fractioned between ethyl acetate and saturated solution of sodium bicarbonate. The crude product was purified by column chromatography (EtOAc: Hexane; 2.5:7.5), afforded 0.150 g of compound **11a** as a cream powder (yield 37%). ^{1}H NMR (400 MHz, DMSO-d_6) δ 11.26 (s, 1H), 10.27 (s, 1H), 9.35 (d, *J* = 1.0 Hz, 1H), 9.04 (d, *J* = 1.2 Hz, 1H), 7.93 (d, *J* = 8.6 Hz, 1H), 7.30 – 7.15 (m, 4H), 2.19 (s, 3H), 1.50 (s, 9H). $C_{18}H_{21}N_5O_4$ [M]: 371.39; MS (ESI) *m/z*: $[M+H]^+$: 372.10 $[M-H]^+$, 370.15

***tert*-butyl(2-(5-acetamidopyrazine-2-carboxamido)-5-fluorophenyl)carbamate (11b)**

Following procedure B, compound **11b** was synthesized from **10a** (0.150 g, 0.8333 mmol) and compound **6** (0.189 g, 0.8333 mmol) as pale pink powder (0.070 g, yield 22%). ^{1}H NMR (400 MHz, DMSO-d_6) δ 11.25 (s, 1H), 10.25 (s, 1H), 9.37 (d, *J* = 1.4 Hz, 1H), 9.22 (s, 1H), 9.02 (d, *J* = 1.4 Hz, 1H), 7.77 (dd, *J* = 9.0, 6.1 Hz, 1H), 7.27 (dd, *J* = 10.4, 2.9 Hz, 1H), 7.10 – 7.05 (m, 1H), 2.19 (s, 3H), 1.49 (s, 9H). $C_{18}H_{20}FN_5O_4$ [M]: 389.38; MS (ESI) *m/z*: $[M+H]^+$: 390.15 $[M-H]^+$, 388.20

***tert*-butyl(2-(5-benzamidopyrazine-2-carboxamido)phenyl) carbamate (11c)**

This compound was prepared from **10b** (0.175 g, 0.7242 mmol) and intermediate **2** (0.150 g, 0.7242 mmol) using described procedure B yielded 0.070 g of off white solid (yield 22.4%). ^{1}H NMR (400 MHz, DMSO-d_6) δ 11.61 (s, 1H), 10.33 (s, 1H), 9.49 (d, *J* = 1.4 Hz, 1H), 9.20 (s, 1H), 9.13 (d, *J* = 1.4 Hz, 1H), 8.11 – 8.08 (m, 2H), 7.95 (dd, *J* = 8.0, 1.4 Hz, 1H), 7.68 – 7.63 (m, 1H), 7.59 – 7.54 (m, 2H), 7.32 – 7.24 (m, 2H), 7.19(td, *J* = 7.6, 1.6 Hz, 1H), 1.52 (s, 9H). $C_{23}H_{23}N_5O_4$ [M]: 433.46; MS (ESI) *m/z*: $[M+H]^+$: 434.20 $[M-H]^+$, 432.15

***tert*-butyl(2-(5-benzamidopyrazine-2-carboxamido)-5-fluorophenyl)carbamate (11d)**

Compound **10b** (0.175 g, 0.7242 mmol) and compound **6** (0.164 g, 0.7242 mmol) were mixed and reacted in presence of other reagents as described in procedure B which afforded 0.077 g of pale pink powder (23.7%). ^{1}H NMR (400 MHz, DMSO-d_6) δ 11.61 (s, 1H), 10.31 (s, 1H), 9.51 (d, *J* = 1.4 Hz, 1H), 9.24 (s, 1H), 9.11 (d, *J* = 1.4 Hz, 1H), 8.11 – 8.08 (m, 2H), 7.79 (dd, *J* = 9.0, 6.1 Hz, 1H), 7.66 (t, *J* = 7.4 Hz, 1H), 7.56 (t, *J* = 7.6 Hz, 2H), 7.29 (dd, *J* = 10.4, 2.9 Hz, 1H), 7.09 (td, *J* = 8.5, 3.0 Hz, 1H), 1.51 (s, 9H). $C_{23}H_{22}FN_5O_4$ [M]: 451.45; MS (ESI) *m/z*: $[M+H]^+$: 452.20 $[M-H]^+$: 450.20

Procedure C. Preparation of 5-acetamido-*N*-(2-aminophenyl)pyrazine-2-carboxamide hydrochloride (12a)

Compound **11a** (0.1 g, 0.3688 mmol) was dissolved in 1 mL of DCM. The mixture was stirred in an ice bath for 15 minutes. 3 mL of 4M dioxane in HCl solution was added and stirred for 90 minutes. The reaction mixture was evaporated to dryness. The sticky mass was washed with n-pentane to get 0.060 g of product **12a** in the form of pale yellow solid (yield 53%).^{1}H NMR (400 MHz, DMSO-d_6) δ 11.30 (s, 1H), 10.72 (s,

1H), 9.44 (d, *J* = 1.2 Hz, 1H), 9.04 (d, *J* = 1.3 Hz, 1H), 7.62 (d, *J* = 7.9 Hz, 2H), 7.55 (d, *J* = 7.7 Hz, 2H), 7.47 – 7.33 (m, 4H), 2.21 (s, 3H).^{13}C NMR (101 MHz, DMSO-d_6) δ 170.08, 162.24, 150.78, 142.55, 139.13, 133.68, 130.74, 127.96, 127.73, 127.27, 126.78, 126.27, 123.90. HPLC Rt: 4.663, this compound was deacetylated in HPLC column and deacetyalated form Rt was 3.070. LC-MS calculated for expected $C_{13}H_{13}N_5O_2$ [M]: 271.27; Found: [M-H]: 270

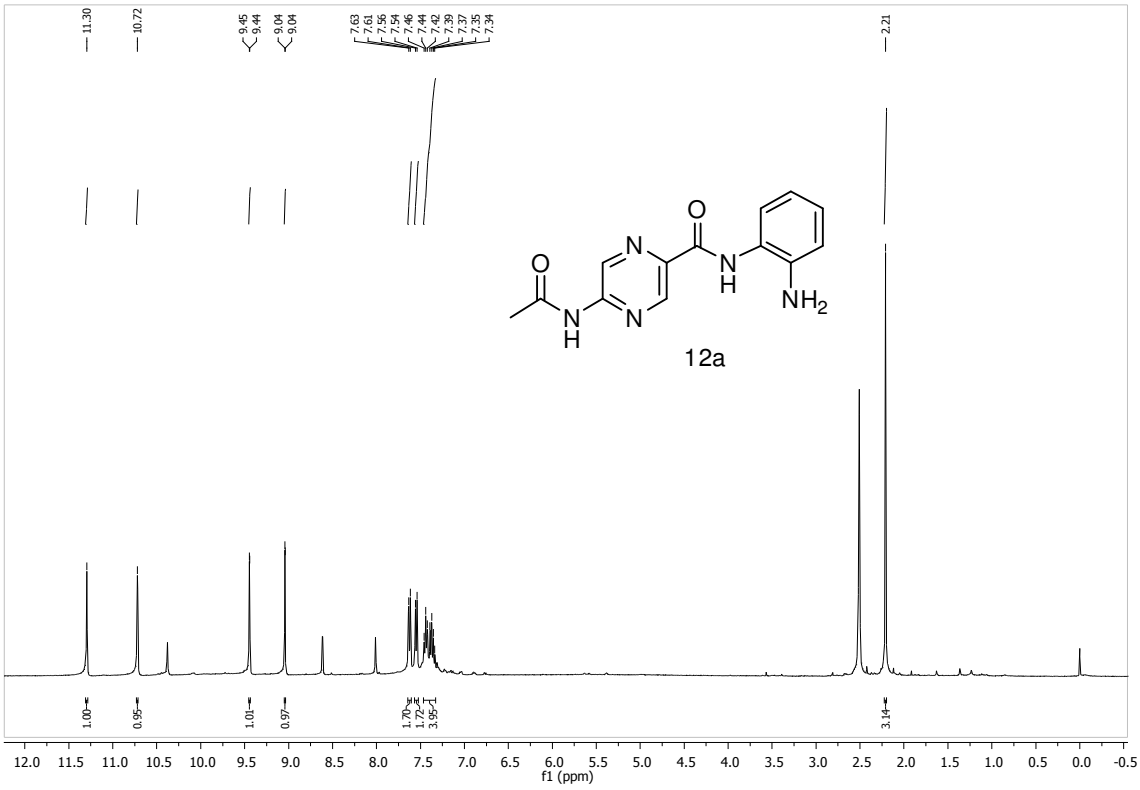

^{1}H NMR of 12a

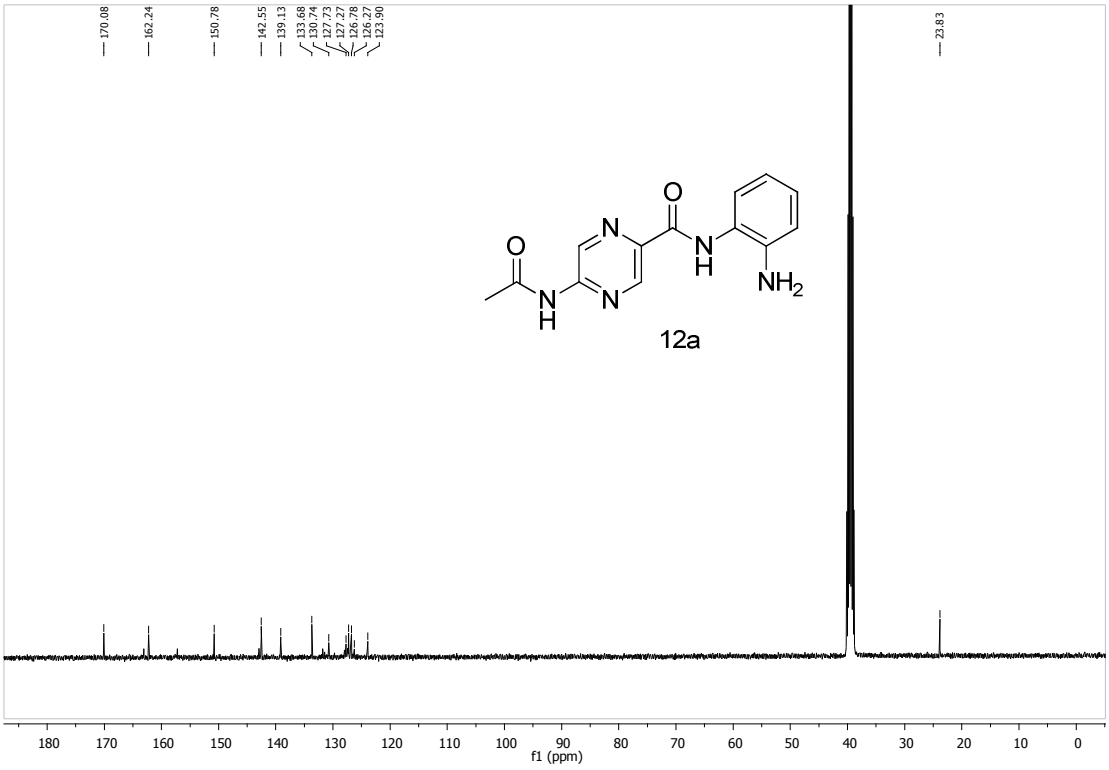

^{13}C NMR of 12a

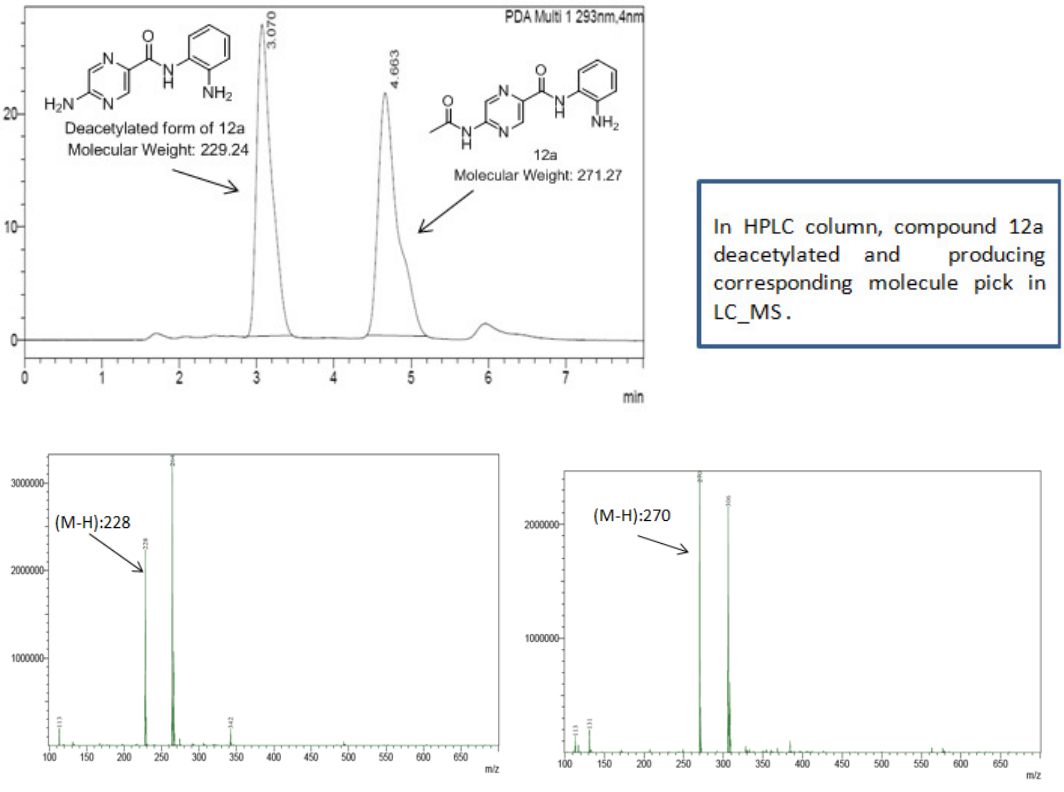

LC/MS of 12a

5-acetamido-*N*-(2-amino-4-fluorophenyl)pyrazine-2-carboxamide hydrochloride (12b)

Following procedure C, Compound **11b** (0.060 g, 0.1542 mmol) was deprotected to get Compound **12b** as beige color powder (yield 0.040 g, 80%). ^{1}H NMR (400 MHz, DMSO-d_6) δ 11.25 (s, 1H), 10.27 (s, 1H), 9.42 (d, *J* = 1.2 Hz, 1H), 9.01 (d, *J* = 1.3 Hz, 1H), 7.43 (dd, *J* = 8.8, 6.0 Hz, 2H), 6.98 (dd, *J* = 10.2, 2.6 Hz, 1H), 6.84 (dd, *J* = 8.5, 2.5 Hz, 1H), 2.20 (s, 3H).^{13}C NMR (101 MHz, DMSO-d_6) δ 170.01, 161.97, 161.41, 159.01, 150.62, 142.36, 139.45, 133.63, 128.46, 128.36, 66.31, 23.80. HPLC Rt: 5.857, this compound was deacetylated in HPLC column and deacetyalated form Rt was 3.676. LC-MS calculated for expected $C_{13}H_{12}FN_5O_2$ [M]: 289.27; Found: $[M-H]^+$: 288

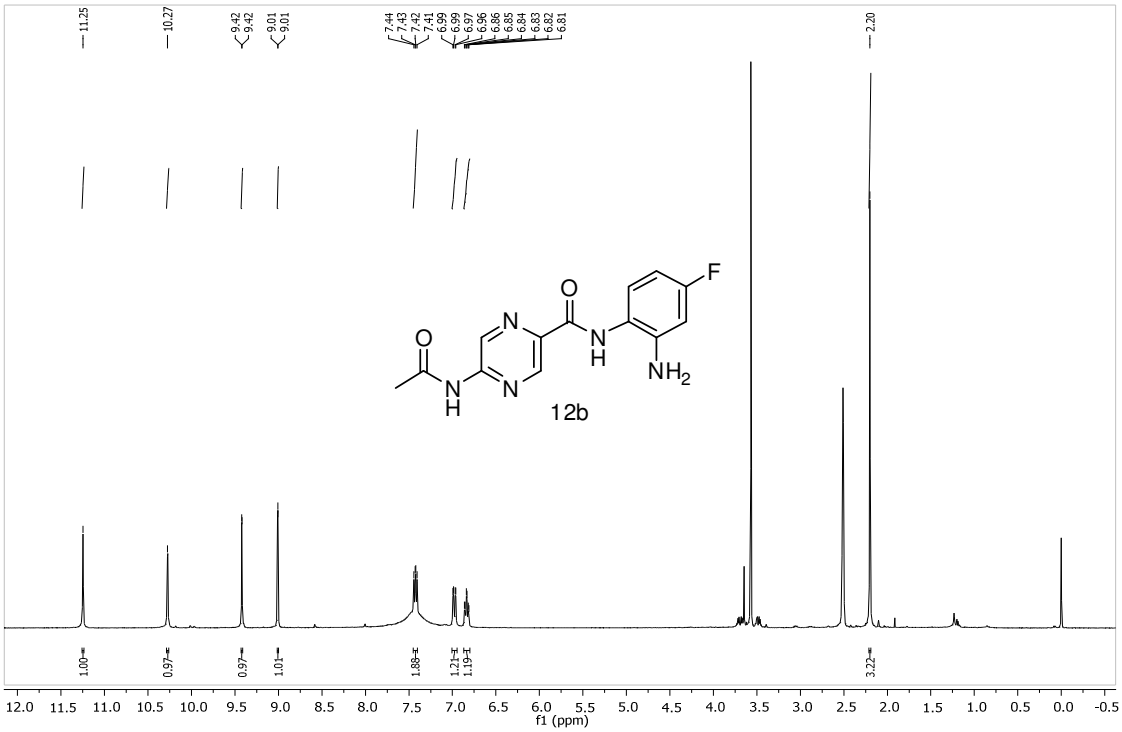

^{1}H NMR of 12b

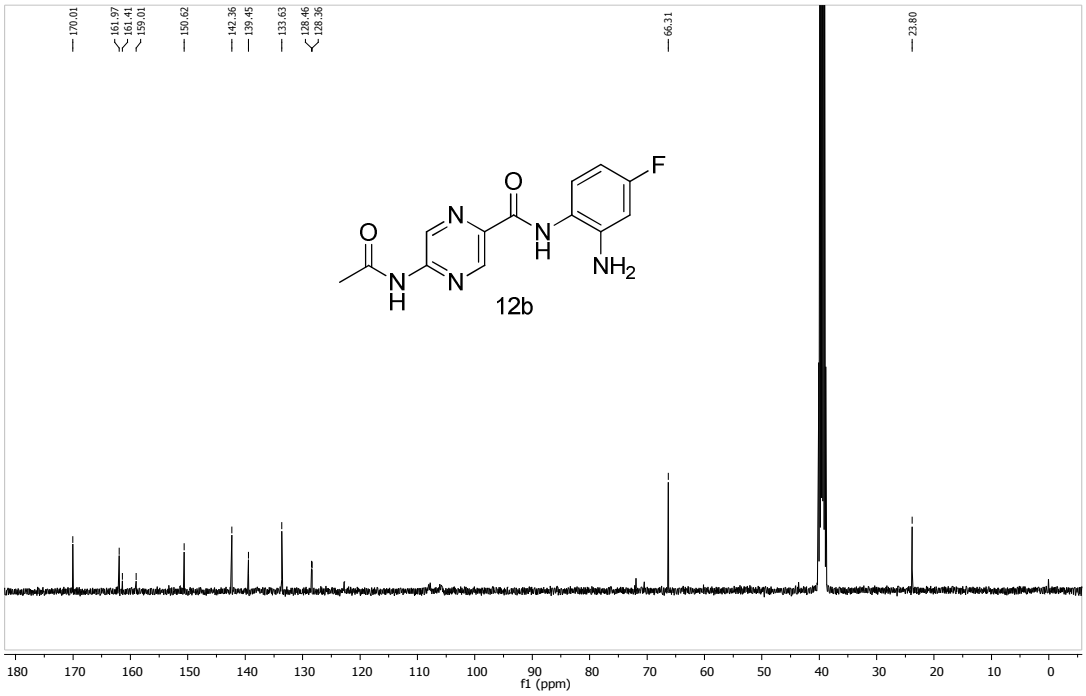

^{13}C NMR of 12b

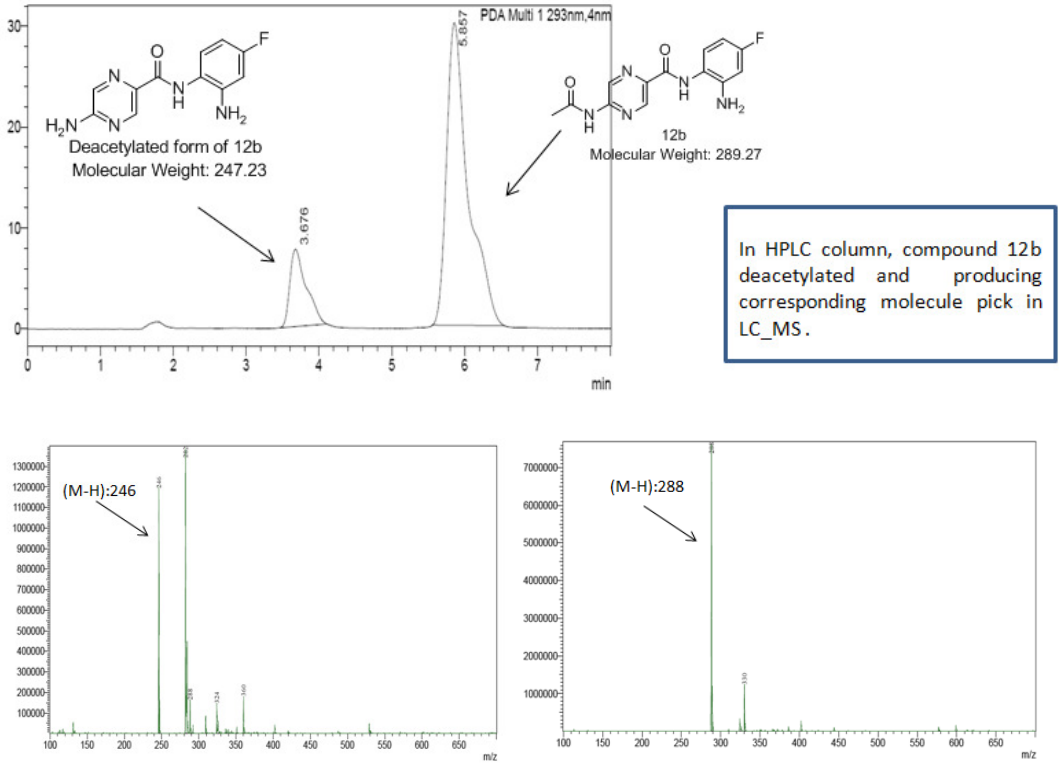

LC/MS of 12b

***N*-(2-aminophenyl)-5-benzamidopyrazine-2-carboxamide hydrochloride (12c)**

This compound was prepared from compound **11c** (0.070 g, 0.1616 mmol) following procedure C to get 0.055 g of product in the form of off white solid (yield 93.2%).[1]H NMR (400 MHz, DMSO-d_6) δ 11.62 (s, 1H), 10.71 (s, 1H), 9.58 (d, *J* = 1.4 Hz, 1H), 9.13 (d, *J* = 1.4 Hz, 1H), 8.13 – 8.08 (m, 2H), 7.69 – 7.54 (m, 5H), 7.47 (dd, *J* = 7.2, 2.0 Hz, 1H), 7.40 – 7.31 (m, 2H).[13]C NMR (101 MHz, DMSO-d_6) δ 166.54, 162.14, 151.21, 142.42, 139.53, 134.93, 132.99, 132.63, 129.93, 128.49, 128.37, 127.10, 126.79, 126.58, 123.12. HPLC Rt: 5.555. LC-MS calculated for expected $C_{18}H_{15}N_5O_2$ [M]: 333.34; Found: $[M-H]^+$: 332

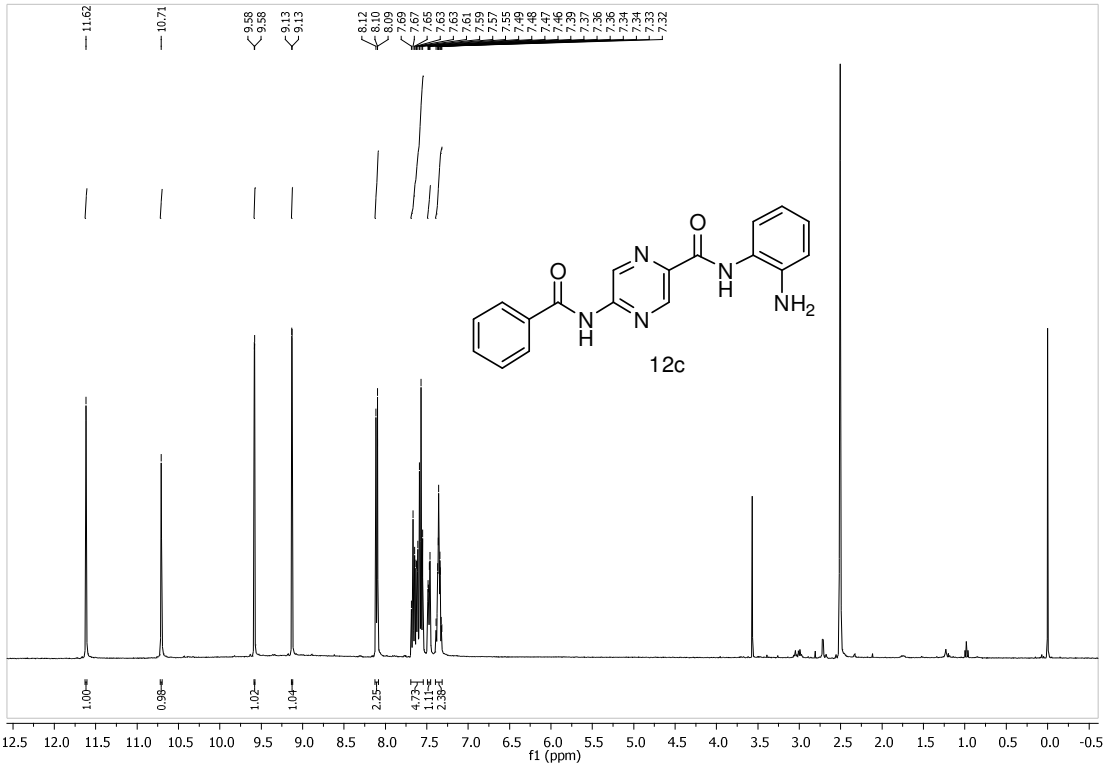

[1]H NMR of 12c

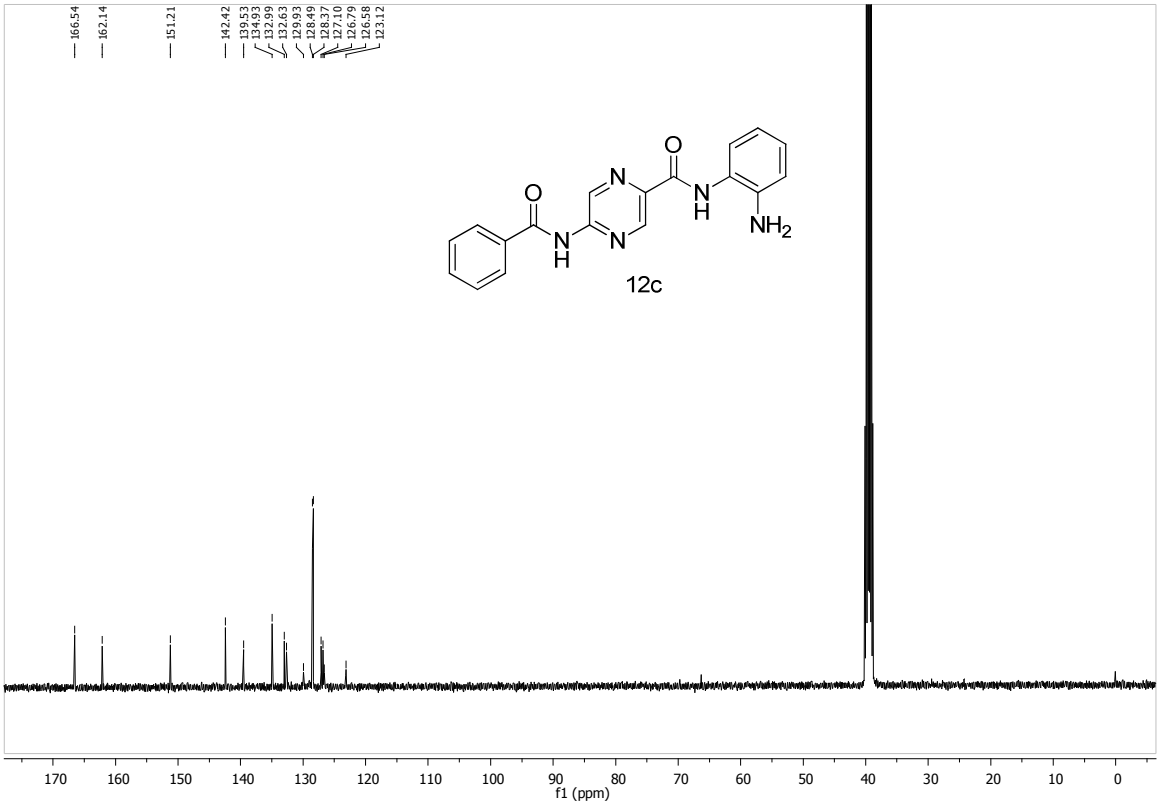

^{13} C of 12c

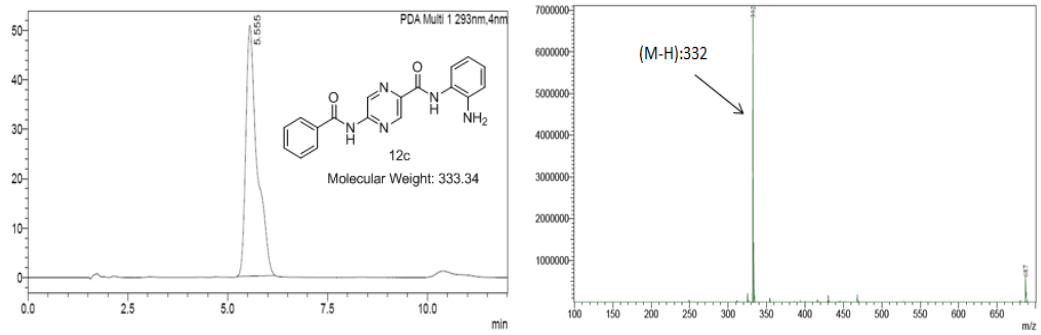

LC/MS of 12c

_N_-(2-amino-4-fluorophenyl)-5-benzamidopyrazine-2-carboxamide hydrochloride (12d)

This compound was prepared from compound **11d** (0.065 g, 0.1441 mmol) following procedure C to get 0.050 g of product in the form of beige color solid (yield 89.5%). ^{1}H NMR (400 MHz, DMSO-d_6) δ 11.58 (s, 1H), 10.31 (s, 1H), 9.56 (d, *J* = 1.3 Hz, 1H), 9.10 (d, *J* = 1.3 Hz, 1H), 8.10 (d, *J* = 7.3 Hz, 2H), 7.69 – 7.39 (m, 5H), 7.10 (s, 2H),

6.94 (dd, *J* = 10.3, 2.5 Hz, 1H), 6.83 – 6.76 (m, 1H). ^{13}C NMR (101 MHz, DMSO-d_6) δ 166.48, 161.95, 161.52, 159.12, 151.03, 142.26, 139.83, 134.88, 133.00, 132.60, 128.48, 128.44, 128.35, 122.31, 66.32. HPLC Rt: 6.387 LC-MS calculated for expected $C_{18}H_{14}FN_5O_2$ [M]: 351.33; Found: $[M-H]^+$: 350

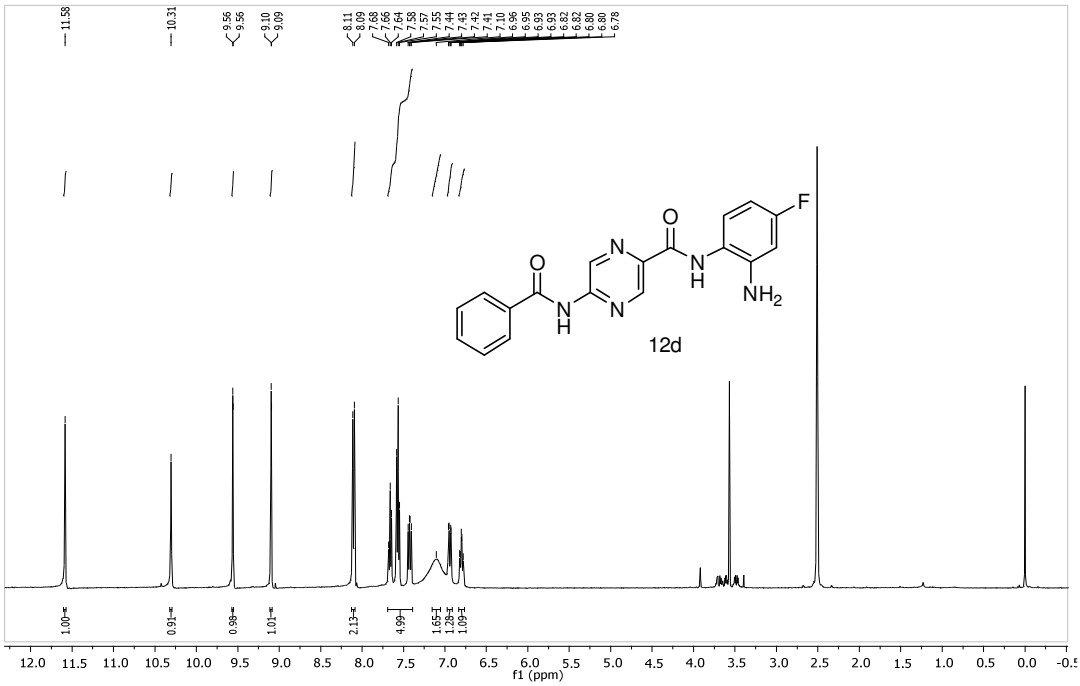

^{1}H NMR of 12d

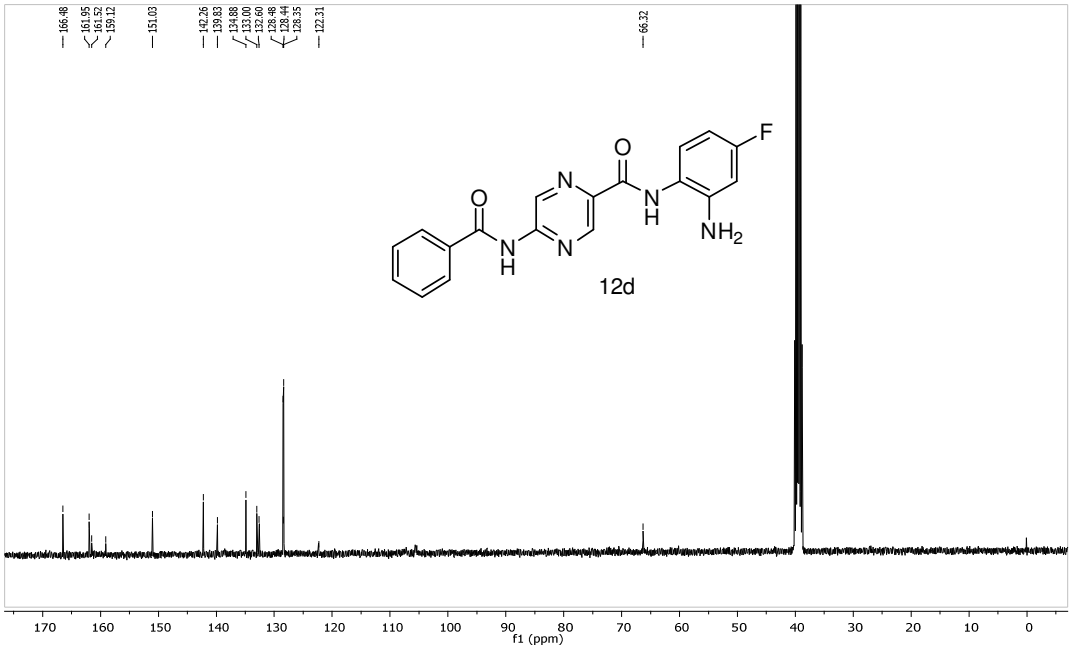

^{13} C of 12d

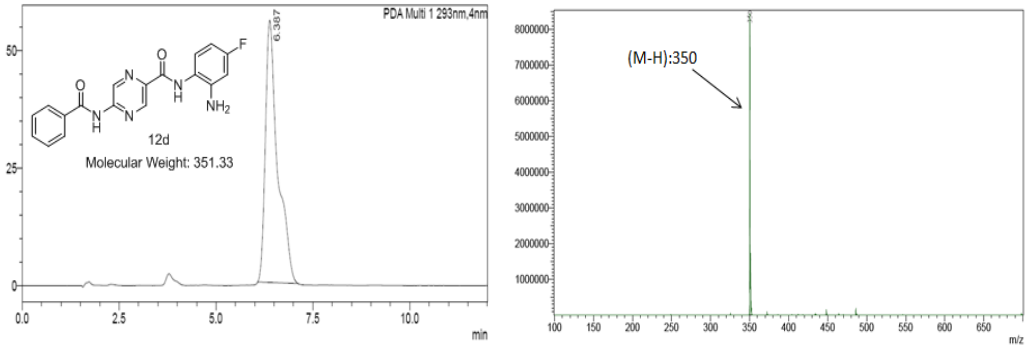

LC/MS of 12d

methyl 6-aminopyrazine-2-carboxylate (14)

Methyl 6-(chloropyrazine)-2-carboxylate (**13**) (2 g, 0.0115 mmol) was dissolved in 80 mL of DMSO. Sodium azide (3 g, 0.0463 mmol) and triphenylphosphene (4.6 g, 0.1738 mmol) were added and refluxed at 120°C for 4 hours. 20 mL of 1N HCl was added and the reaction was continued at 120°C for 2 hours. The mixture was cooled and neutralized by aqueous $NaHCO_3$ solution and product was extracted in ethyl acetate, dried with Na_2SO_4 which was then concentrated and dried with n-pentane to get 1.4 g of compound **14** as yellow solid (yield 82.4%).^{1}H NMR (400 MHz, DMSO-d_6) δ 8.28 – 8.27 (m, 1H), 8.07 (s, 1H), 6.90 (s, 2H), 3.84 (s, 3H). $C_6H_7N_3O_2$ [M]: 153.14; MS (ESI) *m/z*: $[M+H]^+$: 154.05

methyl 6-acetamidopyrazine-2-carboxylate (15)

Compound **14** (1 g, 0.00653 mmol) was heated at 90°C with an excess of acetic anhydride for 5 hours. The reaction mixture was evaporated and washed with $NaHCO_3$ solution. The product was extracted in ethyl acetate and concentrated organic layer was purified by column chromatography (EtOAc: Hexane; 4:6) to get 0.625 g of intermediate **15** as white solid (yield 49.2%). ^{1}H NMR (400 MHz, DMSO-d_6) δ 11.25 (s, 1H), 9.53 (s, 1H), 8.90 (s, 1H), 3.92 (s, 3H), 2.15 (s, 3H). $C_8H_9N_3O_2$ [M]: 195.18; MS (ESI) *m/z*: $[M+H]^+$: 194.05

6-acetamidopyrazine-2-carboxylic acid (16)

Compound **15** (0.626 g, 3.2102 mmol) was dissolved in THF and stirred for 20 minutes at room temperature. Aqueous solution of lithium hydroxide (0.270 g, 6.4205 mmol) was added and stirred for 3 hours. The reaction mixture was neutralized by dilute aqueous solution of HCl and product was extracted in EtOAc. The organic layer was dried and concentrated to get sufficiently pure 0.330 g of compound **16** as white solid (yield 56.8%).^{1}H NMR (400 MHz, DMSO-d_6) δ 11.19 (s, 1H), 9.50 (s, 1H), 8.88 (s, 1H), 2.16 (s, 3H). $C_7H_7N_3O_3$ [M]: 181.15; MS (ESI) *m/z*: $[M+H]^+$: 180.05

***tert*-butyl (2-(6-acetamidopyrazine-2-carboxamido)phenyl)carbamate (17a)**

This compound was synthesized by following procedure B from compound **16** (0.150 g, 0.8287 mmol) and compound **2** (0.190 g, 0.9116 mmol) which yielded 0.143 g of white solid compound **17a** (yield 46.5%). ^{1}H NMR (400 MHz, DMSO-d_6) δ 10.94 (s, 1H), 9.90 (s, 1H), 9.44 (s, 1H), 9.08 (s, 1H), 8.95 (s, 1H), 7.75 – 7.70 (m, 1H), 7.37 (dd, *J* = 6.4, 3.2 Hz, 1H), 7.25 – 7.20 (m, 2H), 2.19 (s, 3H), 1.43 (s, 9H). $C_{18}H_{21}N_5O_4$ [M]: 371.39; MS (ESI) *m/z*: $[M+H]^+$: 372.10 $[M-H]^+$: 370.15

***tert*-butyl(2-(6-acetamidopyrazine-2-carboxamido)-5-fluorophenyl)carbamate (17b)**

Compound **16** (0.160 g, 0.8839 mmol) and compound **6** (0.200 g, 0.8839 mmol) reacted according to procedure B and afforded 0.160 g of product as off white solid (yield 46.5%). ^{1}H NMR (400 MHz, DMSO-d_6) δ 10.95 (s, 1H), 9.83 (s, 1H), 9.45 (s, 1H), 9.16 (s, 1H), 8.93 – 8.92 (m, 1H), 7.60 (dd, *J* = 8.9, 6.1 Hz, 1H), 7.39 (dd, *J* = 10.7, 2.9 Hz, 1H), 7.07 – 7.01 (m, 1H), 2.19 (s, 3H), 1.44 (s, 9H). $C_{18}H_{20}FN_5O_4$ [M]: 389.38; MS (ESI) *m/z*: $[M+H]^+$: 390.15 $[M-H]^+$: 388.20

6-acetamido-*N*-(2-aminophenyl) pyrazine-2-carboxamide hydrochloride (18a)

Compound **17a** (0.130 g, 0.3504 mmol) was deprotected following procedure C to get 0.105 g of one final compound **18a** as white solid (yield 98.13%). ^{1}H NMR (400 MHz, DMSO-d_6) δ 10.98 (s, 1H), 10.57 (s, 1H), 9.49 (s, 1H), 8.98 (s, 1H), 7.69 (d, *J* = 7.3 Hz, 1H), 7.55 (d, J = 7.8 Hz, 1H), 7.42 (dd, *J* = 15.2, 7.0 Hz, 3H), 2.21 (s, 3H).^{13}C NMR (101 MHz, DMSO-d_6) δ 169.71, 162.21, 147.04, 142.25, 138.88, 137.76, 130.48, 127.94, 126.99, 126.89, 126.45, 124.02, 23.68. HPLC Rt: 4.663, this compound was deacetylated in HPLC column and deacetyalated form Rt was 3.070. LC-MS calculated for expected $C_{13}H_{13}N_5O_2$ [M]: 271.27; Found: $[M-H]^+$: 270

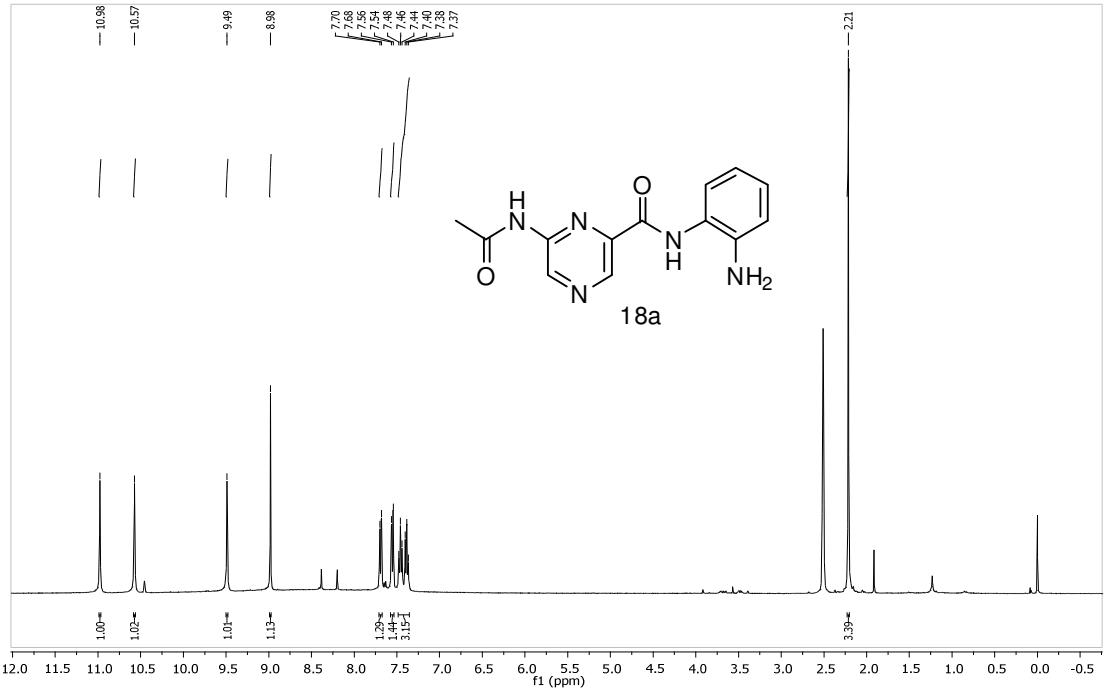

^{1}H NMR of 18a

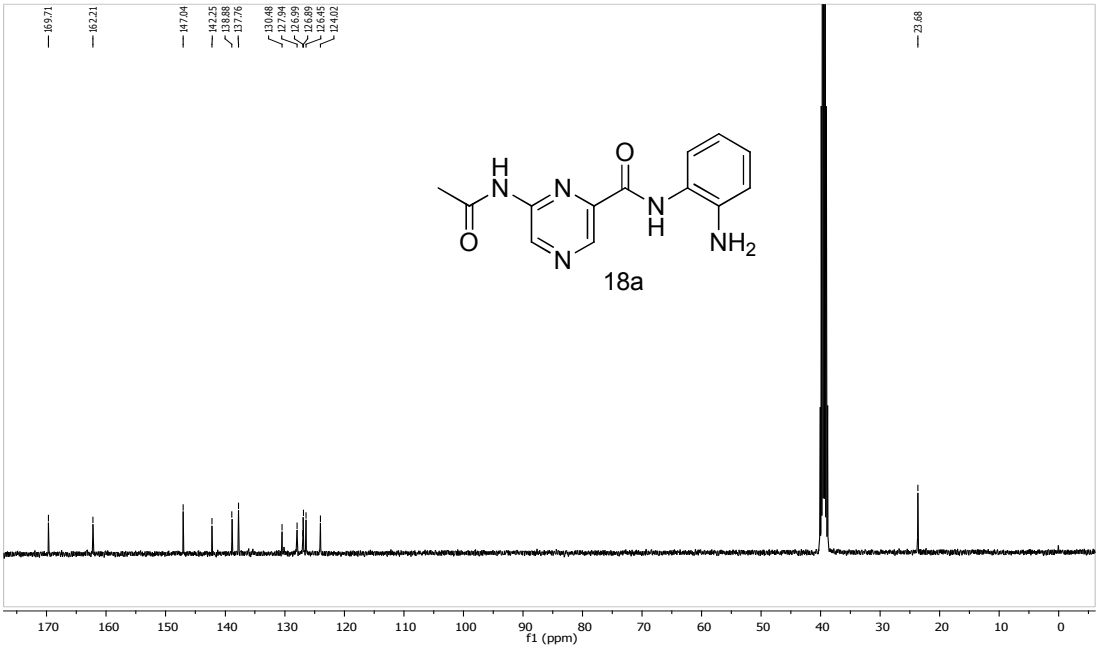

^{13}C NMR of 18a

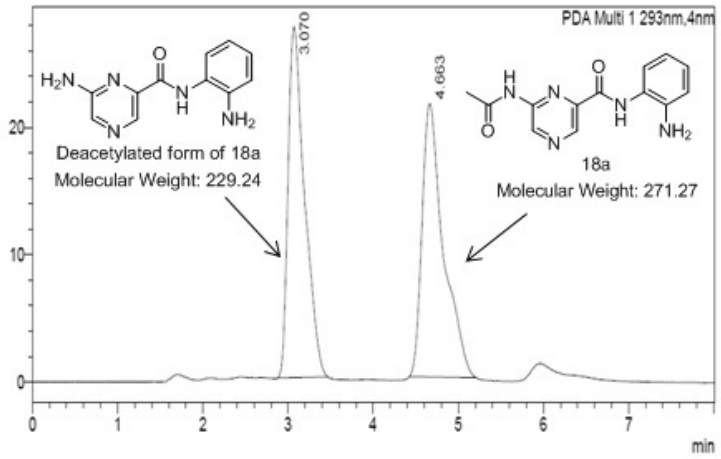

In HPLC column, compound 18a deacetylated and producing corresponding molecule pick in LC_MS.

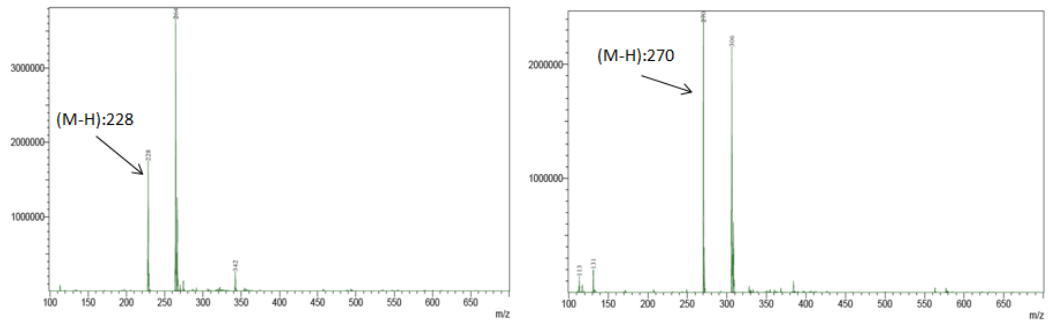

LC/MS of 18a

6-acetamido-*N*-(2-amino-4-fluorophenyl)pyrazine-2-carboxamide hydrochloride (18b)

This compound was prepared by following procedure C from compound **17b** (0.145 g, 0.3727 mmol) to get 0.120 g of another final compound **18b** as off white solid (yield 98.84%). ^{1}H NMR (400 MHz, DMSO-d_6) δ 11.03 (s, 1H), 10.01 (s, 1H), 9.48 (s, 1H), 8.94 (s, 1H), 7.89 (s, 3H), 7.53 (dd, *J* = 8.8, 6.0 Hz, 1H), 7.03 (dd, *J* = 10.1, 2.8 Hz, 1H), 6.88 (dd, *J* = 8.5, 2.7 Hz, 1H), 2.20 (s, 3H). ^{13}C NMR (101 MHz, DMSO-d_6) δ 169.76, 161.98, 161.33, 158.92, 147.04, 142.54, 138.74, 137.65, 127.72, 127.62, 106.44, 106.20, 23.68. HPLC Rt: 5.857, this compound was deacetylated in HPLC column and deacetyalated form Rt was 3.676. LC-MS calculated for expected $C_{13}H_{12}FN_5O_2$ [M]: 289.27; Found:$[M-H]^+$: 288.05

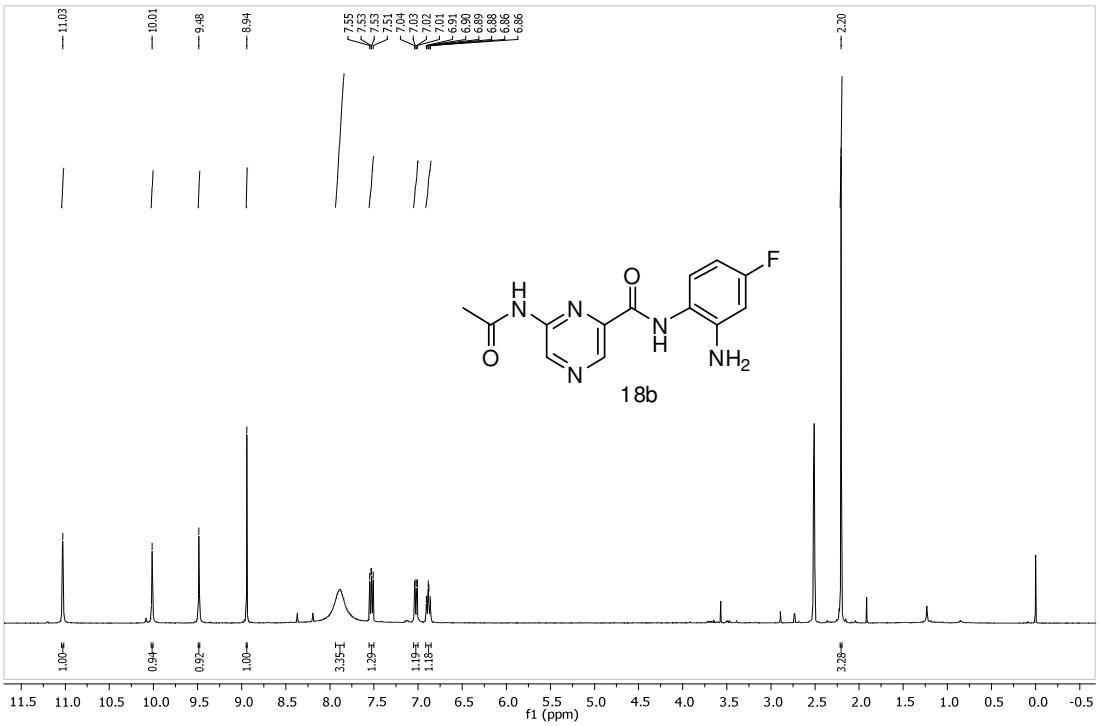

^{1}H NMR of 18b

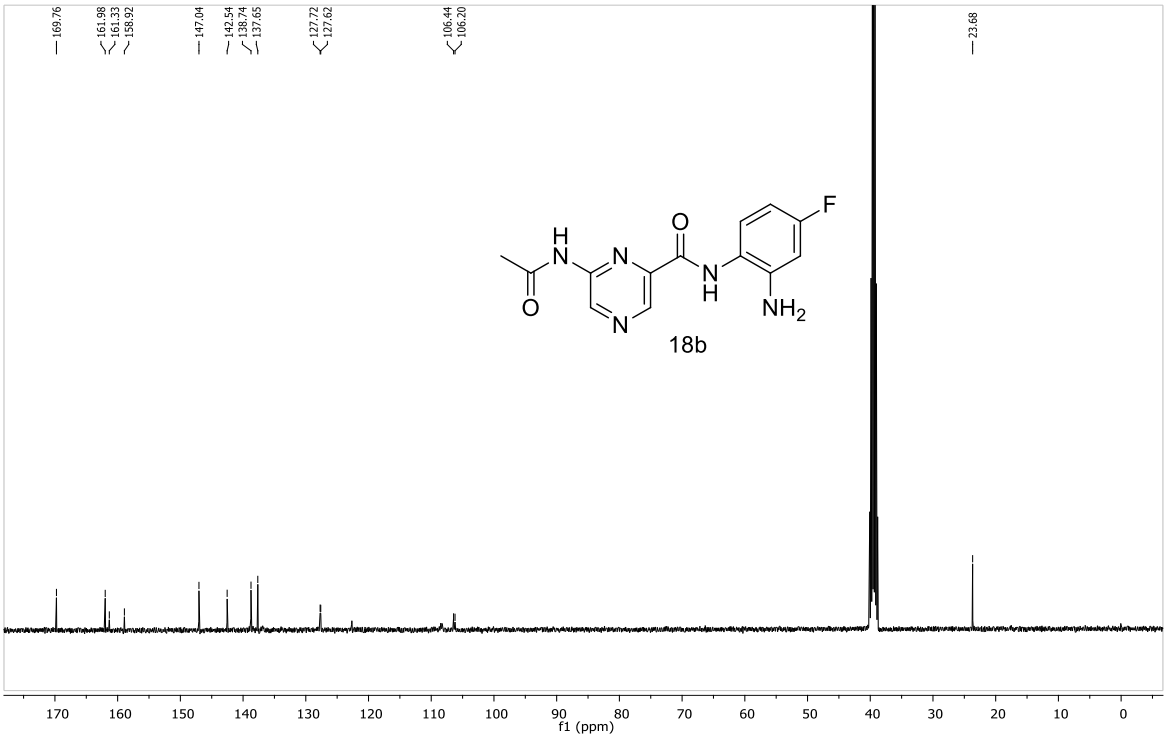

^{13}C NMR of 18b

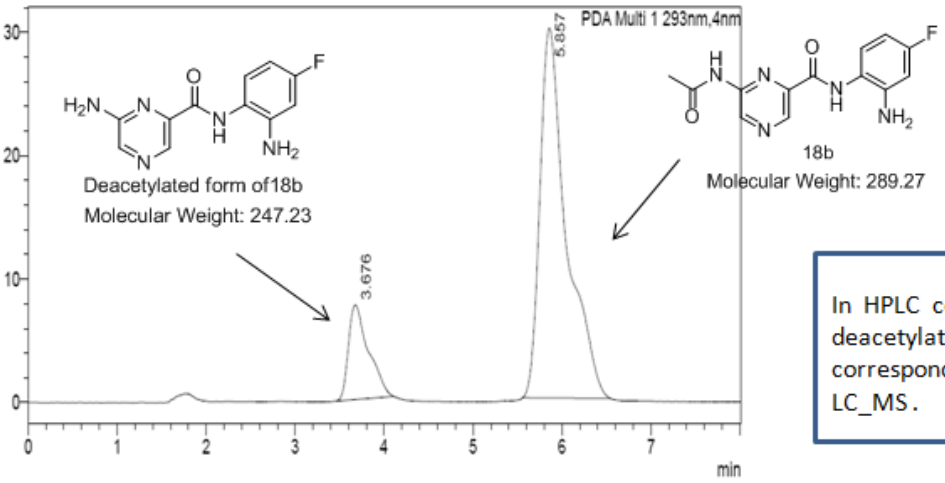

In HPLC column, compound 18b deacetylated and producing corresponding molecule pick in LC_MS.

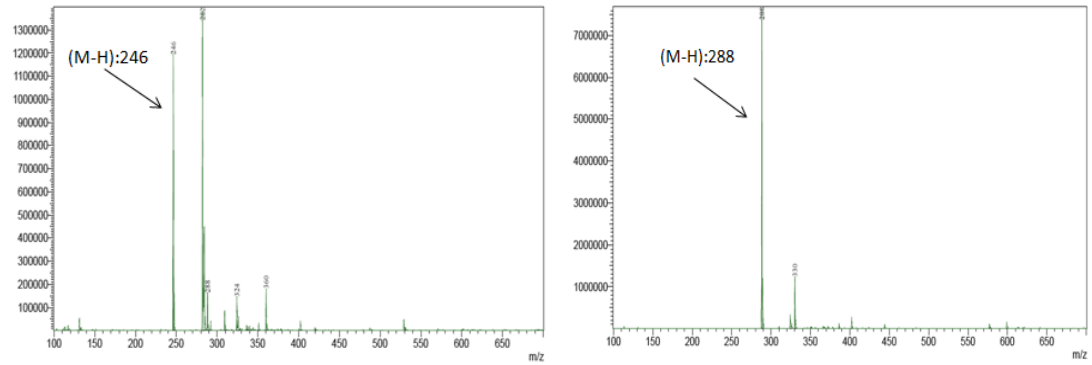

LC/MS of 18b

methyl 5-phenylpyrazine-2-carboxylate (19)

This compound was prepared by following Suzuki coupling mechanism where methyl 5-(chloropyrazine)-2-carboxylate, a commercially available starting material **7** (2 g, 0.0115 mmol) was reacted with phenyl boronic acid (1.4 g, 0.0115 mmol) using bis(triphenylphosphine)palladium(II)dichloride (0.163 g, 0.0002 mmol) as catalyst, potassium carbonate (2.4 g, 0.01737 mmol) as base and 1,4-dioxane as solvent for 12 hour at 100°C. After completion of the reaction, the solvent was evaporated and crude was extracted in ethyl acetate and washed with water. The organic layer was dried over sodium sulphate and crude was purified by column chromatography (hexane: EtOAc; 9:1) to get 1 g of pure white crystalline solid intermediate **19** (yield 40.16%).^{1}H NMR (400 MHz, DMSO-d_6) δ 9.42 (d, *J* = 1.4 Hz, 1H), 9.25 (d, *J* = 1.4 Hz, 1H), 8.27 – 8.23 (m, 2H), 7.62 – 7.57 (m, 3H), 3.95 (s, 3H). $C_{12}H_{12}N_2O_2$ [M]: 214.22; MS (ESI) *m/z*: $[M+H]^+$: 215.10

5-phenylpyrazine-2-carboxylic acid (20)

Intermediate compound **20** (1 g, 0.0046 mmol) was reacted with lithium hydroxide (0.372 g, 0.0093 mmol) according to procedure A to get 0.9 g of white solid compound **20** (yield 96.7%). ^{1}H NMR (400 MHz, DMSO-d_6) δ 13.70 (s, 1H), 9.40 (d, *J* = 1.4 Hz, 1H), 9.24 (d, *J* = 1.4 Hz, 1H), 8.27 – 8.22 (m, 2H), 7.62 – 7.57 (m, 3H). $C_{11}H_8N_2O_2$ [M]: 200.19; MS (ESI) *m/z*: $[M+H]^+$: 201.05, $[M-H]^+$: 199.05

***tert*-butyl (2-(5-phenylpyrazine-2-carboxamido)phenyl)carbamate (21a)**

Compound **20** (0.2 g, 1 mmol) and compound **2** (0.208 g, 1 mmol) were reacted according to procedure B to get cream color solid (0.07g, 17.9%). ^{1}H NMR (400 MHz, DMSO-d_6) δ 10.24 (s, 1H), 9.44 (s, 1H), 9.25 (s, 1H), 8.16 – 8.11 (m, 2H), 7.81 (s, 1H),

7.54 (t, *J* = 12.7 Hz, 4H), 7.00 (t, *J* = 7.6 Hz, 1H), 6.85 – 6.74 (m, 2H), 1.40 (s, 9H). $C_{22}H_{22}N_4O_3$ [M]: 390.17; MS (ESI) *m/z*: $[M-H]^+$: 389.05

***tert*-butyl(5-fluoro-2-(5-phenylpyrazine-2-carboxamido)phenyl)carbamate (21b)**

Compound **20** (0.2 g, 1 mmol) and compound **6** (0.226 g, 1 mmol) were reacted according to procedure B to get compound **21b** as brown color solid (0.06 g, yield 14.7%).^{1}H NMR (400 MHz, DMSO-d_6) δ 10.24 (s, 1H), 9.44 (s, 1H), 9.25 (s, 1H), 8.16 – 8.11 (m, 2H), 7.81 (s, 1H), 7.54 (t, *J* = 12.7 Hz, 4H), 6.85 – 6.74 (m, 2H), 1.40 (s, 9H). $C_{22}H_{21}FN_4O_3$ [M]: 408.43; MS (ESI) *m/z*: $[M-H]^+$: 407.05

***N*-(2-aminophenyl)-5-phenylpyrazine-2-carboxamide hydrochloride (22a)**

Compound **21a** (0.065 g, 0.166 mmol) was deprotected following procedure C to get final compound **22a** (0.054 g, yield 99.1%) as pale pink solid. ^{1}H NMR (400 MHz, DMSO-d_6) δ 10.77 (s, 1H), 9.43 (d, *J* = 1.4 Hz, 1H), 9.35 (d, *J* = 1.4 Hz, 1H), 8.33 – 8.29 (m, 2H), 7.65 – 7.59 (m, 5H), 7.48 (dd, *J* = 6.9, 2.3 Hz, 1H), 7.40 – 7.33 (m, 2H). ^{13}C NMR (101 MHz, DMSO-d_6) δ 162.37, 153.85, 143.44, 142.75, 140.23, 135.01, 130.89, 129.78, 129.20, 127.37, 127.22, 126.94, 126.49, 123.06, 66.32. HPLC Rt: 6.823 LC-MS calculated for expected $C_{17}H_{14}N_4O$ [M]: 290.32; Found: $[M-H]^+$: 289

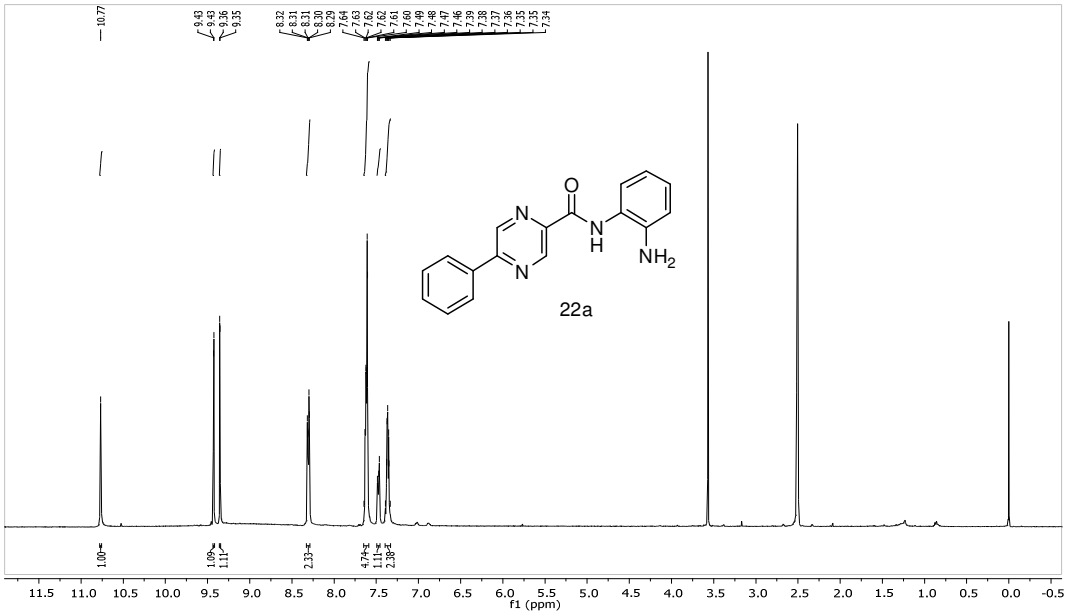

^{1}H NMR of 22a

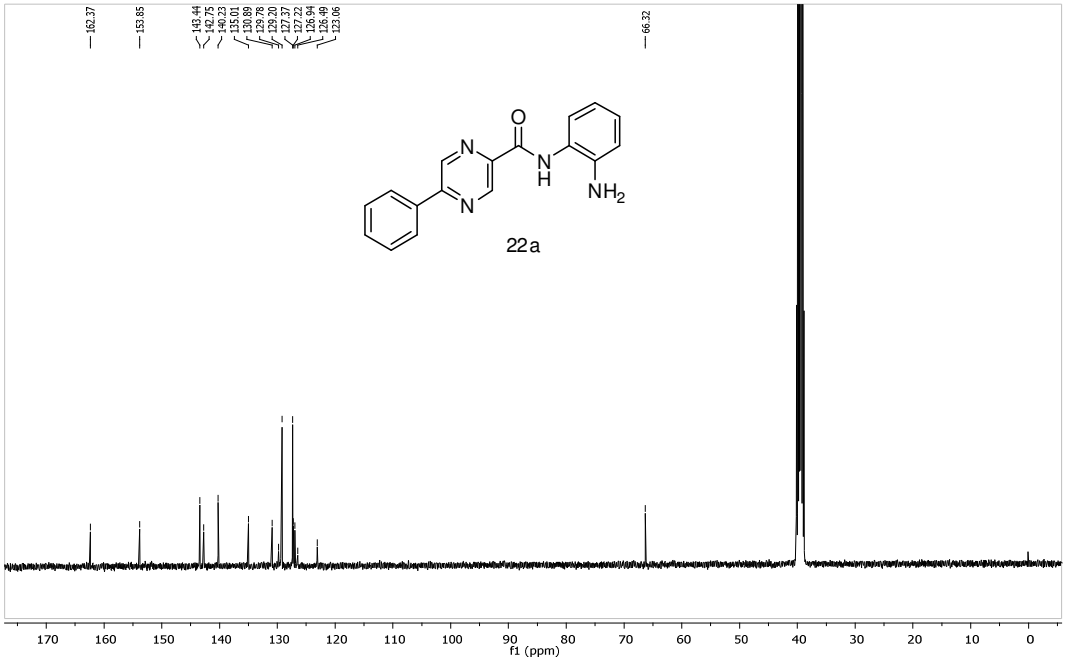

^{13}C NMR of 22a

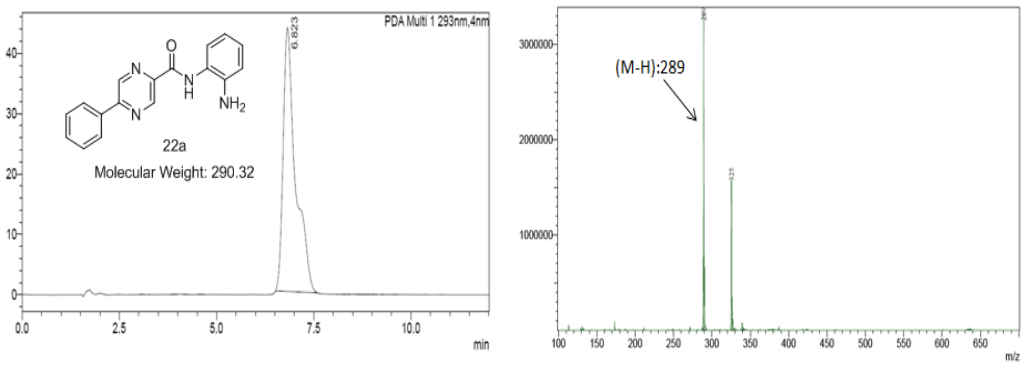

LC/MS of 22a

***N*-(2-amino-4-fluorophenyl)-5-phenylpyrazine-2-carboxamide hydrochloride (22b)**

Compound **21b** (0.055 g, 0.134 mmol) was deprotected following procedure C to get final compound **22b** (0.044 g, yield 95.6%) as pale pink solid. ^{1}H NMR (400 MHz, DMSO-d_6) δ 10.77 (s, 1H), 9.43 (d, *J* = 1.4 Hz, 1H), 9.35 (d, *J* = 1.4 Hz, 1H), 8.33 – 8.29 (m, 2H), 7.65 – 7.59 (m, 5H), 7.40 – 7.33 (m, 2H).^{13}C NMR (101 MHz, DMSO-d_6) δ 162.74, 160.76, 158.36, 153.65, 142.08, 139.63, 133.54, 133.17, 128.82, 128.54, 128.45, 122.54, 119.09, 66.31. HPLC Rt: 7.144 LC-MS calculated for expected $C_{17}H_{13}FN_4O$ [M]: 308.31; Found: $[M-H]^+$: 307.05

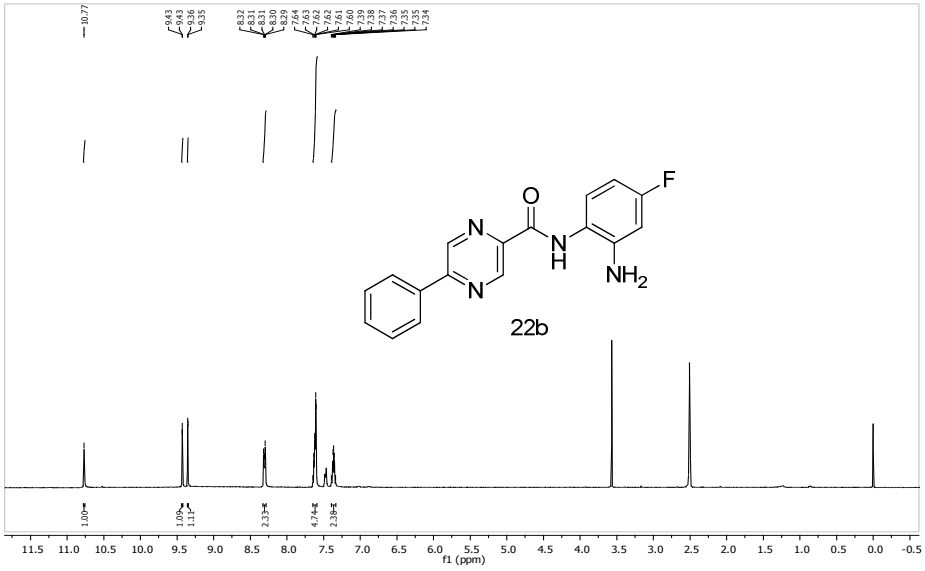

^{1}H NMR of 22b

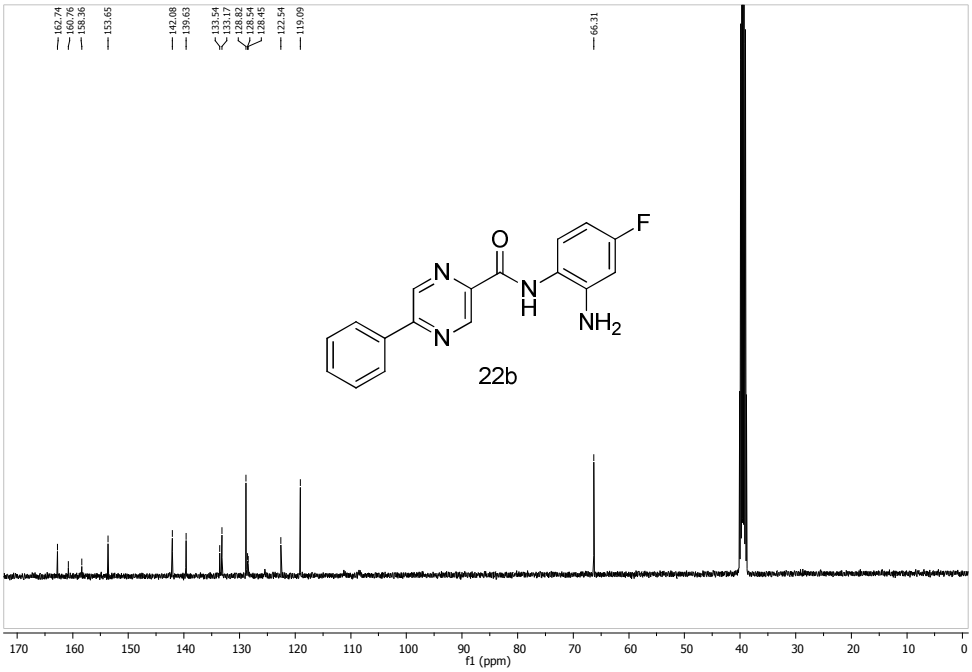

^{13}C NMR of 22b

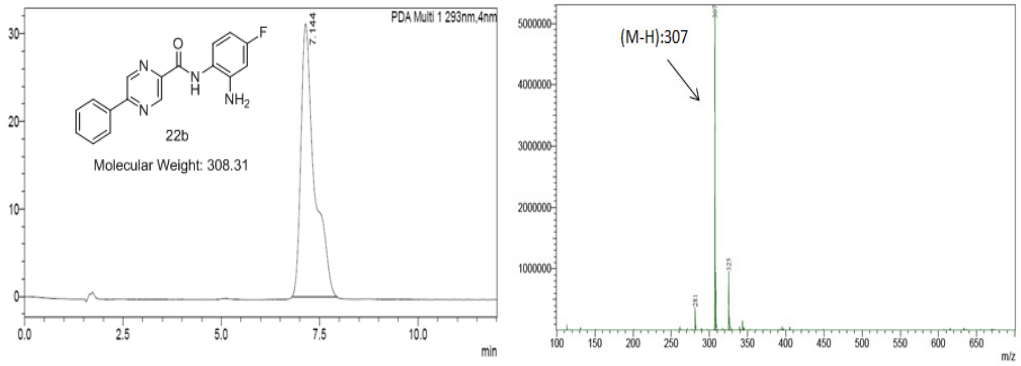

LC/MS of 22b

Procedure D. Preparation of methyl 5-(phenylamino)pyrazine-2-carboxylate (23a)

Methyl 5-(chloropyrazine)-2-carboxylate (1.5 g, 0.00869 mmol), a commercially available starting material **7** was dissolved in 10 mL of 1,4-dioxane. Aniline (0.890 g, 0.00956 mmol) and p-toluene sulphonic acid (2.25 g, 0.01303 mmol) were added and mixture was refluxed at 100°C for 12 hours. Reaction mixture was then concentrated and poured into water, extracted in EtOAc, dried over Na_2SO_4, filtered and evaporated. The crude was purified by column chromatography (EtOAc:Hexane; 3:7) to get 0.320 g

of pale yellow solid compound **23a** (yield 16%). ^{1}H NMR (400 MHz, DMSO-d_6) δ 10.16 (s, 1H), 8.74 (s, 1H), 8.26 (s, 1H), 7.75 (d, *J* = 8.1 Hz, 2H), 7.37 (t, *J* = 7.7 Hz, 2H), 7.07 (t, *J* = 7.3 Hz, 1H), 3.84 (s, 3H). $C_{12}H_{11}N_3O_2$ [M]: 229.23; MS (ESI) *m/z*: $[M+H]^+$: 230.05, $[M-H]^+$: 228.05

methyl 5-(benzylamino)pyrazine-2-carboxylate (23b)

Compound **23b** was also synthesized from methyl 5-(chloropyrazine)-2-carboxylate (1.5 g, 0.00869 mmol) and benzylamine (1.39 g,0.01303 mmol) following procedure D to afford 0.7 g cream color solid compound (yield 33%). ^{1}H NMR (400 MHz, DMSO-d_6) δ 8.59 (d, *J* = 1.2 Hz, 1H), 8.48 (t, *J* = 5.8 Hz, 1H), 8.04 (d, *J* = 1.2 Hz, 1H), 7.34 (d, *J* = 4.4 Hz, 4H), 7.30 – 7.24 (m, 1H), 4.58 (d, *J* = 5.9 Hz, 2H), 3.79 (s, 3H). $C_{13}H_{13}N_3O_2$ [M]: 243.26; MS (ESI) *m/z*: $[M+H]^+$: 244.10, $[M-H]^+$: 242.05

5-(phenylamino) pyrazine-2-carboxylic acid (24a)

Methyl 5-(phenylamino)pyrazine-2-carboxylate (**23a**) (0.320 g, 1.3959 mmol) was reacted with Lithium hydroxide (0.1 g, 4.1879 mmol) following procedure A to get 0.3 g white solid compound **24a** (yield 99.9%). ^{1}H NMR (400 MHz, DMSO-d_6) δ 12.91 (s, 1H), 10.09 (s, 1H), 8.72 (d, *J* = 1.1 Hz, 1H), 8.26 (d, *J* = 1.2 Hz, 1H), 7.77 – 7.74 (m, 2H), 7.39 – 7.33 (m, 2H), 7.06 (t, *J* = 7.4 Hz, 1H).). $C_{11}H_9N_3O_2$ [M]: 215.21; MS (ESI) *m/z*: $[M+H]^+$: 216.00, $[M-H]^+$: 214.05

5-(benzylamino) pyrazine-2-carboxylic acid (24b)

Compound **24b** was synthesized from compound **23a** (0.7 g, 2.8775 mmol) following procedure A. This reaction yielded 0.623 g of product **24b** as white fluffy powder (yield 90%). ^{1}H NMR (400 MHz, DMSO-d_6) δ 12.61 (s, 1H), 8.58 (d, *J* = 1.2 Hz, 1H), 8.40 (t, *J* = 5.8 Hz, 1H), 8.03 (d, *J* = 1.3 Hz, 1H), 7.34 (d, *J* = 4.5 Hz, 4H), 7.26 (t, *J* =

4.5 Hz, 1H), 4.57 (d, *J* = 5.9 Hz, 2H). $C_{12}H_{11}N_3O_2$ [M]: 229.23; MS (ESI) *m/z*: $[M+H]^+$: 230.05, $[M-H]^+$: 228.05

***tert*-butyl (2-(5-(phenylamino)pyrazine-2-carboxamido)phenyl)carbamate (25a)**

Compound **24a** (0.140 g, 0.6505 mmol) was reacted with compound **2** (0.150 g,0.7155 mmol) according to procedure B to get 0.095 g of white powder (yield 37%) ^{1}H NMR (400 MHz, DMSO-d_6) δ 10.11 (d, *J* = 8.4 Hz, 2H), 9.16 (s, 1H), 8.81 (s, 1H), 8.20 (s, 1H), 7.98 (d, *J* = 8.1 Hz, 1H), 7.78 (d, *J* = 8.2 Hz, 2H), 7.38 (t, *J* = 7.7 Hz, 2H), 7.25 (d, *J* = 6.0 Hz, 2H), 7.15 (t, *J* = 7.6 Hz, 1H), 7.06 (t, *J* = 7.3 Hz, 1H), 1.52 (s, 9H). $C_{22}H_{23}N_5O_3$ [M]: 405.45; MS (ESI) *m/z*: $[M+H]^+$: 406.20, $[M-H]^+$: 404.20

***tert*-butyl(5-fluoro-2-(5-(phenylamino)pyrazine-2-carboxamido)phenyl)carbamate (25b)**

Compound **25b** was synthesized from 5-(phenylamino) pyrazine-2-carboxylic acid (**24a**) (0.150 g, 0.6976 mmol) and *tert*-butyl (2-amino-5-fluorophenyl)carbamate (**6**) (0.197 g, 0.7674 mmol) following procedure B. The product obtained as pale pink powder 0.180 g (yield 60.9%). ^{1}H NMR (400 MHz, DMSO-d_6) δ 10.09 (d, *J* = 17.9 Hz, 2H), 9.21 (s, 1H), 8.79 (d, *J* = 1.2 Hz, 1H), 8.21 (d, *J* = 1.2 Hz, 1H), 7.85 – 7.75 (m, 3H), 7.40 – 7.34 (m, 2H), 7.21 (dd, *J* = 10.2, 2.9 Hz, 1H), 7.11 – 7.03 (m, 2H), 1.51 (s, 9H). $C_{22}H_{22}FN_5O_3$ [M]: 423.44; MS (ESI) *m/z*: $[M+H]^+$: 424.15, $[M-H]^+$: 422.15

***tert*-butyl (2-(5-(benzylamino)pyrazine-2-carboxamido) phenyl) carbamate (25c)**

5-(benzylamino) pyrazine-2-carboxylic acid (**24b**) (0.250 g, 1.0906 mmol) and *tert*-butyl (2-aminophenyl) carbamate (**2**) (0.250 g, 1.1996 mmol) were reacted following procedure B and afforded 0.220 g of pale cream powder compound **25c** (yield 48%). ^{1}H NMR (400 MHz, DMSO-d_6) δ 9.99 (s, 1H), 9.09 (s, 1H), 8.65 (s, 1H), 8.38 (t, *J* = 5.9 Hz, 1H), 7.98 – 7.95 (m, 2H), 7.36 (s, 2H), 7.35 (d, *J* = 2.0 Hz, 2H), 7.27 (t, *J* = 7.0 Hz,

1H), 7.22 (t, *J* = 6.8 Hz, 2H), 7.15 – 7.10 (m, 1H), 4.60 (d, *J* = 5.8 Hz, 2H), 1.48 (s, 9H). $C_{23}H_{25}N_5O_3$ [M]: 419.20; MS (ESI) *m/z*: $[M-H]^+$: 418.20

***tert*-butyl(2-(5-(benzylamino)pyrazine-2-carboxamido)-5-fluorophenyl)carbamate (25d)**

5-(benzylamino) pyrazine-2-carboxylic acid (**24b**) (0.195 g, 0.8506 mmol) and *tert*-butyl (2-amino-5-fluorophenyl)carbamate (**6**) (0.240 g, 0.9357 mmol) were reacted following procedure B. The product was obtained as pale pink powder; 0.200 g (yield 53.7%). ^{1}H NMR (400 MHz, DMSO-d_6) δ 9.95 (s, 1H), 9.14 (s, 1H), 8.64 (s, 1H), 8.38 (s, 1H), 7.98 (s, 1H), 7.81 (t, *J* = 7.1 Hz, 1H), 7.35 (s, 4H), 7.27 (s, 1H), 7.19 (d, *J* = 10.2 Hz, 1H), 7.06 (t, *J* = 8.5 Hz, 1H), 4.60 (d, *J* = 4.9 Hz, 2H), 1.48 (s, 9H). $C_{23}H_{24}FN_5O_3$ [M]: 437.47; MS (ESI) *m/z*: $[M+H]^+$: 438.25, $[M-H]^+$: 436.20

***N*-(2-aminophenyl)-5-(phenylamino)pyrazine-2-carboxamide hydrochloride (26a)**

Compound **25a** (0.095 g, 0.2345 mmol) was deprotected following procedure C get one final compound **26a** as yellow color powder. (0.070 g, yield 87.3%).^{1}H NMR (400 MHz, DMSO-d_6) δ 10.56 (s, 1H), 10.52 (s, 1H), 8.82 (d, *J* = 1.2 Hz, 1H), 8.46 (d, *J* = 1.3 Hz, 1H), 7.84 (d, *J* = 7.7 Hz, 2H), 7.65 (d, *J* = 8.0 Hz, 1H), 7.58 (d, *J* = 7.9 Hz, 1H), 7.46 (t, *J* = 7.7 Hz, 1H), 7.40 – 7.38 (m, 1H), 7.38 – 7.34 (m, 2H), 7.06 (t, *J* = 7.4 Hz, 1H), 2.71 (d, *J* = 4.9 Hz, 1H). ^{13}C NMR (101 MHz, DMSO-d_6) δ 162.93, 153.73, 142.28, 139.60, 133.34, 133.25, 131.52, 128.82, 128.28, 127.12, 126.44, 126.33, 124.21, 122.60, 119.13. HPLC Rt: 6.285 LC-MS calculated for expected $C_{17}H_{15}N_5O$ [M]: 305.33; Found: $[M-H]^+$: 304

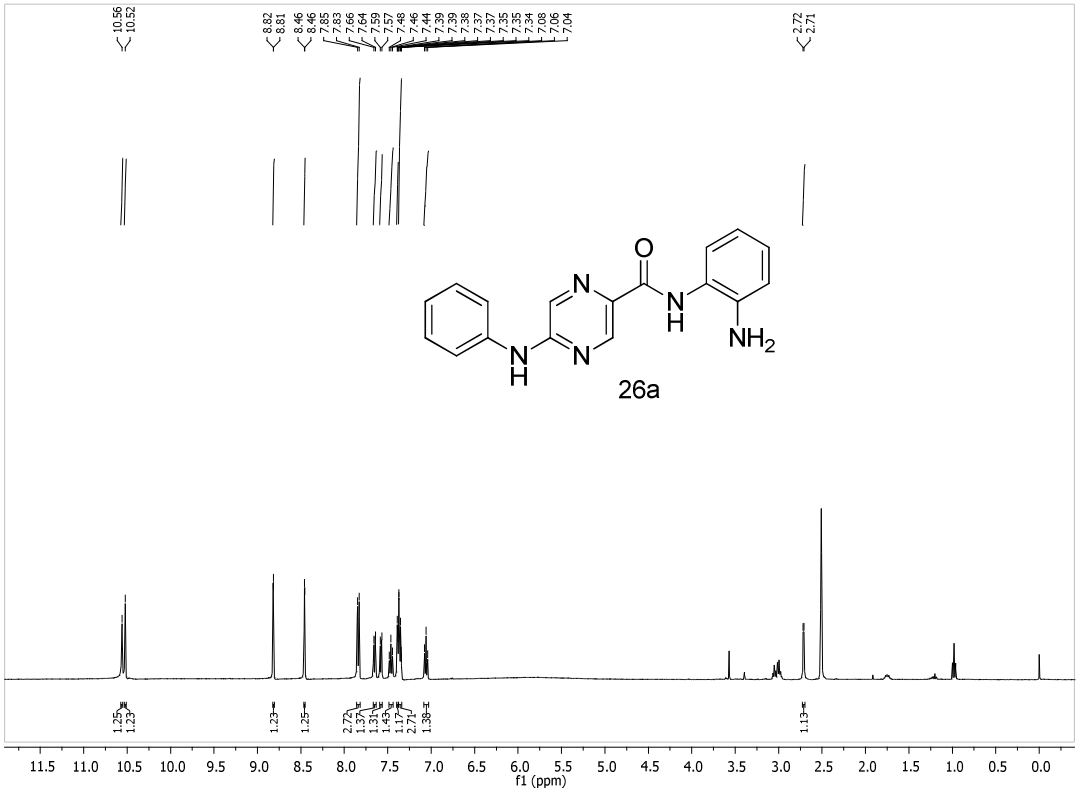

^{1}H NMR of 26a

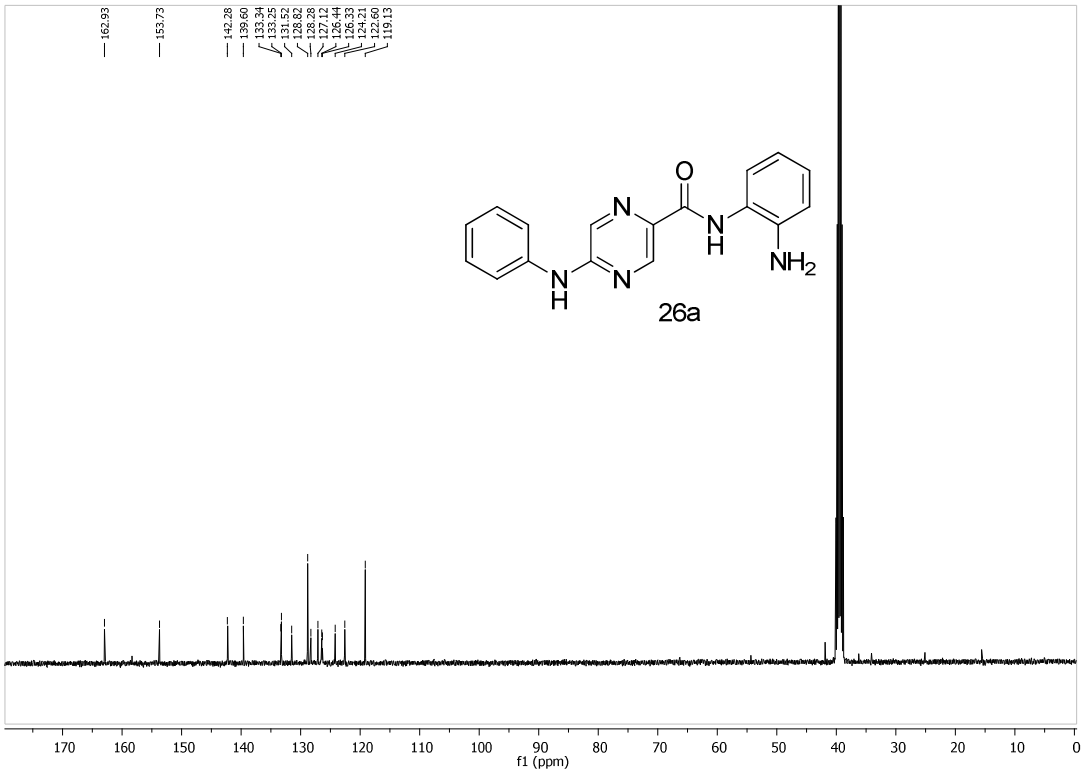

^{13} C NMR of 26a

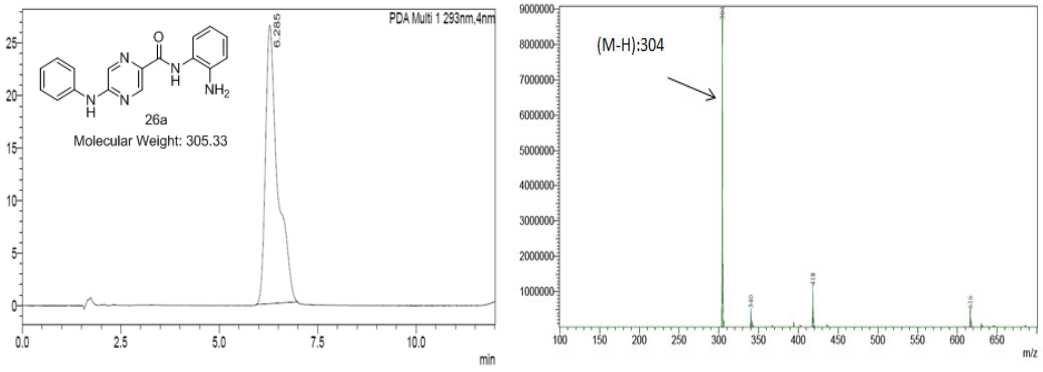

LC/MS of 26a

_N_-(2-amino-4-fluorophenyl)-5-(phenylamino)pyrazine-2-carboxamide hydrochloride (26b)

tert-butyl (5-fluoro-2-(5-(phenylamino) pyrazine-2-carboxamido) phenyl) carbamate (**25b**) (0.130 g, 0.3073 mmol) was depretected as described in procedure C. Compound **26b** was obtained as orange color powder (0.1 g, yield 90.5%). ^{1}H NMR (400 MHz, DMSO-d_6) δ 10.47 (s, 1H), 10.24 (s, 1H), 8.79 (s, 1H), 8.42 (s, 1H), 7.82 (d, *J* = 8.5 Hz, 3H), 7.56 (dd, *J* = 8.9, 5.8 Hz, 1H), 7.40 – 7.34 (m, 3H), 7.22 (d, *J* = 9.6 Hz, 1H), 7.09 (d, *J* = 11.7 Hz, 1H), 7.04 (d, *J* = 8.4 Hz, 1H). ^{13}C NMR (101 MHz, DMSO-d_6) δ 162.74, 160.76, 158.36, 153.65, 142.08, 139.63, 133.54, 133.17, 128.82, 128.54, 128.45, 122.54, 119.09, 66.31. HPLC Rt: 7.144 LC-MS calculated for expected $C_{17}H_{14}FN_5O$ [M]: 323.12; Found: $[M-H]^+$: 322

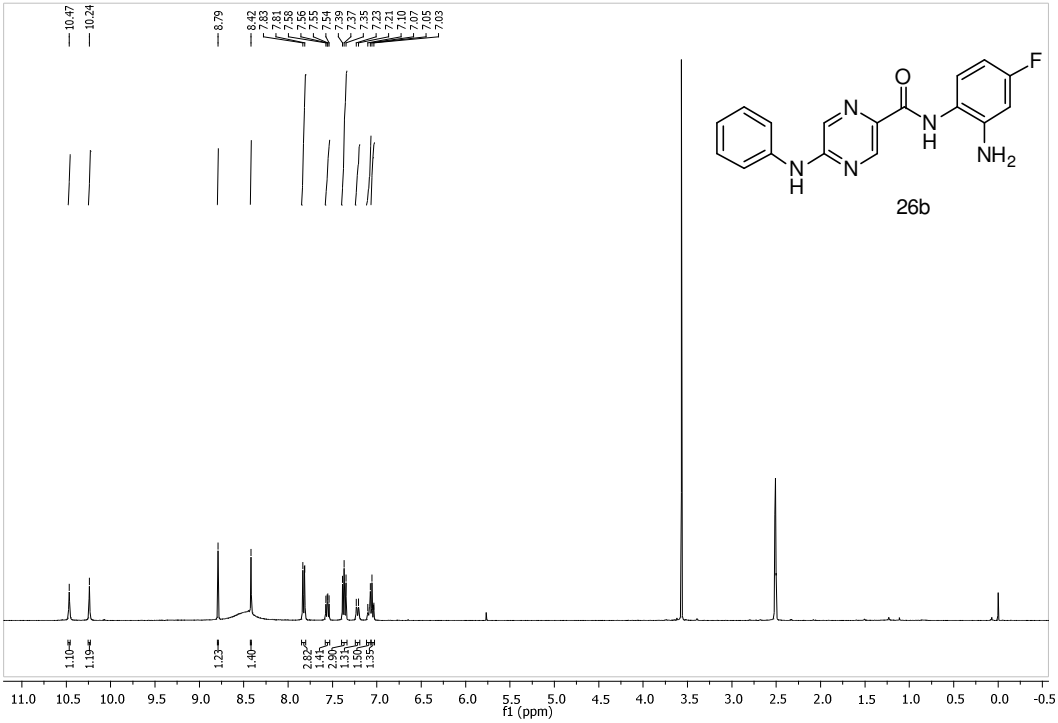

^{1}H NMR of 26b

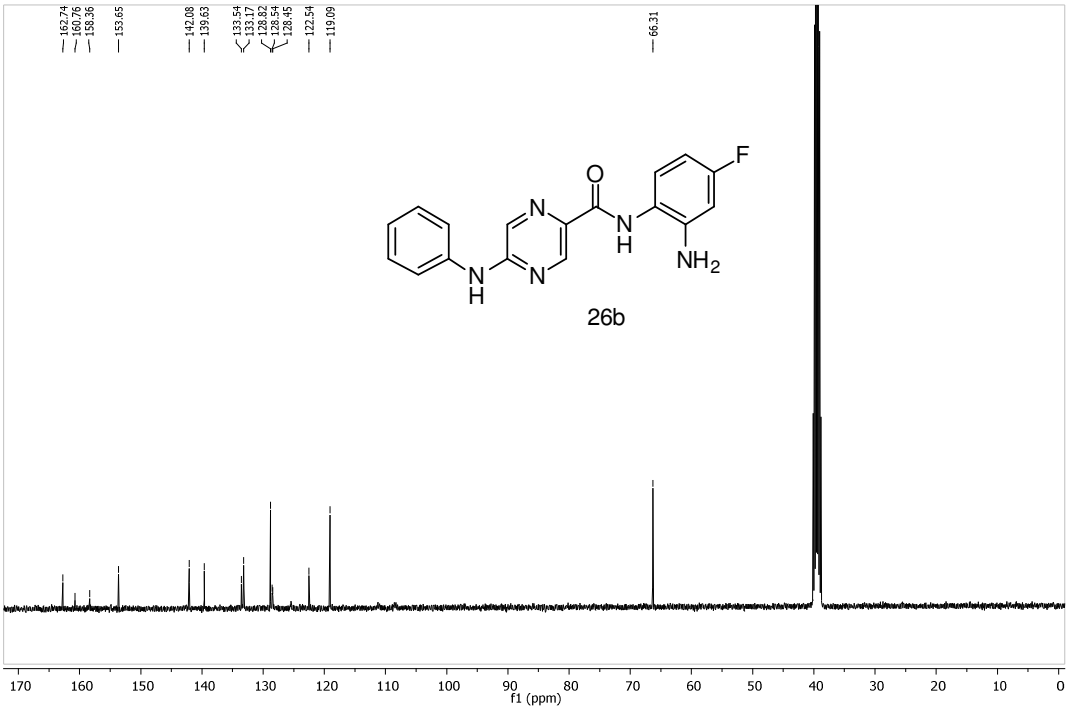

^{13}C NMR of 26b

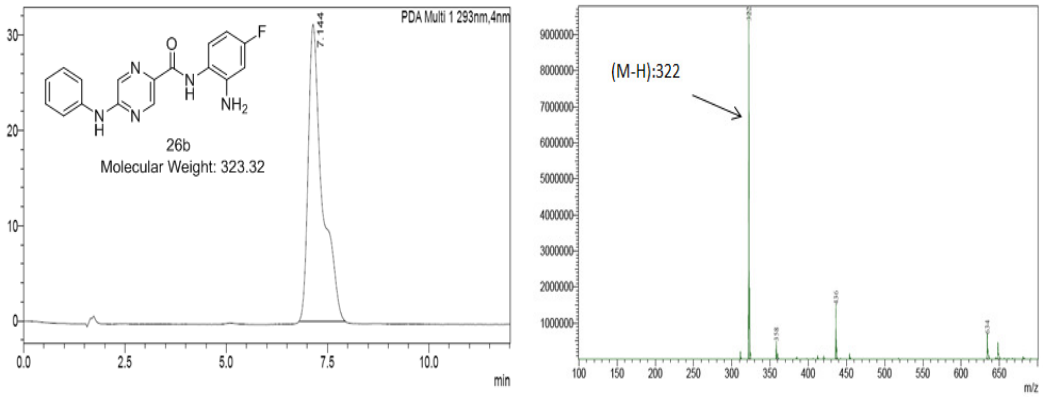

LC/MS of 26b

***N*-(2-aminophenyl)-5-(benzylamino)pyrazine-2-carboxamide hydrochloride (26c)**

The final compound **26c** was prepared by following procedure C from compound **25c** (0.120 g, 0.2860 mmol) to afford **26c** as yellow solid (0.103 g, yield 100%). ^{1}H NMR (400 MHz, DMSO-d_6) δ 10.40 (s, 1H), 8.62 (d, *J* = 32.6 Hz, 2H), 8.13 (s, 1H), 7.63 (dd, *J* = 8.1, 1.3 Hz, 1H), 7.57 (dd, *J* = 7.9, 1.4 Hz, 1H), 7.47 – 7.41 (m, 1H), 7.39 – 7.32 (m, 6H), 7.27 (t, *J* = 7.4 Hz, 1H), 4.62 (s, 2H). ^{13}C NMR (101 MHz, DMSO-d_6) δ 163.19, 155.96, 142.99, 138.78, 131.66, 131.63, 128.39, 128.27, 127.38, 127.01, 126.98, 126.28, 126.17, 124.18, 66.31, 43.71. HPLC Rt: 5.355 LC-MS calculated for expected $C_{18}H_{17}N_5O$ [M]: 319.36; Found: $[M-H]^+$: 318

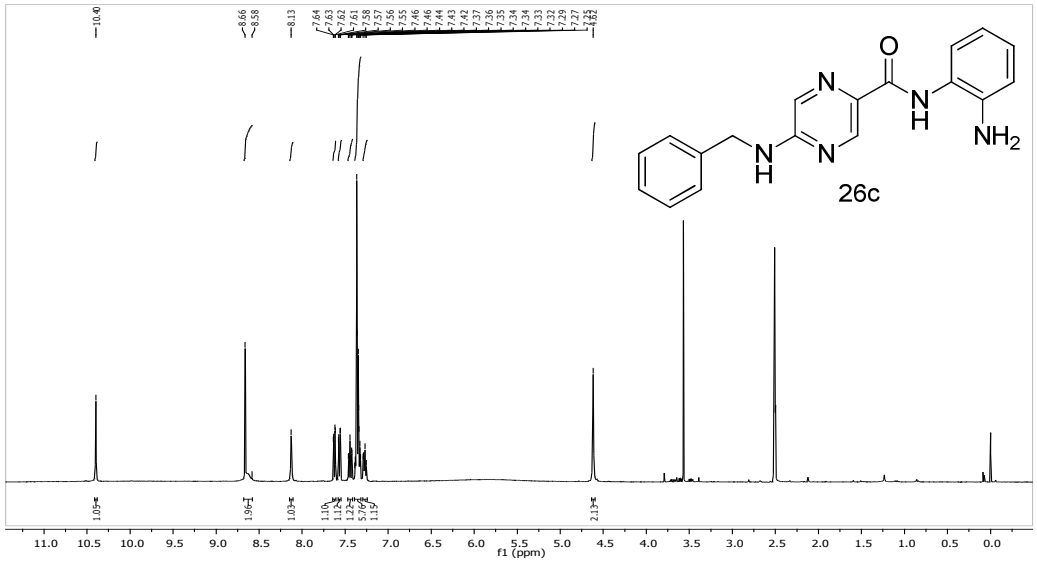

^{1}H NMR of 26c

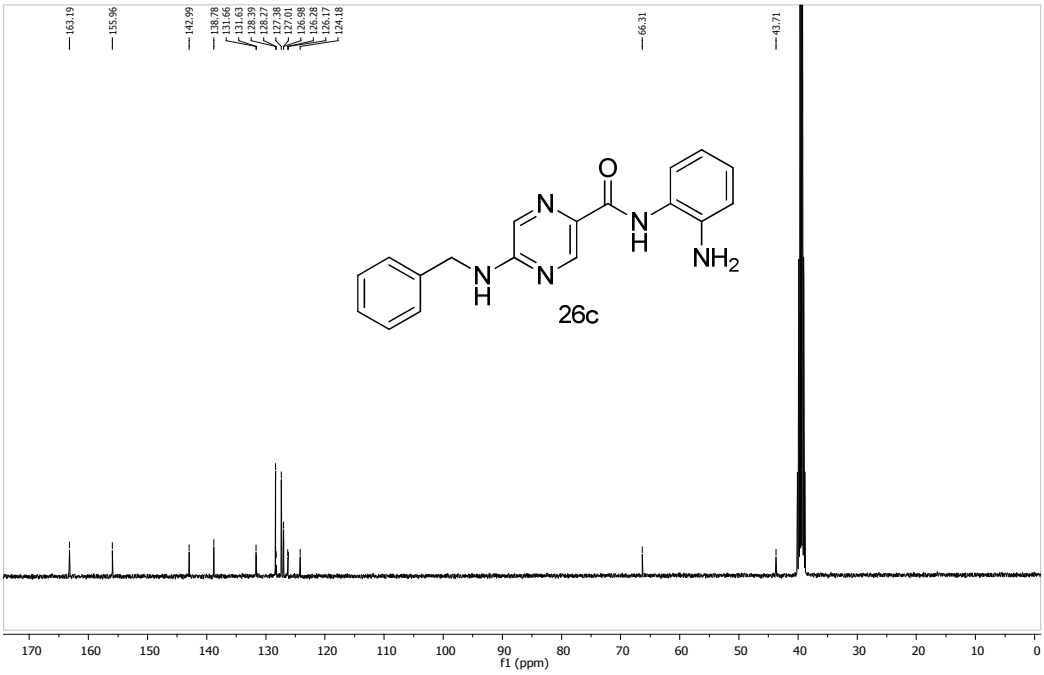

^{13}C NMR of 26c

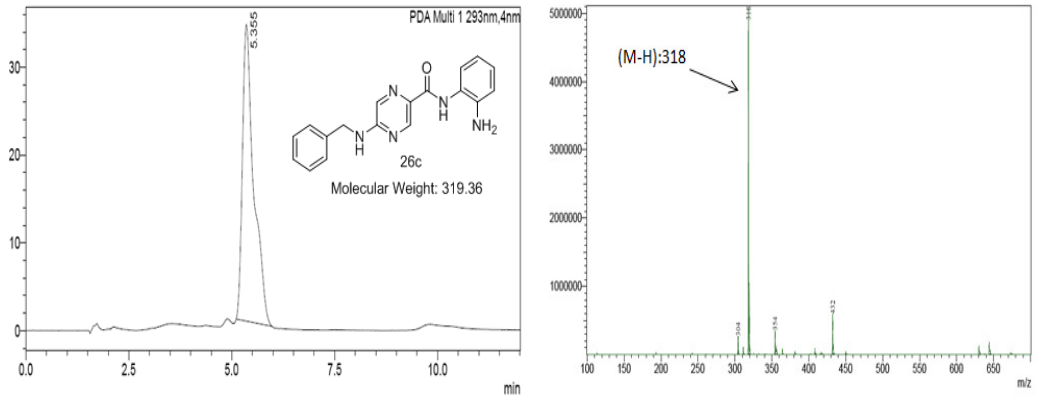

LC/MS of 26c

_N_-(2-amino-4-fluorophenyl)-5-(benzylamino)pyrazine-2-carboxamide hydrochloride (26d)

Compound **26d,** another final compound was prepared from **25d** (0.1g, 0.2285 mmol) following procedure C gave 0.85 g of brown solid (100% conversion). ^{1}H NMR (400 MHz, DMSO-d_6) δ 10.10 (s, 1H), 8.63 (d, *J* = 1.2 Hz, 1H), 8.11 (s, 1H), 7.53 (dd, *J* = 8.9, 5.9 Hz, 1H), 7.39 – 7.32 (m, 6H), 7.29 – 7.24 (m, 2H), 7.20 (dd, *J* = 9.6, 2.7 Hz, 1H), 7.05 (dd, *J* = 8.6, 2.6 Hz, 2H), 4.61 (s, 2H). ^{13}C NMR (101 MHz, DMSO-d_6) δ

162.98, 160.65, 158.27, 155.87, 142.70, 138.80, 131.82, 131.63, 128.38, 128.29, 127.38, 126.98, 126.17, 124.18, 66.32, 43.73 HPLC Rt: 6.082 LC-MS calculated for expected $C_{18}H_{26}FN_5O$ [M]: 337.35; Found: $[M-H]^+$: 336

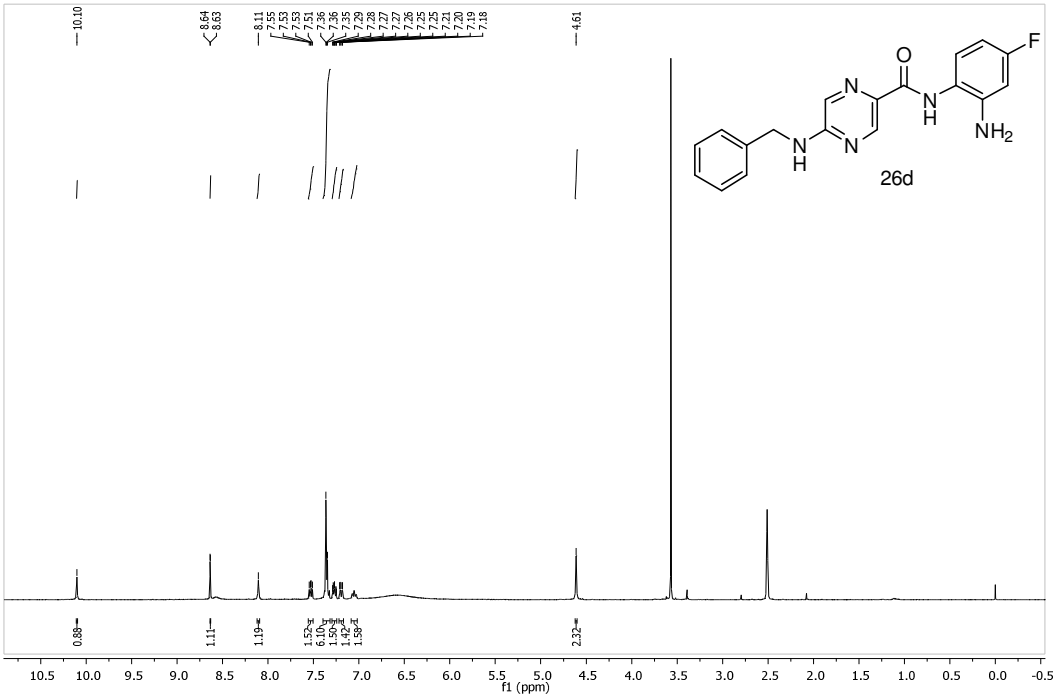

^{1}H NMR of 26d

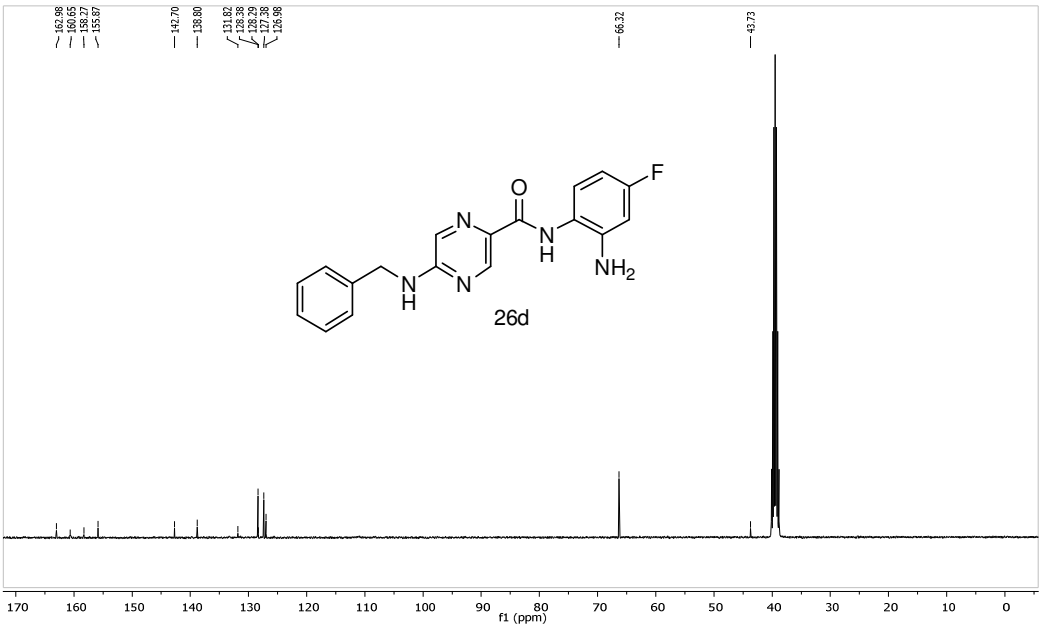

^{13}C of 26d

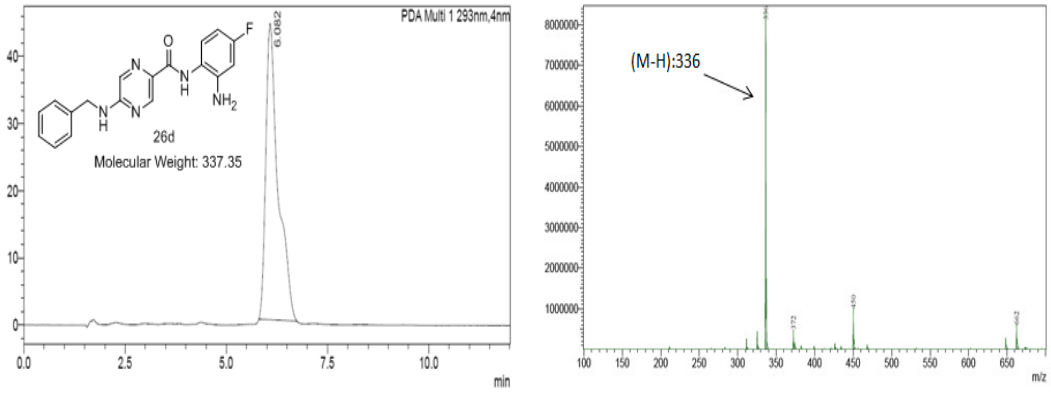

LC/MS of 26d

2.3.2. HDAC inhibition assay

The enzyme inhibition assay was performed using HDAC colorimetric assay kit (BML-AK501, ENZO life sciences). Briefly, 5 µL of Hela nuclear extract (BML-KI137-0500), 10 µL of assay buffer (BML-KI143-0020), 10 µL of sample solution was added per well in a microtiter plate. The reaction was started with addition of 25 µL Color de Lys® substrate solution (BML-KI138-0050). The reaction was incubated in for 30 minutes at 37°C which was terminated by addition of a 50 µl mixture of developer plus stop solution. The plate was incubated for 15 minutes at 37°C and absorbance was measured at 405 nm. All synthesized compounds along with **CI-994** and **BG-45** were screened at 5 µM concentration in duplicate. The promising three test compounds **26b**, **26c**, **26d** at concentration of 0.5 µM, 1 µM, 2 µM, 5 µM, 10 µM and 15 µM along with **BG-45** and **CI-994** (concentration range of 1 µM, 2 µM, 5 µM, 10 µM, 15 µM and 20 µM) were tested in duplicate to find out their IC_{50} values.

2.3.3. HDAC3/NCOR1 assay

This assay was performed using HDAC3/NCOR1 fluorometric drug discovery kit (BML-AK531, ENZO life sciences). Here, 10 µL of sample solution and 15 µL diluted

HDAC3/NCOR1 complex solution (BML-KI574-0030) were added per well in microtiter plate and 25 µL Fluor de Lys® substrate solution (BML-KI177-0005) was added. The plate was incubated for 15 minutes at 37°C. To terminate the reaction, 50 µL of mixture of Fluor de Lys® developer II (BML-KI176-1250) and Trichostatin A ((BML-GR309-9090) was added per well and incubated for 45 minutes at 37°C. The fluorescence intensity was measured at Excitation wavelength 360 nm, Emission wavelength 460 nm using Spectramax M4 (Molecular Devices, USA). First all the synthesized compounds along with **CI-994** and **BG-45** were screened at 1µM concentration in duplicate. Compound **26b, 26c, 26d** and **BG-45** were evaluated at 0.05 µM, 0.1 µM, 0.25 µM, 0.5 µM, 1 µM and 2 µM for IC_{50} determination while **CI-994** was tested at 0.1 µM, 0.25 µM, 0.5 µM, 1 µM, 2 µM and 5 µM in duplicate.

2.3.4. Cell culture and drug treatment

The murine melanoma cell line (B16F10) and human cervical cancer cell line (HeLa) were procured from National center for cell science (NCCS, Pune, India) and cultured in Dulbecco's Modified Eagle Medium (DMEM) (Himedia Laboratories Pvt. Ltd., Mumbai, India), supplemented with 10% heat inactivated fetal bovine serum (Himedia Laboratories Pvt. Ltd., Mumbai, India) and 1 % of antibiotic solution (10000 U Penicillin and 10 mg Streptomycin per mL, Himedia Laboratories Pvt. Ltd., Mumbai, India). Cells were cultured at 37°C in humidified atmosphere with 5% CO_2. Stock solutions of all compounds were prepared in DMSO at a concentration of 100 mM and stored.

2.3.4.1. MTT assay

Antiproliferative activity of all the synthesized compounds was measured by in vitro MTT assay method. 5×10^3 cells were seeded in 96 well plate and incubated overnight.

Cells were treated with **CI-994**, **BG-45** and test compounds in two doses 100μM and 10μM in triplicate and incubated for 72 hours. 50μl of 5mg/mL solution of MTT (3-(4,5-dimethylthiazol-2-yl)-2,5-diphenyltetrazolium bromide; Himedia Laboratories Pvt. Ltd., Mumbai, India) was added. After 4 hours of incubation, the formed formazan crystals were dissolved in DMSO and absorbance was measured at 570nm and 650nm using Spectramax M4 (Molecular Devices, USA).

For, IC_{50} measurement of four selected compounds (**12a, 22a, 26a, 26c, 26d**) along with **CI-994** and **BG-45**, the same procedure was followed as described above. The compounds were explored in a wide range of 0.781, 1.562, 3.125, 6.25, 12.5, 25, 50, 100 and 200 μM. The same experiment was repeated with another batch of cells.

2.3.4.2. Apoptosis assay

For apoptosis assay, $5x10^5$ B16F10 cells were seeded in 6 well plates and incubated overnight at 37°C. The following day, cells were treated with **CI-994**, **BG-45**, **26c** and **26d** and incubated for 72 hours. The cells were trypsinized and suspended in fresh media and centrifuged at 1000 rpm for 5 min at 4°C. The pellet was washed with ice cold PBS and centrifuged. The extent of apoptosis was measured by using Annexin V-FITC and PI dead cell apoptosis kit (Molecular probes, Thermo Fischer Scientific, USA).

2.2.4.3. Cell cycle analysis

Briefly, $5x10^5$ B16F10 cells were seeded in 6 well plates and incubated overnight at 37°C. The following day, cells were treated with **CI-994**, **BG-45**, **26c** and **26d** and incubated for 72 hours. Cells were trypsinized, centrifuged and washed twice with PBS and fixed with 70% ice cold ethanol and stored at -20°C for 24hours. The cells were centrifuged to remove ethanol, washed and resuspended in 500 μL PBS pH 7.4

containing RNAse (100 μg/mL) at room temperature for 20 min. Propidium iodide (PI) (50 μg/mL in PBS) was added to stain cellular DNA and kept in dark for 30 minutes. Flow cytometry analysis was performed and the percentage of cells in each phase of the cell cycle was estimated using the IDEAS Software (version 6.0).

2.4. Conclusion

Here, we have designed and synthesized a series of 2-aminobenzamide derivatives as selective HDAC3 inhibitors. All target compounds were evaluated for their HDAC enzyme inhibition efficiency with HeLa nuclear extract and recombinant HDAC3 enzyme and these compounds were found to be effective HDAC inhibitors with preferential selectivity for HDAC3. These compounds were also tested for their antiproliferative activity in two different cell lines (B16F10 and HeLa). Compound **26c** exhibited potent cell growth inhibition compared to both **CI-994** and **BG45**. One of the lead compound (compound **26c**) showed appreciable selectivity (11.68-fold) in HDAC3 inhibition over pan HDACs which is quite significant than **CI-994** (5.85-fold) and **BG-45** (9.9-fold). Compound **26c** induced significant cell growth arrest in G2/M phase and increased apoptosis level indicating improved anticancer potential compared to **CI-994** and **BG45**. Overall effort to make potent and selective HDAC inhibitors with different structural medication on the overlapping backbone of **BG45** and **CI-994** resulted in compound **26c** as a potential HDAC3 inhibitor. Additionally, all these biological evaluation studies indicated compound **26c** can be further explored as a promising compound for anticancer therapy.

Chapter 3

Design, synthesis and biological activity of novel hydroxamates with piperidine and piperazine linker as HDAC8 inhibitors and potential anticancer agents

3.1. INTRODUCTION

Histone Deacetylase is an amidohydrolase involved in deacetylating the histone lysine residues for chromatin remodeling and thus plays a vital role in the epigenetic regulation of gene expression (Kouzarides 2007). These epigenetic alterations by HDACs suppress gene transcription and lead to the silencing of tumor suppressor genes (Mottamal et al. 2015). Therefore, HDAC inhibition has emerged as potential anticancer target (Manal et al. 2016). In general, HDAC inhibitors have standard pharmacophore model which is structurally similar to HDAC acetyl-lysine substrate (Figure 3.1 and 3.2).

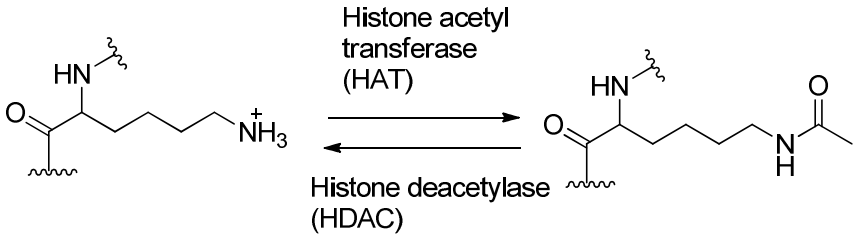

Figure 3.1. The acetylation states of lysine amino acids are governed by the equilibrium activities ofacetyltransferase enzymes and deacetylase enzymes. The lysine residues of histone proteins are key substrates specificity for HDACs.

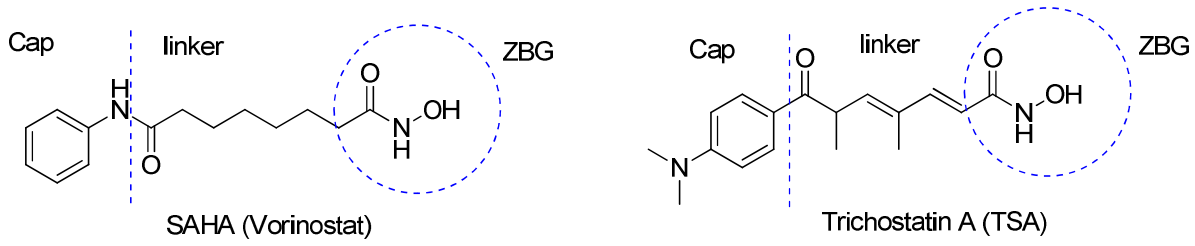

Figure 3.2. Structures of SAHA and Trichostatin A proto type HDAC inhibitors, explaining their design according to general pharmacophore model of HDAC inhibitors.

X-ray crystal structure analysis of SAHA bound in the active site of a bacterial homologue of class I HDAC proteins (HDLP) confirms that the hydroxamic acid (ZBG) coordinates to the catalytic metal atom (zinc) at the bottom of the active site, the anilide capping group interacts with the amino acids the residues at the entrance of active site and the linker lies in a confined hydrophobic channel that appropriately positions the metal-binding moiety and capping group for interactions in the active site (Finnin et al. 1999).

HDAC inhibitors having structural differences in the linker region have been very few. The reason could be that the residues in the hydrophobic channel where linker region lies are highly conserved among the different HDAC isoforms. Therefore, linker region modifications with the groups that can interact with this hydrophobic channel can be exploited to design selective HDAC inhibitors (Wang et al. 2007).

It has been reported that a rigid and bulky linker region that increases the hydrophobic interaction with tunnel residues increases the potency and selectivity within Class I HDACs (Vannini et al. 2004). However, it has also been reported that bulky hydrophobic cap group contributes towards Class-I selectivity (Bieliauskas and Pflum 2008).

3.2. DESIGN OF MOLECULES

Considering these views, here we tried to modify the linker region with piperidine and piperazine moieties. With piperidine and piperazine ring in linker region, we modified cap group with different bulky and hydrophobic groups and designed a series of derivatives (Figure 3.3).

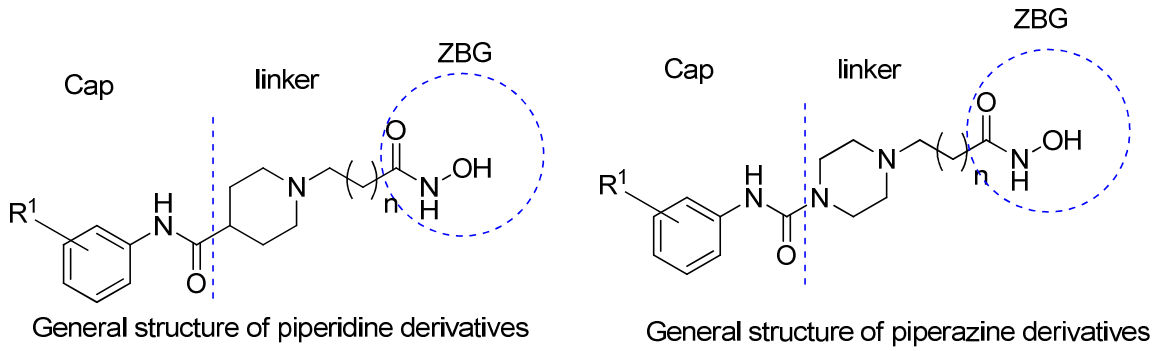

Figure 3.3. Design of novel piperidine and piperazine derivatives

It has been reported in literature with different structure of piperidine and piperazine containing compounds that alkyl side chain attached to ring in linker region shows optimum activity when it has three methylene groups in it (Rossi et al. 2011). In order to check the effect of alkyl side chain length in our design, we tried two methylene and three methylene groups having phenyl in cap group as R^1 and checked the activity. Our initial study suggested the same difference in accordance with the reported observation (Rossi et al. 2011). In our further modifications we kept alkyl side chain length fixed with three methylene groups and modified the cap region to get different hydrophobic cap groups.

3.3. RESULTS AND DISCUSSION

3.3.1. Chemistry

Scheme 3.1 depicts synthesis of piperidine derivatives 5a, 5a', 5b, 5c, 5d and 5e. Here, amine group of 4-piperidine carboxylic acid was protected using di-*tert*-butyl-dicarbonate where, carboxylic acid was converted to its salt form using sodium hydroxide and then it was treated with di-*tert*-butyl-dicarbonate to react with piperidine nitrogen. After completion of reaction, it was neutralized with hydrochloric acid to make carboxylic acid free from its salt from, yielded desired intermediate (Nimbarte et al. 2014). The compound was then

exposed to react with different amines using EDC coupling method to get respective amides. The amide compounds were deprotected with the help of trifluroacetic acid in dichloromethane to make –NH group of piperidine free to attach with aliphatic side chains. Methyl 3-bromopropionate or methyl 4-bromobutanoate was reacted with deprotected piperidine moiety in the presence of potassium carbonate using acetonitrile as solvent. The intermediate esters were converted to hydroxamic acid functional group using 50% (w/v) aqueous hydroxylamine and sodium hydroxide to make final molecules 5a, 5a', 5b, 5c, 5d and 5e.

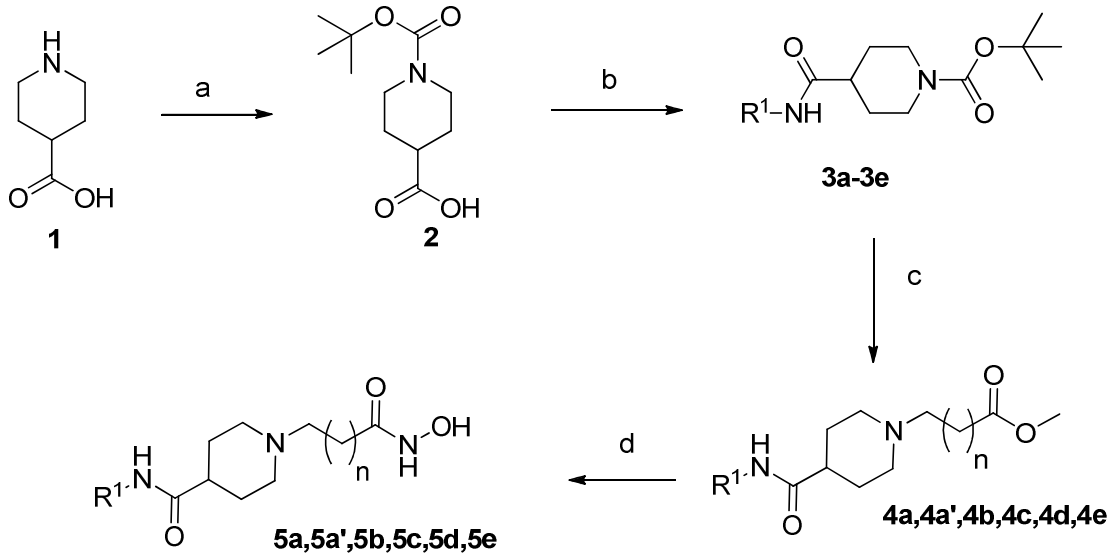

5a: R^1= phenyl, n=0
5a': R^1= phenyl, n=1
5b: R^1= benzyl, n=1
5c: R^1= naphthyl, n=1
5d: R^1= 4-[1,1']biphenyl, n=1
5e: R^1= 4-quinolyl, n=1

Scheme 3.1. *Reagents and conditions:* (a) di-*tert*-butyl-dicarbonate, 1M NaOH, THF, 1M HCl, 0°C, 30 min, rt, overnight (b) R^1NH_2, EDC.HCl, HOBT, TEA, DCM, rt, overnight (c) i. TFA, DCM, 0°C, 2h ii. methyl 3-bromopropanoate (n=0), mehyl 4-bromobutanoate (n=1),

K_2CO_3, acetonitrile, 5h, 90°C (d) 50% w/v aqueous hydroxylamine, 1M NaOH, methanol, 1M HCl, rt, 2h.

Scheme 3.2 describes the protection of piperazine ring using di-*tert*-di-butyl-dicarbonate which is very efficient method to get mono protected piperazine in good yield (Bala et al. 2015). The compound was used as intermediate for the synthesis of piperazine derivatives.

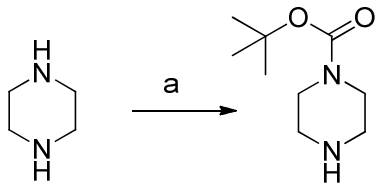

6 **7**

Scheme 3.2. *Reagents and conditions*: (a) di-*tert*-dibuyl-dicarbonate, methanol, $NaHCO_3$, 0°C, 30 min, rt, 4h

Scheme 3.3 describes synthesis of final molecules **11a** and **11b** having piperazine ring attached with aliphatic side chain in linker position. The phenyl isocyanate was reacted with boc protected piperazine (**8**) and produced intermediate **9** (Keith et al. 2012), which was deprotected using TFA in dichloromethane and refluxed with methyl 3-bromopropanoate or methyl 4-bromobutanoate in acetonitrile with K_2CO_3 as base, yielded two derivatives **10a** and **10b**. These compounds were reacted with 50% w/v aqueous hydroxylamine in the presence of sodium hydroxide to get respective hydroxamic acid derivatives.

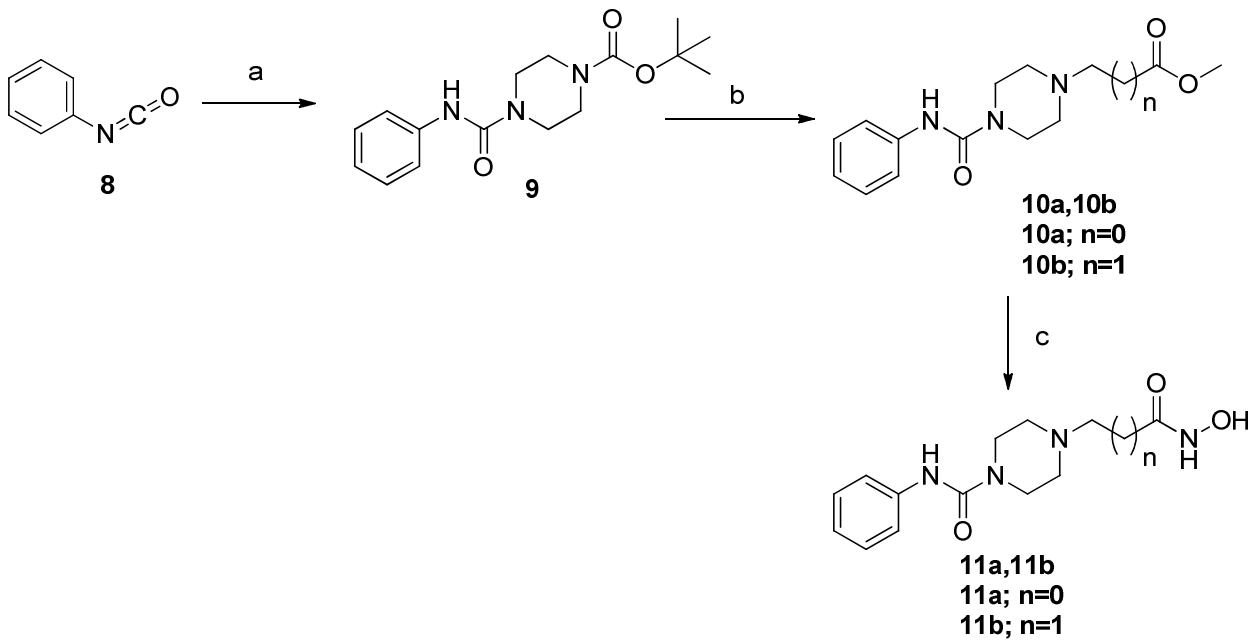

Scheme 3.3. *Reagents and conditions:* (a) Cpd. **7**, DCM, 4h, rt (b) i. TFA, DCM, 0°C, 2h ii. methyl 3-bromopropanoate (n=0), mehyl 4-bromobutanoate (n=1), K_2CO_3, acetonitrile, 5h, 90°C (c) 50% w/v aqueous hydroxylamine, 1M NaOH, methanol, 1M HCl, rt, 2h.

Synthesis of other piperazine derivatives having modification in aryl moiety in cap region using different bulky groups has been described in Scheme 3.4. Here different aryl amines were converted to respective isocyanates using triphosgene in biphasic mixture of DCM and $NaHCO_3$ (Hammock et al. 2016). These isocyanates were combined with boc protected piperazine (**7**) to make respective aryl piperazinyl ureas. These intermediates deprotected using TFA in dichloromethane and refluxed with methyl 3-bromopropanoate or methyl 4-bromobutanoate in acetonitrile with K_2CO_3 as base, yielded **15a-15d**. These compounds were reacted with 50% w/v aqueous hydroxylamine in the presence of sodium hydroxide to get respective hydroxamic acid derivatives.

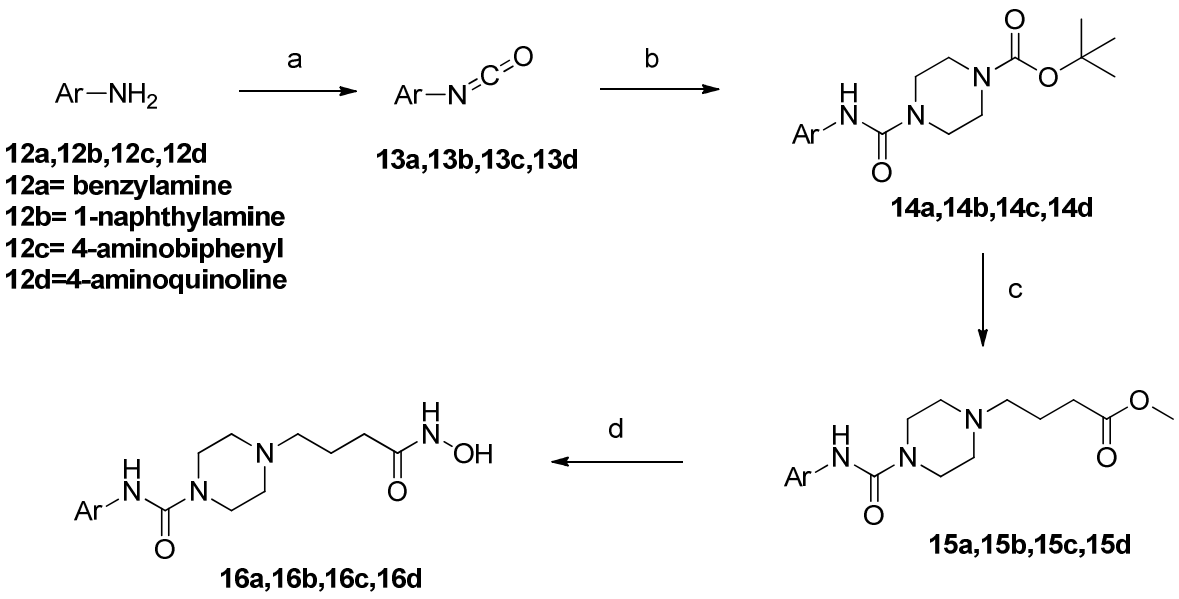

Scheme 3.4. Reagents and conditions: (a) triphosgene, $NaHCO_3$, DCM, 0°C, 1.5h (b) Cpd.**7**, DCM, rt, 4h (c) i. TFA, DCM, 0°C, 2h ii. methyl 3-bromopropanoate (n=0), methyl 4-bromobutanoate (n=1), K_2CO_3, acetonitrile, 5h, 90°C (d) 50% w/v aqueous hydroxylamine, 1M NaOH, methanol, 1M HCl, rt, 2h.

3.3.2. Pan HDAC inhibition assay using HeLa nuclear extract

The target compounds were screened for their HDAC inhibitory activity using *color de lys*® HDAC assay kit (BML-AK501, ENZO life sciences). **SAHA** and **BG45** were used as positive control for the assay. HeLa nuclear extract (expresses HDAC1 and HDAC2 dominantly) (Serebryannyy et al. 2016) was used as a source of HDAC activity. The results are summarized in **Table 3.1**.

Table 3.1. HDAC inhibitory data of target compounds.

Compounds	**% Inhibition at 10μM**		
	HeLa nuclear extract	HDAC3/NCoR1	HDAC8
PT-162 (5a)	35.22	5.93	40.35
PT-199(5a')	36.30	1.93	44.40
PT-241 (5b)	67.52	7.35	63.49
PT-225 (5c)	66.60	10.59	62.16
PT-230 (5d)	64.03	0.05	67.84
PT-250 (5e)	65.34	0.21	72.44
PT-212 (11a)	56.96	8.92	58.35
PT-211 (11b)	62.63	7.95	67.09
PT-251 (16a)	68.95	15.10	69.28
PT-219 (16b)	57.46	9.80	63.24
PT-239 (16c)	63.07	5.35	71.07
PT-254 (16d)	68.36	4.42	74.16
SAHA	91.34	98.99	82.14
BG-45	73.72	85.28	14.27

All compounds were found to show HDAC enzyme inhibition at 10 μM concentration (Table 3.1; Figure 3.4). Most of the compounds exhibit more than 50% enzyme inhibition at 10 μM in HeLa nuclear extract.

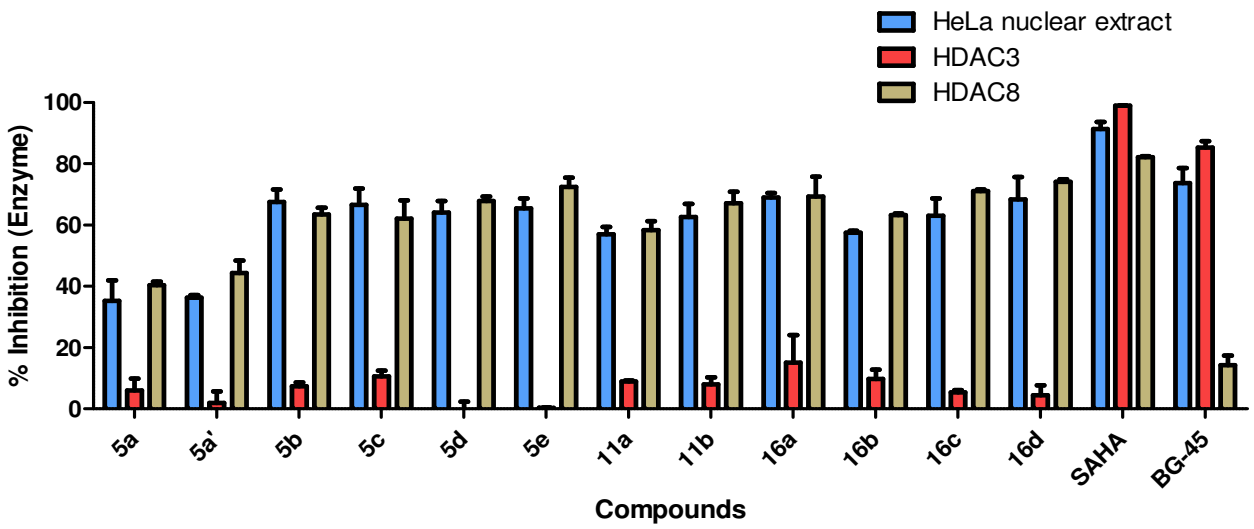

Figure 3.4. HDAC inhibition assay using HeLa nuclear extract, human recombinant HDAC3 and human recombinant HDAC8 enzyme. All compounds including **SAHA** and **BG-45** were screened at 10 μM concentration. All synthesized derivatives exhibit efficient inhibition towards HDAC8 and HeLa nuclear extract, while negligible for HDAC3. Data represents mean ± SD (n=2).

Among these compounds, **5e, 16c, 16d** were further evaluated to find out their IC_{50} values in HeLa nuclear extract by taking **SAHA** and **BG-45** as positive control. These compounds showed less IC_{50} than **BG-45** but more than **SAHA**. Results are summarized in Figure 3.5 and Table 3.2.

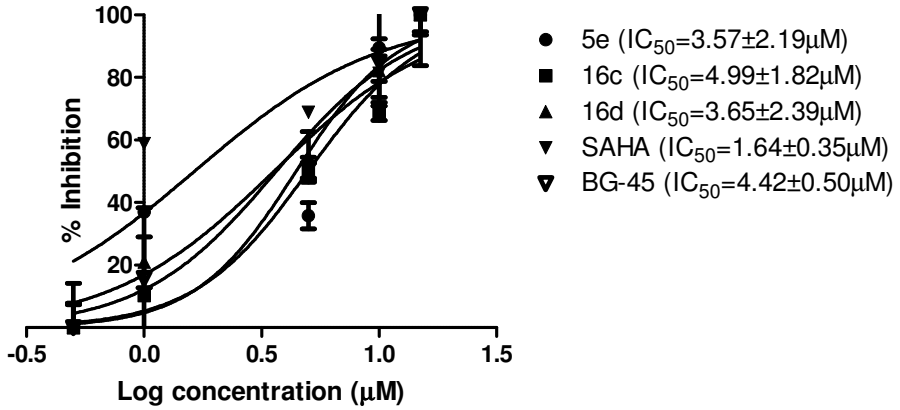

Figure 3.5. Dose response curve of compound **5e, 16c** and **16d** with **SAHA** and **BG-45** for HDAC inhibition assay using HeLa nuclear extract. The data represents mean ± SD (n=2).

Table 3.2. IC_{50} values of promising compounds and their selectivity profile.

Cpd[a]	**IC_{50} (μM)**	
	HeLa nuclear extract (Pan HDAC inhibition)	**HDAC8**
5e	3.57±2.19	3.14±1.01
16c	4.99±1.82	4.29±1.42
16d	3.65±2.39	1.74±0.81
SAHA	1.64±0.35	3.25±2.29
BG45	4.42±0.50	-

[a] Compound number

3.3.3. HDAC3 inhibition assay using human recombinant HDAC3/NCOR1

All synthesized compounds were screened for their HDAC3 inhibition efficiency using HDAC3/NCOR1 fluorometric drug discovery kit (BML-AK531, ENZO life sciences). From the results, it was found that these compounds having negligible inhibition for HDAC3

enzyme (Table-3.1; Figure 3.4) which indicates selectivity of these compounds towards other HDACs HDAC1,2 and HDAC8 than HDAC3.

3.3.4. HDAC8 inhibition assay using human recombinant HDAC8 enzyme

To evaluate selectivity of target compounds, they were further screened for HDAC8 assay using HDAC8 fluorimetric drug discovery kit (BML-AK518). All target compounds, SAHA and BG-45 were tested at 10 μM concentration on human recombinant HDAC8 enzyme according manufacturer's protocol. Interestingly, all compounds were found to show good HDAC8 inhibition. Results displayed higher enzyme inhibition for HDAC8 among HDAC3, HDAC8 and HeLa nuclear extract (Table 3.1). Here, **SAHA** showed comparatively less HDAC8 inhibition than HeLa nuclear extract. BG-45 showed negligible inhibition of HDAC8 and hence not assessed further for IC_{50} determination on HDAC8. To get more precise inhibition potency, the more potent HDAC8 inhibitor compounds **5e**, **16c** and **16d** (72.44%, 71.07% and 74.16% HDAC8 inhibition respectively at 10μM compound concentration) were further evaluated for their IC_{50} values along with **SAHA** (Table 3.2, Figure 3.6). It was observed that the selected compounds have marginal difference in their selectivity towards HDAC8 over HeLa nuclear extract. The analogues exhibited less or similar potency as **SAHA** but preferential selectivity for HDAC8 than prototypical hydroxamate **SAHA**.

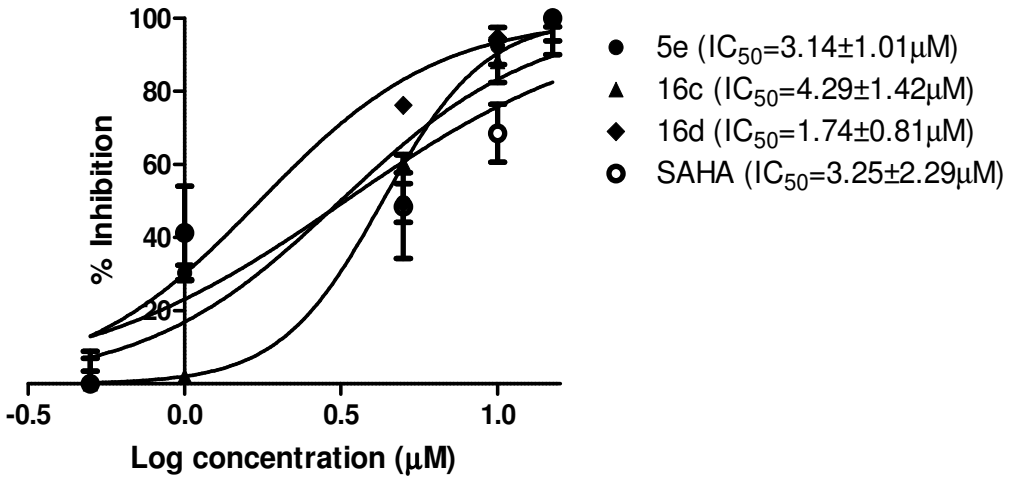

Figure 3.6. Dose response curve of compounds **5e, 16c** and **16d** with **SAHA** in HDAC8 inhibition assay using HDAC8 fluorometric drug discovery kit. The data represents mean ± SD (n=2).

3.3.5. CELLULAR STUDIES USING ANTICANCER CELL LINES

3.3.5.1. Antiproliferative assay using cancer cell lines

Cytotoxicity studies were performed on five different cell lines, i.e., B16F10 (murine melanoma cell line), HeLa (Human cervical cancer cell line), human breast cancer cell line (MCF-7), non-small cell lung cancer cell line (A549) and human acute T cell leukemia (Jurkat E6) by MTT assay method. All the synthesized compounds were evaluated at two different concentrations (100 and 10 μM) in triplicate. **SAHA** and **BG45** were taken as the standard reference compounds in the assay (Figure 3.7 (i-v)). From the assay results, it was observed that majority of the compounds displayed good cytotoxicity on all cell lines in a dose dependent fashion.

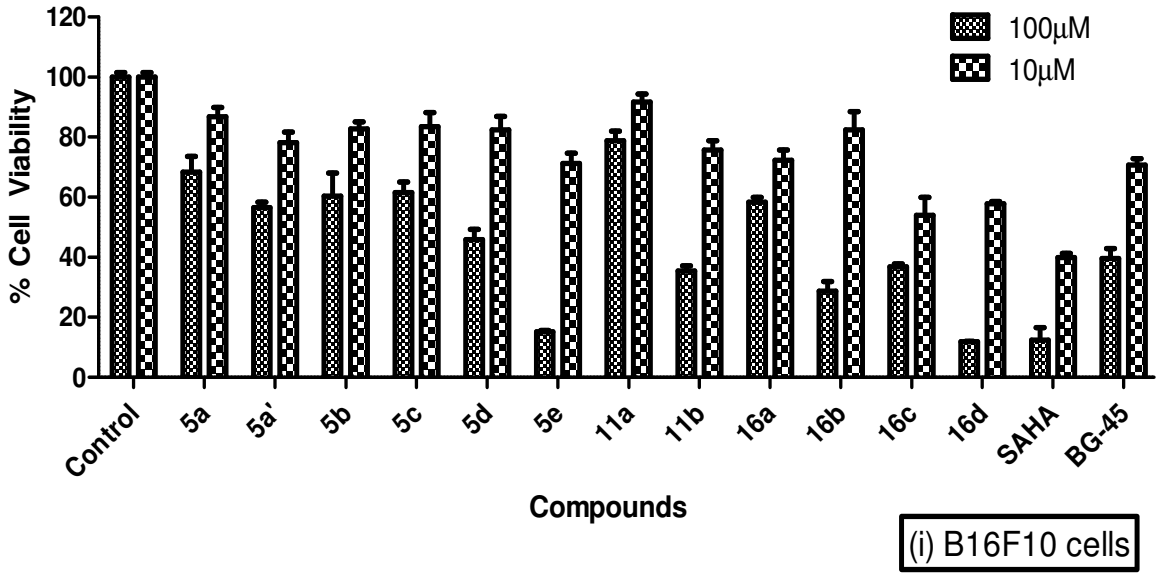

(i) B16F10 cells

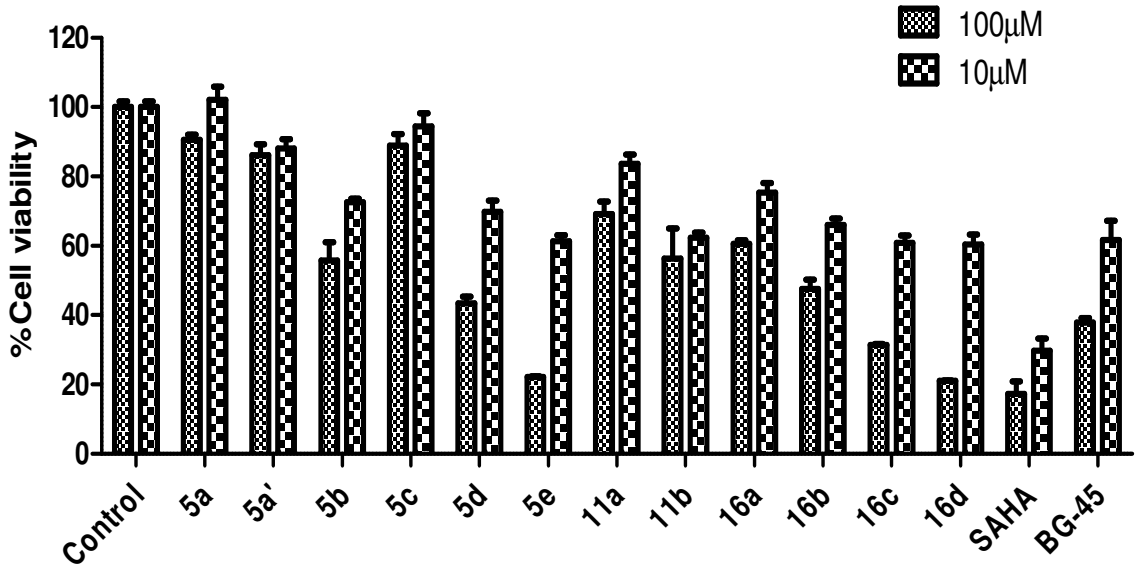

(ii) HeLa cell line

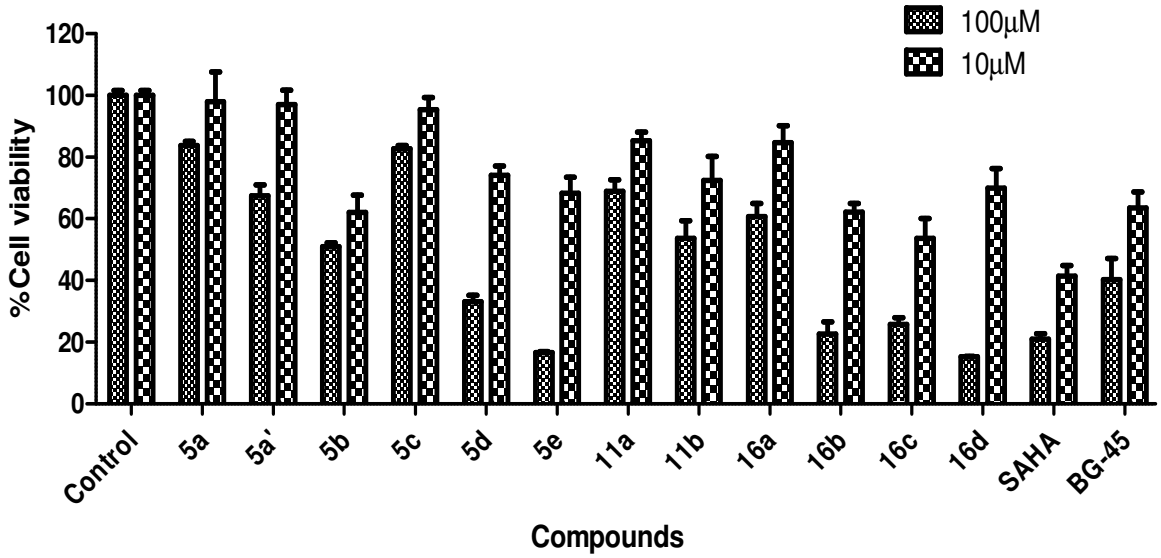

(iii) A-549 cells

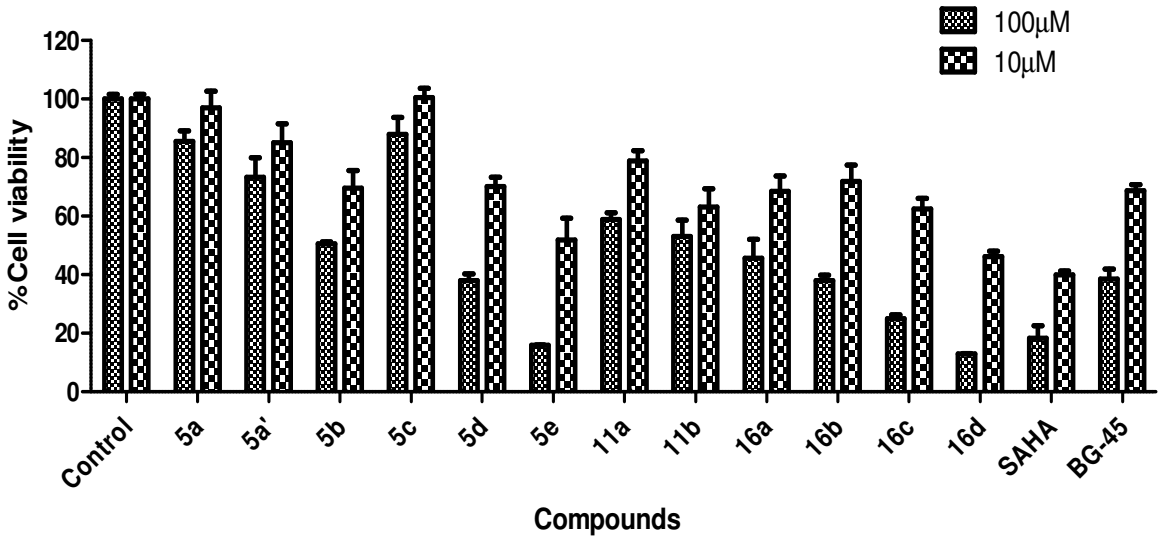

(iv) MCF-7 cells

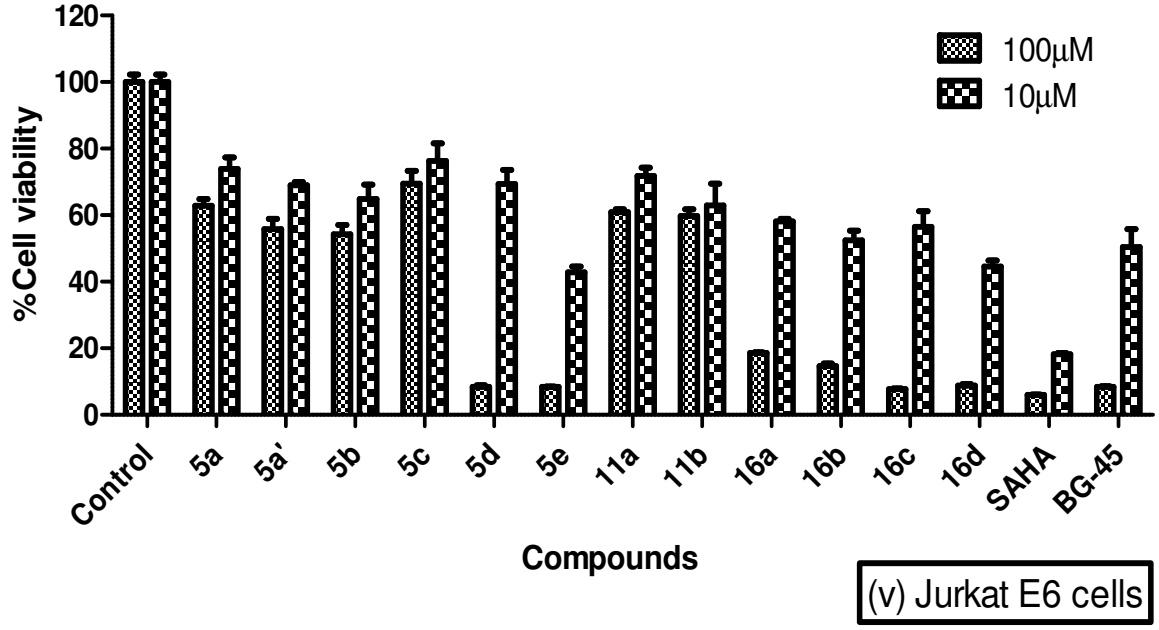

Figure 3.7 (i-v). Anticancer activity of new synthesized compounds in five different cell lines B16F10 (i), HeLa (ii), A-549 (iii), MCF-7 (iv), Jurkat E6 (v). Cells were treated with compounds at 100μM and 10μM in triplicate for 72 hours. Cell viability was measured by MTT reagent. Data represents mean ± SD (n=3).

All compounds were further evaluated for their 50% inhibitory concentration (IC_{50}) with a wider range of concentration. The cell viability after 72 hours of treatment was measured by MTT assay (Figure 3.8 (i-v)). IC_{50} values of all compounds on different five cell lines are represented in Table 3.3.

Table 3.3. IC_{50} values of target compounds on different cancer cell lines.

Compounds	**IC50 (μM)**				
	A-549	HeLa	MCF-7	B16F10	Jurkat E6
PT-162 (5a)	>50	>50	>50	>50	>50
PT-199(5a')	39.53	42.56	39.04	31.66	35.32
PT-241 (5b)	27.49	20.91	25.48	23.80	25.34
PT-225 (5c)	>50	>50	>50	>50	>50
PT-230 (5d)	17.85	18.02	19.12	17.08	14.96
PT-250 (5e)	11.55	11.93	12.16	9.71	8.65
PT-212 (11a)	36.70	44.79	38.19	31.29	28.49
PT-211 (11b)	30.29	34.38	27.92	23.80	27.13
PT-251 (16a)	33.84	25.86	25.98	27.70	30.34
PT-219 (16b)	20.24	15.45	24.43	18.31	17.95
PT-239 (16c)	12.17	12.03	15.24	16.21	13.71
PT-254 (16d)	9.12	10.97	11.42	9.76	7.19
SAHA	3.27	3.31	5.29	5.89	3.79
BG-45	21.43	24.53	26.01	29.60	17.33

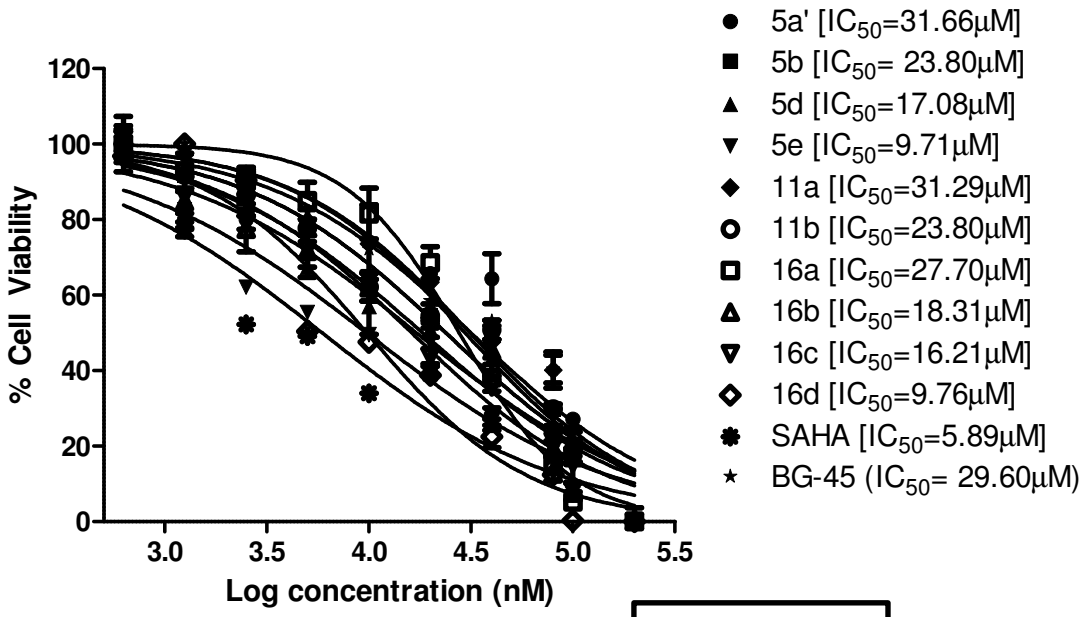

(i) B16F10 cells

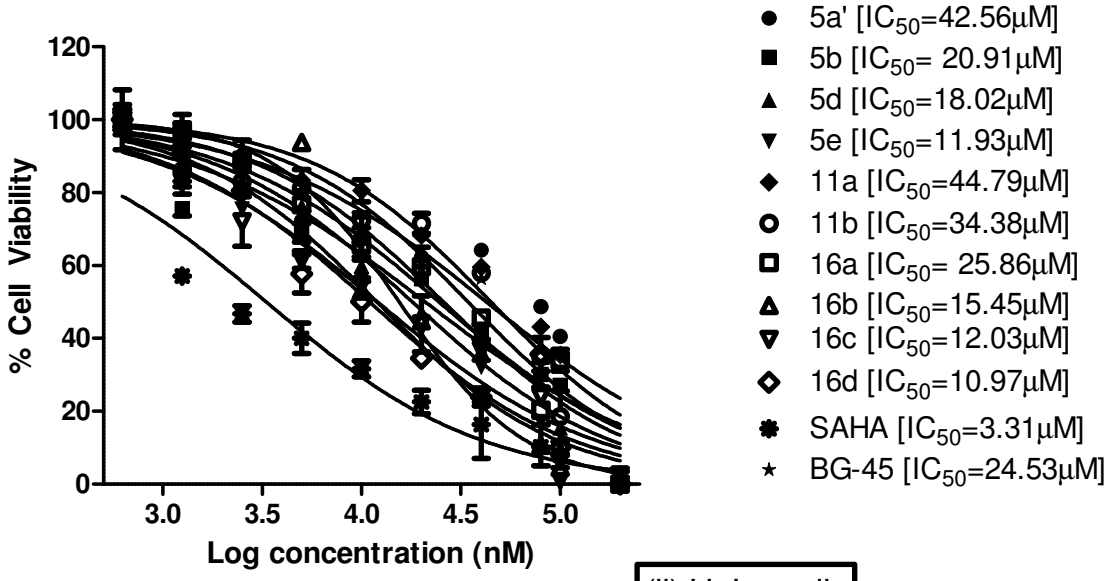

(ii) HeLa cells

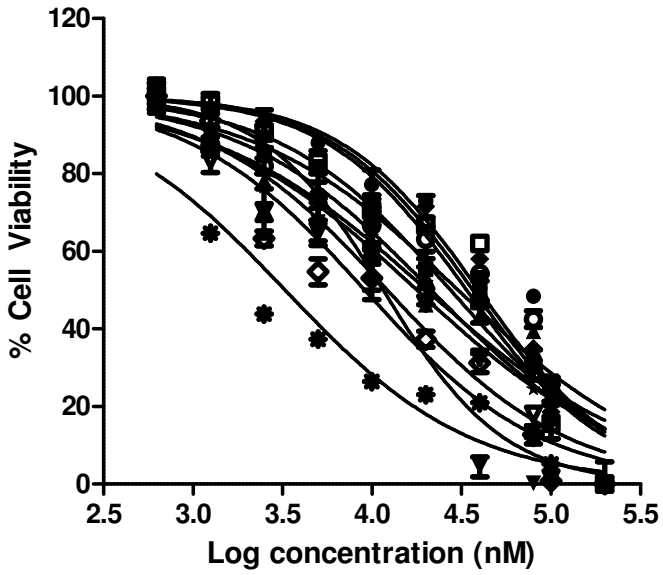

- 5a' (IC_{50}=39.53µM)
- 5b [IC_{50}= 27.49µM]
- 5d [IC_{50}=17.85µM]
- 5e [IC_{50}=11.55µM]
- 11a [IC_{50}=36.70µM]
- 11b [IC_{50}=30.29µM]
- 16a [IC_{50}=33.84µM]
- 16b [IC_{50}=20.24µM]
- 16c [IC_{50}=12.17µM]
- 16d [IC_{50}=9.12µM]
- SAHA [IC_{50}=3.27µM]
- BG-45 [IC_{50}=21.43µM]

(iii) A-549 cells

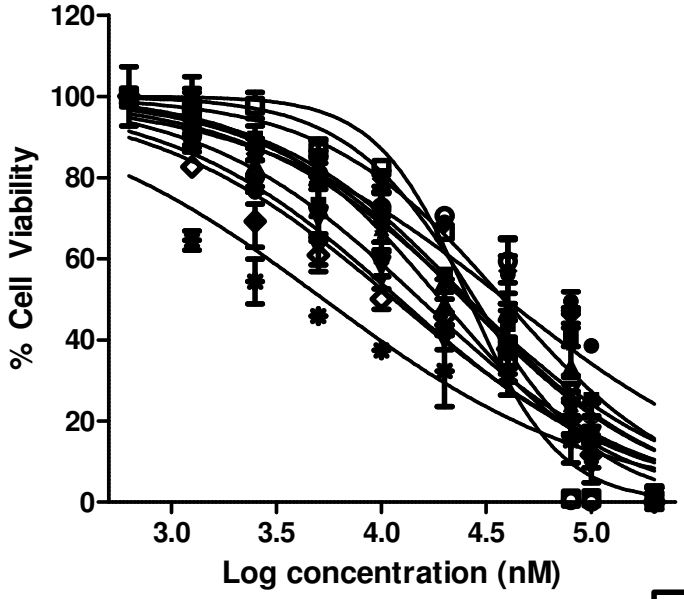

- 5a' [IC_{50}=39.04µM]
- 5b [IC_{50}=25.48µM]
- 5d [IC_{50}=19.12µM]
- 5e [IC_{50}=12.16µM]
- 11a [IC_{50}=38.19µM]
- 11b [IC_{50}=27.92µM]
- 16a [IC_{50}=25.98µM]
- 16b [IC_{50}=24.43µM]
- 16c [IC_{50}=15.24µM]
- 16d [IC_{50}=11.42µM]
- SAHA [IC_{50}=5.29µM]
- BG-45 [IC_{50}=26.01µM]

(iv) MCF-7 cells

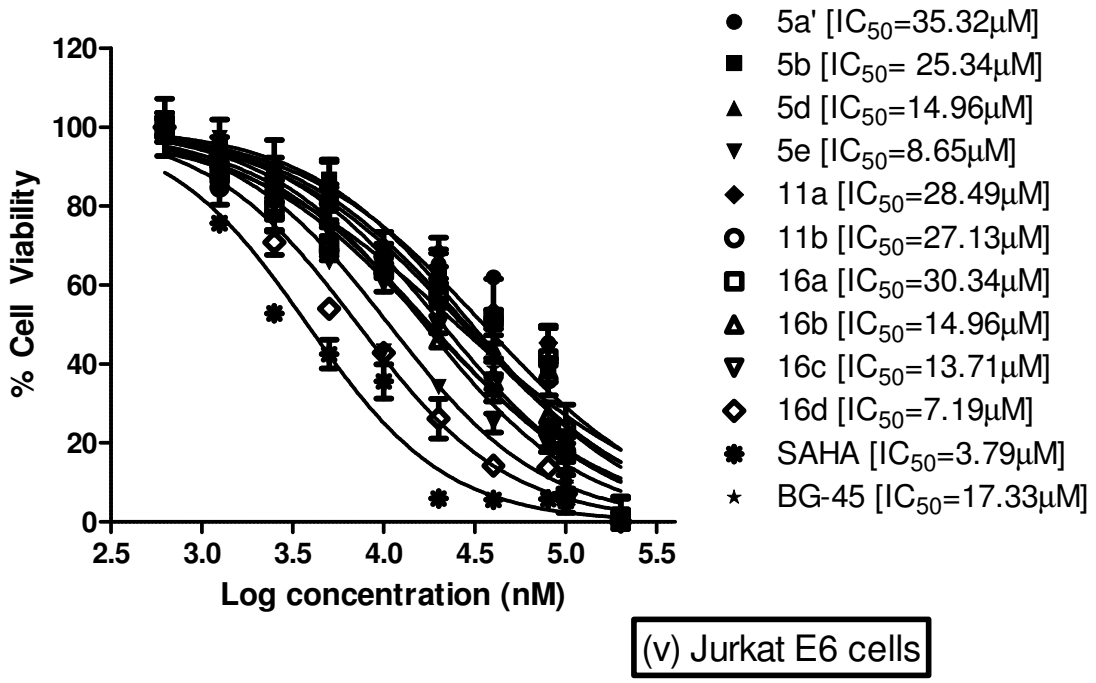

Figure 3.8 (i-v). Dose response curve and IC_{50} values of all novel compounds along with **BG-45** and **SAHA**. All compounds were explored in larger range of ten different concentrations on B16F10 (i), HeLa (ii), A-549 (iii), MCF-7 (iv) and Jurkat E6 (v) cells. Cells were treated with compounds for 72 hours and cell viability was measured by *in vitro* MTT assay method. Data represents mean ± SD (n=2) and plotted in dose response format. IC_{50} was calculated using nonlinear regression analysis method using Graph Pad Prism5.

We have tested the compounds for their anticancer activity on different solid tumor cell lines as well as leukemia cell line. From the result it was found that, all the compounds are showing good potential on all the cell lines with moderate difference with each other. The most potent response among these cell lines was observed in acute T cell leukemia (Jurkat E6) cells. From this series, compound **5e, 16c** and **16d** were found to be more efficient compared to others. The same trend in response we could find in enzyme inhibition assay

also. Hence, these three compounds were further tested to find out their apoptotic potential using Caspase3/7 assay in Jurkat E6 cells.

3.3.5.2. Apo-ONE® Homogeneous Caspase-3/7 Assay

Caspase 3/7 assay was performed using Apo-ONE® Homogeneous Caspase-3/7 Assay kit (Promega, USA). Caspase 3 and Caspase 7 are member of the cysteine-aspartic acid protease (caspase) family which plays central role in the execution-phase of cell apoptosis (Alnemri et al. 1996). Induction of apoptosis and activation of caspases can result from a variety of stimuli including growth factor withdrawal, exposure to radiation or chemotherapeutic agents, or initiation of the Fas/Apo-1 receptor-mediated cell death process (Nicholson and Thornberry 1997). Active caspases participate in a cascade of cleavage events that disable key homeostatic and repair enzymes and bring about systematic structural disassembly of dying cells (Kumar and Lavin 1996; Vaux and Strasser 1996).

Compound **5e**, **16c** and **16d** with **SAHA** and **BG-45** were tested for Caspase3/7 activity using Jurkat E6 cells. Results are displayed in Figure 3.9.

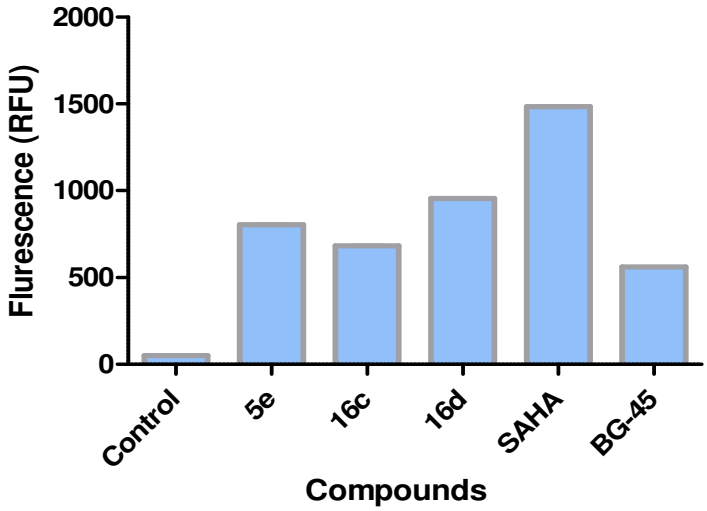

Figure 3.9. Caspase3/7 activation level of **5e, 16 c, 16d**, **SAHA** and **BG-45** in Jurkat E6 cell line compared to control. Compound treatment shows significant difference from control indicates increased apoptosis in cells.

Result demonstrated significant increase in Caspase3/7 activity compared to control cells (vehicle treated cells). Increased caspase3/7 activity indicates the induced apoptosis in cancer cells by the target compounds. This increased apoptosis level proves anticancer potential of novel derivatives.

3.4. MATERIALS AND METHODS

3.4.1. Chemistry

All starting materials and reagents were commercially available and used without further purification. All reactions were monitored by thin layer chromatography (TLC) using precoated plates with silica gel F254 from Merck Millipore Co., USA. UV light as well as staining reagent (ninhydrin solution) was used to detect the spots. ^{1}H and ^{13}C NMR spectrum were recorded in DMSO-d_6 using Bruker-400 MHz and chemical shifts reported in ppm using tetramethylsilane as internal standard. Mass spectroscopy was performed in LCMS-2020, Schimadzu using ESI mode. The Purity of the compounds were analyzed by Analytical LC/MS. Analysis was performed on a LCMS-8040 equipped with a photodiode array detector using a Shiseido C18 4.6×150 mm, 5µ column at a flow rate of 1 mL/min with isocratic flow (40% A: 60% ; Solvent A = water + 0.4% TFA , solvent B = methanol).

Procedure A. preparation of *tert*-butyl 4-(phenylcarbamoyl)piperidine-1-carboxylate (3a)

Compound **2** (1 g, 4.361 mmol) was dissolved in DCM. To this mixture, 1-(3-Dimethyl aminopropyl)-3-ethylcarbodiimide hydrochloride (1.67 g, 8.72 mmol) and 1-hydroxybenzotriazole (1.17 g, 8.72 mmol) was added and stirred for 20 minutes in nitrogen environment. Aniline (0.796 mL, 8.72 mmol) and triethylamine (1.8 mL, 13.08 mmol) was added to above mixture and stirred overnight. Reaction mixture was diluted with DCM and washed with saturated aqueous solution of sodium bicarbonate. DCM layer dried over sodium sulphate and evaporated. The crude was purified by column chromatography (EtOAc: Hexane; 2.5:7.5) to get 0.9 g compound **3a** as white solid (yield 75.35%). ^{1}H NMR (400 MHz, DMSO-d_6) δ 9.97 (s, 1H), 7.62 – 7.58 (m, 2H), 7.31 – 7.25 (m, 2H), 7.04 – 6.99 (m, 1H), 3.99 (d, *J* = 12.3 Hz, 2H), 3.17 – 2.95 (m, 1H), 2.77 (s, 2H), 1.80 – 1.73 (m, 2H), 1.49 (td, *J* = 12.5, 4.5 Hz, 2H), 1.41 (s, 9H). $C_{17}H_{24}N_2O_3$ [M]: 304.18; MS (ESI) *m/z*: $[M+Na]^+$: 304.38 $[M-H]^+$: 303

***tert*-butyl 4-(benzylcarbamoyl)piperidine-1-carboxylate (3b)**

Benzylamine (0.956 mL, 8.72 mmol) and compound **2** (1g, 4.36 mmol) were reacted according to procedure A afforded 0.314 g of cream solid (yield 23%). ^{1}H NMR (400 MHz, DMSO-d_6) δ 8.35 (t, *J* = 5.8 Hz, 1H), 7.31 (dd, *J* = 10.6, 4.3 Hz, 2H), 7.22 (t, *J* = 6.4 Hz, 3H), 4.25 (d, *J* = 5.9 Hz, 2H), 3.95 (d, *J* = 12.2 Hz, 2H), 2.73 (s, 2H), 2.35 (m, 1H), 1.68 (d, *J* = 14.7 Hz, 2H), 1.46 (m, 1H), 1.39 (s, 9H). $C_{18}H_{26}N_2O_3$ [M]: 318.19; MS (ESI) *m/z*: $[M+Na]^+$: 341 $[M-H]^+$: 317

***tert*-butyl 4-(naphthalen-1-ylcarbamoyl)piperidine-1-carboxylate (3c)**

According to procedure A, 1-naphthylamine (0.5 g, 3.49 mmol) and compound **2** (0.4 g, 1.74 mmol) were reacted to get 0.150 g of product as brown semisolid (yield 33.3%). ^{1}H NMR (400 MHz, DMSO-d_6) δ 8.67 (s, 1H), 7.92 (m, 2H), 7.74 (d, *J* = 7.9 Hz, 1H), 7.52 – 7.40 (m, 4H), 3.53 – 3.49 (m, 4H), 3.43 – 3.39 (m, 3H), 1.44 (s, 9H). $C_{21}H_{26}N_2O_3$ [M]: 354.44; MS (ESI) *m/z*: $[M-H]^+$: 353

***tert*-butyl 4-([1,1'-biphenyl]-4-ylcarbamoyl)piperidine-1-carboxylate (3d)**

Following procedure A, compound **3d** was synthesized from 4-aminobiphenyl (0.73 mg, 2.18 mmol) and compound **2** (0.5 g, 2.18 mmol) as cream solid (0.5 g, 60%). ^{1}H NMR (400 MHz, DMSO-d_6) δ 10.02 (s, 1H), 7.70 (d, *J* = 8.7 Hz, 2H), 7.65 – 7.60 (m, 4H), 7.44 (t, *J* = 7.7 Hz, 2H), 7.34 – 7.30 (m, 1H), 4.01 (d, *J* = 12.2 Hz, 2H), 3.33 (s, 5H), 1.79 (d, *J* = 13.3 Hz, 2H), 1.41 (s, 9H). $C_{23}H_{28}N_2O_3$ [M]: 354.44; MS (ESI) *m/z*: $[M-H]^+$: 379

***tert*-butyl 4-(quinolin-4-ylcarbamoyl)piperidine-1-carboxylate (3e)**

4-aminoquinoline (0.5 g, 3.46 mmol) and compound 2 (1.19 g, 5.20 mmol) were reacted following procedure A to get 0.237 g of compound **3e** as pale yellow solid (yield 20%). ^{1}H NMR (400 MHz, DMSO-d_6) δ 10.20 (s, 1H), 8.78 (d, *J* = 5.0 Hz, 1H), 8.36 (dd, *J* = 8.5, 0.7 Hz, 1H), 8.08 (d, *J* = 5.0 Hz, 1H), 8.00 (dd, *J* = 8.4, 0.8 Hz, 1H), 7.77 (m, 1H), 7.64 (m, 1H), 3.34 (s, 5H), 1.89 (dd, *J* = 13.7, 2.8 Hz, 2H), 1.78 (dd, *J* = 13.3, 3.2 Hz, 2H), 1.39 (s, 9H). $C_{20}H_{25}N_3O_3$ [M]: 355.43; MS (ESI) *m/z*: $[M+H]^+$: 356, $[M-H]^+$: 354

Procedure B: General procedure for synthesis of 4a, 4a', 4b, 4c, 4d and 4e

Compound **3a, 3b, 3c, 3d, 3e** were dissolved in DCM and kept in ice bath to get 0°C. Trifluoroacetic acid (50% v/v of total volume of reaction mixture) was added and stirred for

2 hours under nitrogen environment. After completion of the reaction, the solvent was evaporated and product was found pure enough to be used for next step. To the same compound, methyl 3-bromopropionate (1.5 equivalents) for the synthesis of **4a** and methyl 4-bromobutyrate (1.5 equivalents) for the synthesis of **4a', 4b, 4c, 4d** and **4e**, potassium carbonate (3 equivalents) and acetonitrile was added. The reaction mixture was refluxed at 90°C for 5 hours. The mixture was cooled and poured in water. The product was extracted in ethyl acetate, was concentrated and purified by column chromatography (EtOAc: methanol; 9.5:0.5).

methyl 3-(4-(phenylcarbamoyl)piperidin-1-yl)propanoate (4a)

Yield 52.5%, pale brown solid, ^{1}H NMR (400 MHz, DMSO-d_6) δ 9.90 (s, 1H), 7.60 (dd, *J* = 8.6, 1.0 Hz, 2H), 7.31 – 7.25 (m, 2H), 7.02 (t, *J* = 7.4 Hz, 1H), 3.60 (s, 3H), 3.34 (s, 4H), 2.34 (t, *J* = 7.1 Hz, 3H), 1.83 – 1.65 (m, 6H). $C_{16}H_{22}N_2O_3$ [M]: 290.16; MS (ESI) *m/z*: $[M+H]^+$: 291

methyl 4-(4-(phenylcarbamoyl)piperidin-1-yl)butanoate (4a')

Yield 57.8%, pale yellow semi solid, ^{1}H NMR (400 MHz, DMSO-d_6) δ 9.90 (s, 1H), 7.60 (dd, *J* = 8.6, 1.0 Hz, 2H), 7.31 – 7.25 (m, 2H), 7.02 (t, *J* = 7.4 Hz, 1H), 3.60 (s, 3H), 3.34 (s, 4H), 3.00 (s, 2H), 2.34 (t, *J* = 7.1 Hz, 3H), 1.83 – 1.65 (m, 6H). $C_{17}H_{24}N_2O_3$ [M]: 304.18; MS (ESI) *m/z*: $[M+H]^+$: 305

methyl 4-(4-(benzylcarbamoyl)piperidin-1-yl)butanoate (4b)

Yield 80%, pale yellow thick oil, ^{1}H NMR (400 MHz, DMSO-d_6) δ 7.25 (m, 5H), 7.06 (t, *J* = 5.8 Hz, 1H), 4.23 (d, *J* = 5.8 Hz, 2H), 3.58 (s, 4H), 3.30 (dd, *J* = 9.7, 5.0 Hz, 4H), 2.29 (m, 8H), 1.69 (m, 2H). $C_{17}H_{24}N_2O_3$ [M]: 304.18; MS (ESI) *m/z*: $[M+H]^+$: 319

methyl 4-(4-(naphthalen-1-ylcarbamoyl)piperidin-1-yl)butanoate (4c)

Yield 60%, pale yellow semi solid, ^{1}H NMR (400 MHz, DMSO-d_6) δ 8.04 – 8.01 (m, 1H), 7.95 – 7.92 (m, 1H), 7.76 (d, *J* = 8.2 Hz, 1H), 7.64 (d, *J* = 7.4 Hz, 1H), 7.56 – 7.52 (m, 2H), 7.51 – 7.46 (m, 1H), 3.60 (s, 3H), 3.59 -3.58 (m, 2H), 1.91 (s, 3H), 1.76 (m, 5H), 1.25 (d, *J* = 9.3 Hz, 5H). $C_{21}H_{26}N_2O_3$ [M]: 354.44; MS (ESI) *m/z*: $[M+H]^+$: 355

methyl 4-(4-([1,1'-biphenyl]-4-ylcarbamoyl)piperidin-1-yl)butanoate (4d)

Yield 89%, cream color solid, ^{1}H NMR (400 MHz, DMSO-d_6) δ 8.60 (s, 1H), 7.65 – 7.60 (m, 2H), 7.57 (d, *J* = 9.0 Hz, 4H), 7.42 (t, *J* = 7.6 Hz, 2H), 7.30 (t, *J* = 7.8 Hz, 1H), 3.59 (s, 3H), 3.44 (s, 5H), 2.39 – 2.29 (m, 8H), 1.76 – 1.68 (m, 2H). $C_{23}H_{28}N_2O_3$ [M]: 380.48; MS (ESI) *m/z*: $[M+H]^+$: 381, $[M-H]^+$: 379

methyl 4-(4-([1,1'-biphenyl]-4-ylcarbamoyl)piperidin-1-yl)butanoate (4e)

Yield 59%, yellow solid, ^{1}H NMR (400 MHz, DMSO-d_6) δ 10.15 (s, 1H), 8.78 (d, *J* = 5.0 Hz, 1H), 8.36 (d, *J* = 7.8 Hz, 1H), 8.08 (d, *J* = 5.0 Hz, 1H), 7.99 (dd, *J* = 8.4, 0.8 Hz, 1H), 7.77 (m, 1H), 7.63 (m, 1H), 3.60 (s, 3H), 2.94 (d, *J* = 10.3 Hz, 2H), 2.77 – 2.68 (m, 1H), 2.33 (t, *J* = 7.2 Hz, 4H), 1.98 (s, 2H), 1.91 – 1.83 (m, 2H), 1.71 (m,4H). $C_{20}H_{25}N_3O_3$ [M]: 355.43; MS (ESI) m/z: $[M+H]^+$: 356, $[M-H]^+$: 354

Procedure C. General procedure for synthesis of 5a, 5a', 5b, 5c, 5d and 5e

Compound **4a, 4a', 4b, 4c, 4d** and **4e** were dissolved in methanol. 50% w/v aqueous hydroxylamine (18.4 equivalents) was added and mixture was stirred for 15 minutes. 1M NaOH (2 equivalents) was added and reaction was stirred for 2 hours at room temperature. It was concentrated in reduced pressure and resultant solid was dissolved in ice cold water.

The pH was adjusted to 7 with 1M HCl and product was precipitated. No further purification was required. The product was dried in vacuum oven.

1-(3-(hydroxyamino)-3-oxopropyl)-*N*-phenylpiperidine-4-carboxamide (5a)

Yield 40%, brown powder, ^{1}H NMR (400 MHz, DMSO-d_6) δ 10.22 (s, 1H), 7.63 (d, J = 7.7 Hz, 2H), 7.29 (t, J = 7.9 Hz, 2H), 7.04 (t, J = 7.4 Hz, 1H), 3.52 (d, J = 11.6 Hz, 2H), 3.37 (s, 2H), 3.28 (t, J = 7.6 Hz, 2H), 2.86 (t, J = 7.6 Hz, 2H), 2.65 (s, 1H), 2.01 (s, 4H). ^{13}C NMR (101 MHz, DMSO-d_6) δ 172.27, 172.05, 139.62, 129.11, 123.66, 119.67, 51.93, 51.50, 29.03, 26.15. HPLC Rt: 1.986, LC/MS calculated for expected C15H21N3O3 [M]: 291.35; Found: [M]+: 291

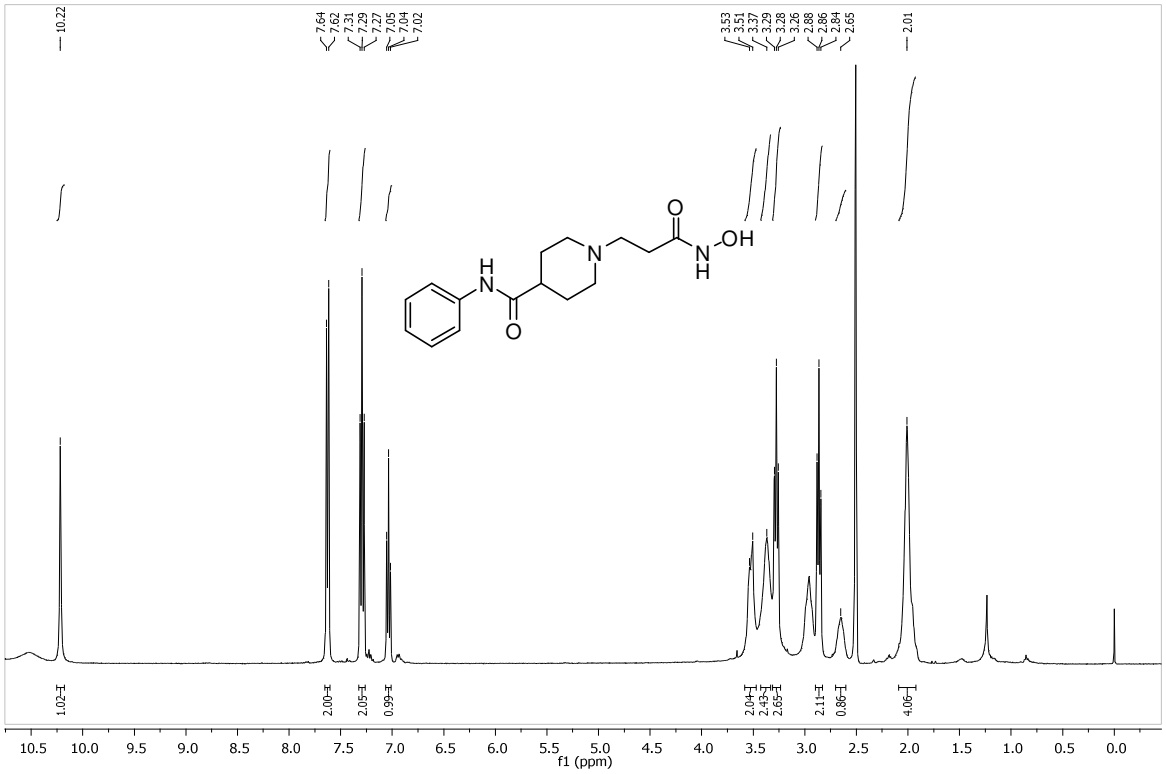

^{1}H NMR of **5a**

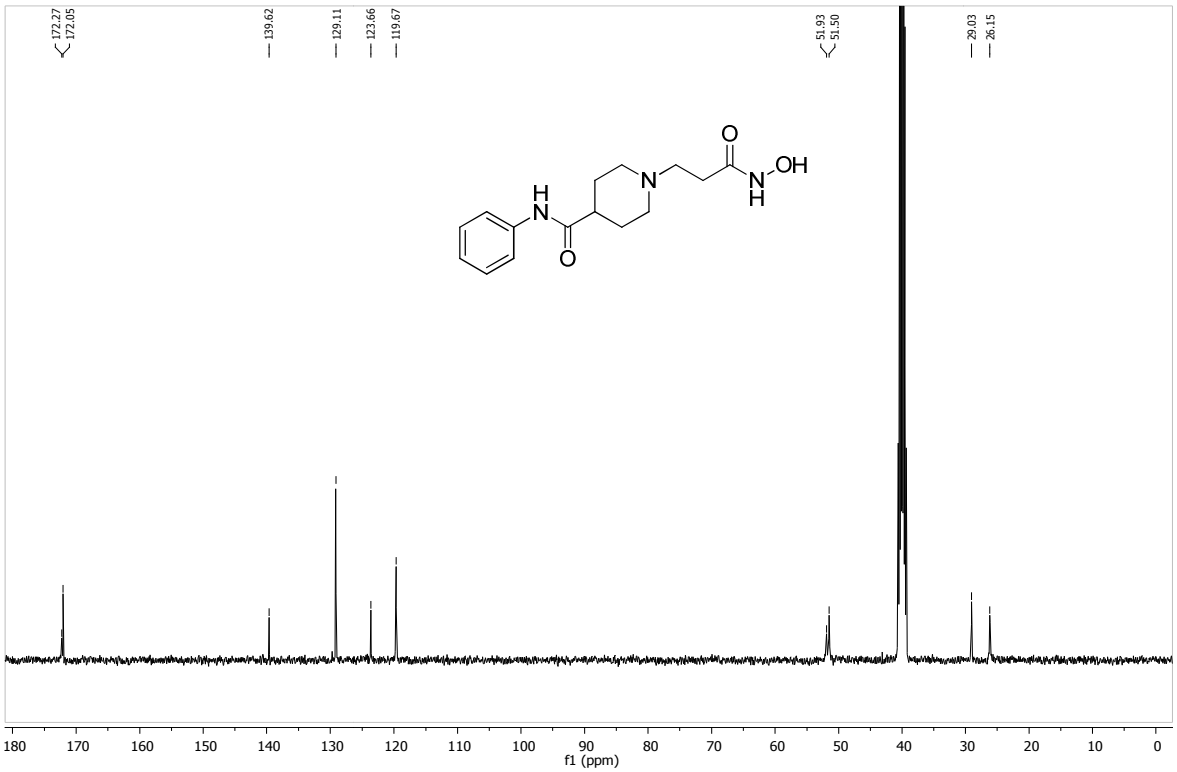

^{13}C NMR of **5a**

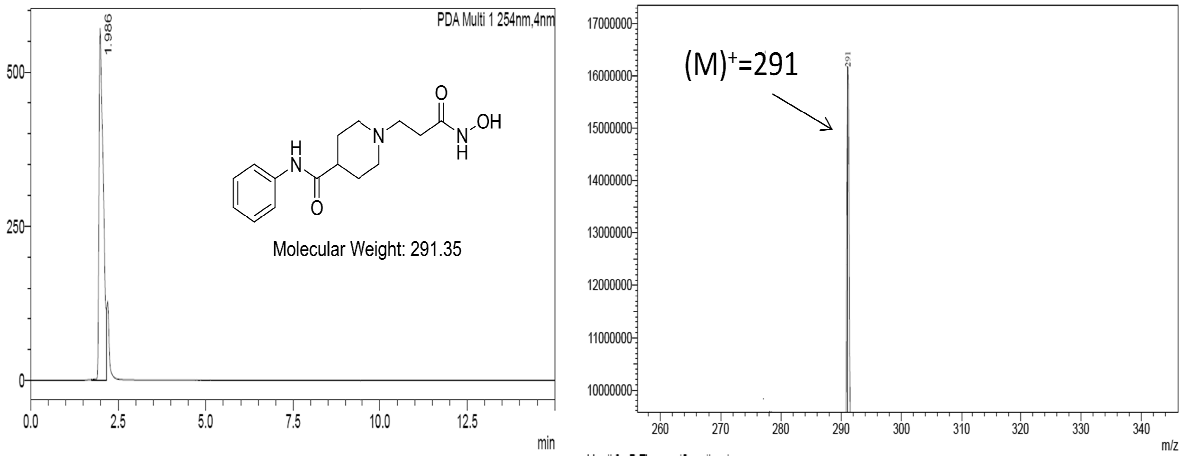

LC/MS of **5a**

1-(4-(hydroxyamino)-4-oxobutyl)-*N*-phenylpiperidine-4-carboxamide (5a')

Yield 66.6%, yellow oil, ^{1}H NMR (400 MHz, DMSO-d_6) δ 7.61 (d, J = 7.6 Hz, 2H), 7.30 (t, J = 7.9 Hz, 2H), 7.04 (t, J = 7.4 Hz, 1H), 3.58 (d, J = 36.1 Hz, 3H), 3.09 – 3.02 (m, 2H), 2.39

(m, 1H), 2.11 – 1.88 (m, 9H). ^{13}C NMR (101 MHz, DMSO-d_6) δ 173.89, 155.13, 140.67, 128.76, 122.48, 120.18, 55.37, 51.12, 44.17, 41.33, 31.25, 19.16 HPLC Rt: 1.995, LC/MS calculated for expected $C_{16}H_{23}N_3O_3$ [M]: 305.37; Found: $[M+H]^+$: 306

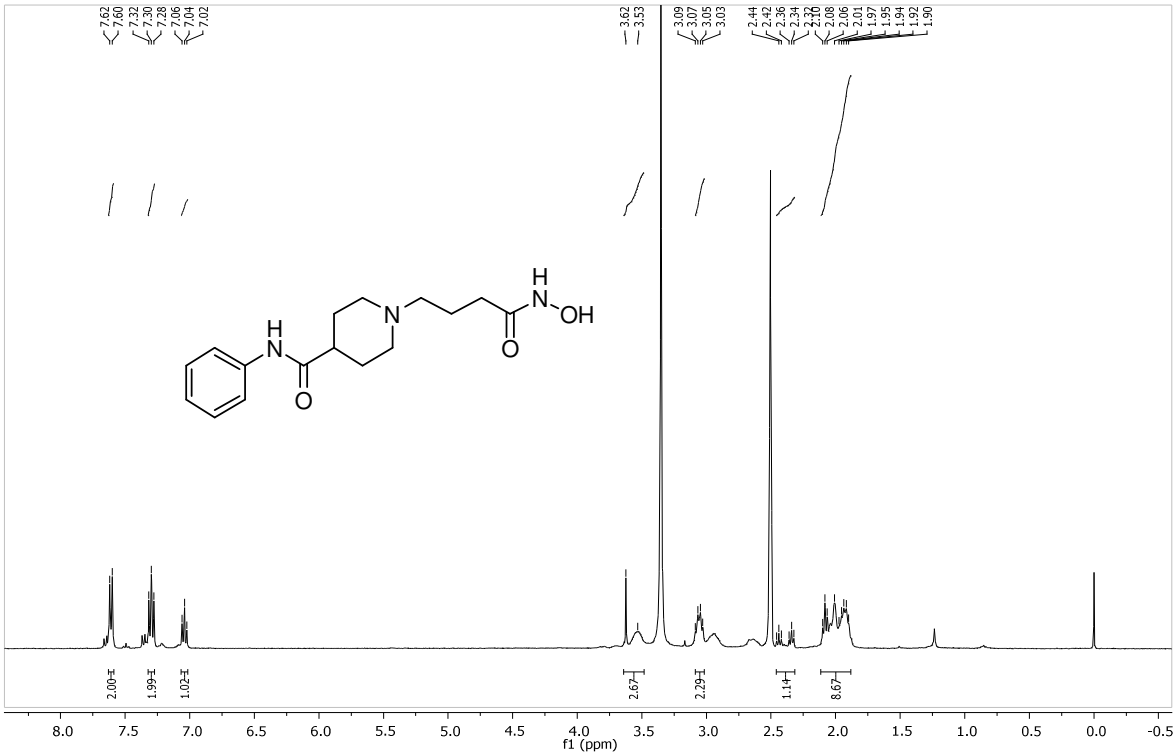

^{1}H NMR of **5a'**

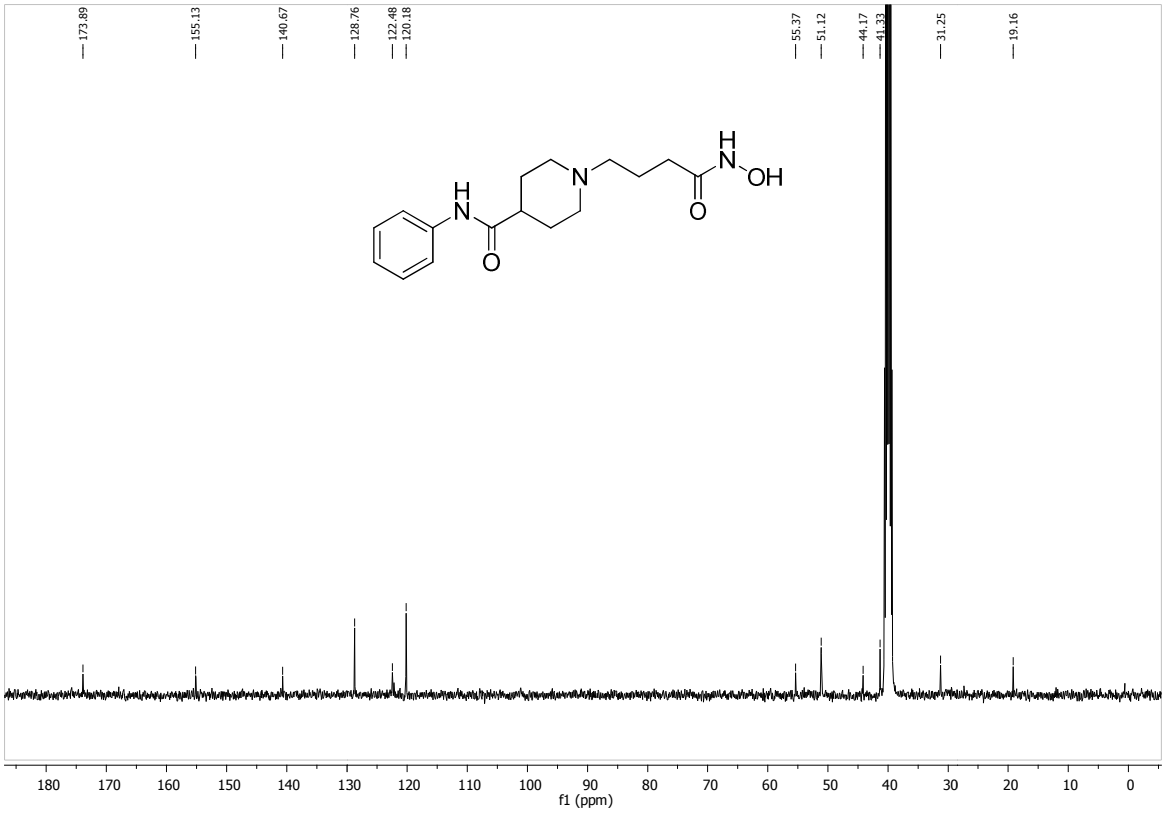

^{13}C NMR of **5a'**

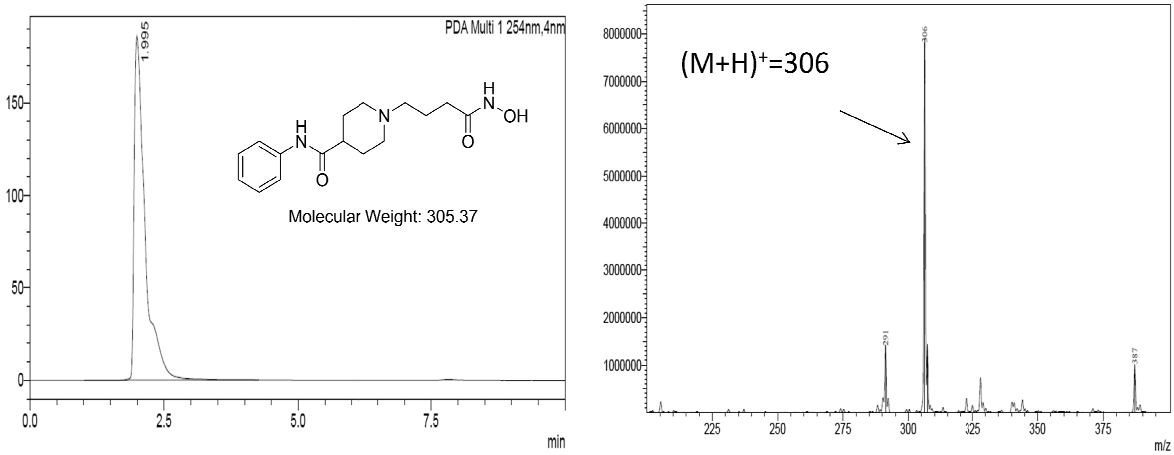

LC/MS of **5a'**

***N*-benzyl-1-(4-(hydroxyamino)-4-oxobutyl)piperidine-4-carboxamide (5b)**

Yield 90%, cream color solid, ^{1}H NMR (400 MHz, DMSO-d_6) δ 7.34 – 7.24 (m, 5H), 7.20 (m, 1H), 4.23 (d, J = 5.7 Hz, 2H), 3.42 (s, 4H), 2.50 (d, J = 4.2 Hz, 4H), 2.46 – 2.40 (m, 2H),

2.24 – 1.99 (m, 2H), 1.71 (m, 2H), 1.30 – 1.21 (m, 1H). ^{13}C NMR (101 MHz, DMSO-d_6) δ 169.53, 157.83, 141.38, 127.49, 126.85, 57.11, 52.56, 43.82, 43.23, 43.04, 30.44, 22.02 HPLC Rt: 2.025, LC/MS calculated for expected $C_{17}H_{25}N_3O_3$ [M]: 319.40; Found: $[M+H]^+$: 320

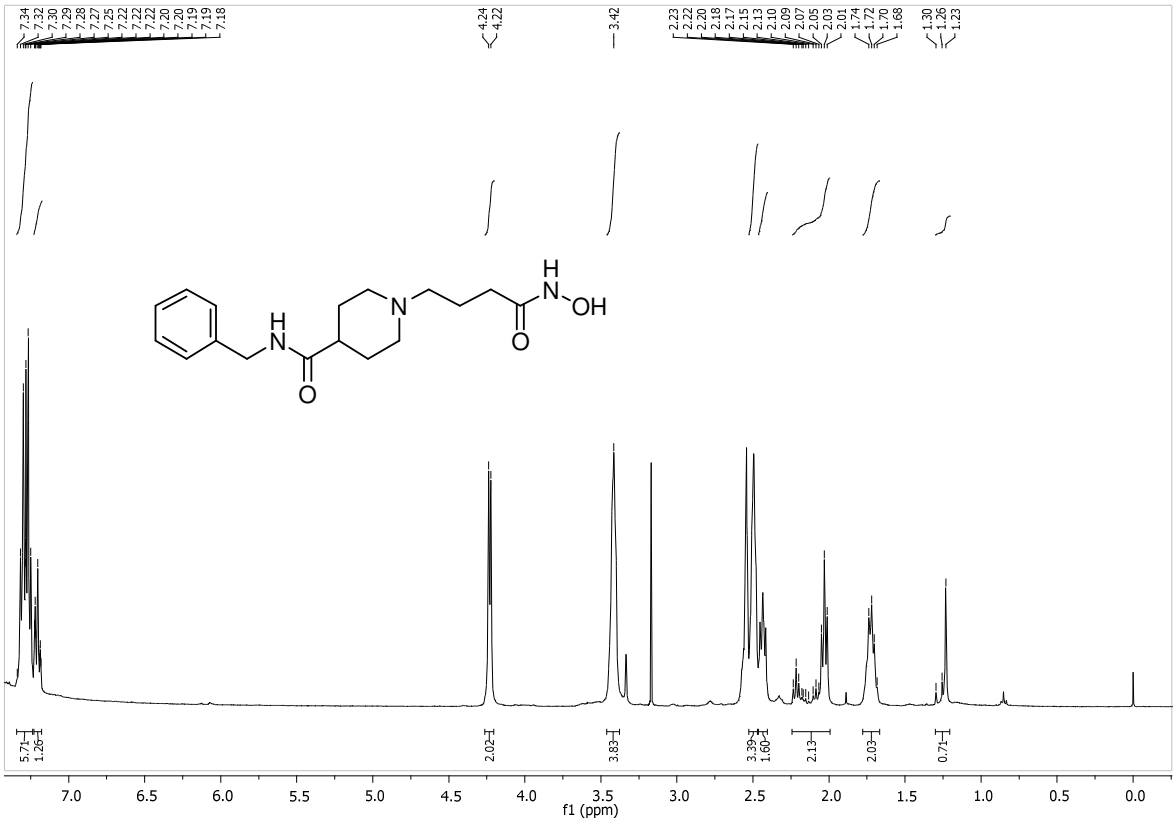

^{1}H NMR of **5b**

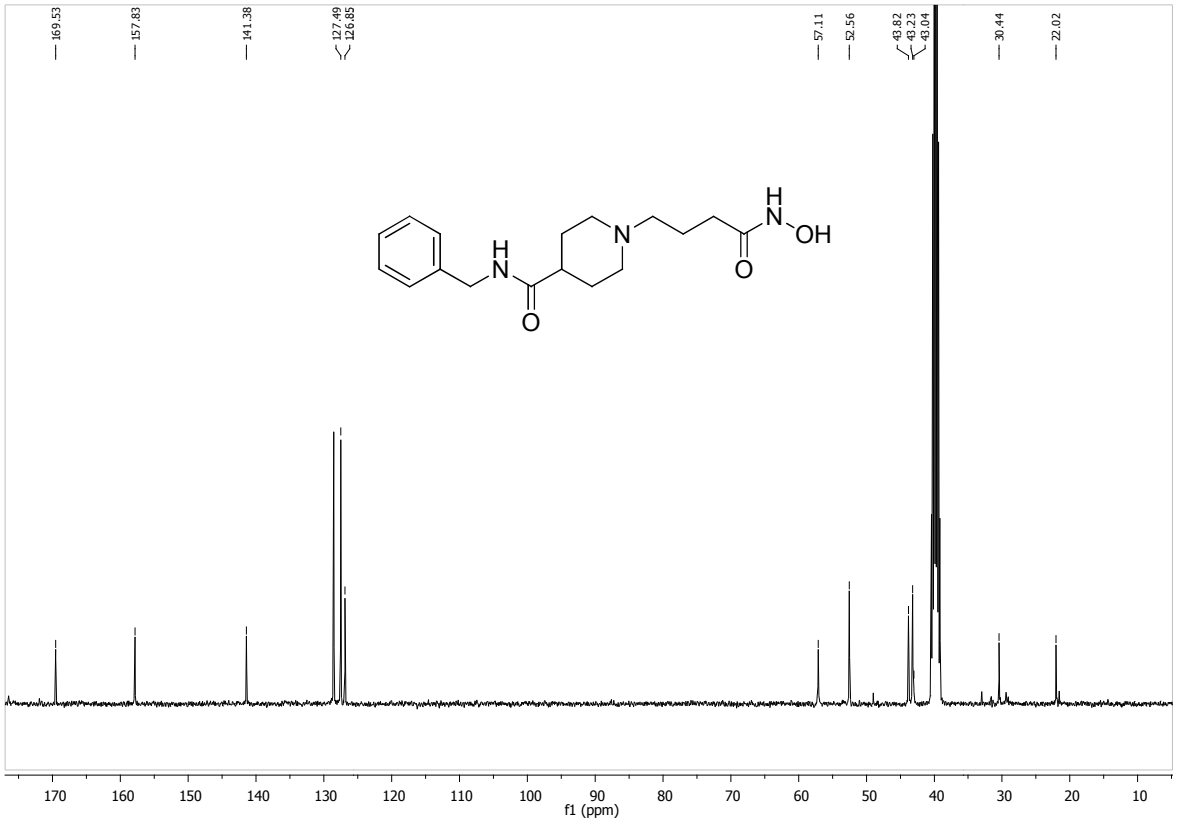

^{13}C NMR of **5b**

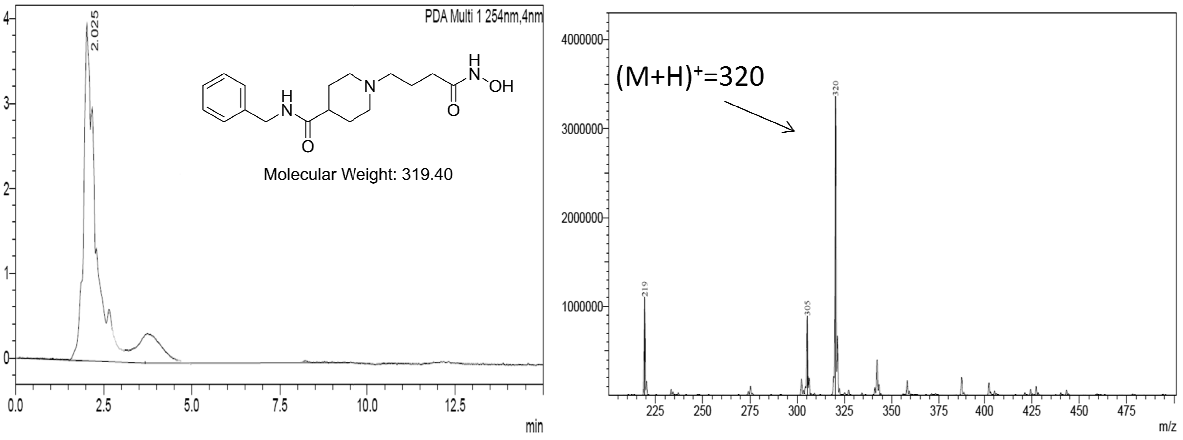

LC/MS of **5b**

1-(4-(hydroxyamino)-4-oxobutyl)-*N*-(naphthalen-1-yl)piperidine-4-carboxamide (5c)

Yield 92%, beige color solid, ^{1}H NMR (400 MHz, DMSO-d_6) δ 9.03 (s, 1H), 7.99 – 7.90 (m, 2H), 7.76 (d, J = 7.8 Hz, 1H), 7.54 – 7.42 (m, 5H), 4.32 (d, J = 8.1 Hz, 2H), 3.21 – 3.09 (m, 5H), 2.37 (m, 4H), 2.14 – 1.88 (m, 4H). ^{13}C NMR (101 MHz, DMSO-d_6) δ 175.09, 173.92, 158.74, 141.69, 138.78, 134.70, 134.25, 126.60, 124.49, 120.21, 116.42, 102.18, 55.62, 51.22, 31.23, 25.92, 25.55, 19.18.HPLC Rt: 2.467, LC/MS calculated for expected $C_{20}H_{25}N_3O_3$ [M]: 355.43; Found: $[M+H]^+$: 356

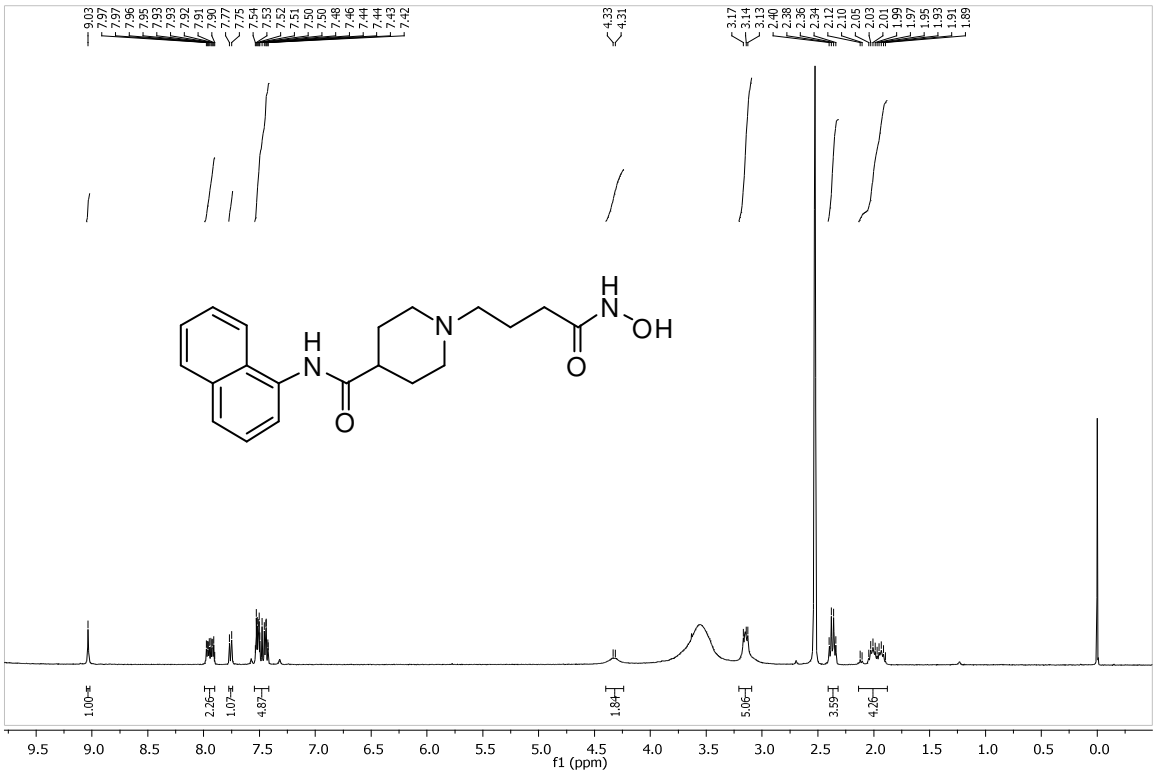

^{1}H NMR of **5c**

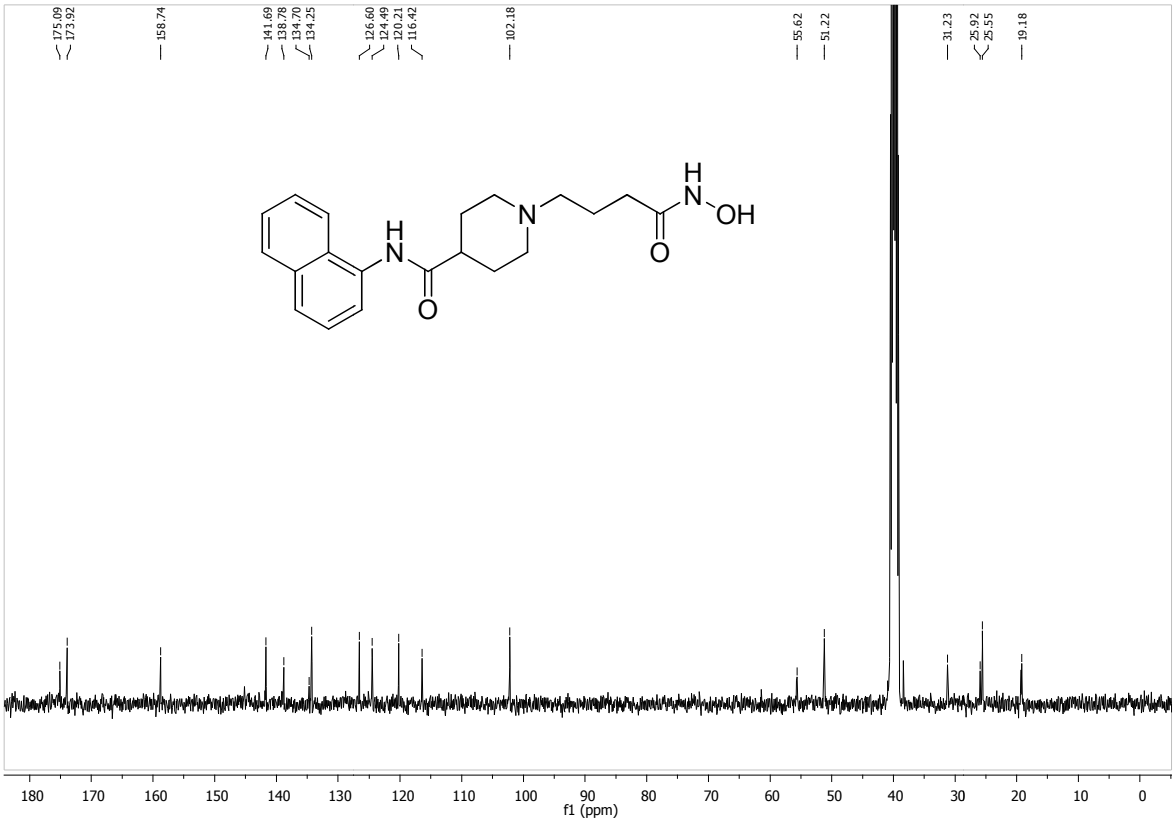

^{13}C NMR of **5c**

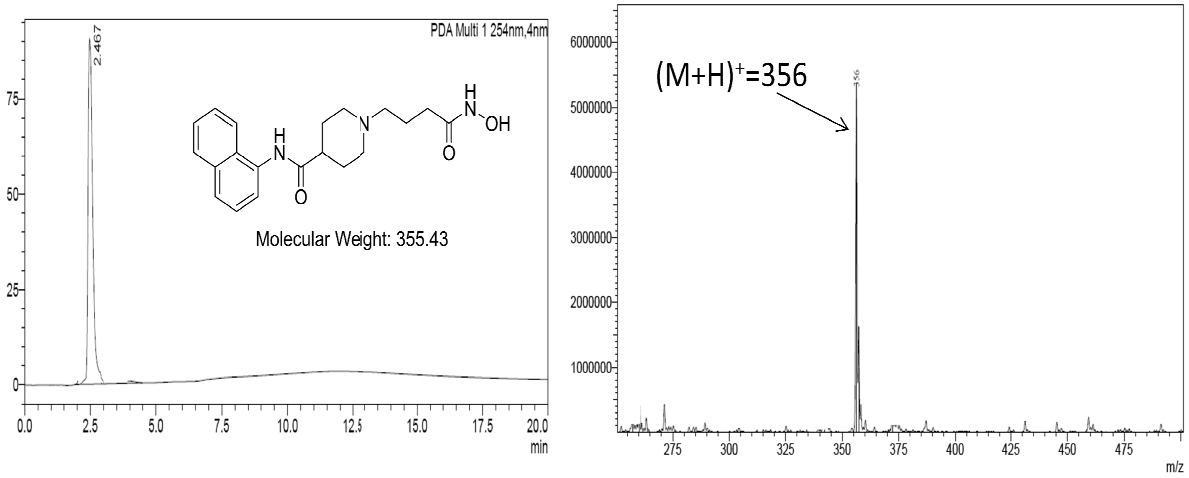

LC/MS of **5c**

***N*-([1,1'-biphenyl]-4-yl)-1-(4-(hydroxyamino)-4-oxobutyl)piperidine-4-carboxamide (5d)**

Yield 82%, creamish yellow solid, ^{1}H NMR (400 MHz, DMSO-d_6) δ 7.76 (d, J = 8.7 Hz, 2H), 7.63 (t, J = 8.4 Hz, 4H), 7.44 (t, J = 7.7 Hz, 2H), 7.33 (t, J = 7.3 Hz, 1H), 3.48 (d, J = 12.0 Hz, 2H), 3.05 (m, 8H), 2.75 (m, 1H), 2.35 (t, J = 7.3 Hz, 1H), 1.98 (m, 6H). ^{13}C NMR (101 MHz, DMSO-d_6) δ 173.94, 172.44, 140.15, 139.21, 135.19, 129.36, 127.45, 127.25, 126.67, 120.01, 55.73, 51.36, 31.21, 26.09, 19.28. HPLC Rt: 2.689, LC/MS calculated for expected $C_{22}H_{27}N_3O_3$ [M]: 381.47; Found: $[M+H]^+$: 382

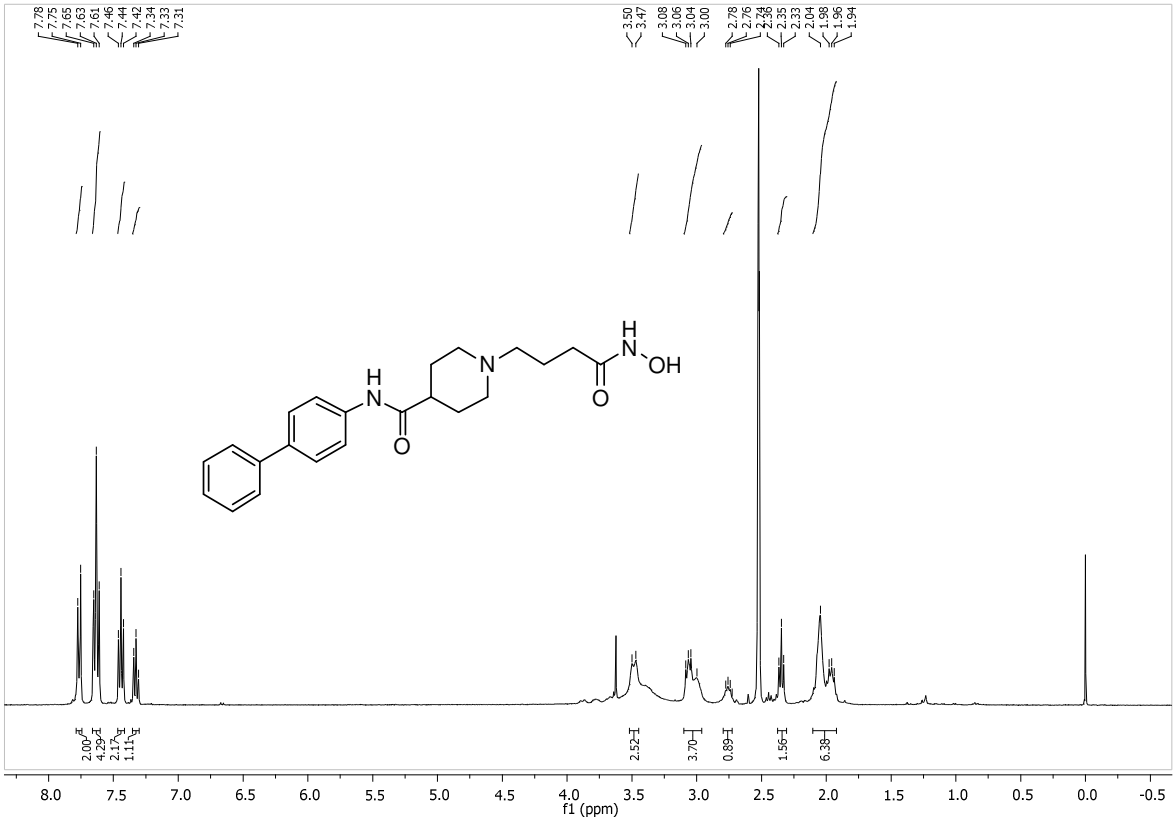

^{1}H NMR of **5d**

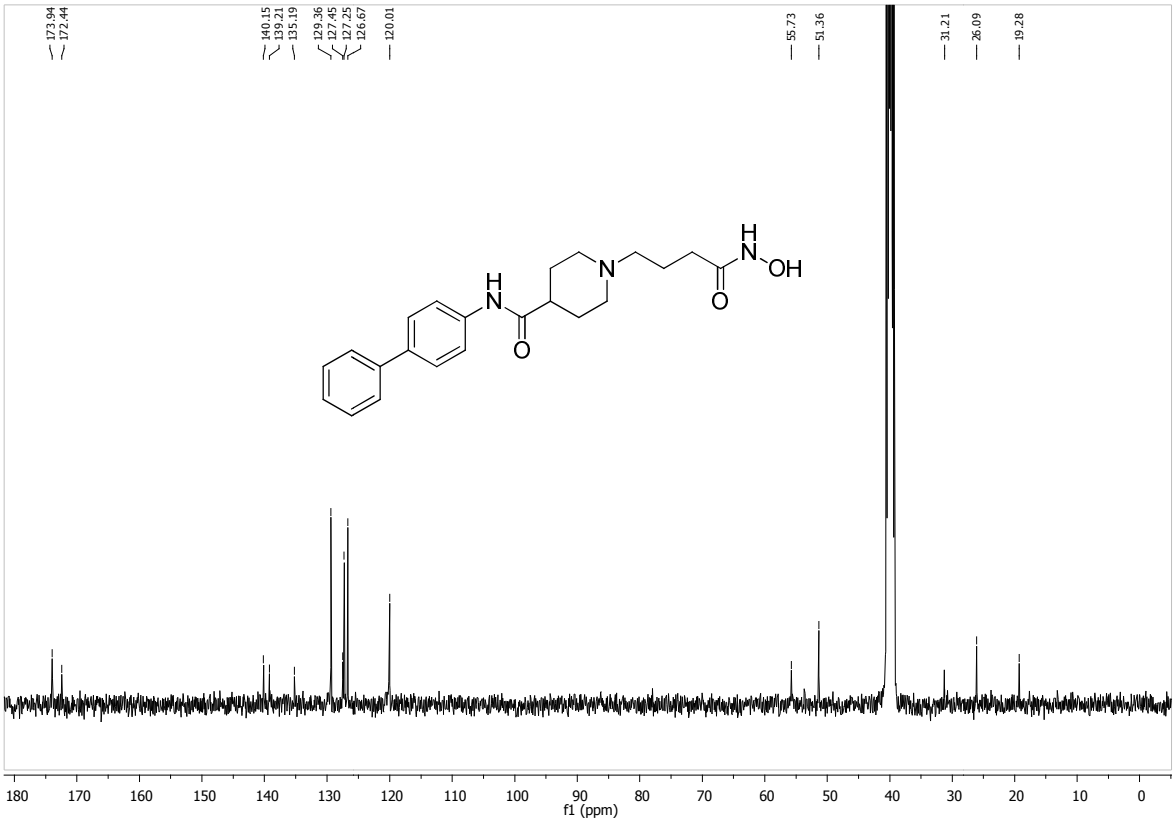

^{13}C NMR of **5d**

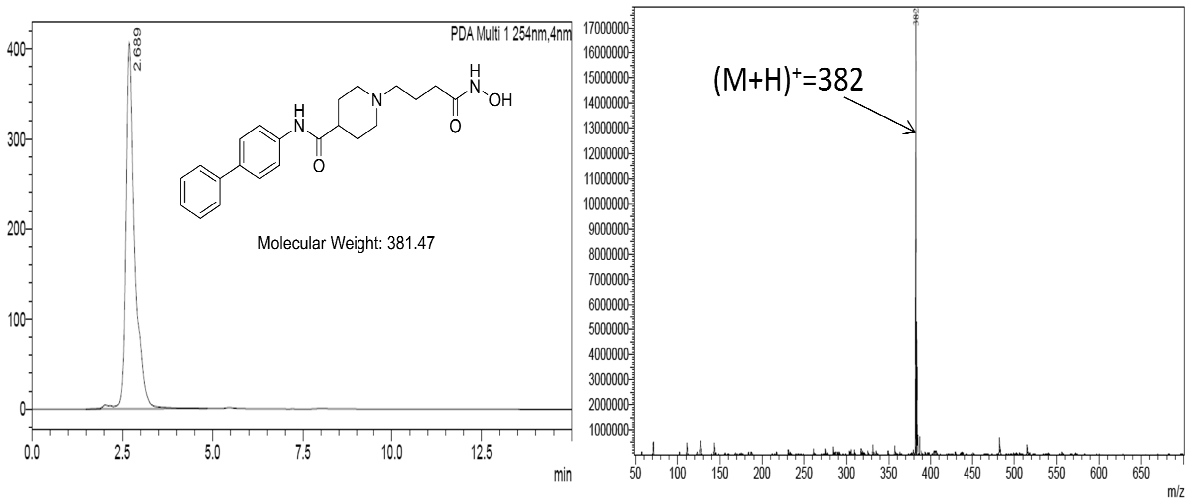

LC/MS of **5d**

1-(4-(hydroxyamino)-4-oxobutyl)-*N*-(quinolin-4-yl)piperidine-4-carboxamide (5e)

Yield 84.3%, yellow color powder, ^{1}H NMR (400 MHz, DMSO-d_6) δ 8.71 (d, J = 6.6 Hz, 1H), 8.61 (d, J = 8.1 Hz, 1H), 8.42 (t, J = 7.7 Hz, 1H), 8.19 – 8.13 (m, 1H), 8.05 (d, J = 8.5 Hz, 1H), 7.95 (m, 1H), 7.67 (m, 1H), 6.92 (d, J = 6.9 Hz, 1H), 3.15 – 2.92 (m, 6H), 2.35 (dd, J = 15.1, 7.3 Hz, 3H), 1.96 (dt, J = 23.8, 13.4 Hz, 7H).^{13}C NMR (101 MHz, DMSO-d_6) δ 175.09, 173.92, 158.74, 141.69, 138.78, 134.25, 126.60, 124.49, 120.21, 116.42, 102.18, 55.62, 51.22, 31.23, 25.92, 25.55, 19.18. HPLC Rt: 2.612, LC/MS calculated for expected $C_{19}H_{24}N_4O_3$ [M]: 356.42; Found: [M+H]+: 357

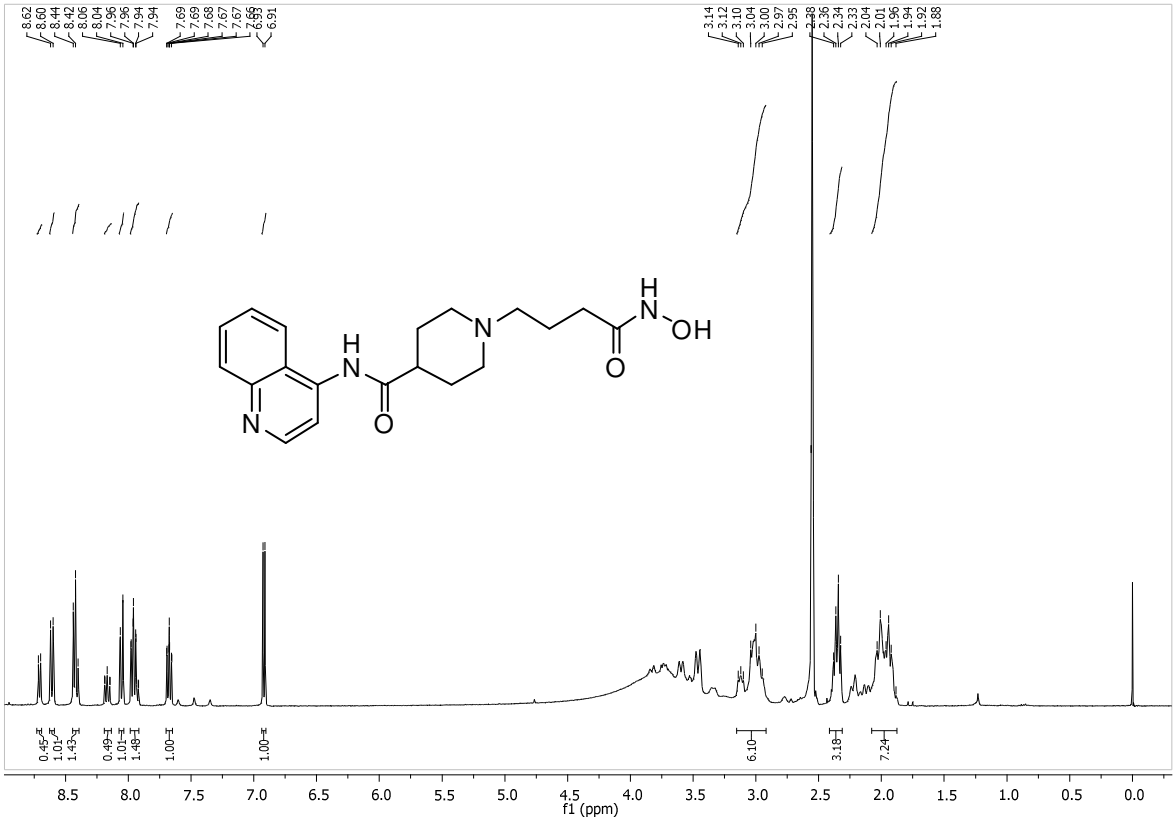

^{1}H NMR of **5e**

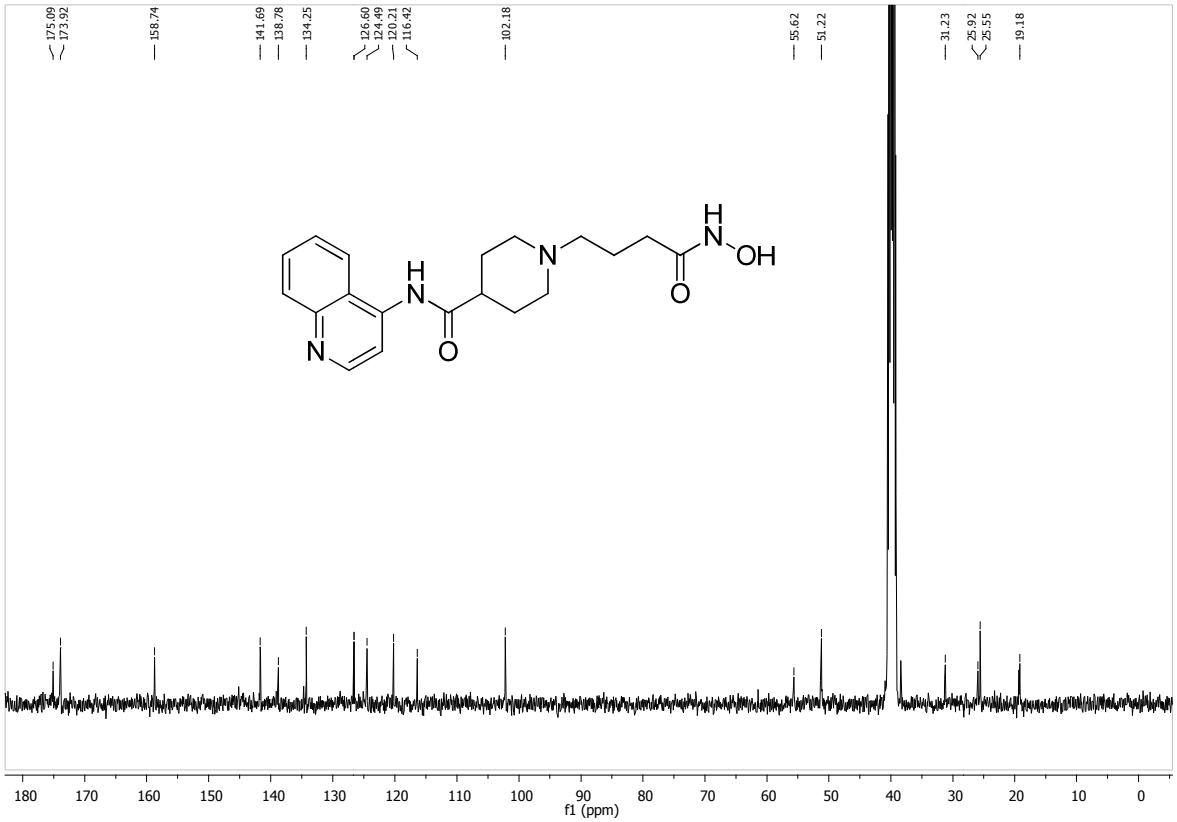

^{13}C NMR of **5e**

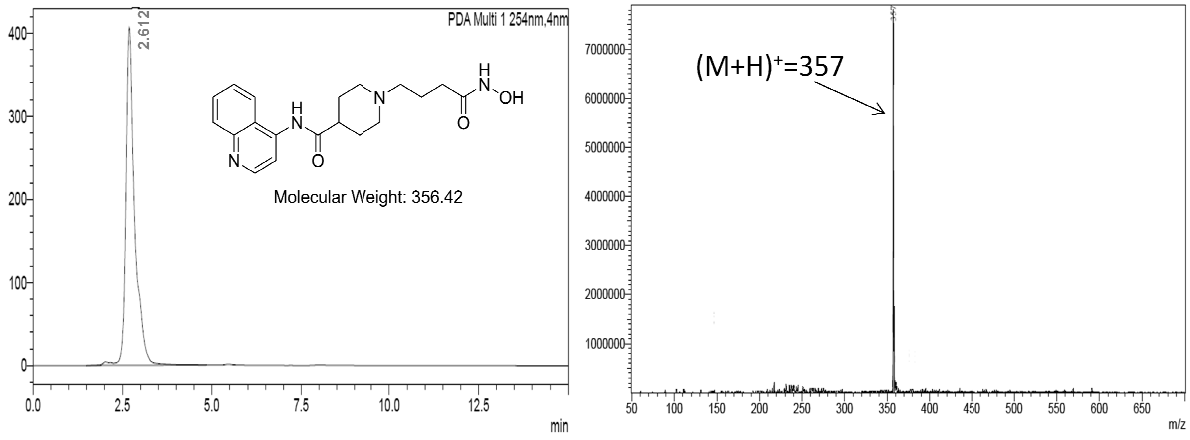

LC/MS of **5e**

***tert*-butyl piperazine-1-carboxylate (7)**

Anhydrous piperazine (5 g, 58.04 mmol) was dissolved in 30 mL of methanol. The reaction mixture was bought to 0°C temperature by keeping it in ice bath. Di-*tert*-butyl-dicarbonate

(10.13g, 46.43 mmol) was mixed with 20 mL of methanol and added to above mixture drop wise. The reaction was stirred for 3 hours at room temperature. After completion of reaction, methanol was evaporated and resultant solid was dissolved in ice cold water. Product was extracted in ethyl acetate and washed with saturated solution of sodium bicarbonate, dried over sodium sulphate and evaporated to get 5.9 g of white solid as a product (yield 54.6%). ^{1}H NMR (400 MHz, DMSO-d_6) δ 3.28 (s, 2H), 3.20 (m, 2H), 2.62 – 2.57 (m, 4H), 1.39 (d, *J* = 4.8 Hz, 9H). $C_9H_{18}N_2O_2$ [M]: 186.25; MS (ESI) *m/z*: $[M+H]^+$: 187

***tert*-butyl 4-(phenylcarbamoyl)piperazine-1-carboxylate (9)**

tert-butyl piperazine-1-carboxylate (**7**) (1 g, 5.36 mmol) was dissolved in 10 mL of DCM. Phenyl isocyanate (**8**) (0.64 g, 5.36 mmol) was added drop wise to above solution and flushed with nitrogen gas. The reaction was stirred for 4 hours. It was diluted with DCM and washed with saturated sodium bicarbonate solution. The DCM layer was collected, dried using sodium sulphate and evaporated to get crude mass. The crude was purified by column chromatography (EtOAc: Hexane; 3:7) to get 0.92 g of white powder (yield 56.4%). ^{1}H NMR (400 MHz, DMSO-d_6) δ 8.56 (s, 1H), 7.46 – 7.43 (m, 2H), 7.26 – 7.20 (m, 2H), 6.96 – 6.91 (m, 1H), 3.42 (m, 4H), 3.35 (m, 4H), 1.42 (s, 9H). $C_{16}H_{23}N_3O_3$ [M]: 305.37; MS (ESI) *m/z*: $[M+H]^+$: 306, $[M-H]^+$: 304

methyl 3-(4-(phenylcarbamoyl)piperazin-1-yl)propanoate (10a)

According to procedure B, compound **10a** was prepared from compound **9** (0.4 g, 1.31 mmol) and methyl 3-bromopropionate (0.328 g, 1.968 mmol) afforded 0.156 g of cream color sticky mass (yield 41%). ^{1}H NMR (400 MHz, DMSO-d_6) δ 7.45 (td, *J* = 8.7, 0.9 Hz, 2H), 7.23 (m, 2H), 6.96 – 6.89 (m, 1H), 3.60 – 3.57 (m, 3H), 3.49 (s, 1H), 3.43 – 3.39 (m,

3H), 2.36 – 2.28 (m, 6H), 1.75 – 1.66 (m, 2H). $C_{15}H_{21}N_3O_3$ [M]: 291.35; MS (ESI) *m/z*: $[M+H]^+$: 292

methyl 4-(4-(phenylcarbamoyl)piperazin-1-yl)butanoate (10b)

According to procedure B, compound **10b** was prepared from compound **9** (0.330 g, 1.08 mmol) and methyl 4-bromobutyrate (0.291g, 1.60 mmol) afforded 0.187 g of cream color solid (yield 56.6%). ^{1}H NMR (400 MHz, DMSO-d_6) δ 7.45 (td, *J* = 8.7, 0.9 Hz, 2H), 7.23 (m, 2H), 6.96 – 6.89 (m, 1H), 3.60 – 3.57 (m, 3H), 3.48 (s, 2H), 3.43 – 3.40 (m, 4H), 2.36 – 2.28 (m, 6H), 1.75 – 1.66 (m, 2H).$C_{16}H_{23}N_3O_3$ [M]: 305.37; MS (ESI) *m/z*: $[M+H]^+$: 306

4-(3-(hydroxyamino)-3-oxopropyl)-N-phenylpiperazine-1-carboxamide (11a)

Following procedure C, compound **11a** was prepared from compound **10a** (0.150 g, 0.51 mmol), produced 0.100 g of product as beige color powder (yield 66.6%). ^{1}H NMR (400 MHz, DMSO-d_6) δ 8.67 (s, 1H), 7.49 (d, J = 8.2 Hz, 2H), 7.26 – 7.20 (m, 2H), 6.95 (q, J = 7.3 Hz, 1H), 3.50 (s, 3H), 3.45 – 3.28 (m, 9H). ^{13}C NMR (101 MHz, DMSO-d_6) δ 155.49, 140.95, 128.79, 128.75, 122.23, 120.15, 51.22, 44.15, 41.38, 28.83. HPLC Rt: 1.957, LC/MS calculated for expected C14H20N4O3 [M]: 292.33; Found: $[M+H]^+$: 293

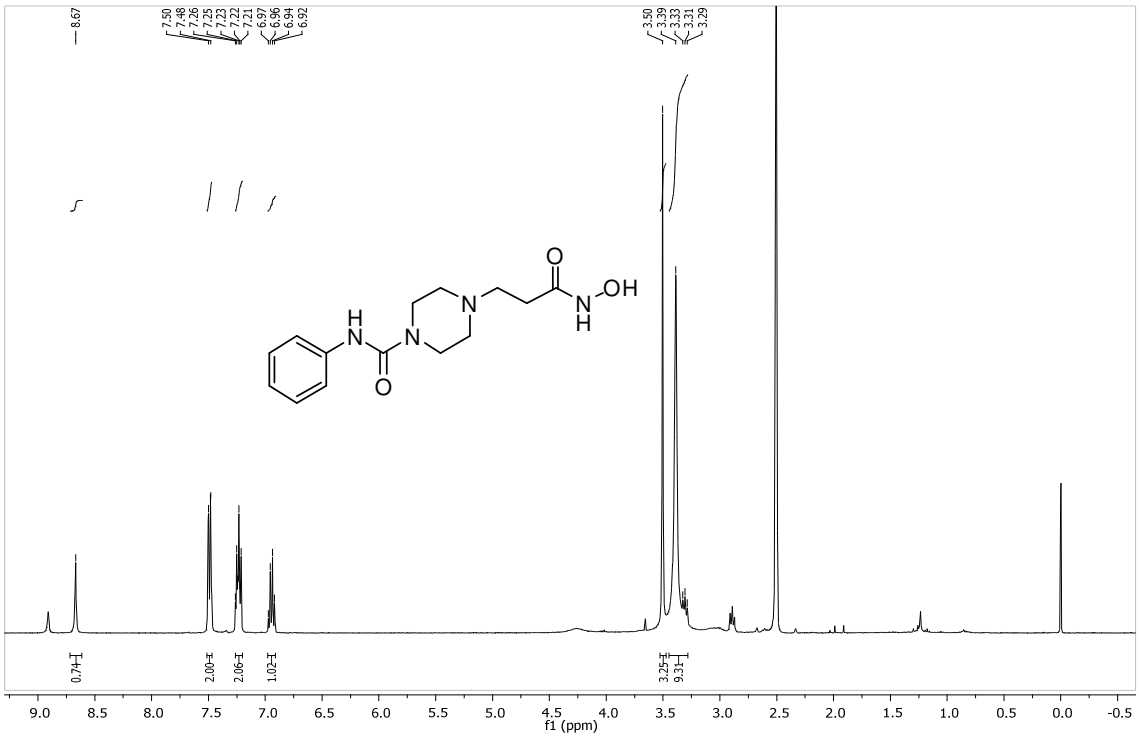

^{1}H NMR of **11a**

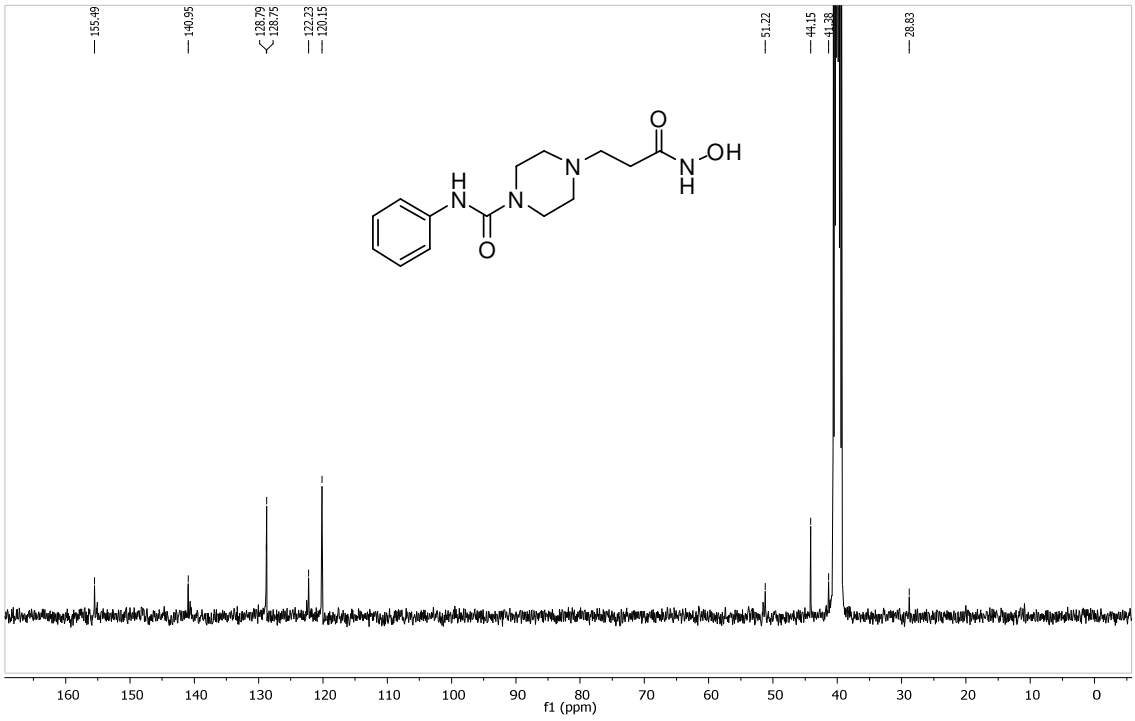

^{13}C NMR of **11a**

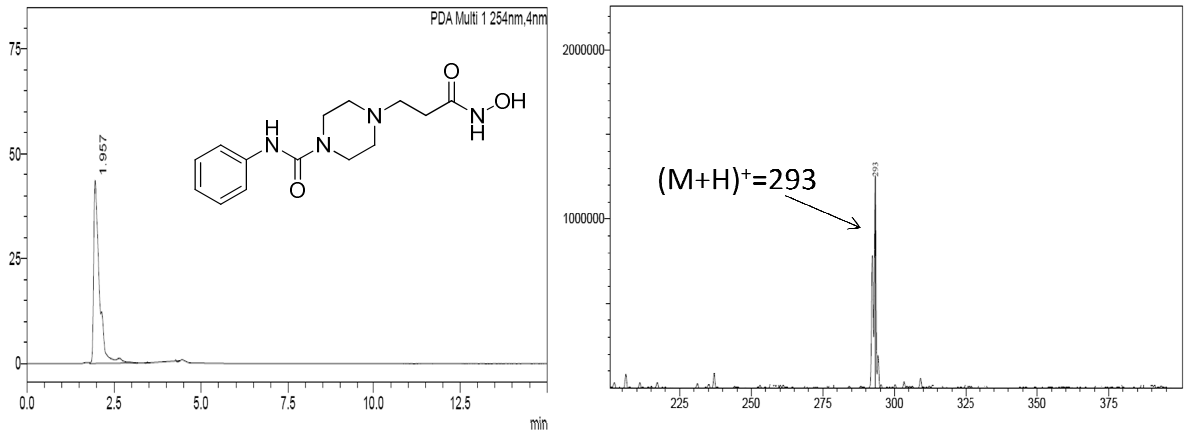

LC/MS of **11a**

4-(4-(hydroxyamino)-4-oxobutyl)-N-phenylpiperazine-1-carboxamide (11b):

According to procedure C, compound **11b** was prepared from compound **10b** (0.180 g, 0.59 mmol), produced 0.130 g of product as cream color powder (yield 72%). ^{1}H NMR (400 MHz, DMSO-d_6) δ 8.97 (s, 1H), 7.50 (d, J = 8.3 Hz, 2H), 7.24 (m, 2H), 6.95 (t, J = 7.3 Hz, 1H), 3.51 (s, 2H), 3.45 (s, 5H), 3.12 – 3.06 (m, 2H), 2.35 (t, J = 7.3 Hz, 2H), 2.01 – 1.93 (m, 2H), 1.30 – 1.22 (m, 1H). ^{13}C NMR (101 MHz, DMSO-d_6) δ 173.89, 155.13, 140.67, 128.76, 122.48, 120.18, 55.37, 51.12, 44.17, 31.25, 19.16. HPLC Rt: 1.980, LC/MS calculated for expected $C_{19}H_{24}N_4O_3$ [M]: 306.36; Found: $[M]^+$: 306

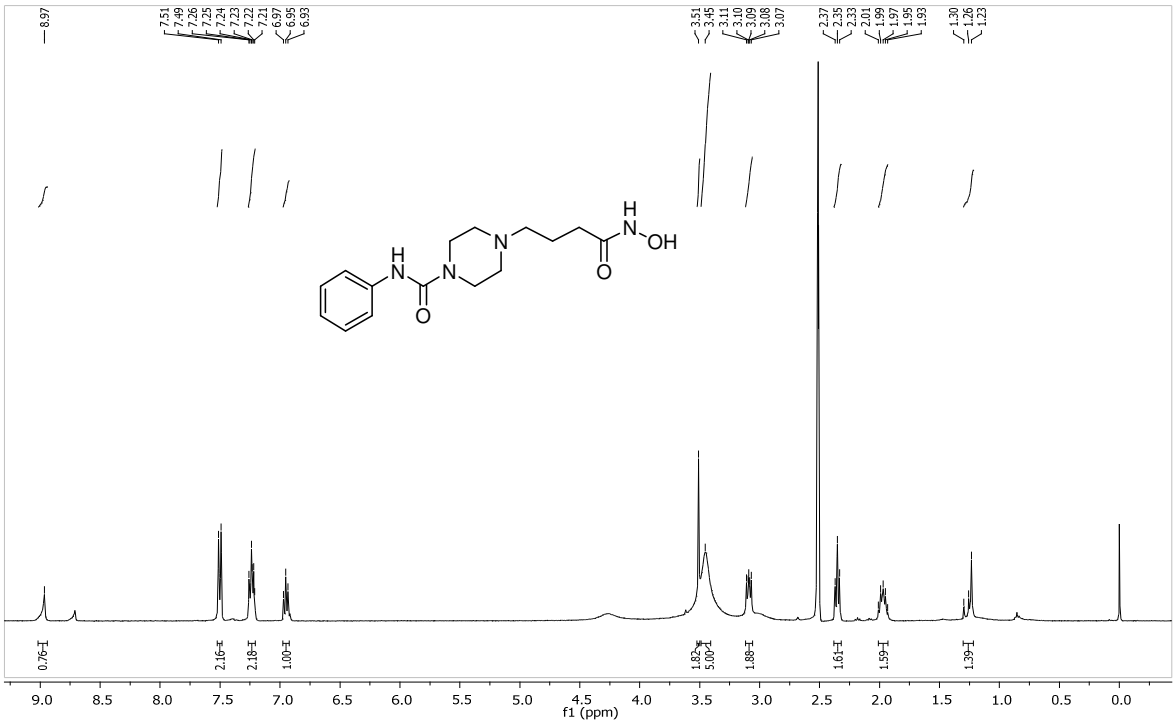

^{1}H NMR of **11b**

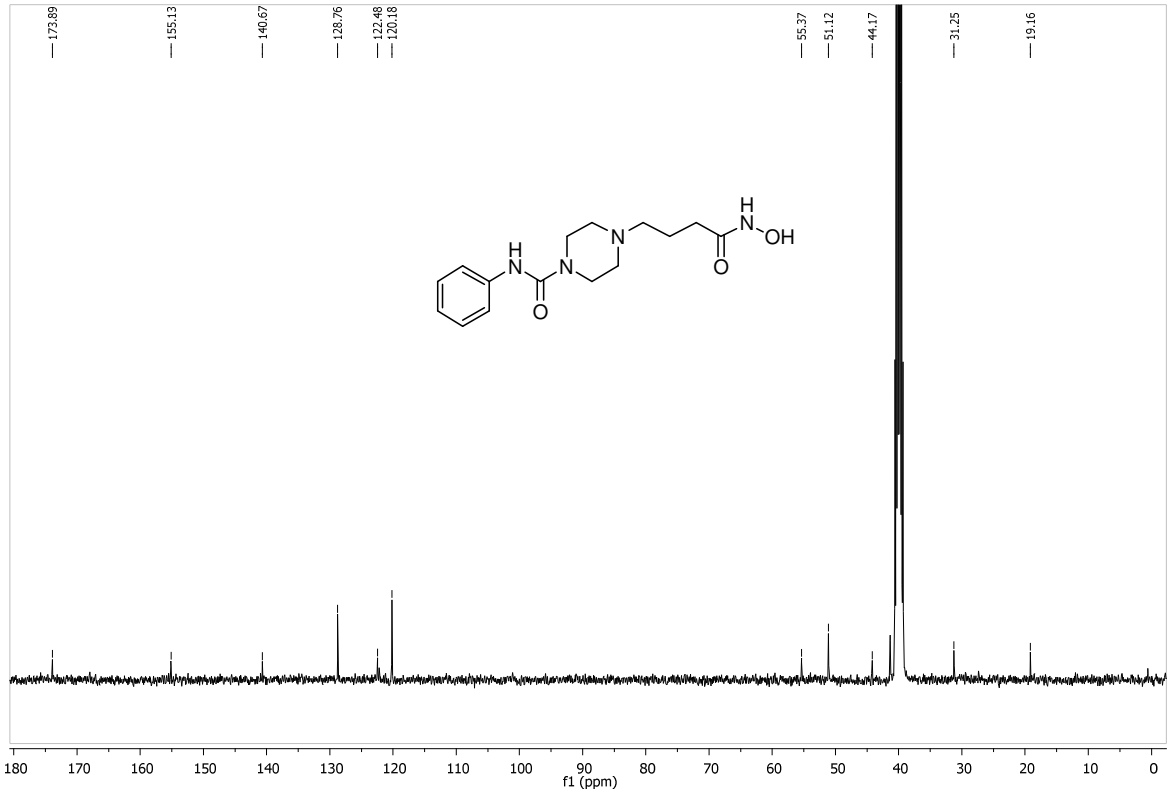

^{13}C NMR of **11b**

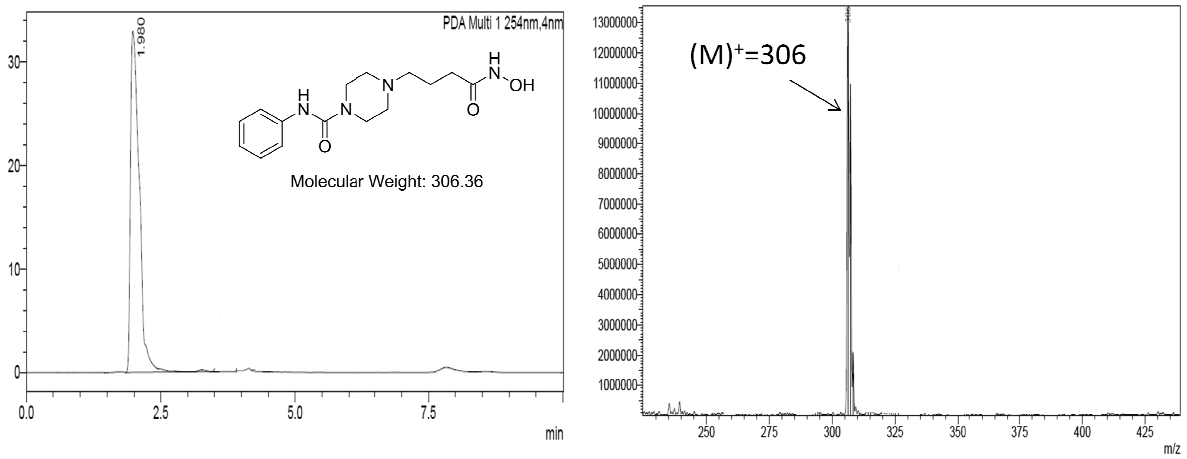

LC/MS of **11b**

Procedure D. General procedure for synthesis of 13a, 13b, 13c, 13d

Aryl amine (**12a**: benzylamine, **12b**: 1-naphthylamine, **12c**: 4-aminobiphenyl, **12d**: 4-amino quinoline) (1 g) was dissolved in 20 mL of DCM. To this solution, 20 mL of $NaHCO_3$ solution was stirred at 0°C. Stirring was stopped momentarily and triphosgene (0.5 equivalents) dissolved in 1 mL of DCM was added with syringe to DCM layer and stirring continued for 1 hour. The DCM layer was separated and passed through bed of celite® and subjected to next reaction immediately.

Procedure E. General procedure for synthesis of 14a, 14b, 14c, 14d

To the DCM layer containing **13a, 13b, 13c** and **13d**, *tert*-butyl piperazine-1-carboxylate (**7**) (1 equivalent) was added and stirred for 4 hours in nitrogen environment. Reaction mixture was diluted with DCM and washed with saturated sodium bicarbonate solution. DCM layer was dried using sodium sulphate, evaporated and purified by column chromatography (EtOAc: Hexane; 3:7).

***tert*-butyl 4-(benzylcarbamoyl)piperazine-1-carboxylate (14a)**

Yield 84%, white solid, ^{1}H NMR (400 MHz, DMSO-d_6) δ 7.33 – 7.19 (m, 6H), 4.24 (dd, *J* = 5.7, 3.6 Hz, 2H), 3.33 (s, 1H), 3.29 (d, *J* = 7.4 Hz, 7H), 1.40 (s, 9H). $C_{17}H_{25}N_3O_3$ [M]: 319.40; MS (ESI) *m/z*: $[M-H]^+$: 318

***tert*-butyl 4-(naphthalen-1-ylcarbamoyl)piperazine-1-carboxylate (14b)**

Yield 75%, white solid, ^{1}H NMR (400 MHz, DMSO-d_6) δ 8.67 (s, 1H), 7.92 (m, 2H), 7.74 (d, *J* = 7.9 Hz, 1H), 7.52 – 7.40 (m, 4H), 3.53 – 3.49 (m, 4H), 3.43 – 3.39 (m, 4H), 1.44 (s, 9H). $C_{20}H_{25}N_3O_3$ [M]: 355.43; MS (ESI) *m/z*: $[M+H]^+$: 356, $[M-H]^+$: 354

***tert*-butyl 4-([1,1'-biphenyl]-4-ylcarbamoyl)piperazine-1-carboxylate (14c)**

Yield 80%, white solid, ^{1}H NMR (400 MHz, DMSO-d_6) δ 8.69 (s, 1H), 7.65 – 7.61 (m, 2H), 7.56 (s, 4H), 7.43 (t, *J* = 7.7 Hz, 2H), 7.30 (t, *J* = 7.3 Hz, 1H), 3.48 – 3.43 (m, 4H), 3.36 (dd, *J* = 9.2, 5.2 Hz, 4H), 1.43 (s, 9H). $C_{22}H_{27}N_3O_3$ [M]: 381.47; MS (ESI) *m/z*: $[M-H]^+$: 380

***tert*-butyl 4-(quinolin-4-ylcarbamoyl)piperazine-1-carboxylate (14d)**

Yield 70%, yellow solid, ^{1}H NMR (400 MHz, DMSO-d_6) δ 10.20 (s, 1H), 8.78 (d, *J* = 5.0 Hz, 1H), 8.36 (dd, *J* = 8.5, 0.7 Hz, 1H), 8.08 (d, *J* = 5.0 Hz, 1H), 8.00 (dd, *J* = 8.4, 0.8 Hz, 1H), 7.77 (m, 1H), 7.64 (m, 1H), 3.34 (s, 4H), 1.89 (dd, *J* = 13.7, 2.8 Hz, 2H), 1.78 (dd, *J* = 13.3, 3.2 Hz, 2H), 1.39 (s, 9H). $C_{22}H_{27}N_3O_3$ [M]: 356.42; MS (ESI) *m/z*: $[M+H]^+$: 357, $[M-H]^+$: 355

methyl 4-(4-(benzylcarbamoyl)piperazin-1-yl)butanoate (15a)

Compound **15a** was synthesized by following procedure B from compound **14a** (1 g, 3.13 mmol) and methyl 4-bromobutanoate (0.850 g, 4.69 mmol) yielded 0.310 g **15a** as cream color sticky solid mass (yield 97%). ^{1}H NMR (400 MHz, DMSO-d_6) δ 7.25 (m, 5H), 7.06 (t,

J = 5.8 Hz, 1H), 4.23 (d, *J* = 5.8 Hz, 2H), 3.58 (s, 3H), 3.30 (dd, *J* = 9.7, 5.0 Hz, 4H), 2.29 (m, 8H), 1.69 (m, 2H). $C_{17}H_{25}N_3O_3$ [M]: 319.40; MS (ESI) *m/z*: $[M+H]^+$: 320

methyl 4-(4-(naphthalen-1-ylcarbamoyl)piperazin-1-yl)butanoate (15b)

Following procedure B, compound **14b** (0.350 g, 0.98 mmol) and methyl 4-bromobutanoate (0.266 g, 1.47 mmol) reacted together to produce compound **15b** as cream color semisolid (0.200 g, 57%). ^{1}H NMR (400 MHz, DMSO-d_6) δ 7.94 (m, 2H), 7.54 – 7.41 (m, 6H), 3.63 (s, 3H), 3.61 (s, 2H), 3.17 – 3.11 (m, 3H), 2.09 – 1.81 (m, 7H), 1.23 (s, 2H). $C_{20}H_{25}N_3O_3$ [M]: 355.43; MS (ESI) *m/z*: $[M+H]^+$: 356, $[M-H]^+$: 354

methyl 4-(4-([1,1'-biphenyl]-4-ylcarbamoyl)piperazin-1-yl)butanoate (15c)

Compound **14c** (0.565 g, 1.48 mmol) and methyl 4-bromobutanoate (0.403 g, 2.22 mmol) were reacted by following procedure B afforded 0.350 g pale brown solid (Yield 62%). ^{1}H NMR (400 MHz, DMSO-d_6) δ 8.60 (s, 1H), 7.65 – 7.60 (m, 2H), 7.57 (d, *J* = 9.0 Hz, 4H), 7.42 (t, *J* = 7.6 Hz, 2H), 7.30 (t, *J* = 7.8 Hz, 1H), 3.59 (s, 3H), 3.44 (s, 4H), 2.39 – 2.29 (m, 8H), 1.76 – 1.68 (m, 2H). $C_{22}H_{27}N_3O_3$ [M]: 381.47; MS (ESI) m/z: $[M+H]^+$: 382, $[M-H]^+$: 380

methyl 4-(4-(quinolin-4-ylcarbamoyl)piperazin-1-yl)butanoate (15d)

Following procedure B, compound **14d** (0.300 g, 0.84 mmol) and methyl 4-bromobutanoate (0.228 g, 1.26 mmol) reacted together to produce compound **15d** as pale yellow solid (0.180 g, 60%). ^{1}H NMR (400 MHz, DMSO-d_6) δ 10.15 (s, 1H), 8.78 (d, *J* = 5.0 Hz, 1H), 8.36 (d, *J* = 7.8 Hz, 1H), 8.08 (d, *J* = 5.0 Hz, 1H), 7.99 (dd, *J* = 8.4, 0.8 Hz, 1H), 7.77 (m, 1H), 7.63 (m, 1H), 3.60 (s, 3H), 2.94 (d, *J* = 10.3 Hz, 2H), 2.33 (t, *J* = 7.2 Hz, 4H), 1.98 (s, 2H), 1.91 – 1.83 (m, 2H), 1.71 (m,4H). $C_{19}H_{24}N_4O_3$ [M]: 356.42; MS (ESI) *m/z*: $[M+H]^+$: 357

N-benzyl-4-(4-(hydroxyamino)-4-oxobutyl)piperazine-1-carboxamide (16a)

Following procedure C, compound **16a** was prepared from compound **15a** (0.360 g, 1.12 mmol), produced 0.300 g of product as cream color sticky solid (Yield 83.3%). ^{1}H NMR (400 MHz, DMSO-d_6) δ 7.34 – 7.24 (m, 5H), 7.20 (m, 1H), 4.23 (d, J = 5.7 Hz, 2H), 3.42 (s, 4H), 2.50 (d, J = 4.2 Hz, 3H), 2.46 – 2.40 (m, 2H), 2.24 – 1.99 (m, 2H), 1.71 (m, 2H), 1.30 – 1.21 (m, 1H). ^{13}C NMR (101 MHz, DMSO-d_6) δ 169.53, 157.83, 141.38, 127.49, 126.85, 57.11, 52.56, 43.82, 43.23, 30.44, 22.02. HPLC Rt: 1.986, LC/MS calculated for expected C16H24N4O3 [M]: 320.18; Found: [M]$^{+}$: 320

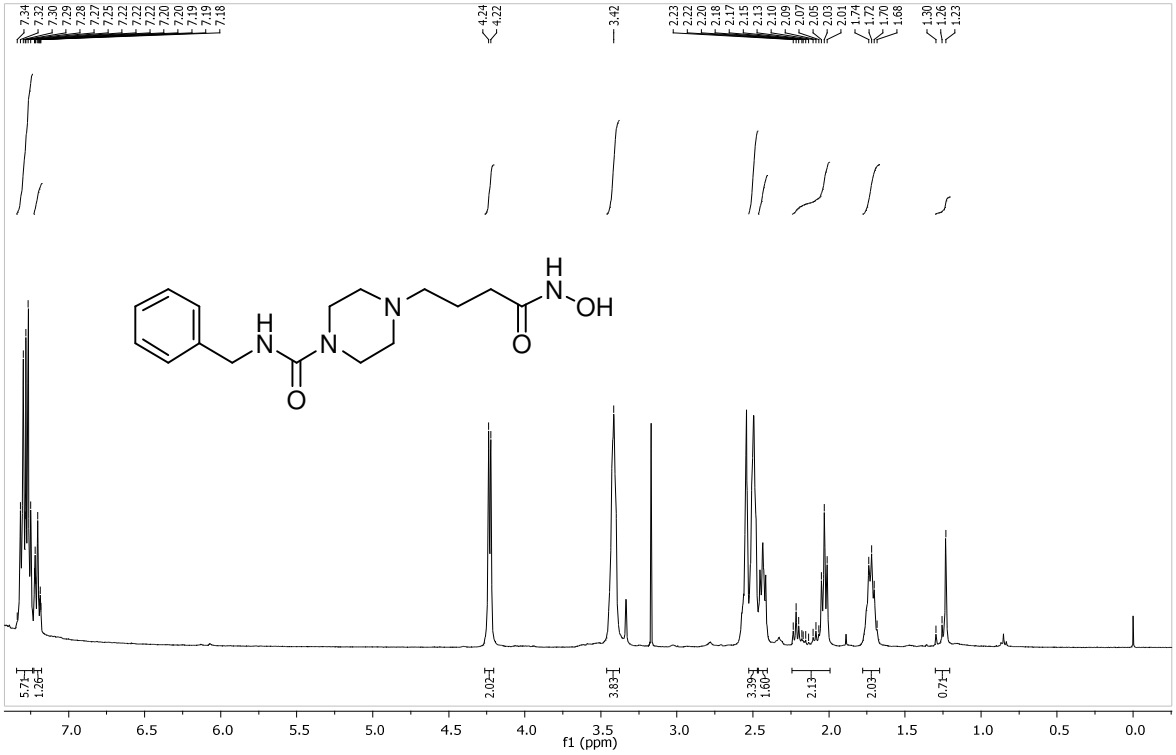

^{1}H NMR of **16a**

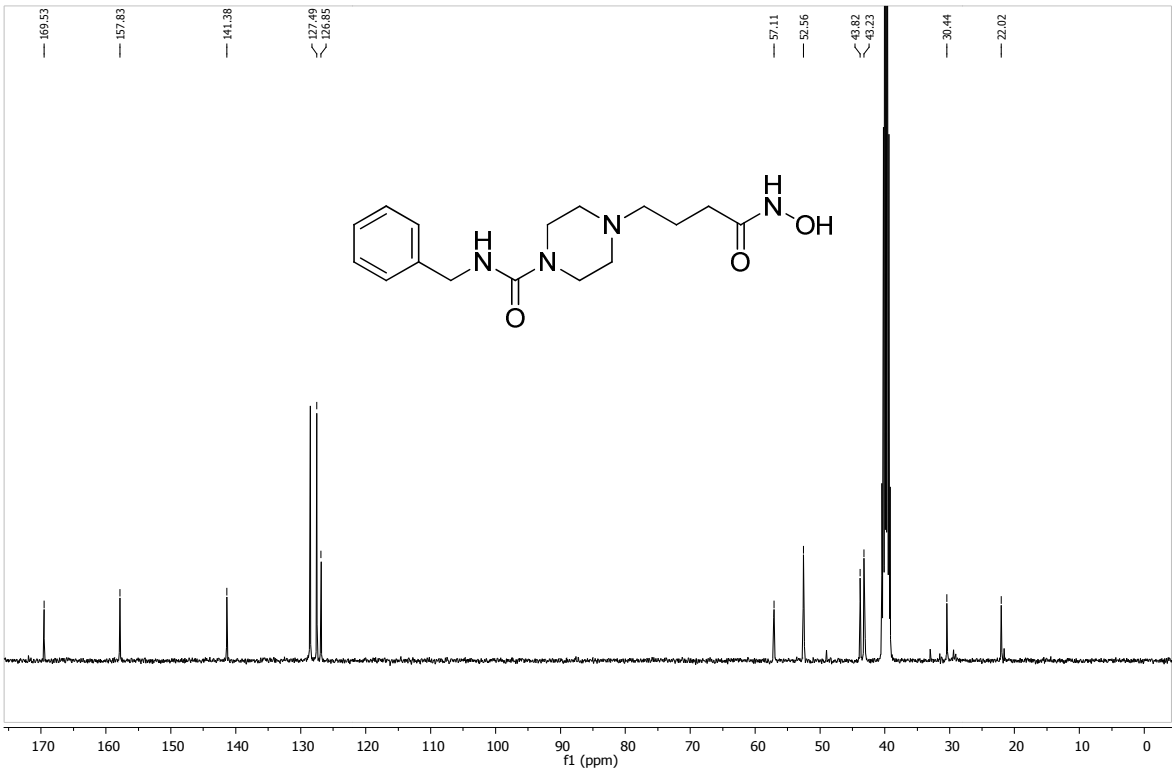

^{13}C NMR of **16a**

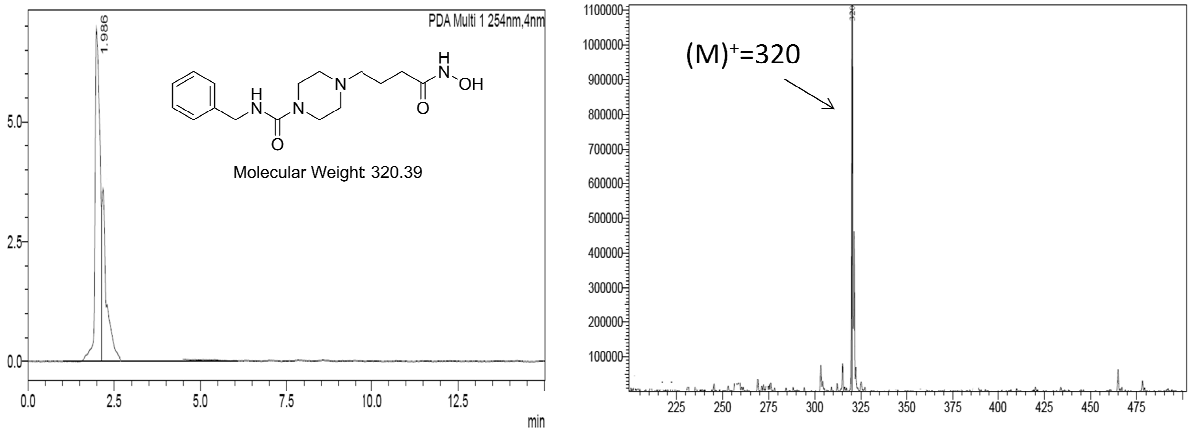

LC/MS of **16a**

4-(4-(hydroxyamino)-4-oxobutyl)-N-(naphthalen-1-yl)piperazine-1-carboxamide (16b)

According to procedure C, compound **16b** was prepared from compound **15b** (0.175 g, 0.49 mmol), produced 0.160 g of product as beige color solid (yield 91.4^{1}H NMR (400 MHz,

DMSO-d_6) δ 9.03 (s, 1H), 7.99 – 7.90 (m, 2H), 7.76 (d, J = 7.8 Hz, 1H), 7.54 – 7.42 (m, 5H), 4.32 (d, J = 8.1 Hz, 2H), 3.21 – 3.09 (m, 5H), 2.37 (m, 4H), 2.14 – 1.88 (m, 4H). ^{13}C NMR (101 MHz, DMSO-d_6) δ 175.09, 173.92, 158.74, 141.69, 138.78, 134.70, 134.25, 126.60, 124.49, 120.21, 116.42, 102.18, 55.62, 51.22, 31.23, 25.55, 19.18. HPLC Rt: 2.008, LC/MS calculated for expected $C_{19}H_{24}N_4O_3$ [M]: 356.18; Found: $[M+H]^+$: 357

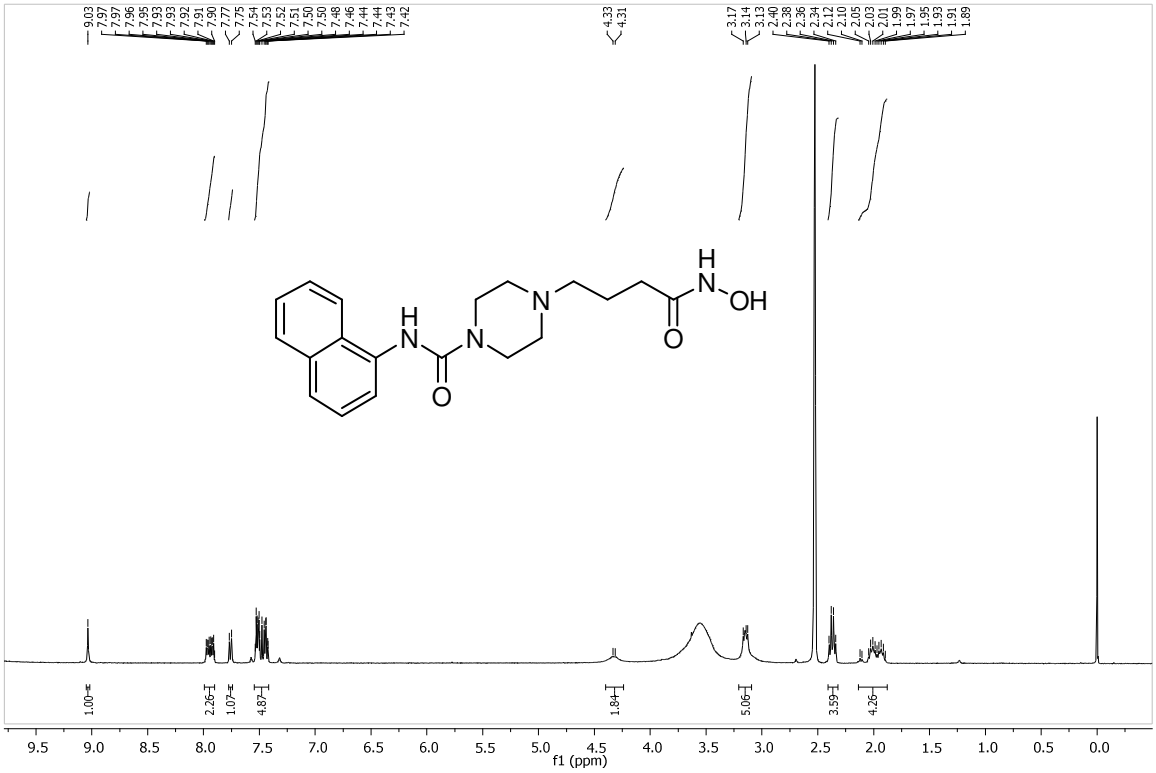

^{1}H NMR of **16b**

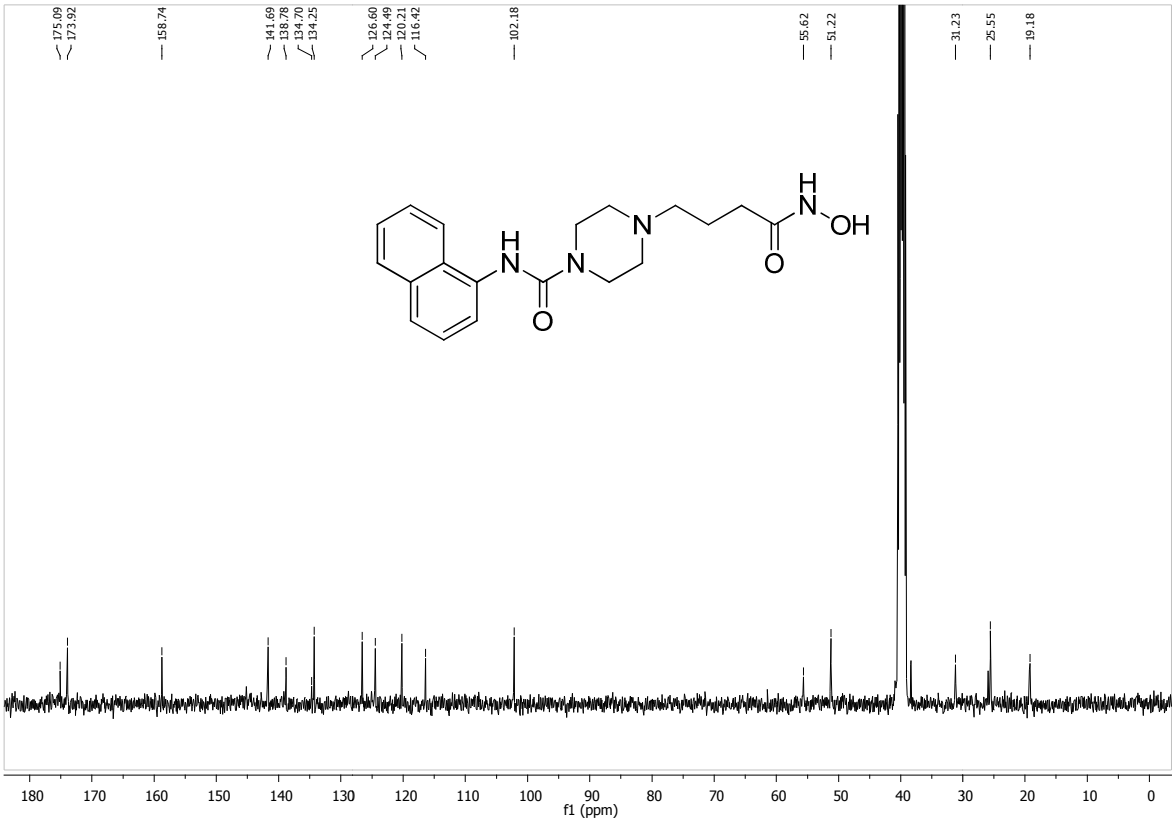

^{13}C NMR of **16b**

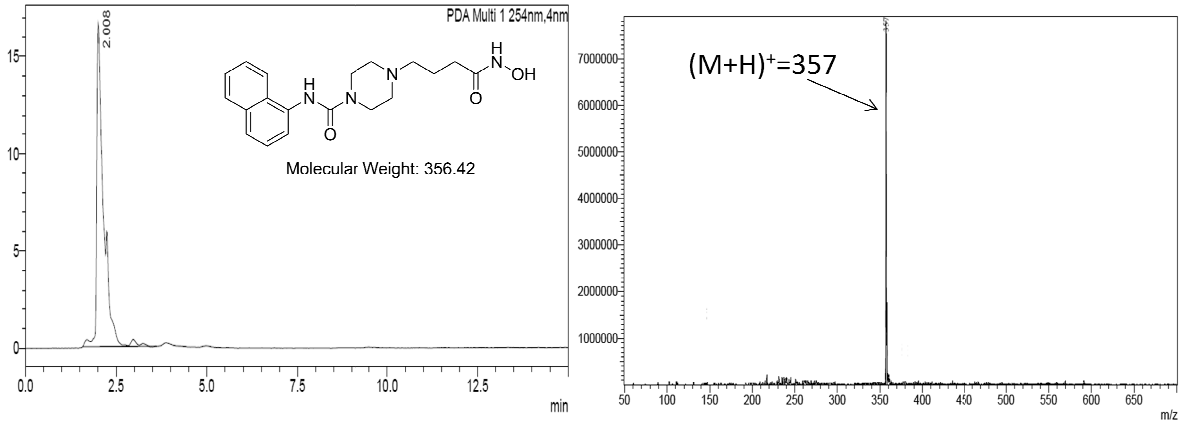

LC/MS of **16b**

N-([1,1'-biphenyl]-4-yl)-4-(4-(hydroxyamino)-4-oxobutyl)piperazine-1-carboxamide (16c)

According to procedure C, compound **16c** was prepared from compound **15c** (0.173g, 0.45mmol), produced 0.165g of product as beige color solid (Yield 95.3%). ^{1}H NMR (400 MHz, DMSO-d_6) δ 7.76 (d, J = 8.7 Hz, 2H), 7.63 (t, J = 8.4 Hz, 4H), 7.44 (t, J = 7.7 Hz, 2H), 7.33 (t, J = 7.3 Hz, 1H), 3.48 (d, J = 12.0 Hz, 2H), 3.05 (m, 8H), 2.75 (m, 1H), 2.35 (t, J = 7.3 Hz, 1H), 1.98 (m, 6H). ^{13}C NMR (101 MHz, DMSO-d_6) δ 173.94, 172.44, 140.15, 139.21, 135.19, 129.36, 127.45, 127.25, 126.67, 120.01, 55.73, 51.36, 31.21, 26.09, 19.28HPLC Rt: 2.513, LC/MS calculated for expected $C_{21}H_{26}N_4O_3$ [M]: 382.46; Found: $[M+H]^+$: 383

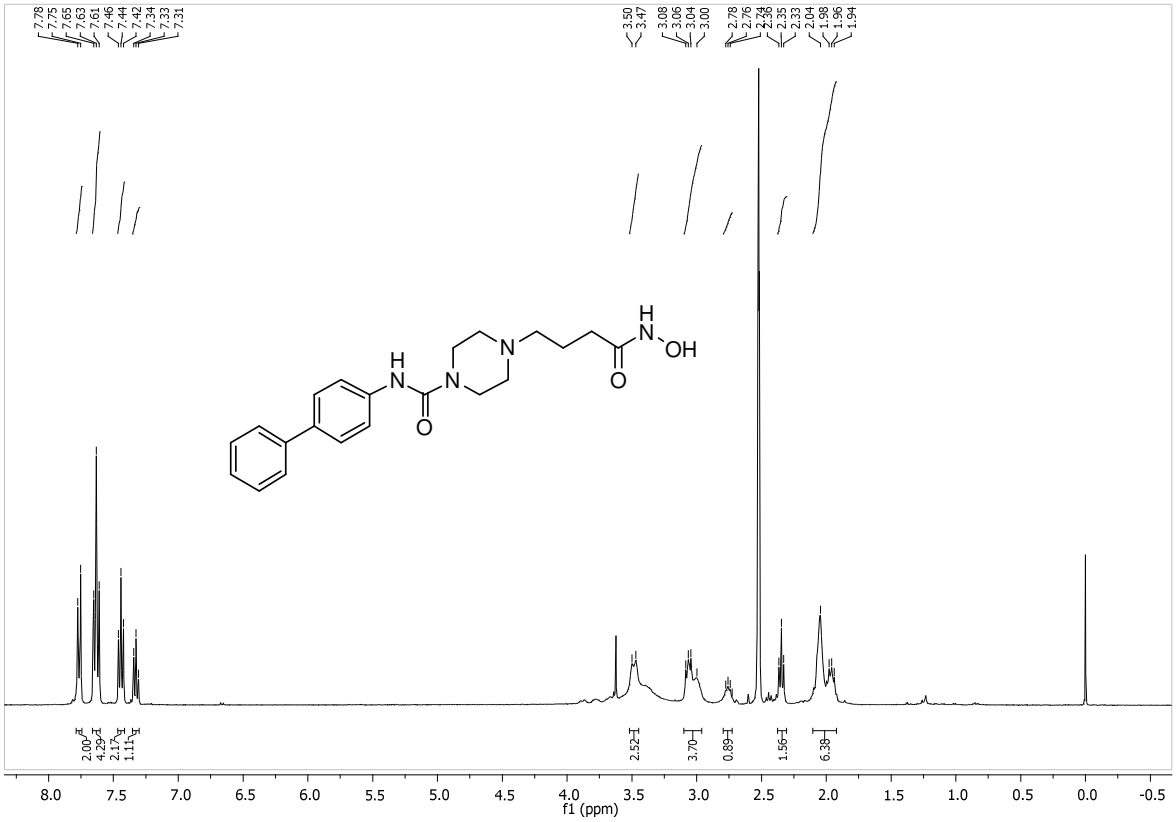

^{1}H NMR of **16c**

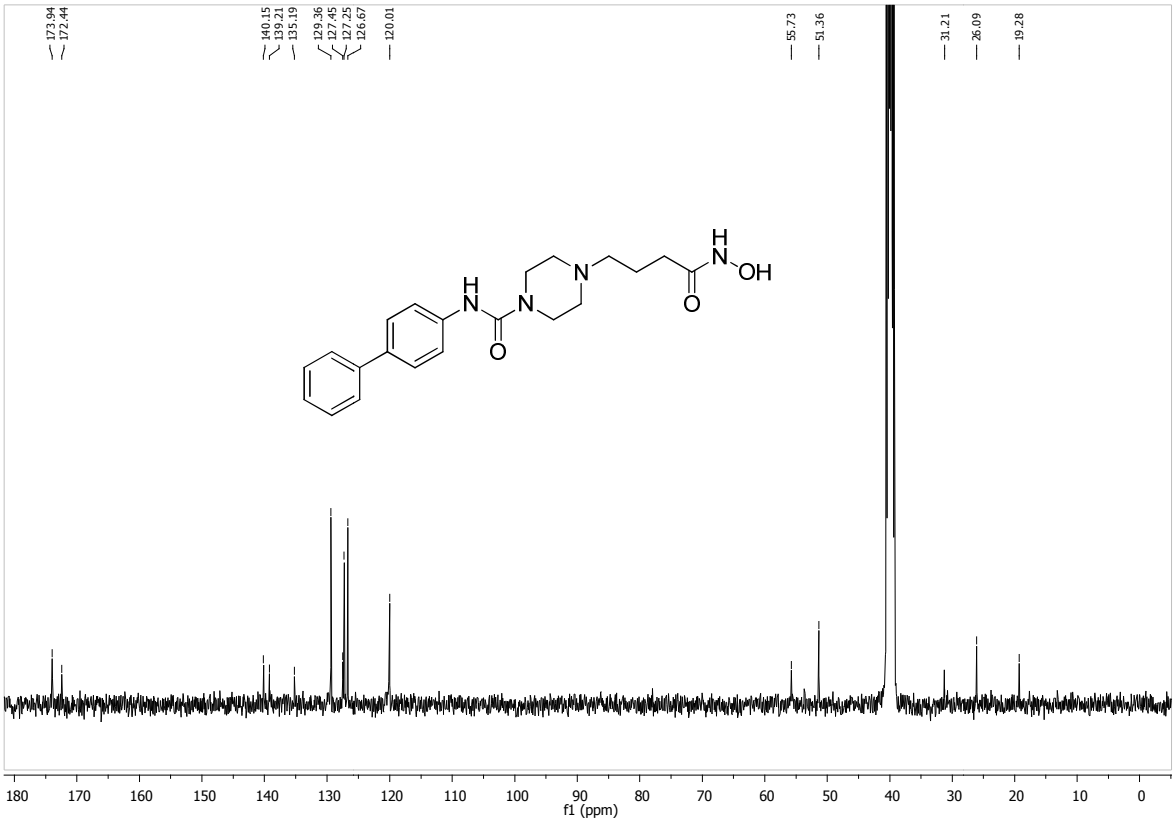

^{13}C NMR of **16c**

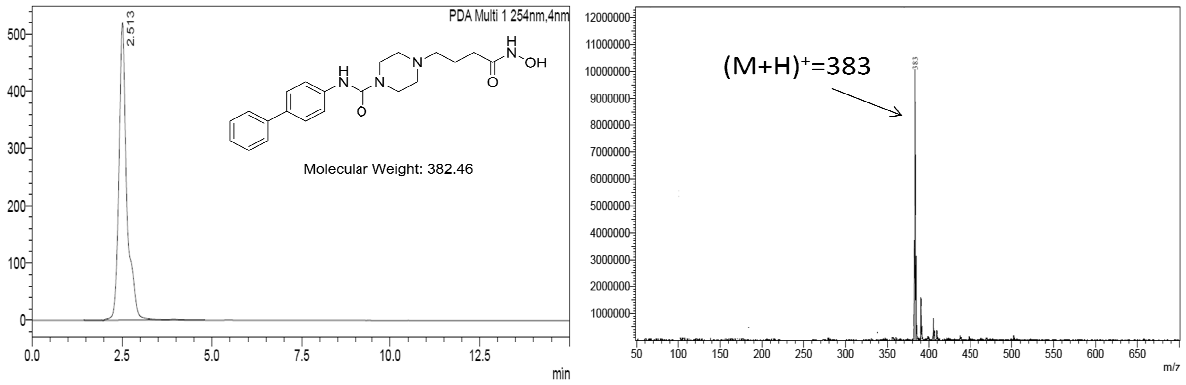

LC/MS of **16c**

4-(4-(hydroxyamino)-4-oxobutyl)-N-(quinolin-4-yl)piperazine-1-carboxamide (16d)

Following procedure C, compound **16d** was prepared from compound **15d** (0.160 g, 0.44 mmol), produced 0.120 g of product as yellow solid (yield 75%). , ^{1}H NMR (400 MHz, DMSO-d_6) δ 8.71 (d, J = 6.6 Hz, 1H), 8.61 (d, J = 8.1 Hz, 1H), 8.42 (t, J = 7.7 Hz, 1H), 8.19

– 8.13 (m, 1H), 8.05 (d, J = 8.5 Hz, 1H), 7.95 (m, 1H), 7.67 (m, 1H), 6.92 (d, J = 6.9 Hz, 1H), 3.15 – 2.92 (m, 6H), 2.35 (dd, J = 15.1, 7.3 Hz, 3H), 1.96 (dt, J = 23.8, 13.4 Hz, 7H).^{13}C NMR (101 MHz, DMSO-d_6) δ 175.09, 173.92, 158.74, 141.69, 138.78, 134.25, 126.60, 124.49, 120.21, 116.42, 102.18, 55.62, 51.22, 31.23, 25.92, 25.55, 19.18. HPLC Rt: 2.467, LC/MS calculated for expected $C_{18}H_{23}N_5O_3$ [M]: 357.41; Found: $[M+H]^+$: 358

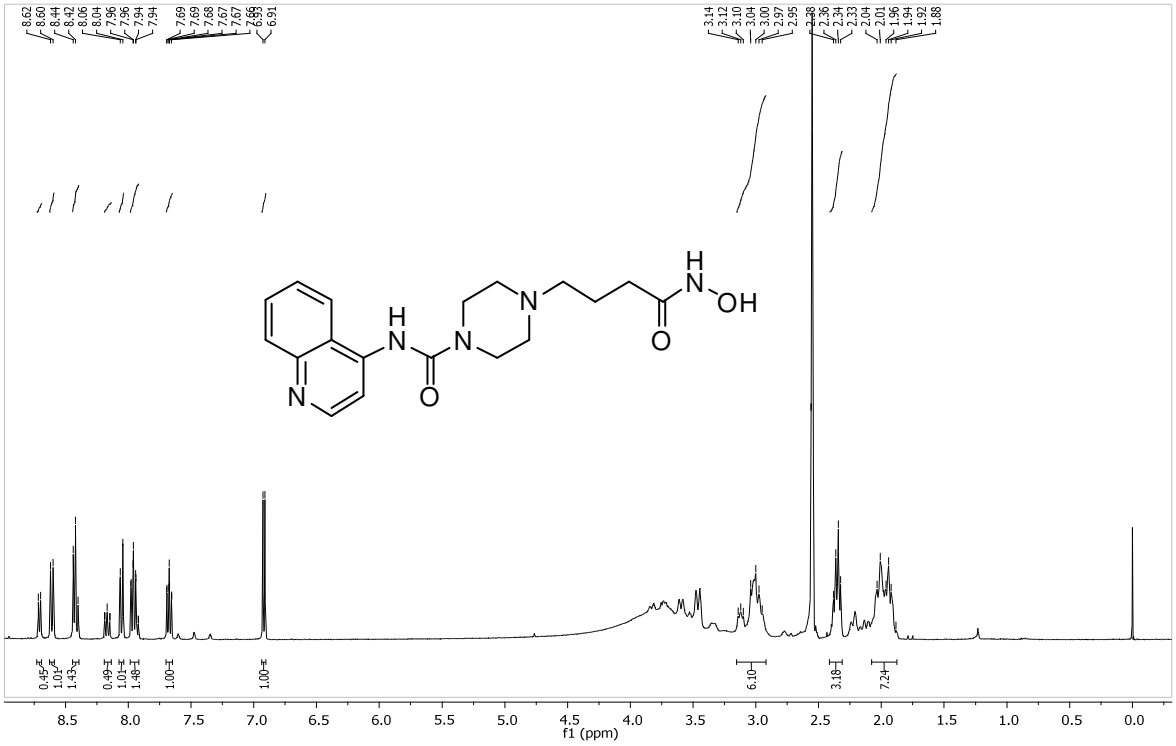

^{1}H NMR of **16d**

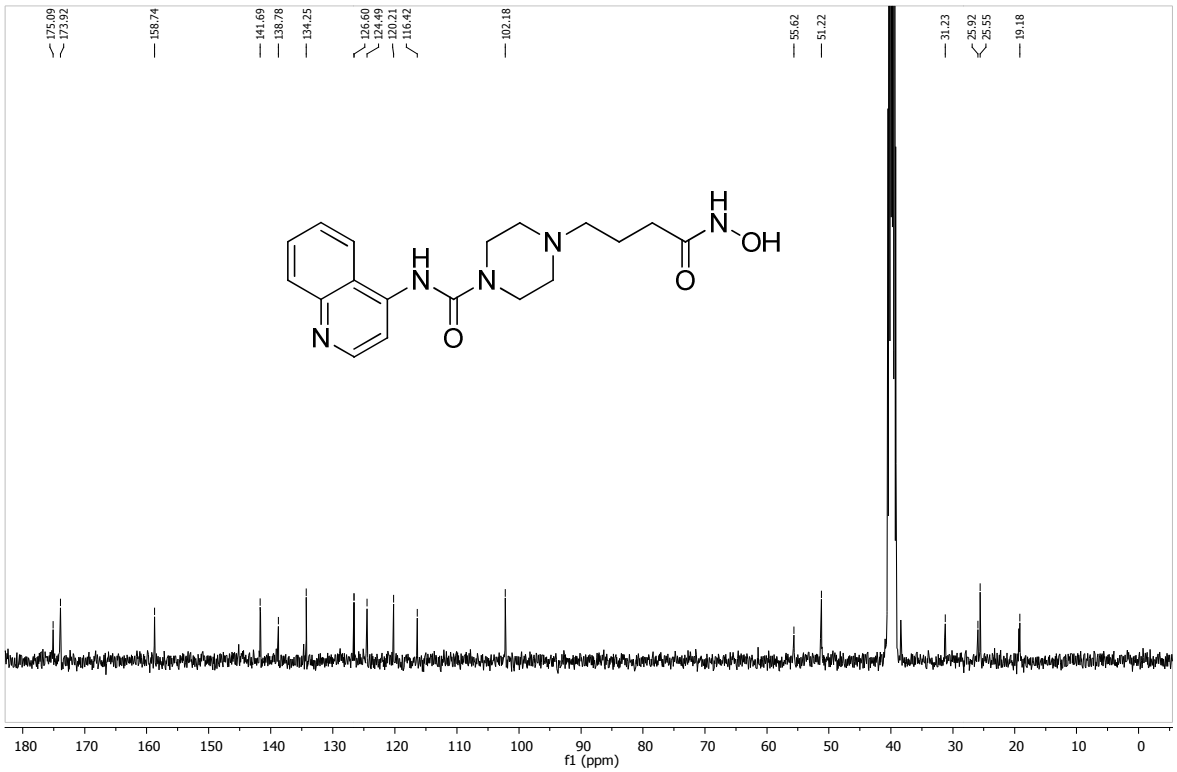

^{13}C NMR of **16d**

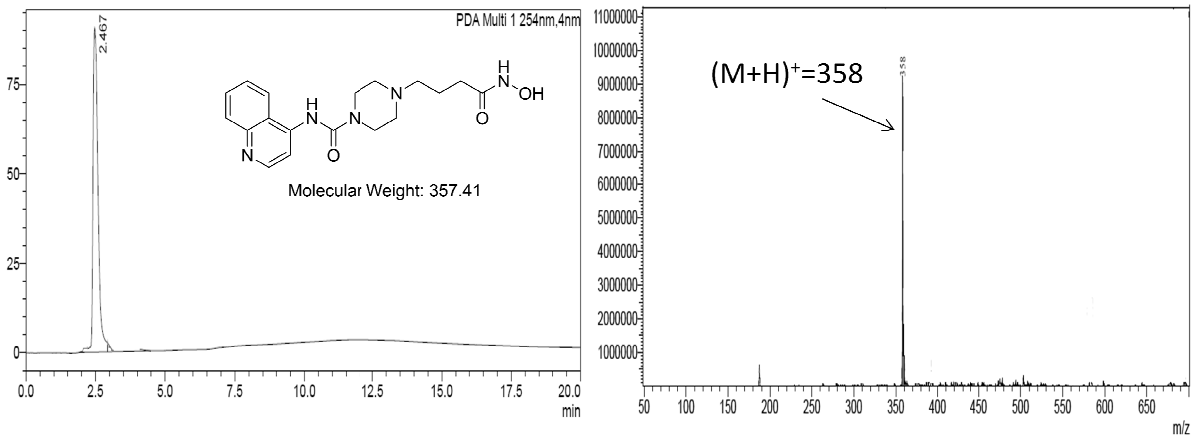

LC/MS of **16d**

3.4.2. HDAC inhibition assay using HeLa nuclear extract

The HDAC enzyme inhibition assay was performed using HDAC colorimetric assay kit (BML-AK501, ENZO life sciences) following vendor's proocol. Briefly, 5 µL of HeLa nuclear extract (BML-KI137-0500), 10 µL of assay buffer (BML-KI143-0020), 10 µL of

sample solution was added per well in a microtiter plate. The reaction was started with addition of 25 µL Color de Lys® substrate solution (BML-KI138-0050). The reaction was incubated in for 30 minutes at 37°C which was terminated by addition of a 50 µL mixture of developer plus stop solution. The plate was incubated for 15 minutes at 37°C and absorbance was measured at 405 nm. All synthesized compounds along with **SAHA** and **BG-45** were screened at 10 µM concentration in duplicate. Compound **5e, 16c** and **16d** were further tested to find out their IC_{50} values in the same way described above. Here, compounds were tested with the concentrations 0.5µM, 1µM, 5µM, 10µM, 15µM.

3.4.3. HDAC3/NCOR1 assay using human recombinant HDAC3 enzyme

HDAC3 enzyme inhibition assay was performed using HDAC3/NCOR1 fluorometric drug discovery kit (BML-AK531, ENZO life sciences) following vendor's protocol. Here, 10 µL of sample solution and 15 µL diluted HDAC3/NCOR1 complex solution (BML-KI574-0030) were added per well in microtiter plate and 25 µL Fluor de Lys® substrate solution (BML-KI177-0005) was added. The plate was incubated for 15 minutes at 37°C. To terminate the reaction, 50 µL of mixture of Fluor de Lys® developer II (BML-KI176-1250) and Trichostatin A (BML-GR309-9090) was added per well and incubated for 45 minutes at 37°C. The fluorescence intensity was measured at Excitation wavelength 360 nm, Emission wavelength 460 nm using Spectramax M4 (Molecular Devices, USA). All synthesized compounds along with **SAHA** and **BG-45** were screened at 10 µM concentration in duplicate.

3.4.4. HDAC8 assay using recombinant HDAC8 enzyme

HDAC8 inhibition assay was performed using HDAC8 fluorimetric drug discovery kit (BML-AK518, Enzo life science) following vendor's protocol. Briefly, 15 µL of diluted

human recombinant HDAC8 enzyme (BML-SE145-0100) was incubated with 10 µL of test inhibitor (10 µM) and 25 µl of *Fluor de Lys*®- HDAC8, deacetylase substrate (BML-KI178-0005). After 10 minutes incubation, reaction was terminated by adding 50 µL stop solution which contains *Fluor de Lys*®- Developer II (BML-KI176-1250) and trichostatin A. The plate was incubated for 45 minutes at 37°C and fluorescence intensity was measured at excitation wavelength 360 nm, emission wavelength 460 nm using Spectramax M4 (Molecular Devices, USA). The promising compound **5e, 16c** and **16d** were further tested to find out their IC_{50} values in the same manner as described above. Here, compounds were tested in the concentration range from 0.5µM, 1 µM, 5 µM, 10 µM, 15 µM.

3.4.5. Cell culture and drug treatment

The murine melanoma cell line (B16F10), human cervical cancer cell line (HeLa), human breast cancer cell line (MCF-7), non-small cell lung cancer cell line (A549) and human acute T cell leukemia (Jurkat E6) were procured from National center for cell science (NCCS, Pune, India). HeLa, B16F10 and MCF-7 cells were cultured in Dulbecco's Modified Eagle Medium (DMEM) (Himedia Laboratories Pvt. Ltd., Mumbai, India), A-549 cells were cultured in Dulbecco's Modified Eagle Medium/ Nutrient Mixture F-12 Ham (DMEM/F12,1:1 mixture, (Himedia Laboratories Pvt. Ltd., Mumbai, India), and *J*urkat E6 cells were cultured in Roswell Park Memorial Institute (RPMI-1640, Himedia Laboratories Pvt. Ltd., Mumbai, India) supplemented with 10% heat inactivated fetal bovine serum (Himedia Laboratories Pvt. Ltd., Mumbai, India) and 1% of antibiotic solution (10000 U Penicillin and 10 mg Streptomycin per mL, Himedia Laboratories Pvt. Ltd., Mumbai, India). Cells were cultured at 37°C in humidified atmosphere with 5% CO_2. Stock solutions of all compounds were prepared in DMSO-d6 at a concentration of 100 mM and stored.

3.4.5.1. MTT assay

Antiproliferative activity of all the synthesized compounds was measured by *in vitro* MTT assay method. 5×10^3 cells (B16F10, HeLa, A-549 and MCF-7) were seeded in 96 well plate and incubated overnight. Cells were treated with **SAHA**, **BG-45** and test compounds in two doses 100 and 10 μM in triplicate and incubated for 72 hours. 50 μL of 5 mg/mL solution of MTT (3-(4,5-dimethylthiazol-2-yl)-2,5-diphenyltetrazolium bromide; Himedia Laboratories Pvt. Ltd., Mumbai, India) was added. After 4 hours of incubation, the formazan crystals were dissolved in DMSO-d6 and absorbance was measured at 570nm and 650nm using Spectramax M4 (Molecular Devices, USA).

For, IC_{50} measurement of all synthesized compounds along with **SAHA** and **BG-45**, the same procedure was followed as described above. The concentration used for IC_{50} measurement were 0.625, 1.25, 2.5, 5, 10, 20, 40, 80, 100 and 200 μM. The same experiment was repeated with another batch of cells.

For Jurkat E6 cells, 2×10^4 cells in 100 μl were seeded in 96 well plates and incubated overnight. Treatment concentrations of compounds were same for all experiments as described above for other cell lines. After 72 hours of incubation with compounds, cells were treated with 22μl of Prestoblue™(Invitrogen, life technologies, United States) reagent. Plate was incubated for 2 hours and fluorescence intensity was measured at excitation wavelength 560 nm, emission wavelength 590 nm using Spectramax M4 (Molecular Devices, USA).

3.4.5.2. Apo-ONE® Homogeneous Caspase-3/7 Assay

Caspase 3/7 assay was performed using Apo-ONE® Homogeneous Caspase-3/7 Assay kit (Promega, USA) following vendor's protocol. Briefly, 2×10^4 Jurkat E6 cells were seeded in

white tissue culture plate and incubated overnight. The cells were treated with 10 µM of compound **5e**, **16c** and **16d** for 72 hours. Apo-ONE® Homogeneous Caspase-3/7 reagent was prepared by mixing Caspase Substrate Z-DEVD-R110 (100X) and Apo-ONE® Homogeneous Caspase-3/7 Buffer. 100 µL of reagent was added to the wells and mixed by shaking it on plate shaker for 30 seconds at 300 rpm. Then plate was incubated for 40 minutes at room temperature and fluorescence intensity was measured at 485 nm excitation wavelength and 527 nm emission wavelength using Spectramax M4 (Molecular Devices, USA).

3.5. CONCLUSION

Here, we have designed and synthesized piperidine and piperazine derivatives containing hydroxamic acid as zinc binding group and different bulky cap groups. The modification of linker region is somewhat least explored in the drug design and discovery of inhibitor of potent and/or selective small molecules. The long chain methylene linker modification with piperidine and piperazine is promising approach of drug design. Compared to piperidine linkers, piperazine derivatives are found to be more effective may be because of urea linkage between cap group and piperazine ring provides favorable hetero atom for hydrogen bonding within the enzyme pocket.

In consideration of cap group modifications, it was observed that increased bulkiness and hydrophobicity increased activity of the compounds (naphthyl, 4-amino[1,1’]biphenyl derivatives compared to phenyl and benzyl derivatives). Further activity was enhanced by introduction of heterocyclic nitrogen atom by 4-aminoquiniline substituent indicates the scope of heterocyclic modifications for further design and development of these compounds.

From the biological characterization of this series of compounds, it was found that the compounds possess potent antiproliferative activity in various cancer cell lines. They displayed efficient activity on solid tumor cell lines as well as leukemia cell line. The compounds showed increased Caspase3/7 activity which provided the evidence of their anticancer potential by activation of apoptotic pathways.

In biochemical enzyme inhibition assays, the compounds exhibited significant HDAC enzyme inhibition in HeLa nuclear extract showing their potential as HDAC inhibitors. To evaluate their activity within Class I HDACs, we screened them against human recombinant HDAC3/NCoR1 enzyme and human recombinant HDAC8 enzyme. Significant HDAC8 inhibition and negligible HDAC3 inhibition proven their selectivity towards HDAC8 compared to HDAC3, though further characterization on other HDACs are needed for more specific insights.

Modifications in hydroxamates with different linker and cap group could not increase potency of the HDAC inhibitors than its prototype SAHA, however they could show similar anticancer potential to SAHA. These newer analogues are more selective towards HDAC8 than SAHA. Vorinostat (SAHA) inhibits HDAC3 and HDAC8 with almost similar potential while newer analogues show remarkable difference between them.

Overall efforts to derivatize hydroxamates with rigid and bulky piperidine and piperazine linkers with bulky cap group modifications yielded novel series of analogues with efficient anticancer potential and preferential HDAC8 inhibition. From the series, compound **16d** having alkyl piperazinyl urea in linker region and 4-aminoquinoline substituent in surface

recognition site came out as lead compound, which can be further modified to design more efficacious and selective HDAC inhibitors.

Chapter 4

Synthesis and biological characterization of selective HDAC8 inhibitors

4.1. INTRODUCTION

Aberrant expression of various HDACs has been observed in many human diseases especially in cancer, which makes them important therapeutic targets for many human cancers (Barneda-Zahonero and Parra 2012). Overexpression of classical HDACs has been represented in pathological situation (Fraga et al. 2005). Hence, histone deacetylase inhibitors (HDACIs) have emerged as promising cancer therapeutic agents.

Classical histone deacetylases are divided in three main classes; Class I HDACs (HDAC1, 2, 3, 8), Class IIa HDACs (HDAC4, 5, 7, 9), Class IIb HDACs (HDAC6 and 10), Class IV HDACs (HDAC11). Class III HDACs are called sirtuins and different in their mechanism from classical HDACs (De Ruijter et al. 2003).

Many of the HDAC inhibitors currently in the clinic are broad-spectrum or pan- HDAC inhibitors (mainly hydroxamates) which inhibit many of the Class I, II and IV isoforms. These include SAHA, panobinostat, PCI-24781, belinostat, JNJ-26481585 and ITF-2357 (Figure 4.1). These compounds have been shown to inhibit most of the HDAC isoforms with nanomolar potency; interestingly, the isoform that is inhibited least potently in each case is the Class I isoform HDAC8 suggesting that the active site of HDAC8 may be structurally distinct (Kinzel et al. 2009; Suzuki et al. 2005).

HDAC8 is an isoform expressed in tumor cell lines and various tissues. HDAC8 is essential for cell survival, and it is implicated in the recently described Cornelia de Lange syndrome (CdLS), which is a congenital malformation disorder (Deardorff et al. 2012; Deardorff et al. 2016). It plays an important role in some diseases, including smooth muscle cell

contractions, acute myeloid leukemia, neuroblastoma, and T cell lymphoma (Ononye et al. 2013).

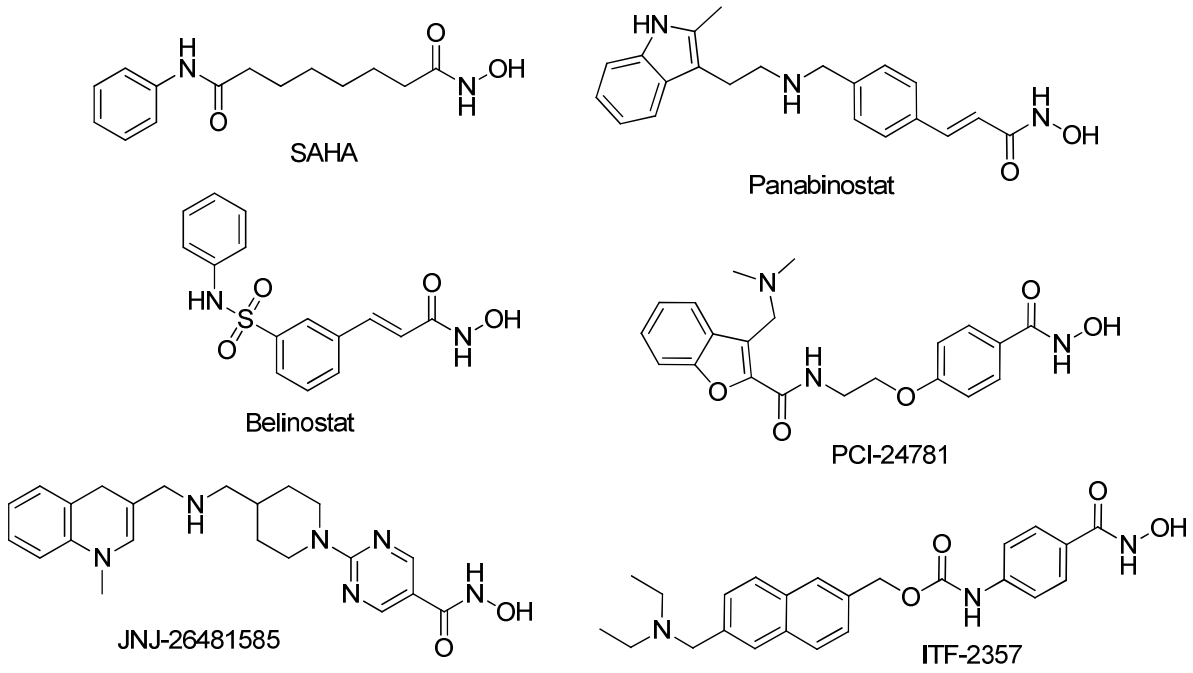

Figure 4.1. Structure of hydroxamic acid containing HDAC inhibitors which are in clinic or in clinical trials

It has been reported in literature that Class I enzymes have an internal pocket at the bottom of the tube-like channel leading to the zinc ion. This 14 Å hydrophobic internal cavity is formed by the same residues for all class I isoforms, with minor differences. HDAC1, HDAC2, and HDAC3 in that order contain the longest cavities, and HDAC-8 has the smallest cavity (Bertrand 2010). Recent reports reveal that HDAC8 possesses a deep hydrophobic pocket adjacent to the active site channel, allowing the design of HDAC8 selective compounds that interact with both the active site Zn^{2+} ion and this sub pocket. These unique features can be exploited to design selective compounds for class I HDACs

(Bourguet et al. 2017). Few HDAC8 selective inhibitors with different structures are represented in Figure 4.2.

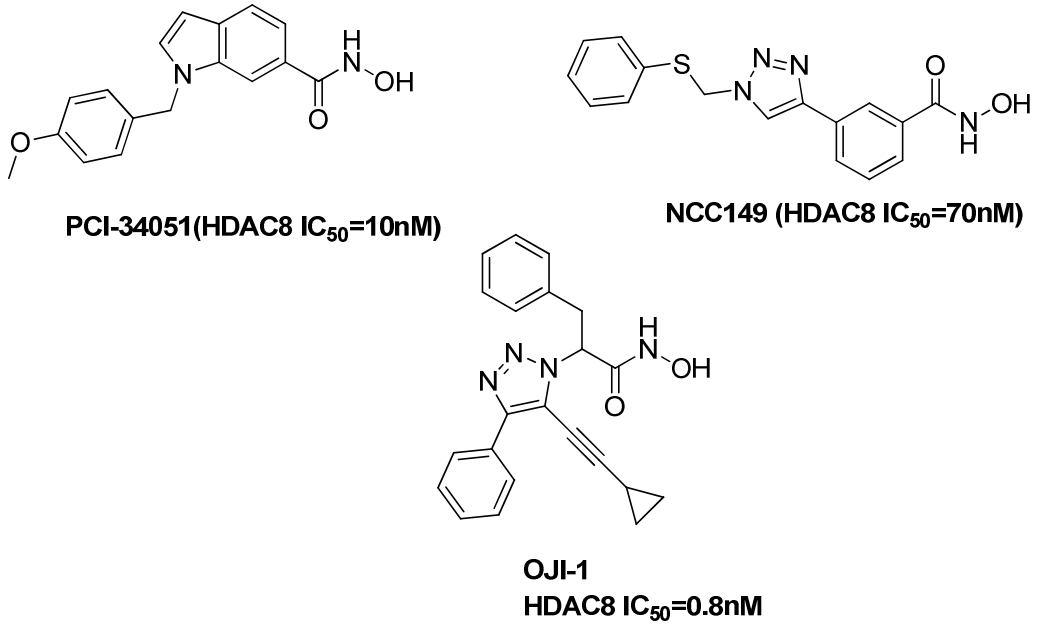

Figure 4.2. Structure of HDAC8 selective inhibitors

From the figure 4.2, it is clear that these compounds have short length of linker as well as side chain attached to linker improves activity (e.g. **OJI-1**)(Amin et al. 2017). With these perspectives in mind, we have synthesized a series of compounds having aliphatic side chain as linker with a hanging aliphatic moiety between the ZBG and cap region. The synthesized novel compounds have been screened for HDAC inhibition potency and selectivity as well as their anticancer activity.

4.2. RESULTS AND DISCUSSION

4.2.1. Chemistry

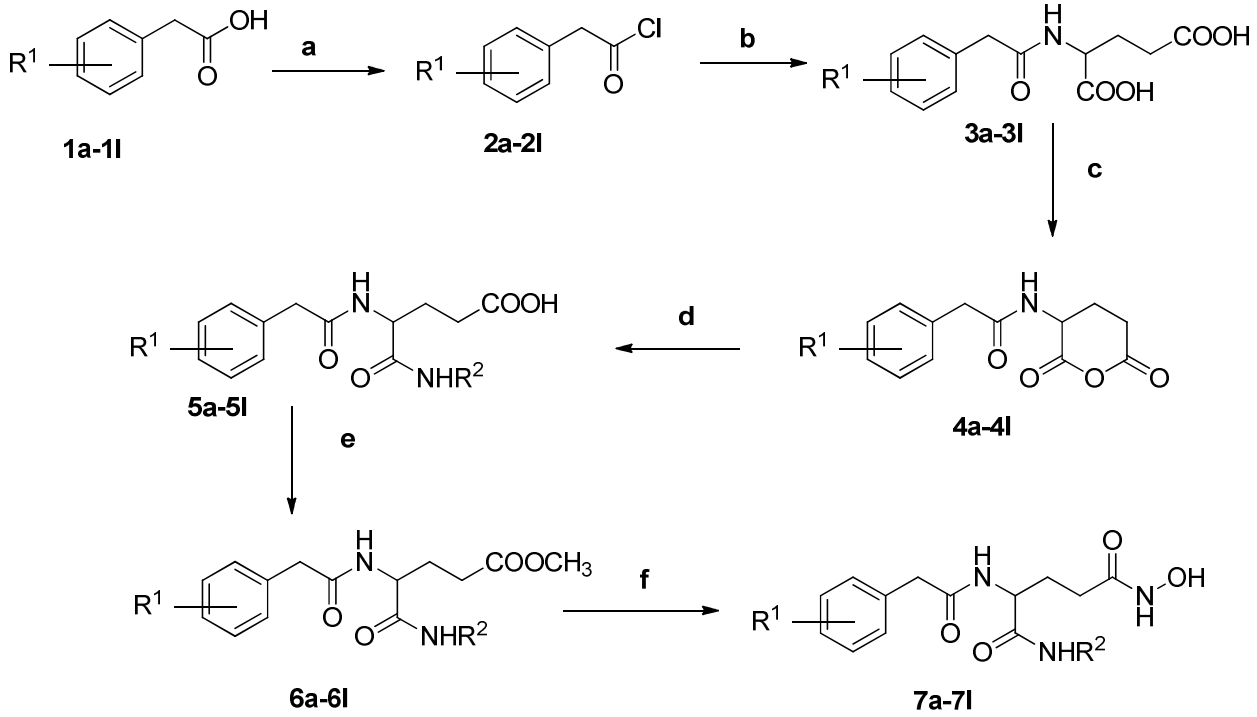

Scheme 4.1. *Reagents & conditions:* (a) i. thionyl chloride ii. benzene (b) i. L(+) glutamic acid ii.2N NaOH iii. 1N HCl (c) i. DCC ii. Chloroform (d) i. R_2NH_2 ii. 1N Na_2CO_3 iii. 1N HCl (e) i. thionyl chloride, ii. anhydrous methanol, 12h, 0°C (f) i: 50% w/v aqueous hydroxylamine solution, ii: 1N sodium hydroxide, iii: methanol (1:1), 2h, RT iv.1M hydrochloric acid

A series of novel compounds have been synthesized as described in Scheme 4.1. Purity of these final compounds was evaluated using ^{1}H NMR, ^{13}C NMR and LC/MS analysis. Spectral data of these compounds are provided in experimental methods.

4.2.2. HDAC inhibition assay and selectivity of compounds

All target compounds were screened for their HDAC enzyme inhibition efficiency. First we tested these compounds on HeLa nuclear extract which is rich in HDAC1 and HDAC2

(Serebryannyy et al. 2016). It was observed that compounds **7c, 7d, 7e, 7f, 7h, 7i, 7k, 7l** were showing good inhibition (Figure 4.3 and Table 4.1). Again they were tested on human recombinant HDAC8 at the same concentration (10 μM). Almost all compounds were found to show promising HDAC8 inhibition. Particularly compound **7d, 7f, 7h, 7i, 7k** and **7l** were showing more than 80% HDAC8 inhibition. Another Class I HDAC, HDAC3 was also screened for inhibition by these compounds. These compounds found to show minimal inhibition of HDAC3. These results demonstrate selectivity of these compounds towards HDAC8.

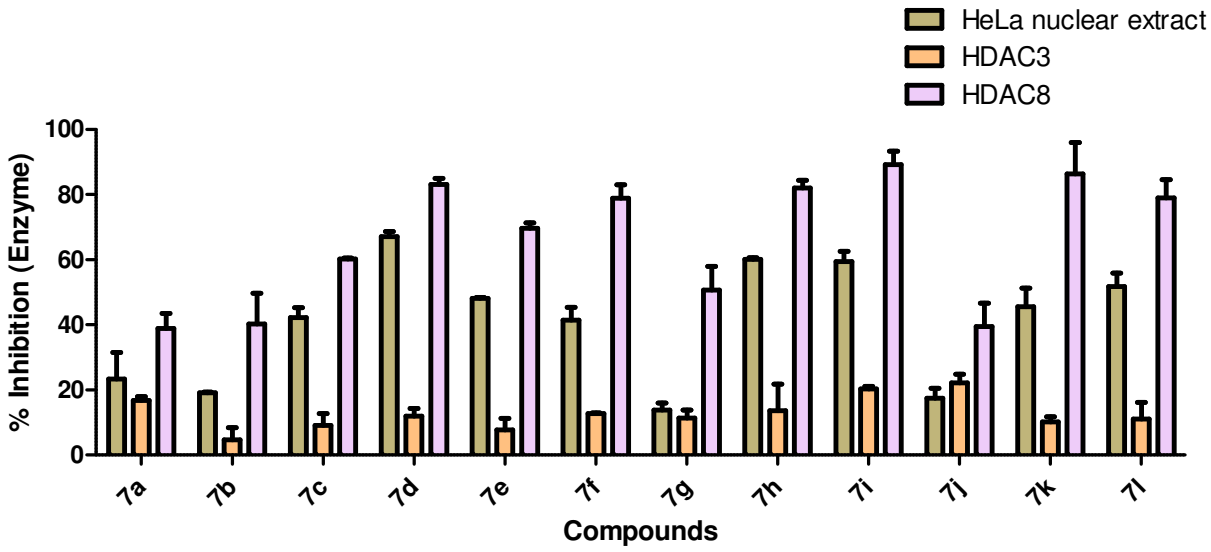

Figure 4.3. HDAC inhibition efficiency of all target compounds. All novel compounds were screened at 10μM concentration on HeLa nuclear extract, human recombinant HDAC3 and human recombinant HDAC8.

Table 4.1. %HDAC inhibition of target compounds in HeLa nuclear extract, human recombinant HDAC3 and human recombinant HDAC8

Cpd	R^1	R^2	% Inhibition at 10μM		
			HeLa nuclear extract	HDAC3/NCoR1	HDAC8
7a	2-Br	n-C_5H_{11}	23.25	16.71	38.84
7b	2-F	i-C_4H_9	19.14	4.65	40.17
7c	4-Br	n-C_5H_{11}	42.24	9.02	60.24
7d	4-Br	n-C_6H_{13}	67.16	11.96	83.14
7e	4-Cl	n-C_4H_9	48.12	7.73	69.66
7f	4-Cl	n-C_5H_{11}	41.46	12.67	78.84
7g	4-NO_2	n-C_4H_9	13.77	11.36	50.61
7h	2,4-dichloro	n-C_4H_9	60.11	13.63	82.05
7i	2,4-dichloro	n-C_5H_{11}	59.42	20.33	89.17
7j	2,4-dichloro	C_6H_5	17.43	22.11	39.44
7k	-	n-C_5H_{11}	45.52	10.10	86.38
7l	-	n-C_6H_{13}	51.69	11.08	78.94

4.2.3. Cellular studies using anticancer cell lines

4.2.3.1. Antiproliferative assay using cancer cell lines

Cytotoxicity studies were performed on three different cell lines, i.e., B16F10 (murine melanoma cell line), non-small cell lung cancer cell line (A549) and human acute T cell

leukemia (Jurkat E6) by MTT assay method. All the synthesized compounds were evaluated at two different concentrations (100 and 10 μM) in triplicate (Figure 4.4 (i-iii)). From the assay results, it was observed that few compounds displayed good cytotoxicity in similar trend on cell lines.

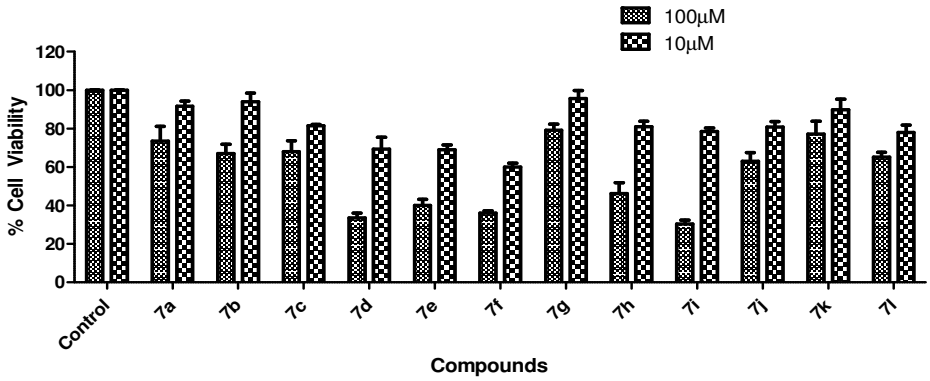

[i] B16F10 cells

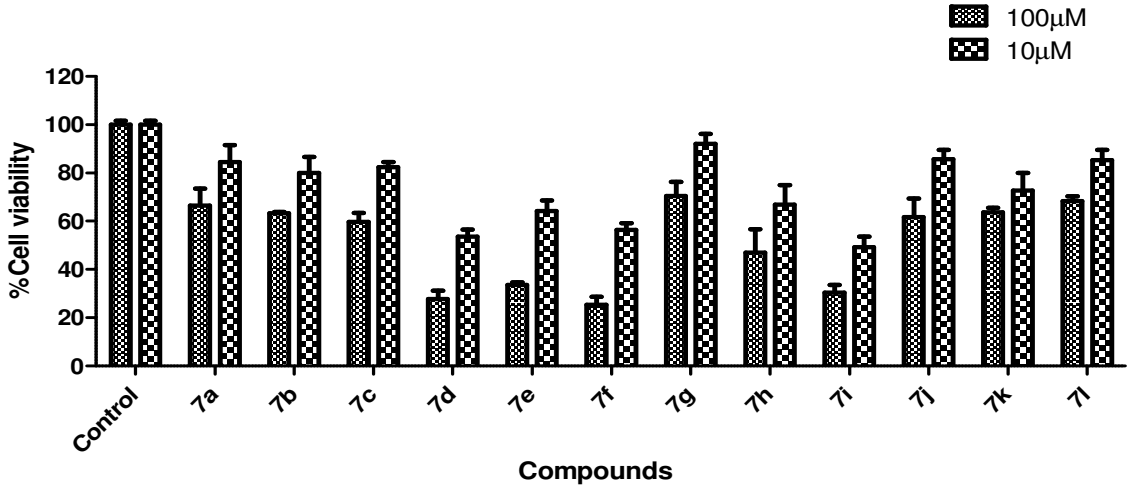

[ii] A-549 cells

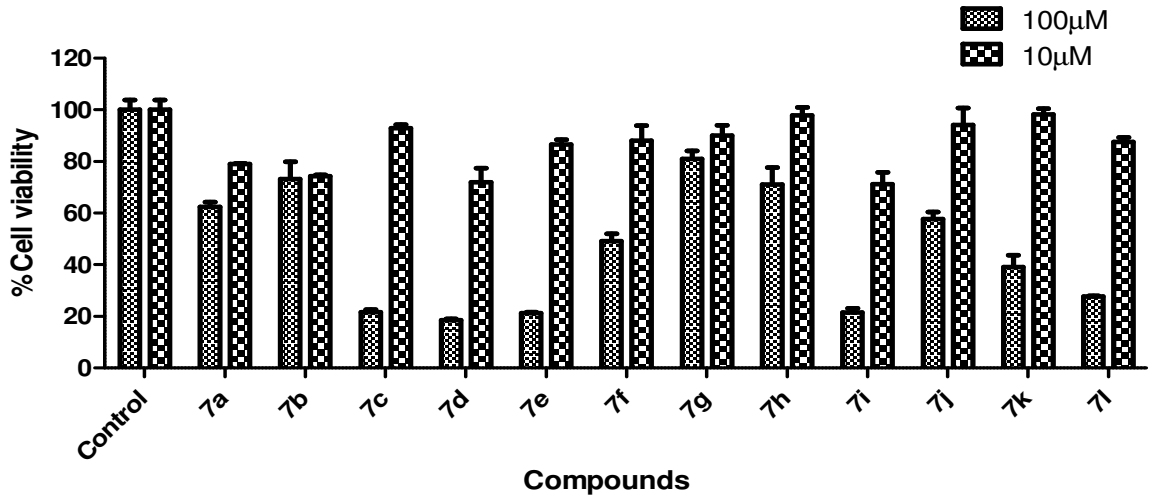

[iii] Jurkat E6 cells

Figure 4.4. MTT assay of novel synthesized compounds on B16F10 cells [i], A549 cells [ii] and Jurkat E6 cells [iii]. Cells were treated for 72 hours and cell viability was measured by MTT reagent. Data represents mean ± SD (n=3).

Promising compounds (**7d, 7e, 7f, 7h, 7i**) were further screened to find out their IC_{50} values in all three cell lines. Results are displayed in Figure 4.5 (i-iii) and Table 4.2.

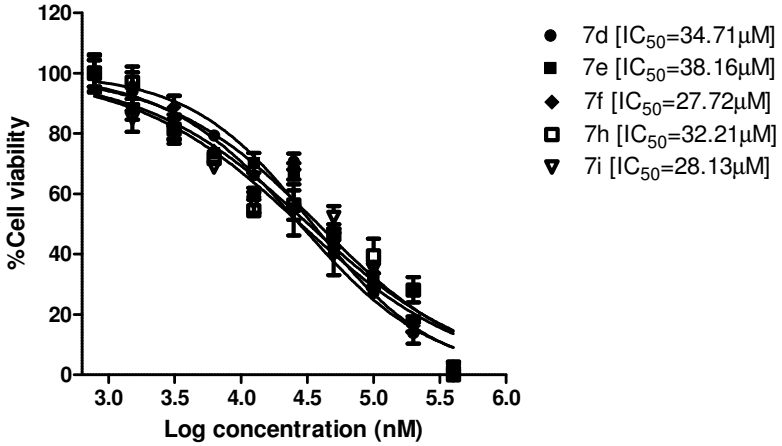

[i] B16F10 cells

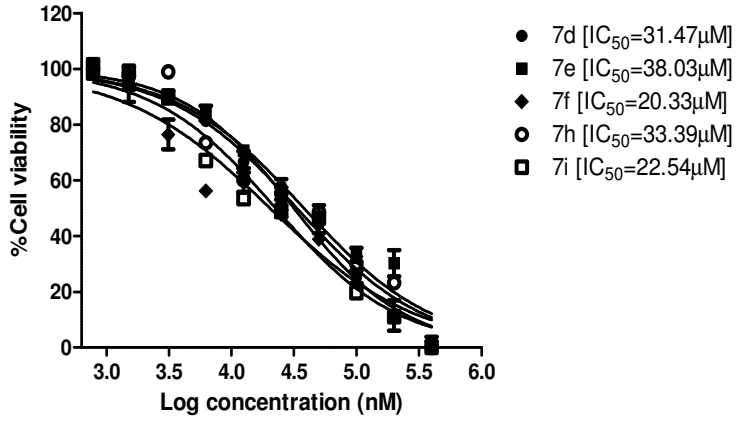

[ii] A-549 cells

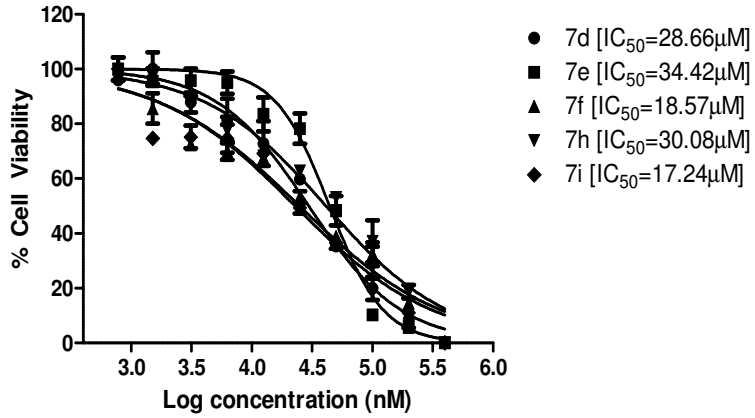

[iii] Jurkat E6 cells

Figure 4.5. Dose response curve of **7d, 7e, 7f, 7h** and **7i** on B16F10 cells [i], A549 cells [ii] and Jurkat E6 cells [iii]. These compounds were tested in 10 different doses and incubated for 72 hours. Cell viability was measured using MTT reagent. Data represents mean ± SD (n=2).

Table 4.2. IC_{50} values of target compounds in different cancer cell lines

Cpd	R^1	R^2	IC_{50} (µM) in B16F10 cells	IC_{50} (µM) in A549 cells	IC_{50} (µM) in Jurkat E6 cells
7a	2-Br	n-C_5H_{11}	> 50	> 50	> 50
7b	2-F	i-C_4H_9	> 50	> 50	> 50

7c	4-Br	n-C_5H_{11}	> 50	> 50	> 50
7d	4-Br	n-C_6H_{13}	34.71	31.47	28.66
7e	4-Cl	n-C_4H_9	38.16	38.03	34.42
7f	4-Cl	n-C_5H_{11}	27.72	20.33	18.57
7g	4-NO_2	n-C_4H_9	> 50	> 50	> 50
7h	2,4-dichloro	n-C_4H_9	32.21	33.39	30.08
7i	2,4-dichloro	n-C_5H_{11}	28.13	22.54	17.24
7j	2,4-dichloro	C_6H_5	> 50	> 50	> 50
7k	-	n-C_5H_{11}	> 50	> 50	> 50
7l	-	n-C_6H_{13}	> 50	> 50	> 50

It was found that among three cell lines, highest activity was seen in Jurkat E6 cells. Increased activity was observed with compounds having alkyl side chain with five carbon atoms. This length found most suitable as four carbon and six carbon chain showed comparatively lesser activity. Again substitution on phenyl ring showed impact on activity. It has been noticed that chloro substitution on phenyl ring is favorable.

4.2.3.2. Cell cycle analysis

We further investigated the effect of **7d** and **7i** on cell cycle progression in B16F10 cells (Figure 4.6). From the result, it was found that compound **7d** and **7i** induced growth arrest at G2/M phase of cell growth. Compound **7i** induced significant growth arrest around 42.5% in G2/M phase compared to control showing 9.32%, while G0/G1 phase decreased to 10.5% from 74.6%. The similar pattern of growth arrest was found for **7d** also. These results

indicated that compound **7i** might produce anticancer activity with the growth arrests at G2/M phase.

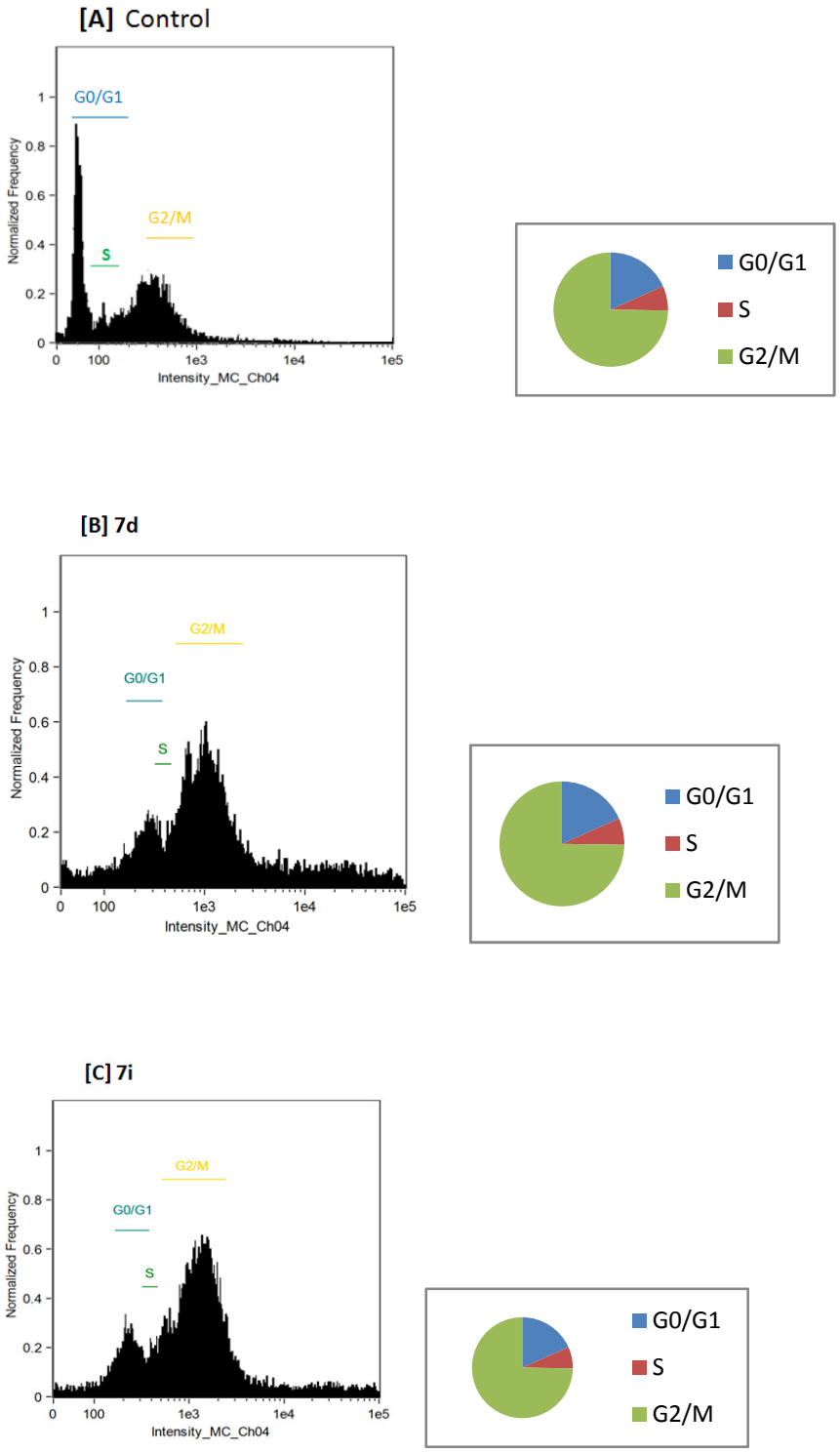

G0/G1	74.6
S	2.31
G2/M	9.32

G0/G1	9.69
S	4.22
G2/M	35.5

G0/G1	10.5
S	3.98
G2/M	42.8

Figure 4.6. Cell cycle arrest induced in B16F10 cells by (A) **Control**, (B) **7d**, (C) **7i**.

4.3. MATERIAL AND METHODS

4.3.1. Chemistry

All starting material and reagents were commercially available and used without further purification. All reactions were monitored by thin layer chromatography (TLC) using precoated plates with silica gel F254 from Merck Millipore Co., USA. ^{1}H and ^{13}C NMR spectrum were recorded in DMSO-d_6 using Nuclear Magnetic Resonance (NMR) Spectrophotometer High Performance-400 MHz (Bruker Biospin, Switzerland). Mass spectroscopy was performed in LCMS-2020, Schimadzu using ESI mode. The Purity of the compounds were analyzed by Analytical LC/MS. Analysis was performed on a LCMS-8040 equipped with a photodiode array detector using a Shiseido C18 4.6×150 mm, 5µ column at a flow rate of 1 mL/minute with isocratic flow (20% A: 80%B ; Solvent A = water + 0.4% TFA , solvent B = methanol).

Synthesis of substituted phenylacetyl chlorides/napthylacetyl chloride (2a-2l)

Substituted phenyl acetic acid or naphthyl acetic acid (1a-1l) was dissolved in benzene. Thionyl chloride (0.5 equivalents) was added drop-wise from the dropping funnel. Anhydrous condition was maintained in the reaction flask. The reaction mixture was refluxed for 3–4 hours until HCl gas evolution stops. The evolution of HCl gas was checked by Congo red paper. The excess of thionyl chloride was removed by distillation with dry benzene to obtain the products (2a-2l) which were used immediately in the next reaction without further purification.

Synthesis of 2-*N*-(substituted phenylacetyl)-L(+)-isoglutamic acids (3a-3j) and 2-*N*-napthylacetyl-L(+)-isoglutamic acid (3k-3l)

L(+)-Glutamic acid (1 equivalent) was taken in a round bottom flask. Sodium hydroxide solution (2 N) was added slowly to the above flask till all glutamic acid dissolved and the mixture become slightly alkaline (pH 7.5–8.0). The reaction mixture was stirred in ice bath at 0°C temperature. Substituted phenylacetyl chlorides or napthylacetyl chlorides (2a-2l) (1 equivalent) was added in small portion at a time to the reaction mixture with constant stirring, and sodium hydroxide (2 N) was added in between to keep the reaction mixture alkaline. The progress of reaction was monitored by TLC. After the completion of the reaction, the reaction mixture was washed with diethyl ether. The aqueous solutions were then acidified with 6 N HCl in ice cold condition to precipitate the solid products. The precipitated products were filtered, washed several time with distilled water and dried under vacuum. These products were obtained in quantitative yield (>90%) and good purity, therefore subjected for next reaction without further characterization.

Synthesis of substituted pentanoic acid (5a-5l)

Substituted acids (3a-3l) were dissolved in dry chloroform. The reaction mixture was stirred on a magnetic stirrer with the temperature maintained at 0–5°C under anhydrous condition. The *N,N*-dicyclohexylcarbidiimide (DCC) (1 equivalent) was dissolved in 20 ml dry chloroform and it was added slowly and gradually to the reaction mixture with continuous stirring. After 1 h of stirring, substituted amine (2 equivalents) was added to the reaction mixture and continuously stirred for 5–6 h. After the reaction was over, the reaction mixture was kept in the refrigerator for overnight. The solution was filtered and both the solid part [dicyclohexylurea (DCU)] and the liquid (chloroform) layer were extracted with cold 1 N sodium carbonate (Na_2CO_3) solution. The aqueous part was then acidified to pH 2 with 1 N HCl in cold condition to obtain solid precipitations of these products separately. The product

was extracted with ethyl acetate and was dried with anhydrous sodium sulphate overnight. It was evaporated to get the crude residues. The residues were recrystallized from ethanol and dried to obtain the target compounds as white solid.

4-(2-(2-bromophenyl)acetamido)-5-oxo-5-(pentylamino)pentanoic acid (5a)

Yield 86%, white powder, ^{1}H NMR (400 MHz, DMSO-d_6) δ 8.23 (d, *J* = 8.1 Hz, 1H), 7.91 (t, *J* = 5.6 Hz, 1H), 7.59 – 7.56 (m, 1H), 7.36 – 7.29 (m, 2H), 7.18 (m, 1H), 4.25 m, 1H), 3.65 (d, *J* = 5.6 Hz, 2H), 3.04 (qd, *J* = 13.1, 6.0 Hz, 2H), 2.32 (t, *J* = 7.8 Hz, 2H), 1.97 – 1.72 (m, 2H), 1.43 – 1.34 (m, 2H), 1.24 (t, *J* = 15.2 Hz, 5H), 0.85 (t, *J* = 7.0 Hz, 3H). $C_{18}H_{25}BrN_2O_4$ [M]: 413.31; MS (ESI) *m/z*: $[M]^+$: 413,$[M+2]^+$:415

4-(2-(2-fluorophenyl)acetamido)-5-(isobutylamino)-5-oxopentanoic acid (5b)

Yield 93.6%, white solid, ^{1}H NMR (400 MHz, DMSO-d_6) δ 8.27 (d, *J* = 8.1 Hz, 1H), 7.93 (t, *J* = 5.8 Hz, 1H), 7.34 – 7.24 (m, 2H), 7.17 – 7.10 (m, 2H), 4.27 (td, *J* = 8.3, 5.7 Hz, 1H), 3.54 (d, *J* = 3.8 Hz, 2H), 2.96 – 2.80 (m, 2H), 2.30 (t, *J* = 7.9 Hz, 2H), 1.96 – 1.61 (m, 3H), 0.82 (d, *J* = 6.7 Hz, 6H). $C_{17}H_{23}FN_2O_4$ [M]: 338.37; MS (ESI) *m/z*: $[M+H]^+$: 339

4-(2-(4-bromophenyl)acetamido)-5-oxo-5-(pentylamino)pentanoic acid (5c)

Yield 72.5%, cream color solid, ^{1}H NMR (400 MHz, DMSO-d_6) δ 8.26 (d, *J* = 8.1 Hz, 1H), 7.92 (t, *J* = 5.6 Hz, 1H), 7.50 – 7.46 (m, 2H), 7.22 (d, *J* = 8.4 Hz, 2H), 4.20 (td, *J* = 8.2, 5.8 Hz, 1H), 3.45 (d, *J* = 3.2 Hz, 2H), 3.08 – 2.94 (m, 2H), 2.26 (t, *J* = 7.8 Hz, 2H), 1.40 – 1.32 (m, 2H), 1.29 – 1.17 (m, 6H), 0.84 (t, *J* = 7.1 Hz, 3H). $C_{18}H_{25}BrN_2O_4$ [M]: 413.31; MS (ESI) *m/z*: $[M]^+$: 413, $[M+2]^+$:415

4-(2-(4-bromophenyl)acetamido)-5-(hexylamino)-5-oxopentanoic acid (5d)

Yield 70%, cream color powder, ^{1}H NMR (400 MHz, DMSO-d_6) δ 8.27 (d, *J* = 8.2 Hz, 1H), 7.92 (t, *J* = 5.6 Hz, 1H), 7.48 (d, *J* = 6.5 Hz, 2H), 7.21 (d, *J* = 8.4 Hz, 2H), 4.20 (dd, *J* = 14.0, 8.2 Hz, 1H), 3.45 (d, *J* = 3.1 Hz, 2H), 3.09 – 2.93 (m, 2H), 2.25 (t, *J* = 7.9 Hz, 2H), 1.93 – 1.69 (m, 2H), 1.38 – 1.32 (m, 2H), 1.22 (d, *J* = 3.0 Hz, 6H), 0.85 (t, *J* = 6.8 Hz, 3H). $C_{19}H_{27}BrN_2O_4$ [M]: 427.33; MS (ESI) *m/z*: $[M]^+$: 427, $[M+2]^+$:429

5-(butylamino)-4-(2-(4-chlorophenyl)acetamido)-5-oxopentanoic acid (5e)

Yield 92.7%, pale cream color powder, ^{1}H NMR (400 MHz, DMSO-d_6) δ 8.26 (d, *J* = 8.2 Hz, 1H), 7.91 (t, *J* = 5.6 Hz, 1H), 7.35 (d, *J* = 8.4 Hz, 2H), 7.27 (d, *J* = 8.4 Hz, 2H), 4.20 (dd, *J* = 14.0, 8.2 Hz, 1H), 3.47 (d, *J* = 3.4 Hz, 2H), 2.25 (t, *J* = 7.9 Hz, 2H), 1.37 – 1.19 (m, 8H), 0.85 (t, *J* = 7.3 Hz, 3H). $C_{17}H_{23}ClN_2O_4$ [M]: 354.83; MS (ESI) *m/z*: $[M+2]^+$: 356

4-(2-(4-chlorophenyl)acetamido)-5-oxo-5-(pentylamino)pentanoic acid (5f)

Yield 75%, white powder, ^{1}H NMR (400 MHz, DMSO-d_6) δ 8.26 (d, *J* = 8.2 Hz, 1H), 7.92 (t, *J* = 5.6 Hz, 1H), 7.34 (d, *J* = 8.5 Hz, 2H), 7.28 (d, *J* = 8.5 Hz, 2H), 4.25 – 4.18 (m, 1H), 3.48 (d, *J* = 3.4 Hz, 2H), 2.26 (t, *J* = 7.9 Hz, 2H), 1.94 – 1.71 (m, 2H), 1.41 – 1.16 (m, 8H), 0.84 (t, *J* = 7.1 Hz, 3H). $C_{18}H_{25}ClN_2O_4$ [M]: 368.86; MS (ESI) *m/z*: $[M+H]^+$: 369

5-(butylamino)-4-(2-(4-nitrophenyl)acetamido)-5-oxopentanoic acid (5g)

Yield 83%, yellow powder, ^{1}H NMR (400 MHz, DMSO-d_6) δ 8.39 (d, *J* = 8.1 Hz, 1H), 8.17 (d, *J* = 8.8 Hz, 2H), 7.96 (t, *J* = 5.5 Hz, 1H), 7.54 (d, *J* = 8.8 Hz, 2H), 4.22 (t, *J* = 11.1 Hz, 1H), 3.66 (d, *J* = 3.0 Hz, 2H), 3.09 – 2.97 (m, 2H), 2.27 (t, *J* = 7.8 Hz, 2H), 1.94 – 1.70 (m, 2H), 1.38 – 1.19 (m, 4H), 0.84 (t, *J* = 7.3 Hz, 3H). $C_{17}H_{23}N_3O_6$ [M]: 365.38; MS (ESI) *m/z*: $[M+H]^+$: 366

5-(butylamino)-4-(2-(2,4-dichlorophenyl)acetamido)-5-oxopentanoic acid (5h)

Yield 73%, Cream color solid, ^{1}H NMR (400 MHz, DMSO-d_6) δ 8.28 (d, *J* = 8.2 Hz, 1H), 7.91 (t, *J* = 5.6 Hz, 1H), 7.58 (t, *J* = 1.1 Hz, 1H), 7.38 (d, *J* = 1.2 Hz, 2H), 4.24 (m, 1H), 3.65 (d, *J* = 5.6 Hz, 2H), 3.10 – 2.98 (m, 2H), 2.33 – 2.28 (m, 2H), 1.82 (m, 2H), 1.39 – 1.23 (m, 4H), 0.86 (t, *J* = 7.3 Hz, 3H). $C_{17}H_{22}Cl_2N_2O_4$ [M]: 389.27; MS (ESI) *m/z*: $[M]^+$: 389, $[M+2]^+$: 391

4-(2-(2,4-dichlorophenyl)acetamido)-5-oxo-5-(pentylamino)pentanoic acid (5i)

Yield 82.8%, White solid, ^{1}H NMR (400 MHz, DMSO-d_6) δ 8.66 (d, *J* = 8.1 Hz, 1H), 7.91 (t, *J* = 5.6 Hz, 1H), 7.68 (s, 1H), 7.50 (d, *J* = 0.9 Hz, 2H), 4.34 (m, 1H), 3.14 – 3.01 (m, 2H), 2.12 – 1.75 (m, 4H), 1.39 (dd, *J* = 13.1, 6.4 Hz, 2H), 1.31 – 1.15 (m, 6H), 0.86 (t, *J* = 6.7 Hz, 3H). $C_{18}H_{24}Cl_2N_2O_4$ [M]: 403.30; MS (ESI) *m/z*:$[M]^-$:403, [M-2]: 401

4-(2-(2,4-dichlorophenyl)acetamido)-5-oxo-5-(phenylamino)pentanoic acid (5j)

Yield 67%, off white powder, ^{1}H NMR (400 MHz, DMSO-d_6) δ 8.75 (d, *J* = 8.0 Hz, 1H), 8.50 (t, *J* = 5.9 Hz, 1H), 7.69 (t, *J* = 1.1 Hz, 1H), 7.51 (d, *J* = 1.1 Hz, 2H), 7.34 – 7.23 (m, 5H), 4.46 (m, 1H), 4.32 (d, *J* = 6.0 Hz, 2H), 2.44 – 2.39 (m, 2H), 2.09 – 1.83 (m, 2H). $C_{19}H_{18}Cl_2N_2O_4$ [M]: 409.26; MS (ESI) *m/z*:$[M+H]^+$: 410

4-(2-(naphthalen-2-yl)acetamido)-5-oxo-5-(pentylamino)pentanoic acid (5k)

Yield 75.65%, white powder, ^{1}H NMR (400 MHz, DMSO-d_6) δ 8.38 (d, *J* = 8.2 Hz, 1H), 8.10 – 8.07 (m, 1H), 7.94 – 7.90 (m, 2H), 7.81 (dd, *J* = 7.1, 2.3 Hz, 1H), 7.52 – 7.47 (m, 2H), 7.43 (dd, *J* = 7.1, 5.1 Hz, 2H), 4.24 (td, *J* = 8.2, 5.7 Hz, 1H), 3.97 (q, *J* = 15.0 Hz, 2H), 3.02 (m, 2H), 2.32 – 2.26 (m, 2H), 1.40 – 1.16 (m, 8H), 0.84 (t, *J* = 7.0 Hz, 3H). $C_{22}H_{28}N_2O_4$ [M]: 384.47; MS (ESI) *m/z*: $[M+H]^+$: 385

5-(hexylamino)-4-(2-(naphthalen-2-yl)acetamido)-5-oxopentanoic acid (5l)

Yield 79%, white powder, ^{1}H NMR (400 MHz, DMSO-d_6) δ 10.43 (s, 1H), 8.42 (d, *J* = 8.1 Hz, 1H), 8.12 – 8.05 (m, 1H), 7.93 – 7.87 (m, 2H), 7.81 (dd, *J* = 6.3, 3.0 Hz, 1H), 7.53 – 7.41 (m, 4H), 4.24 – 4.17 (m, 1H), 3.98 (d, *J* = 2.8 Hz, 2H), 3.07 – 2.96 (m, 2H), 2.03 – 1.68 (m, 5H), 1.39 – 1.18 (m, 9H), 0.85 (t, *J* = 6.7 Hz, 3H). $C_{23}H_{30}N_2O_4$ [M]: 398.50; MS (ESI) *m/z*: $[M+H]^+$: 399

Synthesis of substituted pentanoate (6a-6l)

The substituted pentanoic acids (**5a-5l**) were dissolved in anhydrous methanol and flask was kept in ice bath to get 0°C temperature. Thionylchloride (1.5-2ml) was added drop wise to the above mixture and stirred overnight. The reaction mixture was concentrated and diluted with ethyl acetate. The organic layer was washed with aqueous saturated sodiumbicarbonate solution and brine solution. The crude organic mixture was purified by column chromatography EtOAc:Hexane (3:7) as a mobile phase.

methyl 4-(2-(2-bromophenyl)acetamido)-5-oxo-5-(pentylamino)pentanoate (6a)

Yield 56.09%, white powder, ^{1}H NMR (400 MHz, DMSO-d_6) δ 8.23 (d, *J* = 8.1 Hz, 1H), 7.91 (t, *J* = 5.6 Hz, 1H), 7.59 – 7.56 (m, 1H), 7.36 – 7.29 (m, 2H), 7.18 (m, 1H), 4.25 m, 1H), 3.65 (d, *J* = 5.6 Hz, 2H), 3.58 (s, 3H), 3.04 (qd, *J* = 13.1, 6.0 Hz, 2H), 2.32 (t, *J* = 7.8 Hz, 2H), 1.97 – 1.72 (m, 2H), 1.43 – 1.34 (m, 2H), 1.24 (t, *J* = 15.2 Hz, 5H), 0.85 (t, *J* = 7.0 Hz, 3H). $C_{19}H_{27}BrN_2O_4$ [M]: 427.33; MS (ESI) *m/z*: $[M]^+$: 427, $[M+2]^+$: 429

methyl 4-(2-(2-fluorophenyl)acetamido)-5-(isobutylamino)-5-oxopentanoate (6b)

Yield 73.6%, white solid, ^{1}H NMR (400 MHz, DMSO-d_6) δ 8.27 (d, *J* = 8.1 Hz, 1H), 7.93 (t, *J* = 5.8 Hz, 1H), 7.34 – 7.24 (m, 2H), 7.17 – 7.10 (m, 2H), 4.27 (td, *J* = 8.3, 5.7 Hz, 1H),

3.58 (s, 3H), 3.54 (d, *J* = 3.8 Hz, 2H), 2.96 – 2.80 (m, 2H), 2.30 (t, *J* = 7.9 Hz, 2H), 1.96 – 1.61 (m, 3H), 0.82 (d, *J* = 6.7 Hz, 6H). $C_{18}H_{25}FN_2O_4$ [M]: 352.40; MS (ESI) *m/z*: $[M+H]^+$: 353

methyl 4-(2-(4-bromophenyl)acetamido)-5-oxo-5-(pentylamino)pentanoate(6c)

Yield 62.15%, cream powder, ^{1}H NMR (400 MHz, DMSO-d_6) δ 8.26 (d, *J* = 8.1 Hz, 1H), 7.92 (t, *J* = 5.6 Hz, 1H), 7.50 – 7.46 (m, 2H), 7.22 (d, *J* = 8.4 Hz, 2H), 4.20 (td, *J* = 8.2, 5.8 Hz, 1H), 3.57 (s, 3H), 3.45 (d, *J* = 3.2 Hz, 2H), 3.08 – 2.94 (m, 2H), 2.26 (t, *J* = 7.8 Hz, 2H), 1.40 – 1.32 (m, 2H), 1.29 – 1.17 (m, 6H), 0.84 (t, *J* = 7.1 Hz, 3H). $C_{19}H_{27}BrN_2O_4$ [M]: 427.33; MS (ESI) *m/z*: $[M]^+$: 427, $[M+2]^+$: 429

methyl 4-(2-(4-bromophenyl)acetamido)-5-(hexylamino)-5-oxopentanoate (6d)

Yield 30%, cream color powder, ^{1}H NMR (400 MHz, DMSO-d_6) δ 8.27 (d, *J* = 8.2 Hz, 1H), 7.92 (t, *J* = 5.6 Hz, 1H), 7.48 (d, *J* = 6.5 Hz, 2H), 7.21 (d, *J* = 8.4 Hz, 2H), 4.20 (dd, *J* = 14.0, 8.2 Hz, 1H), 3.56 (s, 3H), 3.45 (d, *J* = 3.1 Hz, 2H), 3.09 – 2.93 (m, 2H), 2.25 (t, *J* = 7.9 Hz, 2H), 1.93 – 1.69 (m, 2H), 1.38 – 1.32 (m, 2H), 1.22 (d, *J* = 3.0 Hz, 6H), 0.85 (t, *J* = 6.8 Hz, 3H). $C_{20}H_{29}BrN_2O_4$ [M]: 441.36; MS (ESI) *m/z*: $[M]^+$: 441, $[M+2]^+$:443

methyl 5-(butylamino)-4-(2-(4-chlorophenyl)acetamido)-5-oxopentanoate (6e)

Yield 92.7%, pale cream color powder, ^{1}H NMR (400 MHz, DMSO-d_6) δ 8.26 (d, *J* = 8.2 Hz, 1H), 7.91 (t, *J* = 5.6 Hz, 1H), 7.35 (d, *J* = 8.4 Hz, 2H), 7.27 (d, *J* = 8.4 Hz, 2H), 4.20 (dd, *J* = 14.0, 8.2 Hz, 1H), 3.57 (s, 3H), 3.47 (d, *J* = 3.4 Hz, 2H), 2.25 (t, *J* = 7.9 Hz, 2H), 1.37 – 1.19 (m, 8H), 0.85 (t, *J* = 7.3 Hz, 3H). $C_{18}H_{25}ClN_2O_4$ [M]: 368.86; MS (ESI) *m/z*: $[M+2]^+$: 369

methyl 4-(2-(4-chlorophenyl)acetamido)-5-oxo-5-(pentylamino)pentanoate (6f)

Yield 68%, white powder, ^{1}H NMR (400 MHz, DMSO-d_6) δ 8.26 (d, *J* = 8.2 Hz, 1H), 7.92 (t, *J* = 5.6 Hz, 1H), 7.34 (d, *J* = 8.5 Hz, 2H), 7.28 (d, *J* = 8.5 Hz, 2H), 4.25 – 4.18 (m, 1H), 3.57 (s, 3H), 3.48 (d, *J* = 3.4 Hz, 2H), 2.26 (t, *J* = 7.9 Hz, 2H), 1.94 – 1.71 (m, 2H), 1.41 – 1.16 (m, 8H), 0.84 (t, *J* = 7.1 Hz, 3H). $C_{19}H_{27}ClN_2O_4$ [M]: 382.88; MS (ESI) *m/z*: $[M+H]^+$: 383

methyl 5-(butylamino)-4-(2-(4-nitrophenyl)acetamido)-5-oxopentanoate (6g)

Yield 53%, yellow powder, ^{1}H NMR (400 MHz, DMSO-d_6) δ 8.39 (d, *J* = 8.1 Hz, 1H), 8.17 (d, *J* = 8.8 Hz, 2H), 7.96 (t, *J* = 5.5 Hz, 1H), 7.54 (d, *J* = 8.8 Hz, 2H), 4.22 (t, *J* = 11.1 Hz, 1H), 3.66 (d, *J* = 3.0 Hz, 2H), 3.56 (s, 3H), 3.09 – 2.97 (m, 2H), 2.27 (t, *J* = 7.8 Hz, 2H), 1.94 – 1.70 (m, 2H), 1.38 – 1.19 (m, 4H), 0.84 (t, *J* = 7.3 Hz, 3H). $C_{18}H_{25}N_3O_6$ [M]: 379.17; MS (ESI) *m/z*: $[M+H]^+$: 380

methyl 5-(butylamino)-4-(2-(2,4-dichlorophenyl)acetamido)-5-oxopentanoate (6h)

Yield 43%, Cream color solid, ^{1}H NMR (400 MHz, DMSO-d_6) δ 8.28 (d, *J* = 8.2 Hz, 1H), 7.91 (t, *J* = 5.6 Hz, 1H), 7.58 (t, *J* = 1.1 Hz, 1H), 7.38 (d, *J* = 1.2 Hz, 2H), 4.24 (m, 1H), 3.65 (d, *J* = 5.6 Hz, 2H), 3.58 (s, 3H), 3.10 – 2.98 (m, 2H), 2.33 – 2.28 (m, 2H), 1.82 (m, 2H), 1.39 – 1.23 (m, 4H), 0.86 (t, *J* = 7.3 Hz, 3H). $C_{18}H_{24}Cl_2N_2O_4$ [M]: 403.30; MS (ESI) *m/z*: $[M]^-$: 403, [M-2]: 401

methyl 4-(2-(2,4-dichlorophenyl)acetamido)-5-oxo-5-(pentylamino)pentanoate (6i)

Yield 61.8%, White solid, ^{1}H NMR (400 MHz, DMSO-d_6) δ 8.66 (d, *J* = 8.1 Hz, 1H), 7.91 (t, *J* = 5.6 Hz, 1H), 7.68 (s, 1H), 7.50 (d, *J* = 0.9 Hz, 2H), 4.34 (m, 1H), 3.58 (s, 3H), 3.14 –

3.01 (m, 2H), 2.12 – 1.75 (m, 4H), 1.39 (dd, *J* = 13.1, 6.4 Hz, 2H), 1.31 – 1.15 (m, 6H), 0.86 (t, *J* = 6.7 Hz, 3H). $C_{19}H_{26}Cl_2N_2O_4$ [M]: 417.33; MS (ESI) *m/z*: $[M]^-$: 417, [M-2]: 415

methyl 4-(2-(2,4-dichlorophenyl)acetamido)-5-oxo-5-(phenylamino)pentanoate (6j)

Yield 47%, off white powder, ^{1}H NMR (400 MHz, DMSO-d_6) δ 8.75 (d, *J* = 8.0 Hz, 1H), 8.50 (t, *J* = 5.9 Hz, 1H), 7.69 (t, *J* = 1.1 Hz, 1H), 7.51 (d, *J* = 1.1 Hz, 2H), 7.34 – 7.23 (m, 5H), 4.46 (m, 1H), 4.32 (d, *J* = 6.0 Hz, 2H), 3.59 (s, 3H), 2.44 – 2.39 (m, 2H), 2.09 – 1.83 (m, 2H). $C_{20}H_{20}Cl_2N_2O_4$ [M]: 423.29; MS (ESI) *m/z*: $[M]^+$: 423, $[M+2]^+$: 425, $[M-2]^+$: 421

methyl 4-(2-(naphthalen-2-yl)acetamido)-5-oxo-5-(pentylamino)pentanoate (6k)

Yield 35.65%, white powder, ^{1}H NMR (400 MHz, DMSO-d_6) δ 8.38 (d, *J* = 8.2 Hz, 1H), 8.10 – 8.07 (m, 1H), 7.94 – 7.90 (m, 2H), 7.81 (dd, *J* = 7.1, 2.3 Hz, 1H), 7.52 – 7.47 (m, 2H), 7.43 (dd, *J* = 7.1, 5.1 Hz, 2H), 4.24 (td, *J* = 8.2, 5.7 Hz, 1H), 3.97 (q, *J* = 15.0 Hz, 2H), 3.57 (s, 3H), 3.02 (m, 2H), 2.32 – 2.26 (m, 2H), 1.40 – 1.16 (m, 8H), 0.84 (t, *J* = 7.0 Hz, 3H). $C_{23}H_{30}N_2O_4$ [M]: 398.50; MS (ESI) *m/z*: $[M+H]^+$: 399.

methyl 5-(hexylamino)-4-(2-(naphthalen-2-yl)acetamido)-5-oxopentanoate (6l)

Yield 52%, white powder, ^{1}H NMR (400 MHz, DMSO-d_6) δ 10.43 (s, 1H), 8.42 (d, *J* = 8.1 Hz, 1H), 8.12 – 8.05 (m, 1H), 7.93 – 7.87 (m, 2H), 7.81 (dd, *J* = 6.3, 3.0 Hz, 1H), 7.53 – 7.41 (m, 4H), 4.24 – 4.17 (m, 1H), 3.98 (d, *J* = 2.8 Hz, 2H), 3.57 (s, 3H), 3.07 – 2.96 (m, 2H), 2.03 – 1.68 (m, 5H), 1.39 – 1.18 (m, 9H), 0.85 (t, *J* = 6.7 Hz, 3H). $C_{24}H_{32}N_2O_4$ [M]: 412.52; MS (ESI) *m/z*: $[M+H]^+$: 413

Synthesis of substituted hydroxamic acid (7a-7l)

The intermediate substituted esters (6a-6l) were dissolved in methanol. 50% w/v aqueous hydroxylamine (18.5 equivalents) was added to it and stirred for 30 minutes at room

temperature. To the above mixture sodium hydroxide (1M, 2 equivalents) was added and stirred for 1.5 hour. The reaction mixture was concentrated and poured in ice cold water. It was neutralized by 1M hydrochloric acid. The product was extracted in ethyl acetate, dried over sodium sulphate and evaporated to get the final product (7a-7l).

2-(2-(2-bromophenyl) acetamido)-*N*^{5}-hydroxy-*N*^{1}-pentylpentanediamide (7a)

Yield 56.09%, white solid, ^{1}H NMR (400 MHz, DMSO-d_6) δ 10.42 (s, 1H), 8.25 (d, *J* = 8.1 Hz, 1H), 7.90 (t, *J* = 5.4 Hz, 1H), 7.58 (d, *J* = 7.9 Hz, 1H), 7.32 (q, *J* = 7.5 Hz, 2H), 7.21 – 7.15 (m, 1H), 4.22 (dd, *J* = 13.7, 8.0 Hz, 1H), 3.71 – 3.60 (m, 2H), 3.11 – 2.97 (m, 2H), 2.06 – 1.67 (m, 4H), 1.43 – 1.16 (m, 7H), 0.85 (t, *J* = 6.9 Hz, 3H), ^{13}C NMR (101 MHz, DMSO-d_6) δ 170.73, 168.77, 168.50, 136.03, 132.18, 131.80, 128.54, 127.49, 124.45, 52.34, 42.10, 38.39, 28.86, 28.65, 28.47, 21.77, 13.88. HPLC Rt: 2.303, LC/MS calculated for expected $C_{18}H_{26}BrN_3O_4$ [M]: 428.32; Found: $[M]^+$: 428, $[M+2]^+$: 430

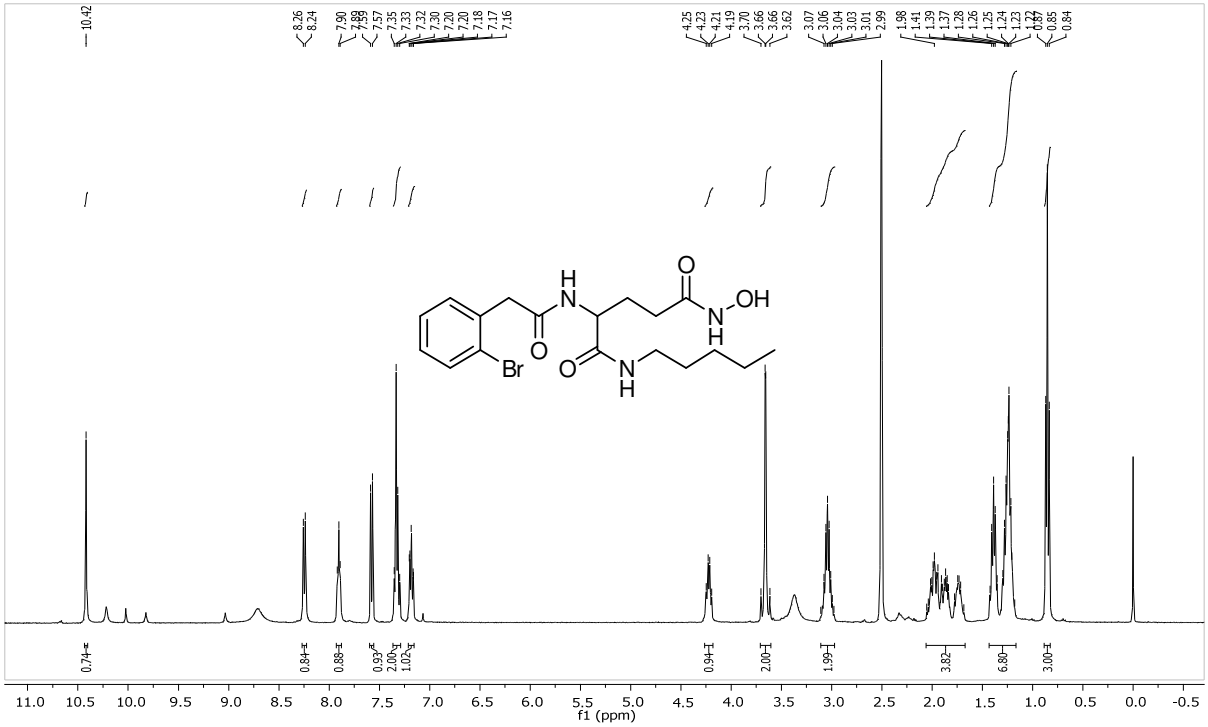

^{1}H NMR of **7a**

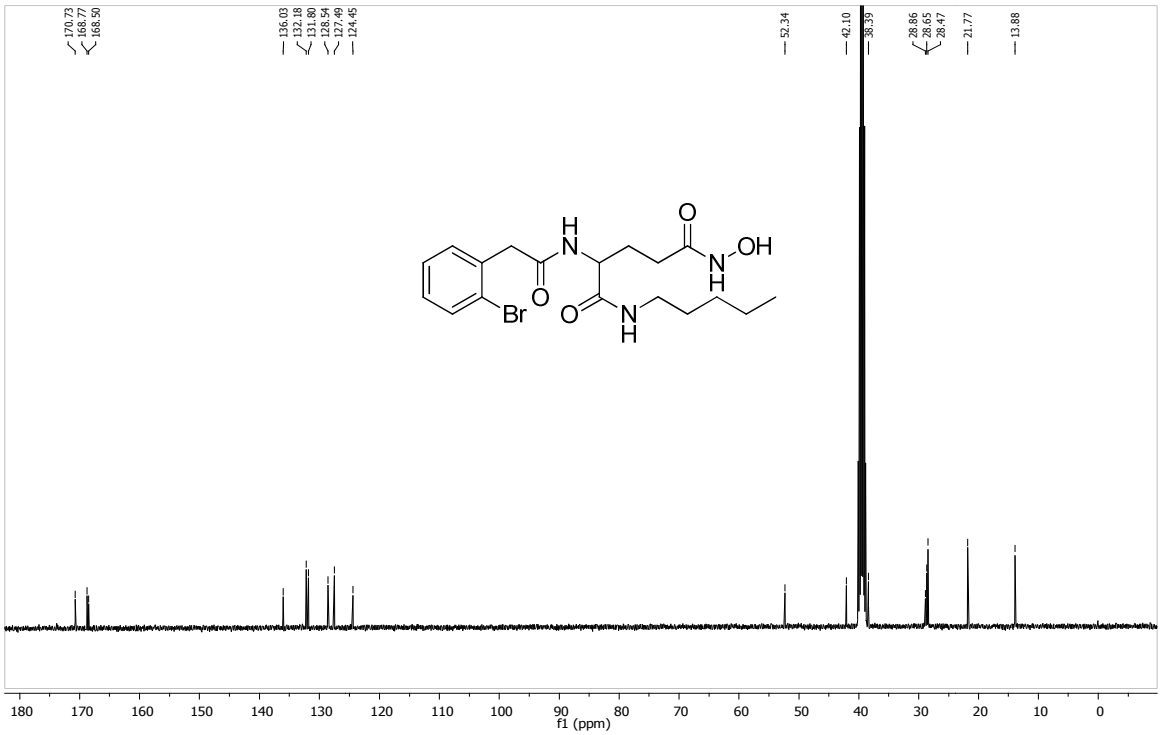

^{13}C NMR **7a**

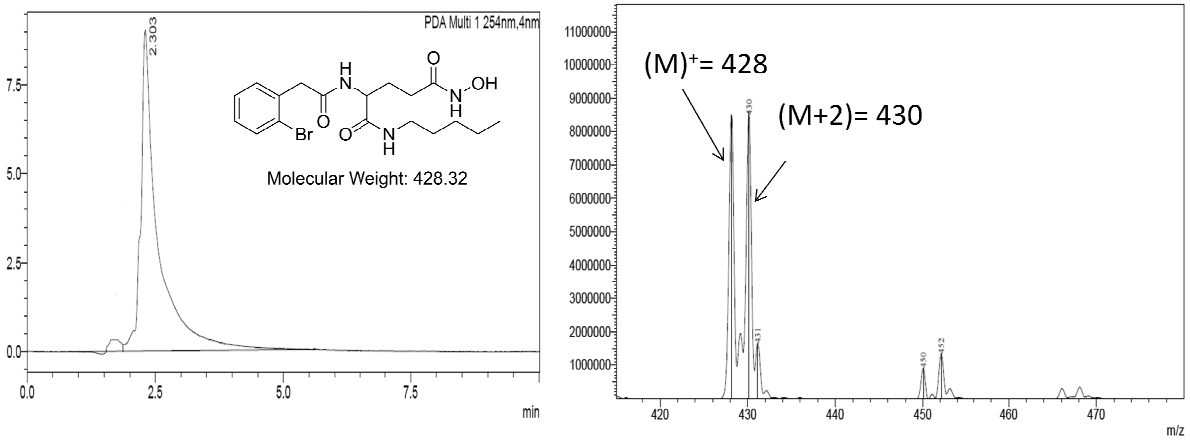

LC/MS of **7a**

2-(2-(2-fluorophenyl)acetamido)-*N*^{5}-hydroxy-*N*^{1}-isobutylpentanediamide (7b)

Yield 57.46%, white powder, ^{1}H NMR (400 MHz, DMSO-d$_6$) δ 10.43 (s, 1H), 8.71 (s, 1H), 8.29 (d, *J* = 8.1 Hz, 1H), 7.92 (t, *J* = 5.8 Hz, 1H), 7.34 – 7.24 (m, 2H), 7.16 – 7.10 (m, 2H), 4.24 (td, *J* = 8.2, 5.7 Hz, 1H), 3.55 (s, 2H), 2.96 – 2.80 (m, 2H), 2.01 – 1.61 (m, 5H), 0.82 (d, *J* = 6.7 Hz, 6H). ^{13}C NMR (101 MHz, DMSO-d$_6$) δ 170.93, 169.00, 168.49, 161.75,

159.32, 131.66, 128.52, 124.09, 115.01, 52.39, 45.91, 34.96, 28.84, 28.51, 27.96, 20.00

HPLC Rt: 2.361 LC/MS calculated for [M]: 353.39; Found: $[M+H]^+$: 354

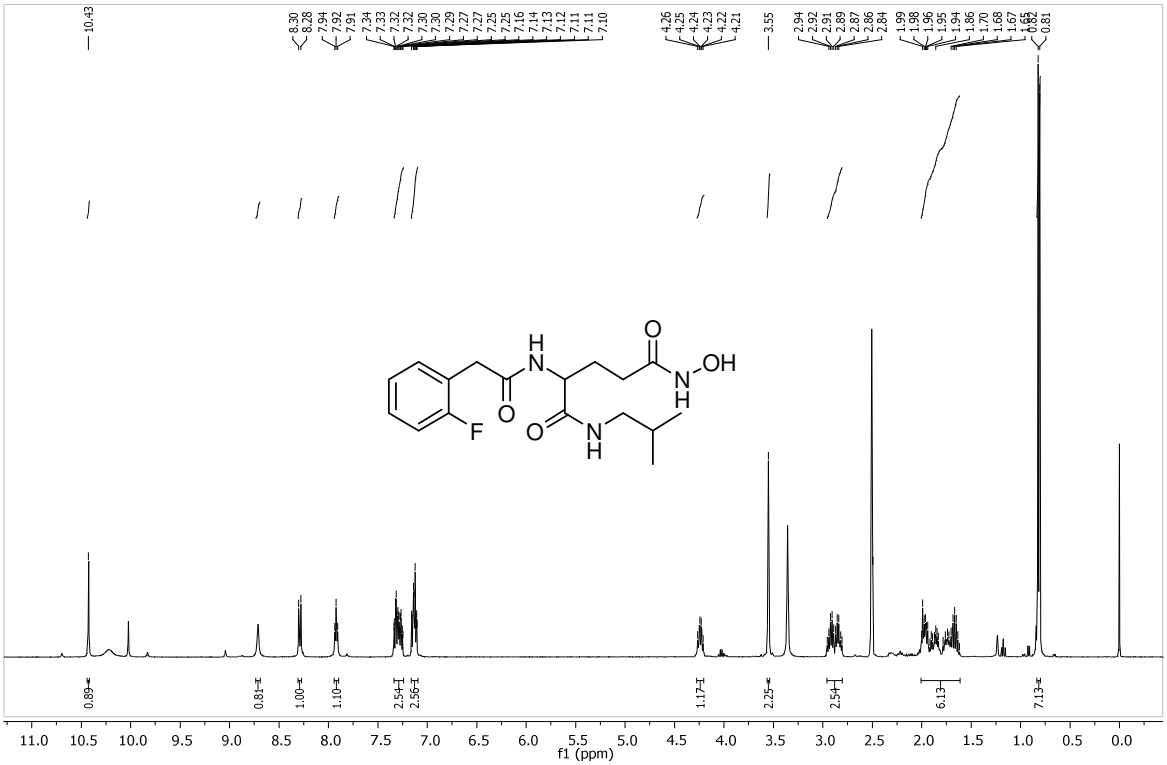

^{1}H NMR of **7b**

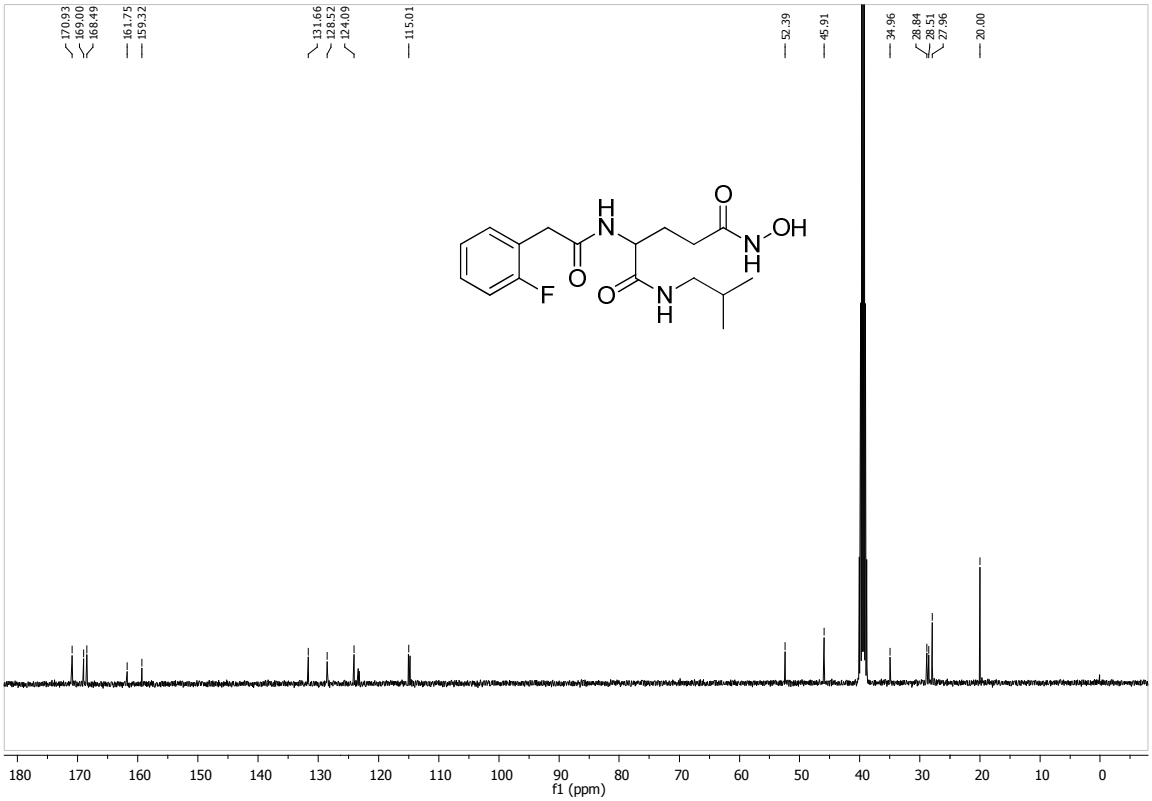

^{13}C NMR of **7b**

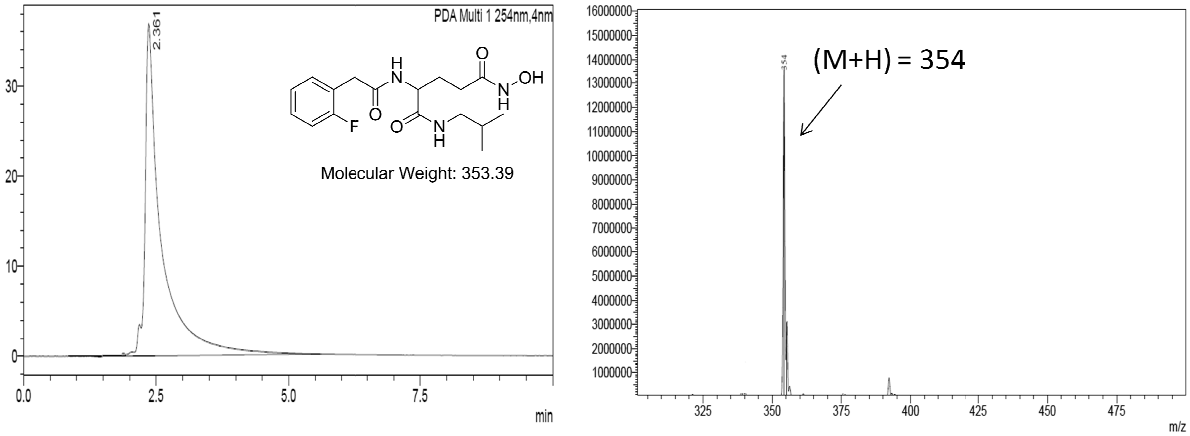

LC/MS of **7b**

2-(2-(4-bromophenyl)acetamido)-*N*^{5}-hydroxy-*N*^{1}-pentylpentanediamide (7c)

Yield 48%, cream color solid, ^{1}H NMR (400 MHz, DMSO-d_6) δ 8.29 (d, *J* = 8.1 Hz, 1H), 7.90 (t, *J* = 5.5 Hz, 1H), 7.47 (d, *J* = 8.4 Hz, 2H), 7.22 (d, *J* = 8.4 Hz, 2H), 4.17 (dd, *J* = 14.9, 6.9 Hz, 1H), 3.50 – 3.41 (m, 2H), 3.02 (m, 2H), 1.98 – 1.66 (m, 4H), 1.36 (m, 2H),

1.29 – 1.17 (m, 5H), 0.84 (t, *J* = 7.1 Hz, 3H), ^{13}C NMR (101 MHz, DMSO-d_6) δ 171.26, 170.10, 168.93, 136.33, 131.78, 131.46, 119.96, 52.79, 41.71, 38.88, 29.32, 29.10, 28.94, 22.25, 14.36. HPLC Rt: 2.474 LC/MS calculated for expected $C_{18}H_{26}BrN_3O_4$ [M]: 428.32; Found: $[M]^+$: 428, $[M+2]^+$: 430, $[M+Na]^+$: 452

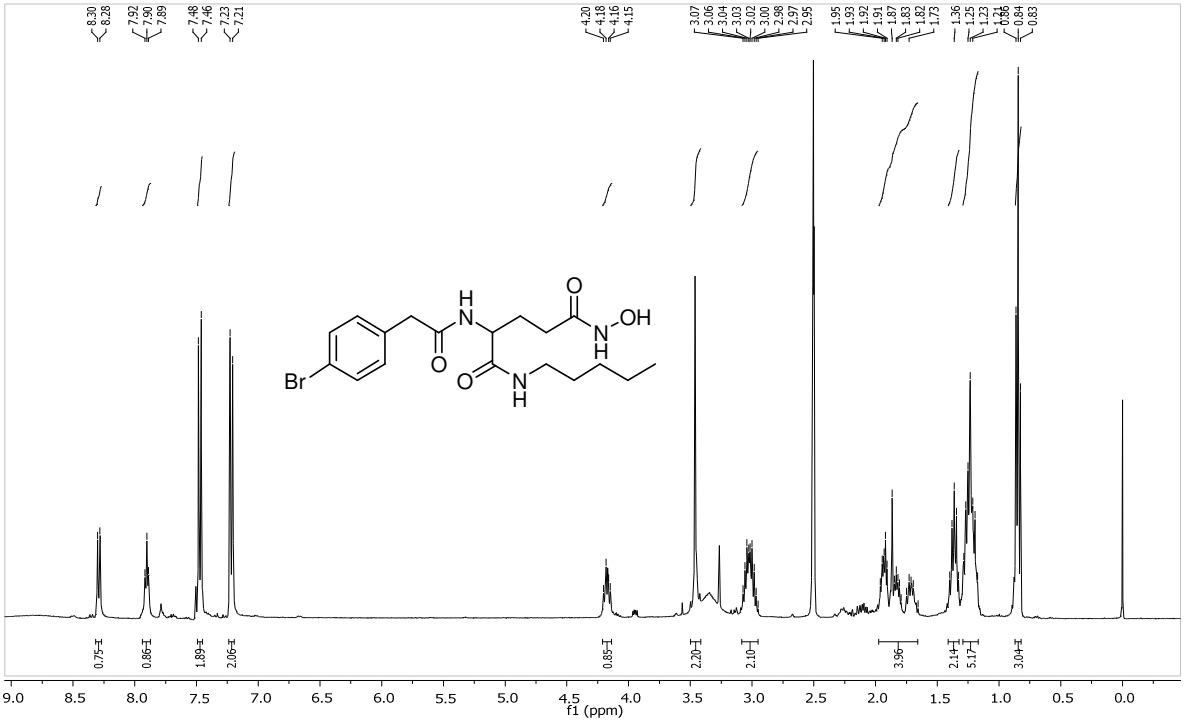

^{1}H NMR **7c**

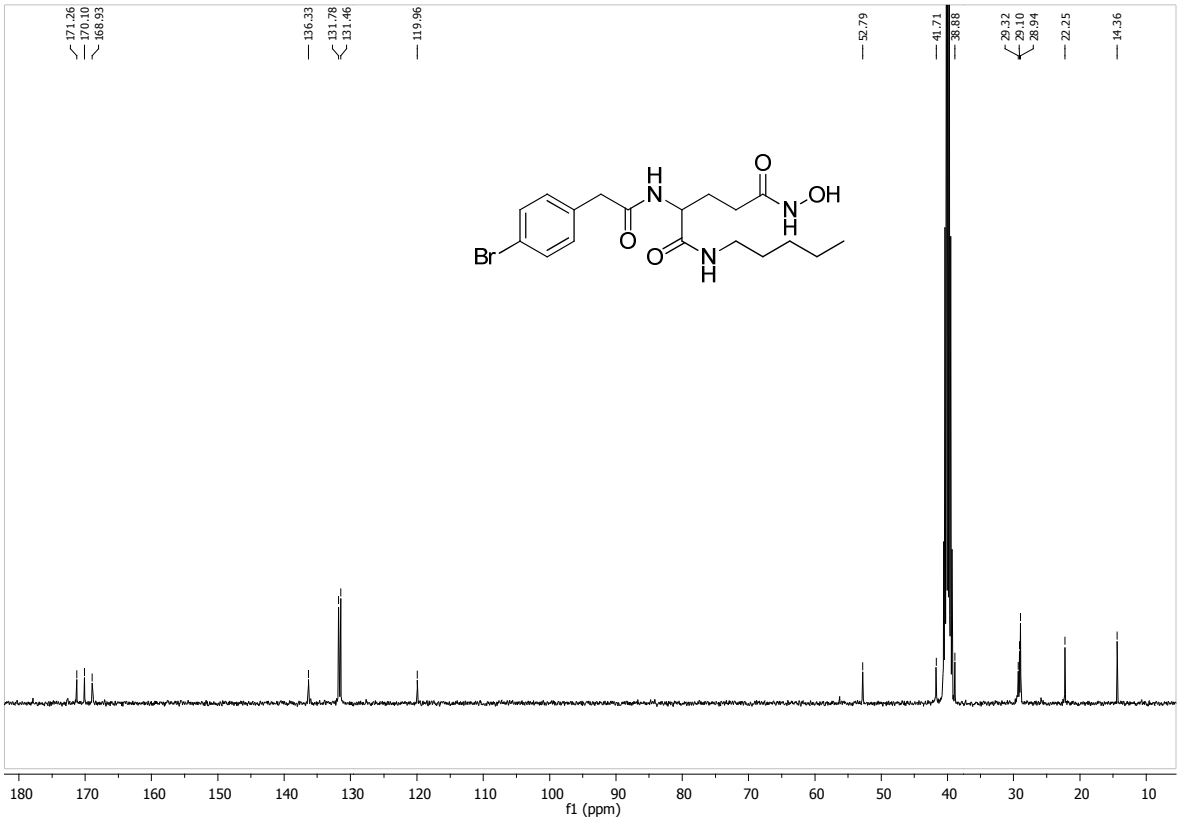

^{13}C NMR **7c**

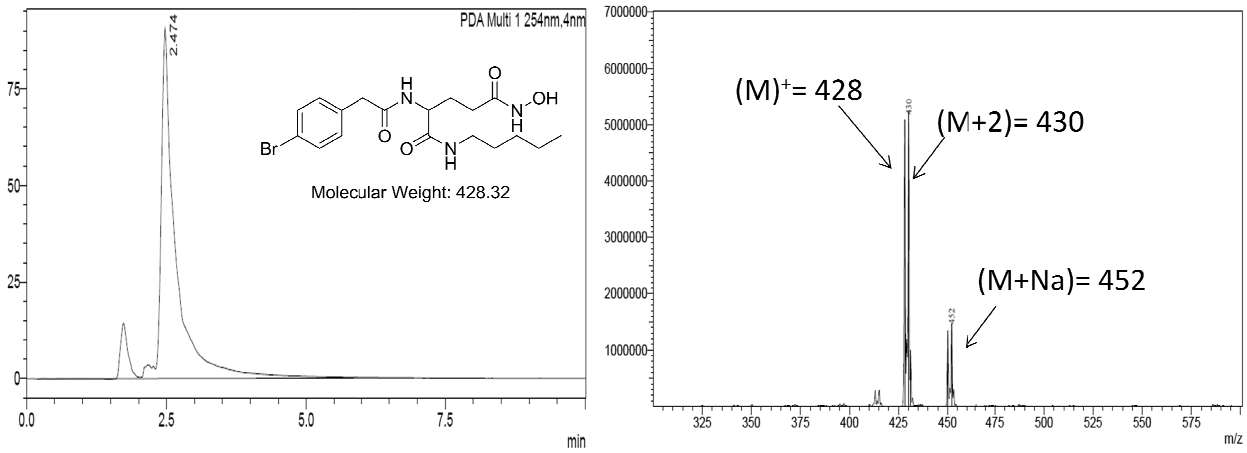

LC/MS of **7c**

2-(2-(4-bromophenyl)acetamido)-*N*^{1}-hexyl-*N*^{5}-hydroxypentanediamide (7d)

Yield 92.7%, cream powder, ^{1}H NMR (400 MHz, DMSO-d$_6$) δ 10.41 (s, 1H), 8.29 (t, *J* = 8.5 Hz, 1H), 7.91 (t, *J* = 5.5 Hz, 1H), 7.47 (d, *J* = 8.4 Hz, 2H), 7.22 (d, *J* = 8.3 Hz, 2H), 4.17

(dd, *J* = 14.0, 8.2 Hz, 1H), 3.46 (s, 2H), 3.09 – 2.95 (m, 2H), 2.20 – 1.66 (m, 4H), 1.34 (dd, *J* = 13.2, 6.5 Hz, 2H), 1.23 (d, *J* = 4.6 Hz, 6H), 0.85 (dd, *J* = 8.5, 5.0 Hz, 3H), ^{13}C NMR (101 MHz, DMSO-d_6) δ 170.75, 169.57, 168.43, 135.84, 131.28, 130.95, 119.45, 52.30, 41.20, 38.40, 30.90, 28.90, 28.84, 28.45, 25.91, 22.00, 13.88. HPLC Rt: 2.447 LC/MS calculated for expected $C_{19}H_{28}BrN_3O_4$ [M]: 442.35; Found: $[M]^+$: 442, $[M+2]^+$: 444

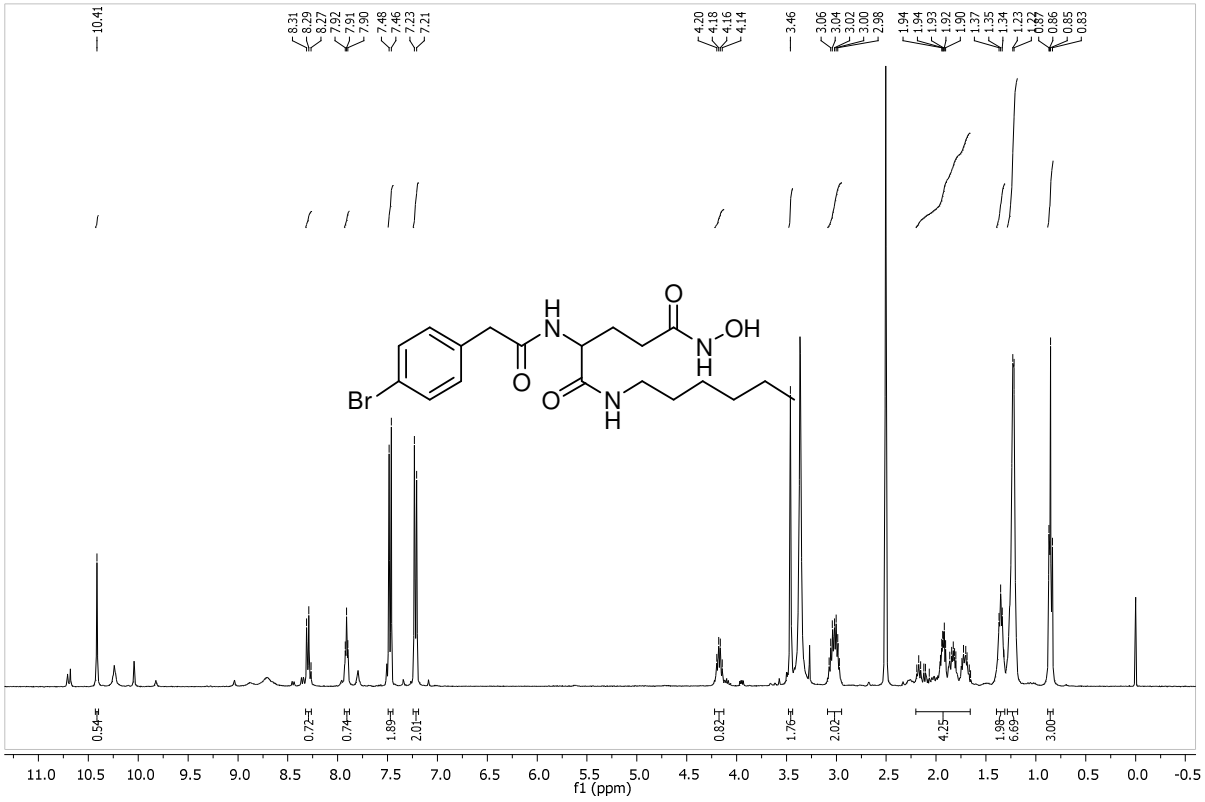

^{1}H NMR **7d**

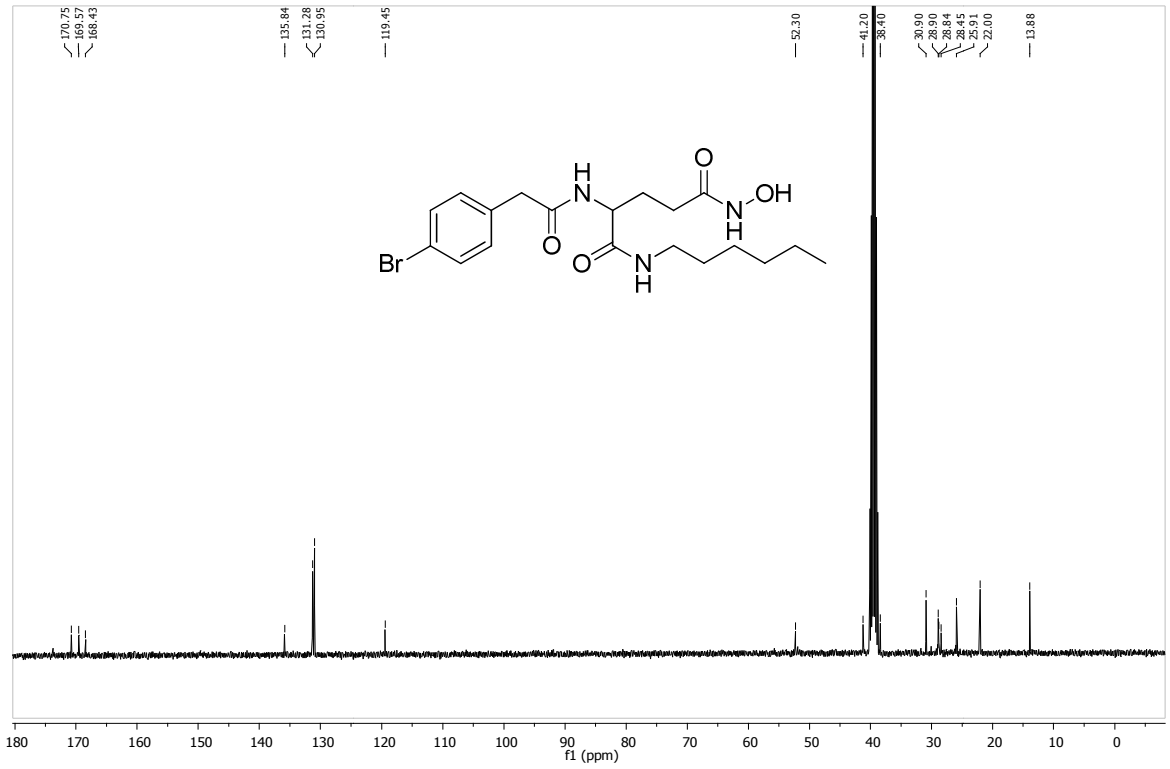

^{13}C NMR OF **7d**

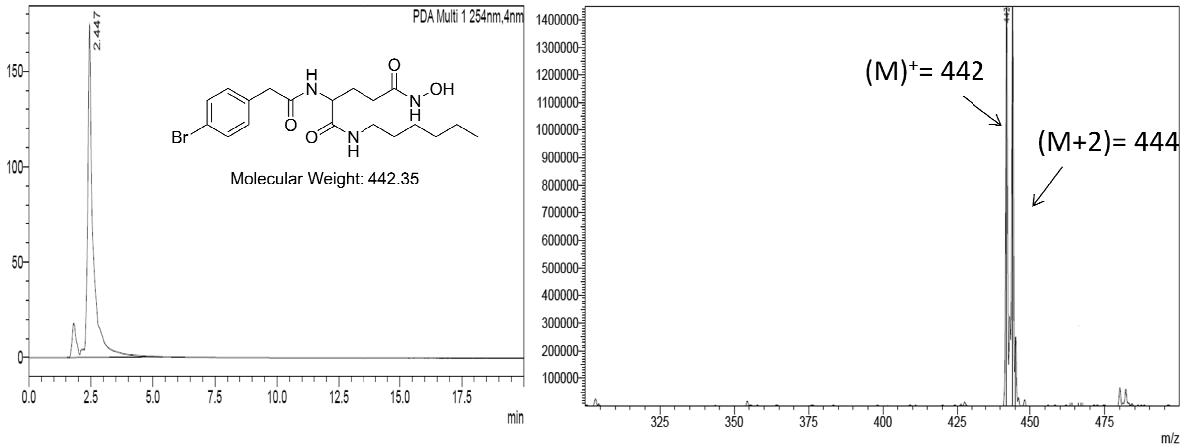

LC/MS of **7d**

N^1-butyl-2-(2-(4-chlorophenyl)acetamido)-N^5-hydroxypentanediamide (7e)

Yield 60%, cream color solid, ^{1}H NMR (400 MHz, DMSO-d_6) δ 10.39 (s, 1H), 8.26 (d, *J* = 8.1 Hz, 1H), 7.88 (t, *J* = 5.6 Hz, 1H), 7.38 – 7.33 (m, 2H), 7.28 (d, *J* = 8.5 Hz, 2H), 4.22 – 4.12 (m, 1H), 3.48 (s, 1H), 3.03 (m, 1H), 1.97 – 1.60 (m, 2H), 1.40 – 1.17 (m, 7H), 0.86 (m,

3H). ^{13}C NMR (101 MHz, DMSO-d_6) δ 171.25, 170.15, 168.91, 167.46, 135.91, 132.18, 132.06, 131.49, 131.38, 131.25, 129.13, 128.54, 67.87, 52.77, 41.65, 38.58, 31.56, 30.26, 29.48, 29.30, 28.95, 28.83, 23.71, 22.86, 19.92, 14.36, 14.11, 11.27. HPLC Rt: 2.955 LC/MS calculated for expected $C_{17}H_{24}ClN_3O_4$ [M]: 369.84; Found: $[M+H]^+$: 370, $[M+Na]^+$: 392

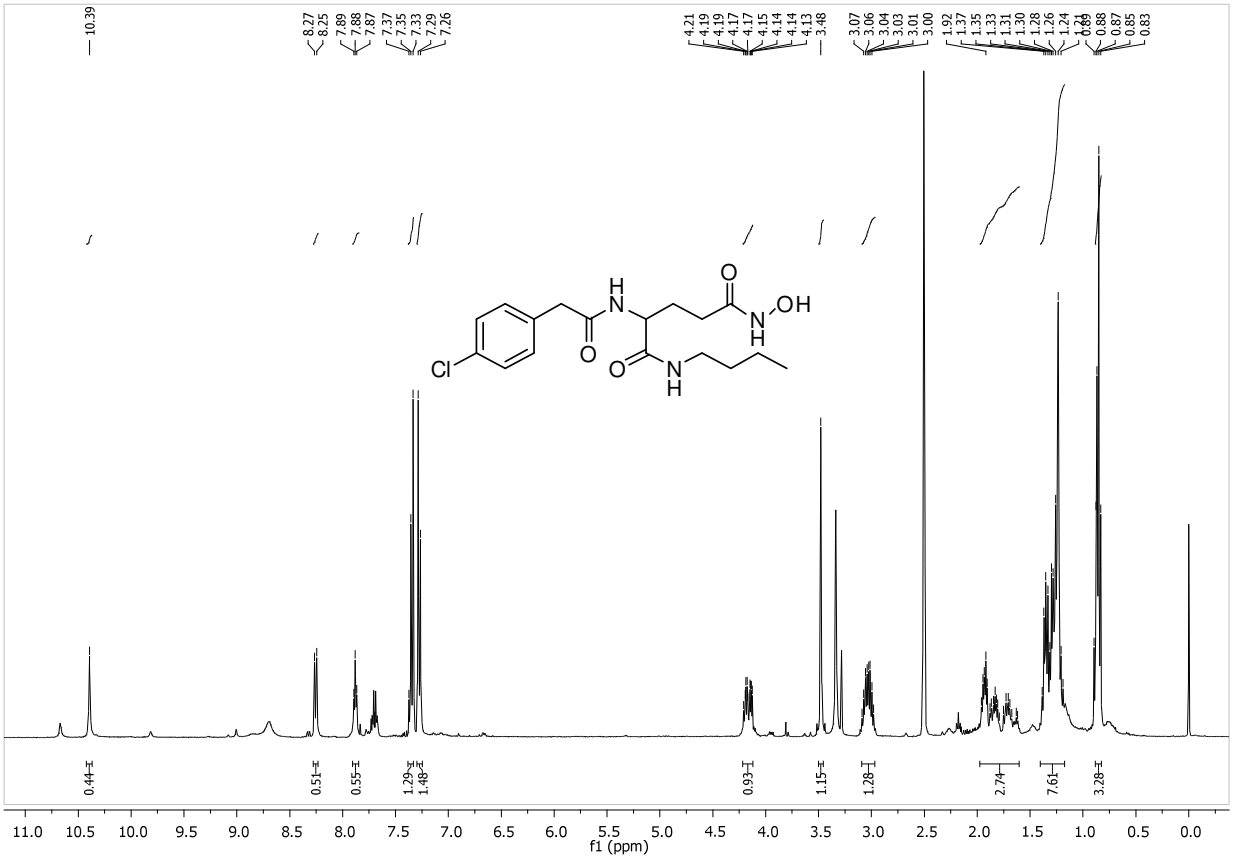

^{1}H NMR **7e**

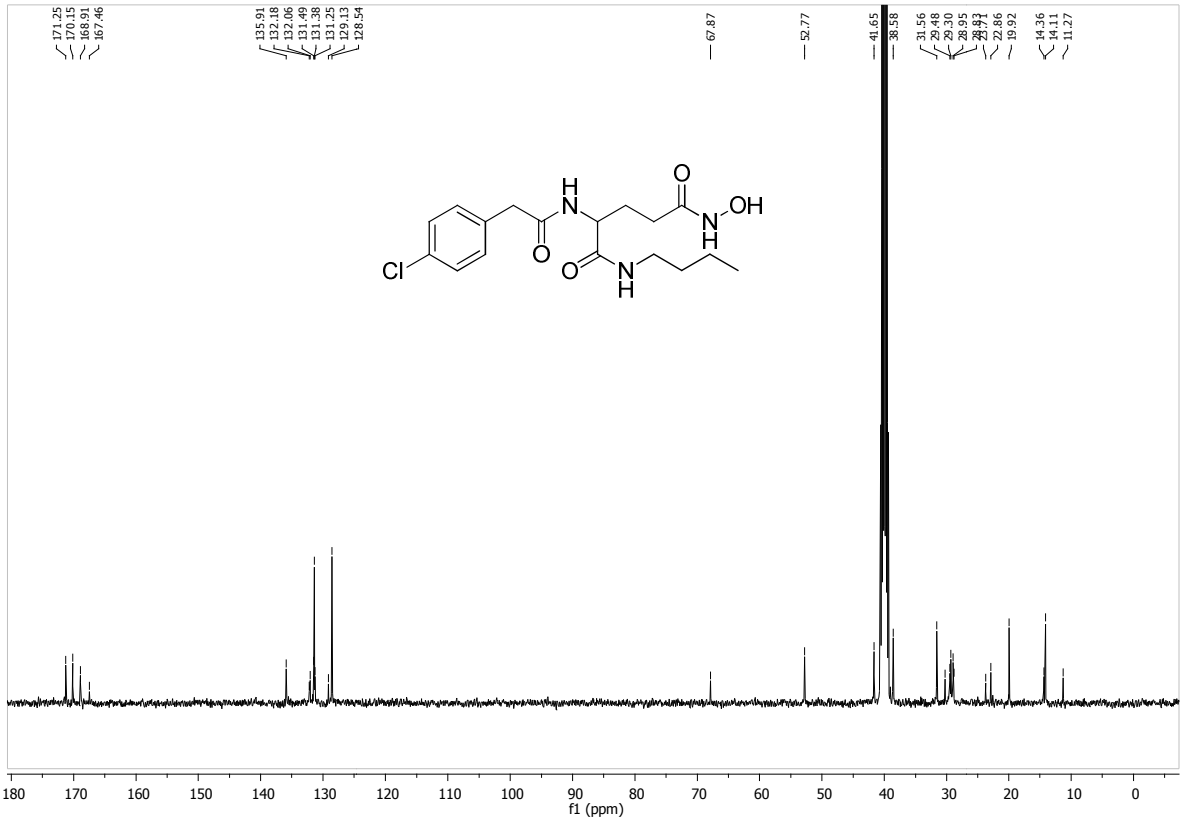

^{13}C NMR **7e**

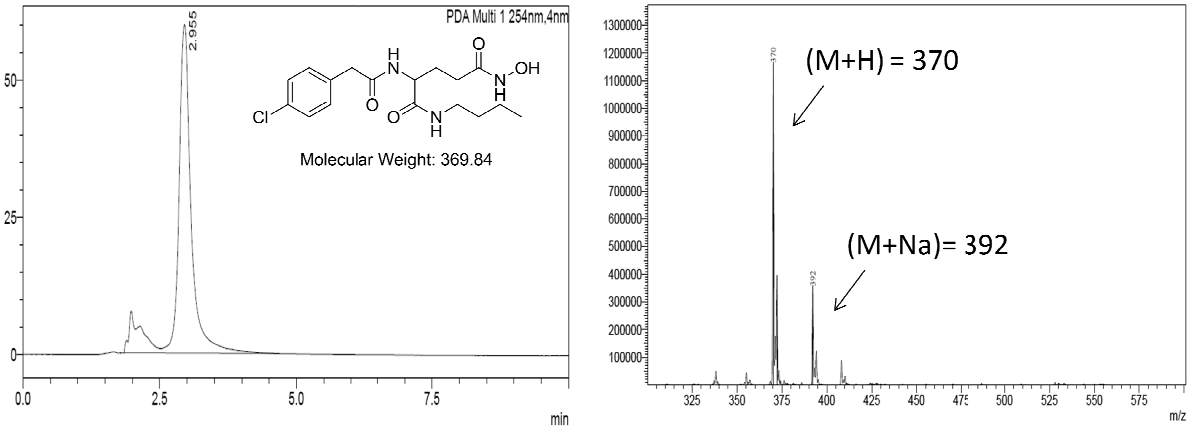

LC/MS of **7e**

2-(2-(4-chlorophenyl)acetamido)-*N*^{5}-hydroxy-*N*^{1}-pentylpentanediamide (7f)

Yield 80%, white crystals, ^{1}H NMR (400 MHz, DMSO-d$_6$) δ 8.31 (d, *J* = 8.1 Hz, 1H), 7.92 (t, *J* = 5.4 Hz, 1H), 7.34 (d, *J* = 8.4 Hz, 2H), 7.28 (d, *J* = 8.4 Hz, 2H), 4.18 (dd, *J* = 13.7, 7.9 Hz, 1H), 3.48 (s, 2H), 3.02 (m, 2H), 1.98 – 1.67 (m, 4H), 1.41 – 1.32 (m, 2H), 1.24 (m, 5H),

0.84 (t, *J* = 7.0 Hz, 3H). ^{13}C NMR (101 MHz, DMSO-d_6) δ 171.28, 170.19, 168.94, 135.90, 131.50, 131.38, 128.53, 52.81, 29.32, 29.10, 28.94, 22.24, 14.35. HPLC Rt: 2.362, LC/MS calculated for expected $C_{18}H_{26}ClN_3O_4$ [M]: 383.87; $[M+H]^+$: 384, $[M+Na]^+$: 406

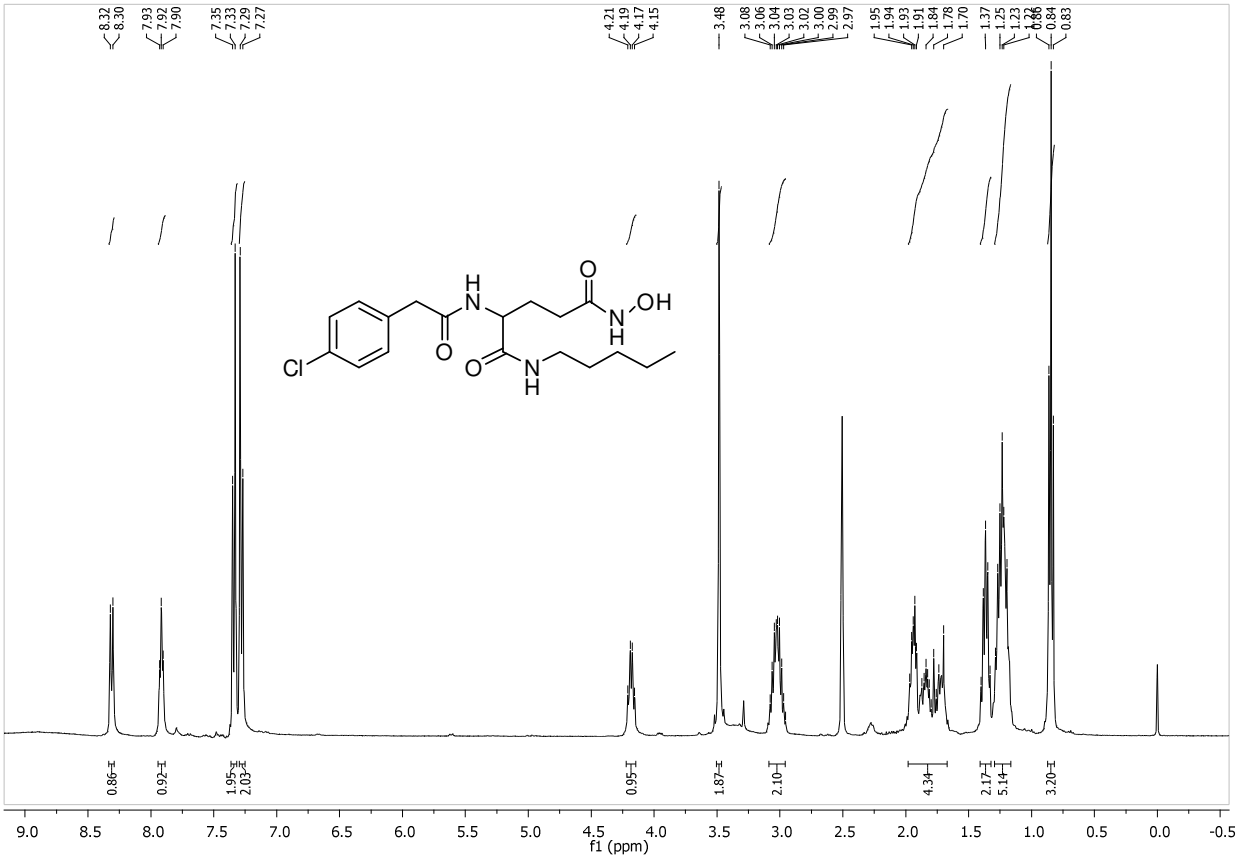

^{1}H NMR of **7f**

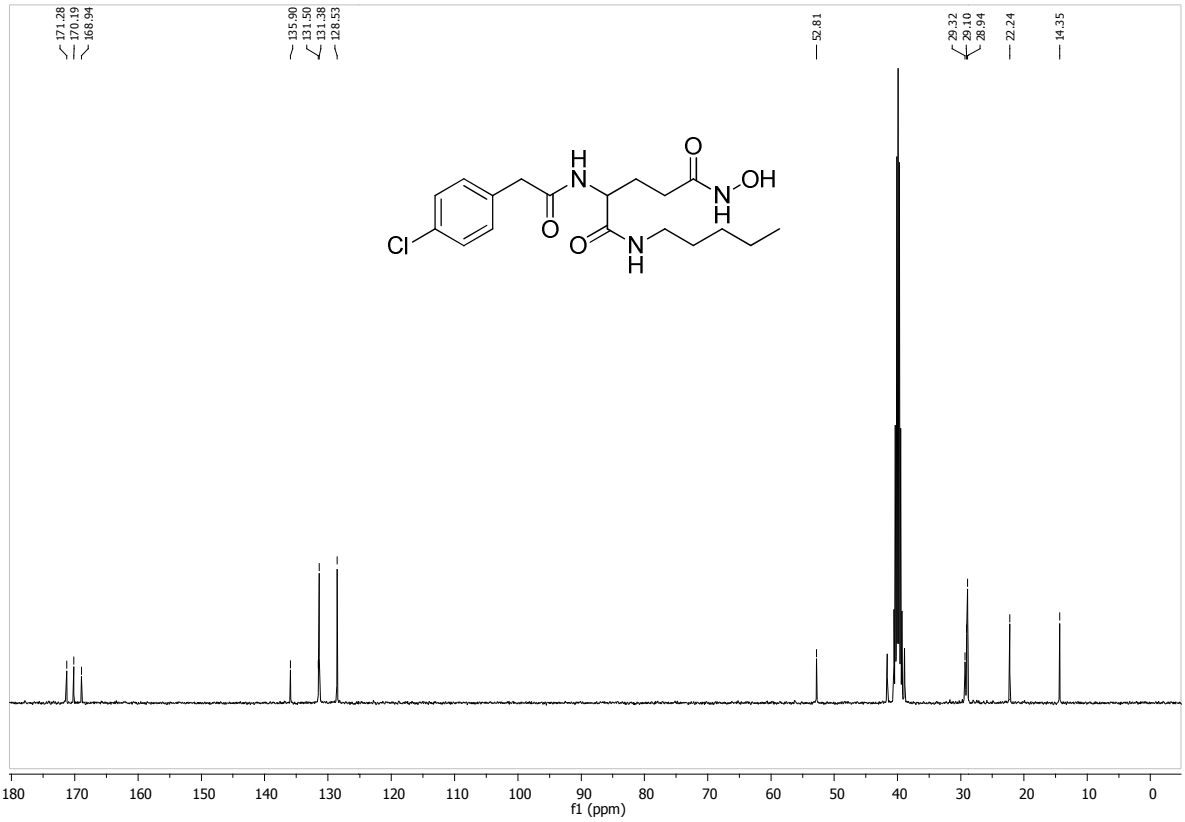

^{13}C NMR of **7f**

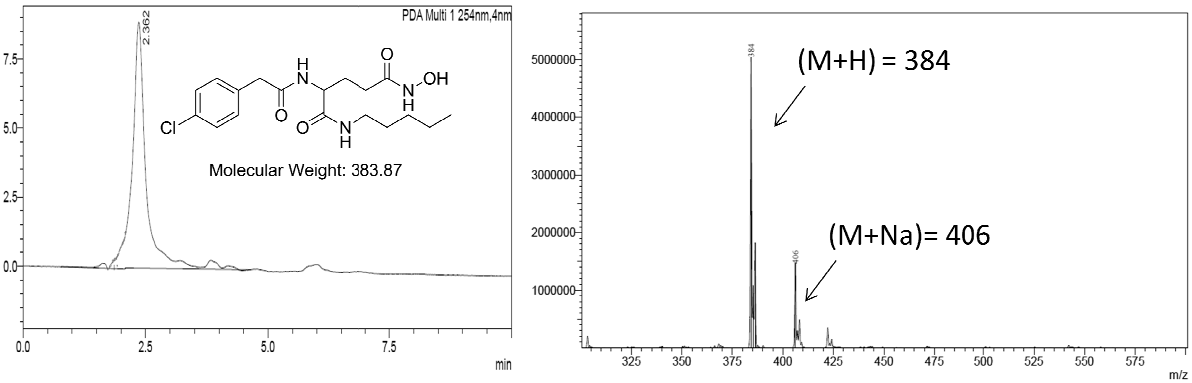

LC/MS of **7f**

N^1-butyl-N^5-hydroxy-2-(2-(4-nitrophenyl)acetamido)pentanediamide (7g)

Yield 57.9%, pale yellow powder, ^{1}H NMR (400 MHz, DMSO-d_6) δ 8.44 (d, J = 8.1 Hz, 1H), 8.17 (d, J = 8.7 Hz, 2H), 7.95 (t, J = 5.5 Hz, 1H), 7.54 (d, J = 8.8 Hz, 2H), 4.19 (dd, J = 13.8, 8.2 Hz, 1H), 3.67 (s, 2H), 3.04 (m, 2H), 1.98 – 1.67 (m, 3H), 1.39 – 1.19 (m, 5H), 0.87

– 0.82 (m, 3H), ^{13}C NMR (101 MHz, DMSO-d_6) δ 170.69, 168.89, 168.41, 146.18, 144.55, 130.37, 123.22, 52.39, 41.61, 38.09, 31.06, 28.81, 28.46, 19.42, 13.60. HPLC Rt: 3.388, LC/MS calculated for expected $C_{17}H_{24}N_4O_6$ [M]: 380.40; $[M+H]^+$: 381, $[M+Na]^+$: 403

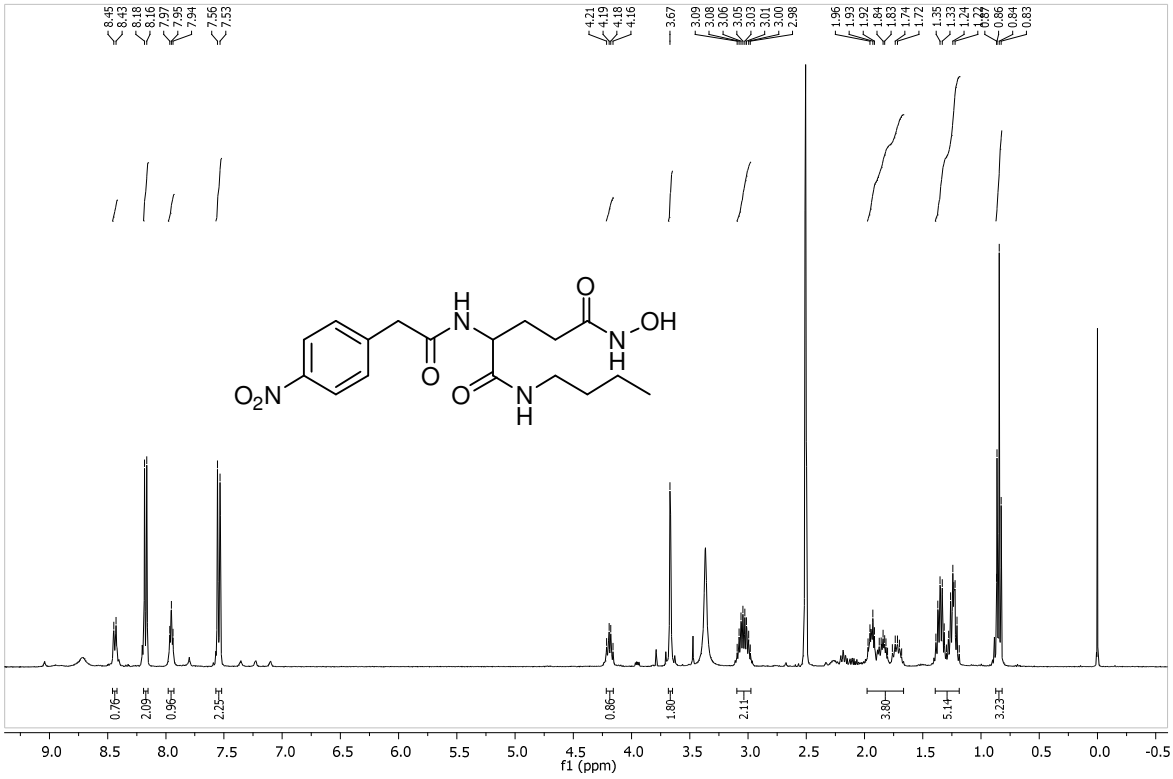

^{1}H NMR of **7g**

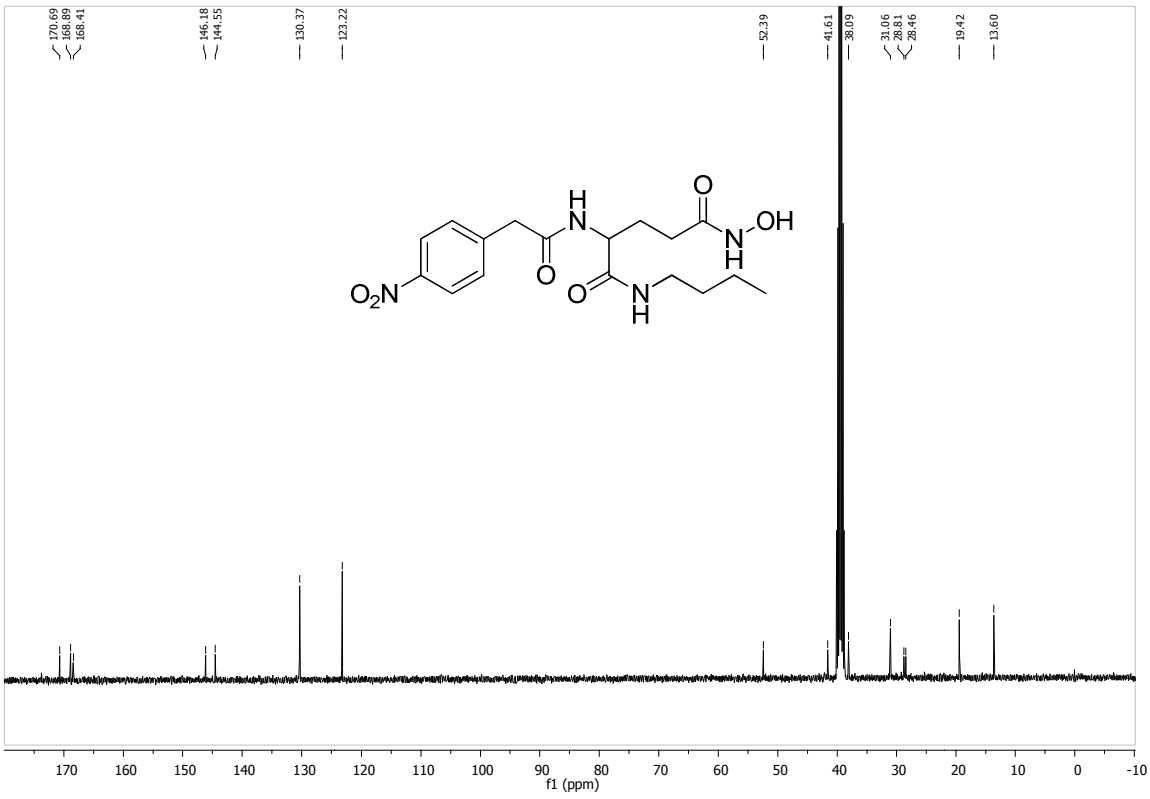

^{13}C NMR of **7g**

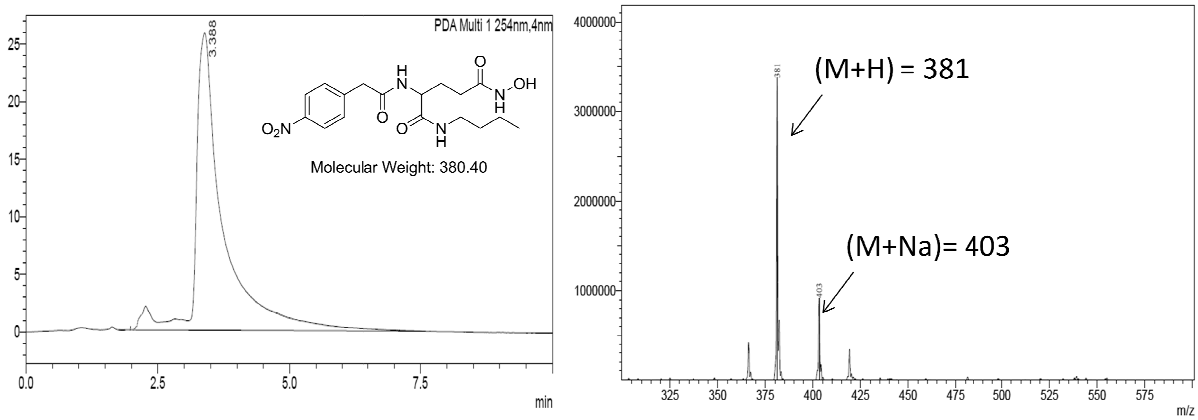

LC/MS of **7g**

N^1-butyl-2-(2-(2,4-dichlorophenyl)acetamido)-N^5-hydroxypentanediamide (7h)

Yield 92%, Cream powder, ^{1}H NMR (400 MHz, DMSO-d_6) δ 8.29 (d, *J* = 8.1 Hz, 1H), 7.90 (t, *J* = 5.6 Hz, 1H), 7.57 (s, 1H), 7.38 (s, 2H), 4.21 (m, 1H), 3.65 (d, *J* = 3.0 Hz, 2H), 3.11 – 2.99 (m, 2H), 2.01 – 1.69 (m, 3H), 1.41 – 1.21 (m, 5H), 0.86 (t, *J* = 7.3 Hz, 3H), ^{13}C NMR

(101 MHz, DMSO-d_6) δ 173.81, 170.69, 168.46, 134.53, 133.53, 133.13, 131.91, 128.34, 127.04, 52.34, 38.09, 31.08, 30.10, 28.82, 28.45, 19.43, 13.62. HPLC Rt: 2.526, LC/MS calculated for expected $C_{17}H_{23}Cl_2N_3O_4$ [M]: 404.29; $[M]^+$: 404, [M+2]: 406

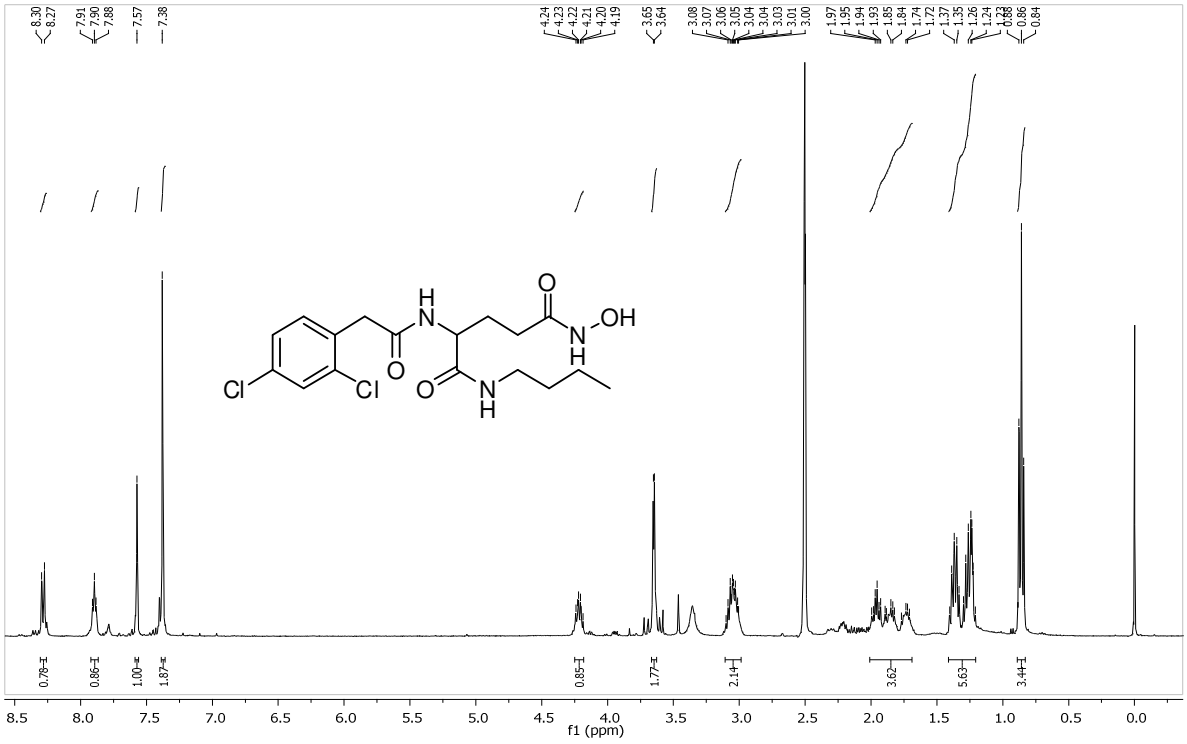

^{1}H NMR of **7h**

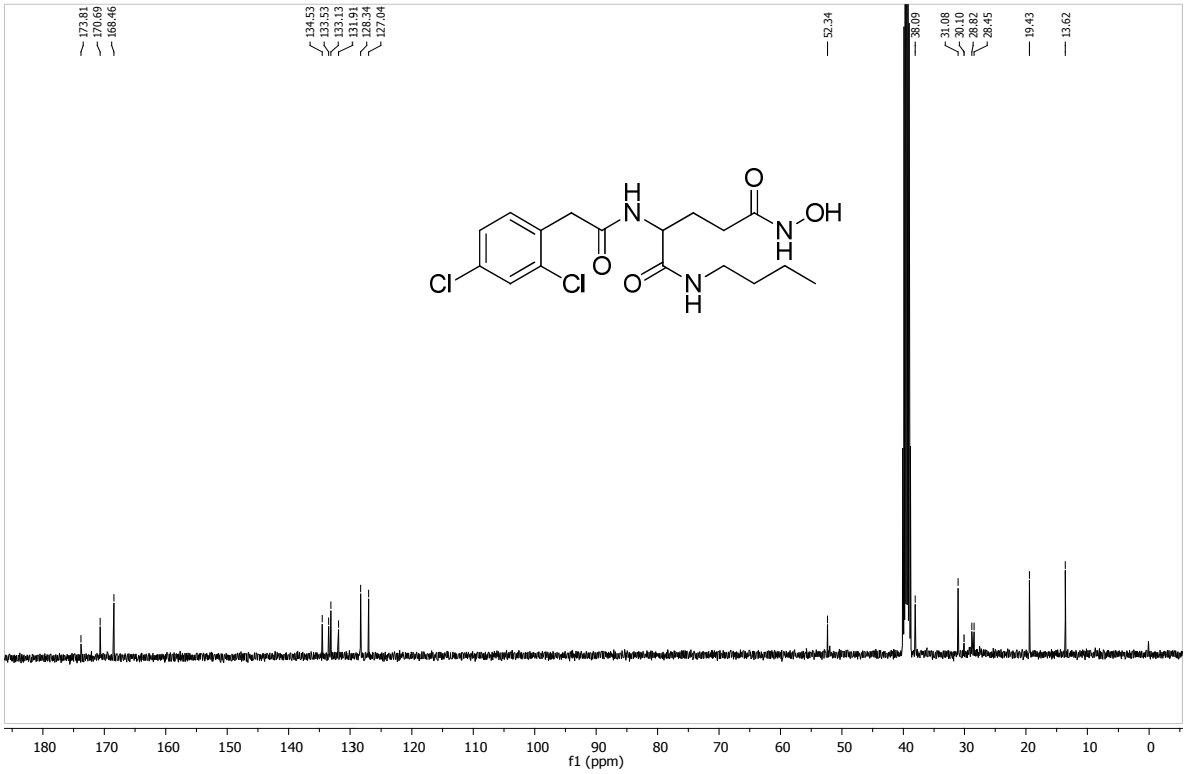

^{13}C NMR of **7h**

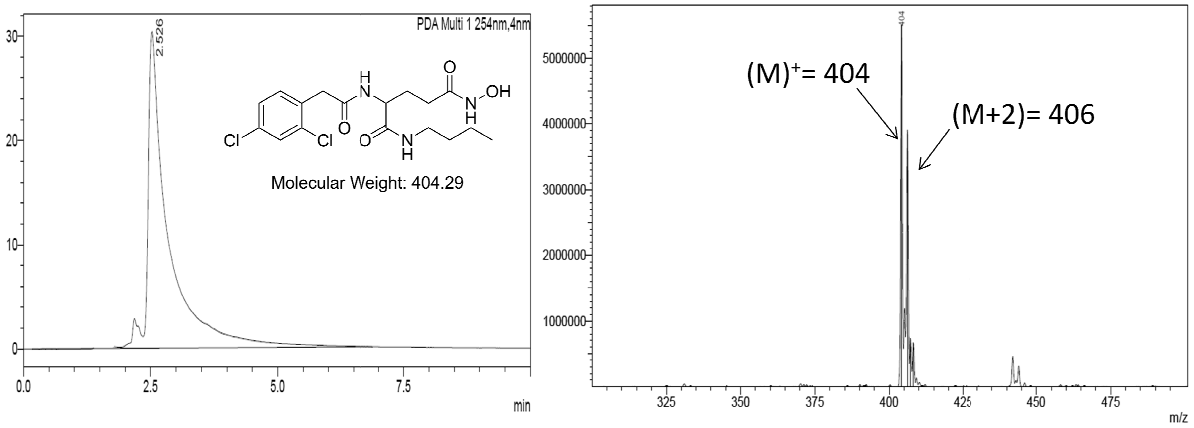

LC/MS of **7h**

2-(2-(2,4-dichlorophenyl)acetamido)-*N*^{5}-hydroxy-*N*^{1}-pentylpentanediamide (7i)

Yield 88.6%, white powder, ^{1}H NMR (400 MHz, DMSO-d$_6$) δ 8.72 (s, 1H), 8.66 (d, *J* = 8.1 Hz, 1H), 7.91 (t, *J* = 5.6 Hz, 1H), 7.68 (s, 1H), 7.50 (d, *J* = 0.9 Hz, 2H), 4.34 (m, 1H), 3.14 – 3.01 (m, 2H), 2.12 – 1.75 (m, 4H), 1.39 (dd, *J* = 13.1, 6.4 Hz, 2H), 1.31 – 1.15 (m, 6H), 0.86 (t, *J* = 6.7 Hz, 3H), ^{13}C NMR (101 MHz, DMSO-d$_6$) δ 170.36, 168.44, 165.29, 135.30,

134.49, 131.23, 130.51, 129.02, 127.11, 52.93, 38.49, 30.93, 28.95, 28.91, 27.96, 25.93, 22.02, 13.88. HPLC Rt: 2.810, LC/MS calculated for expected $C_{18}H_{25}Cl_2N_3O_4$ [M]: 418.31; $[M]^+$: 418, $[M+2]^+$: 420.

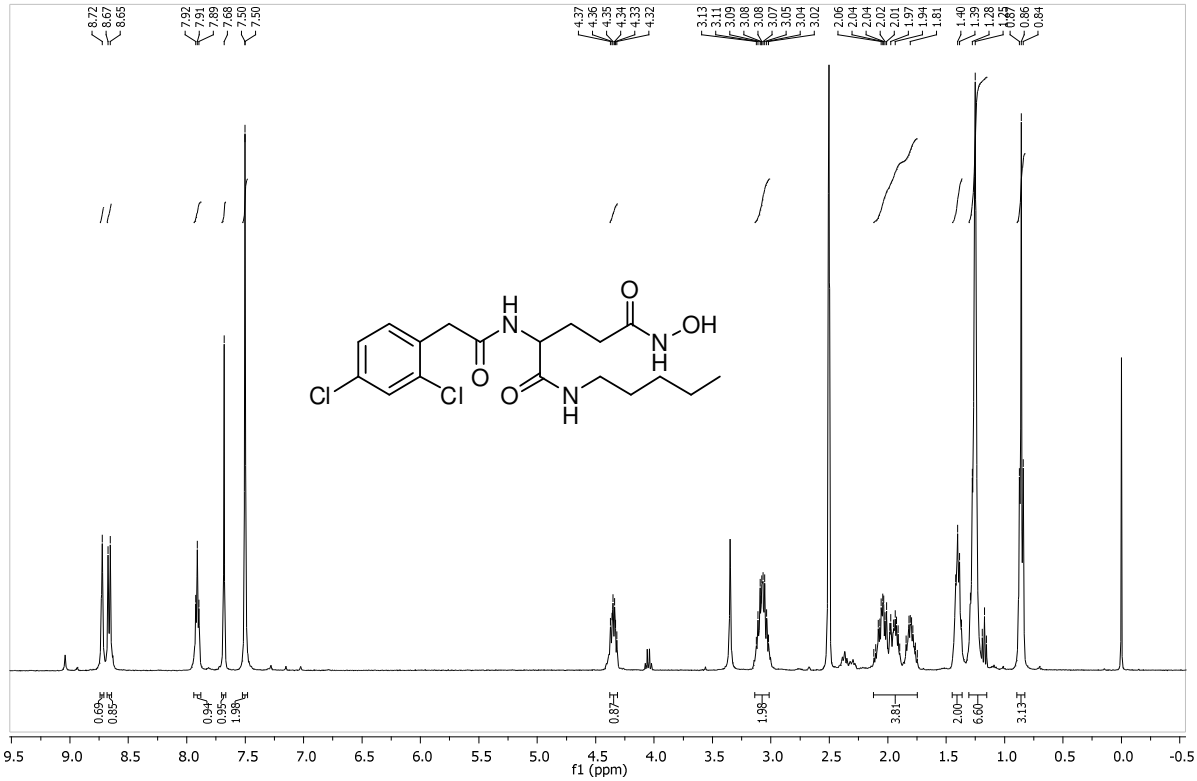

^{1}H NMR of **7i**

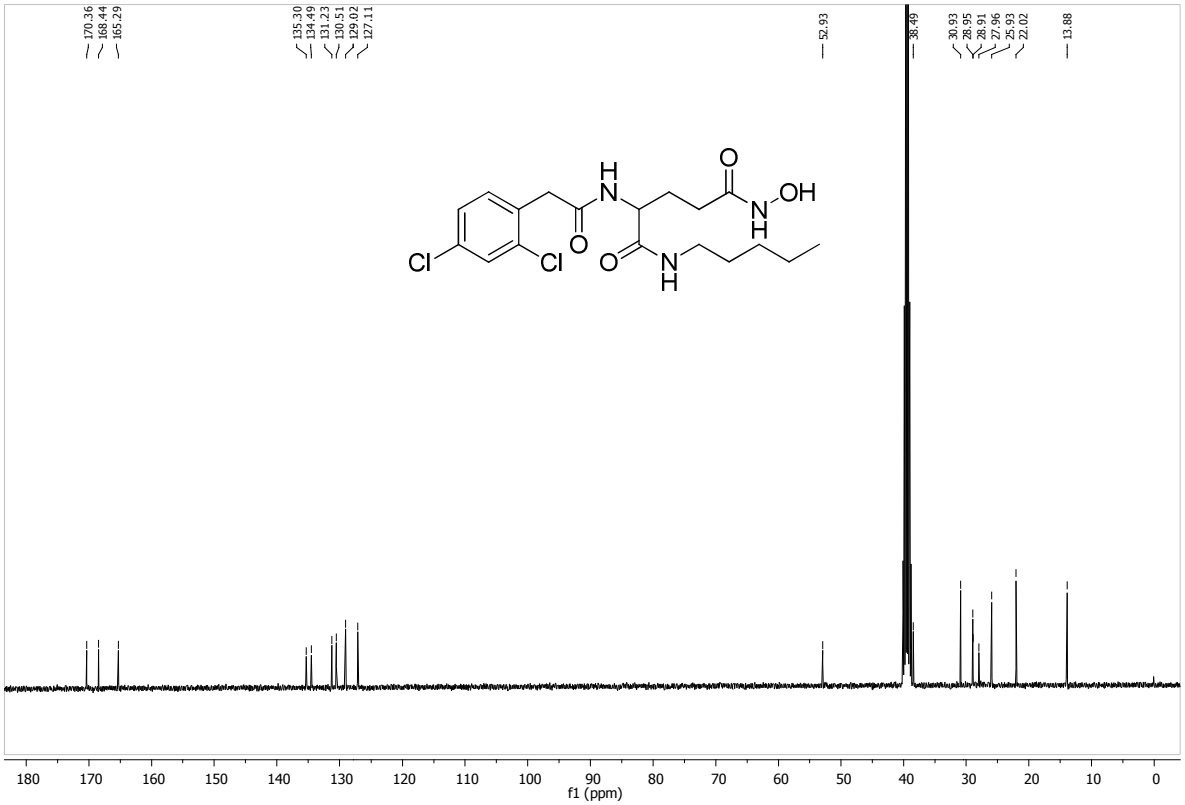

^{13}C NMR of **7i**

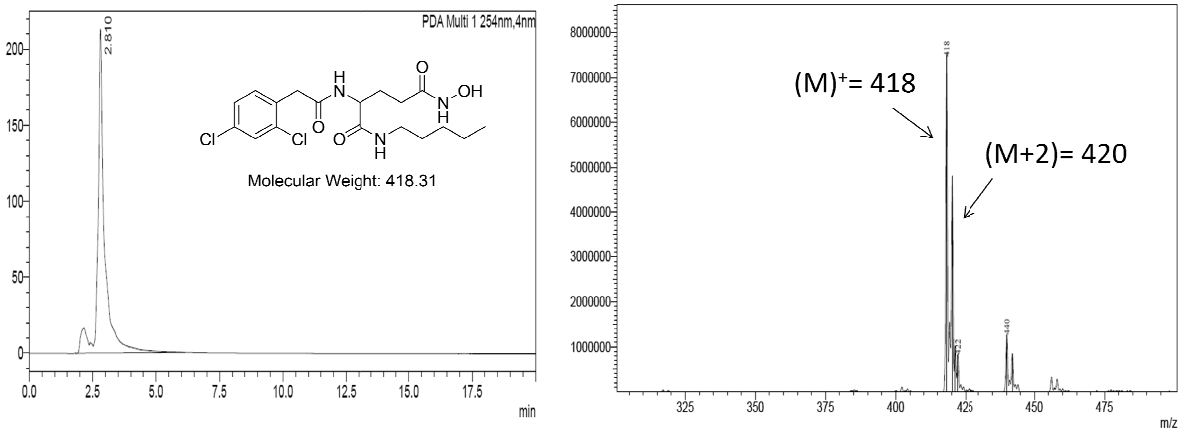

LC/MS of **7i**

2-(2-(2,4-dichlorophenyl)acetamido)-*N*^{5}-hydroxy-*N*^{1}-phenylpentanediamide (7j)

Yield 40%, off white powder, ^{1}H NMR (400 MHz, DMSO-d$_6$) δ 8.75 (t, *J* = 9.0 Hz, 1H), 8.48 (t, *J* = 5.8 Hz, 1H), 7.68 (d, *J* = 1.2 Hz, 1H), 7.55 – 7.48 (m, 2H), 7.35 – 7.21 (m, 5H), 4.42 (m, 1H), 4.32 (d, *J* = 5.8 Hz, 2H), 2.15 – 1.95 (m, 3H), 1.91 – 1.80 (m, 1H), ^{13}C NMR

(101 MHz, DMSO-d_6) δ 170.74, 170.72, 168.43, 165.45, 139.27, 139.23, 135.24, 134.53, 131.28, 130.56, 129.03, 128.23, 127.11, 127.04, 126.74, 53.06, 42.07, 28.94, 27.79. HPLC Rt: 2.712 LC/MS calculated for expected $C_{19}H_{19}Cl_2N_3O_4$ [M]: 424.28; $[M]^+$: 424, $[M+2]^+$: 426.

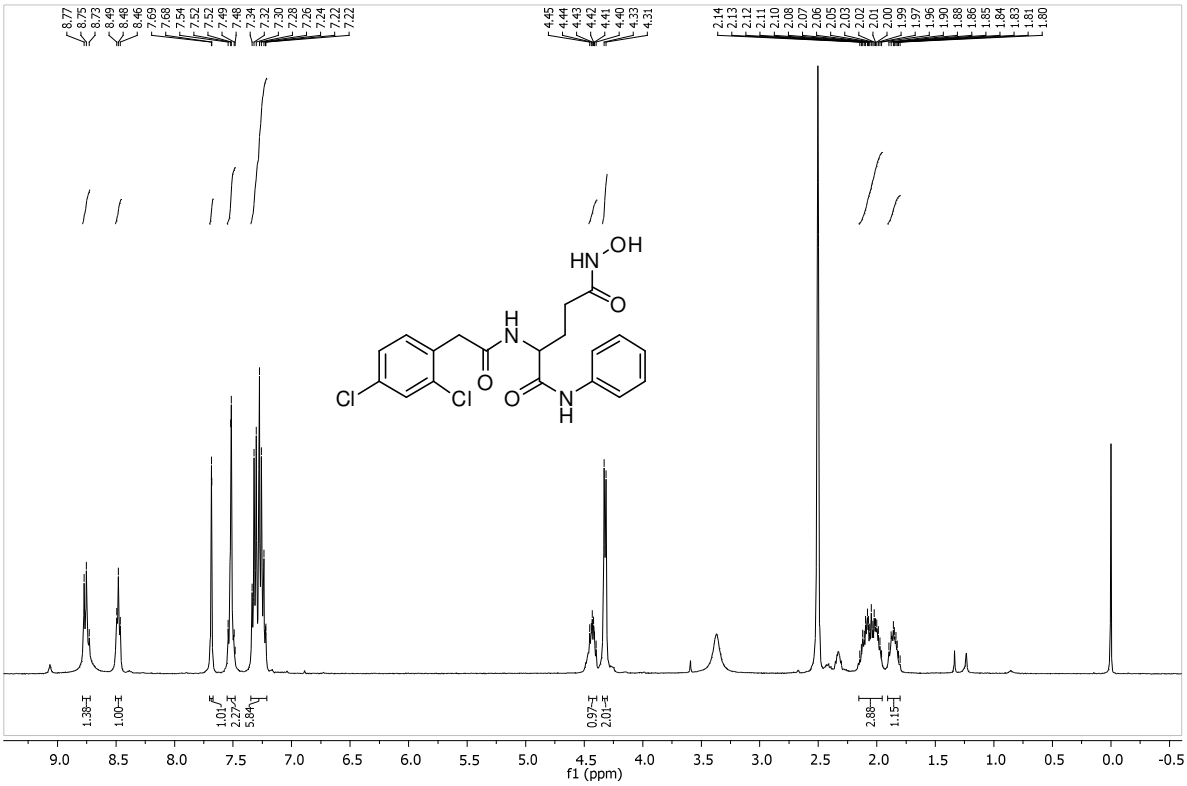

^{1}H NMR of **7j**

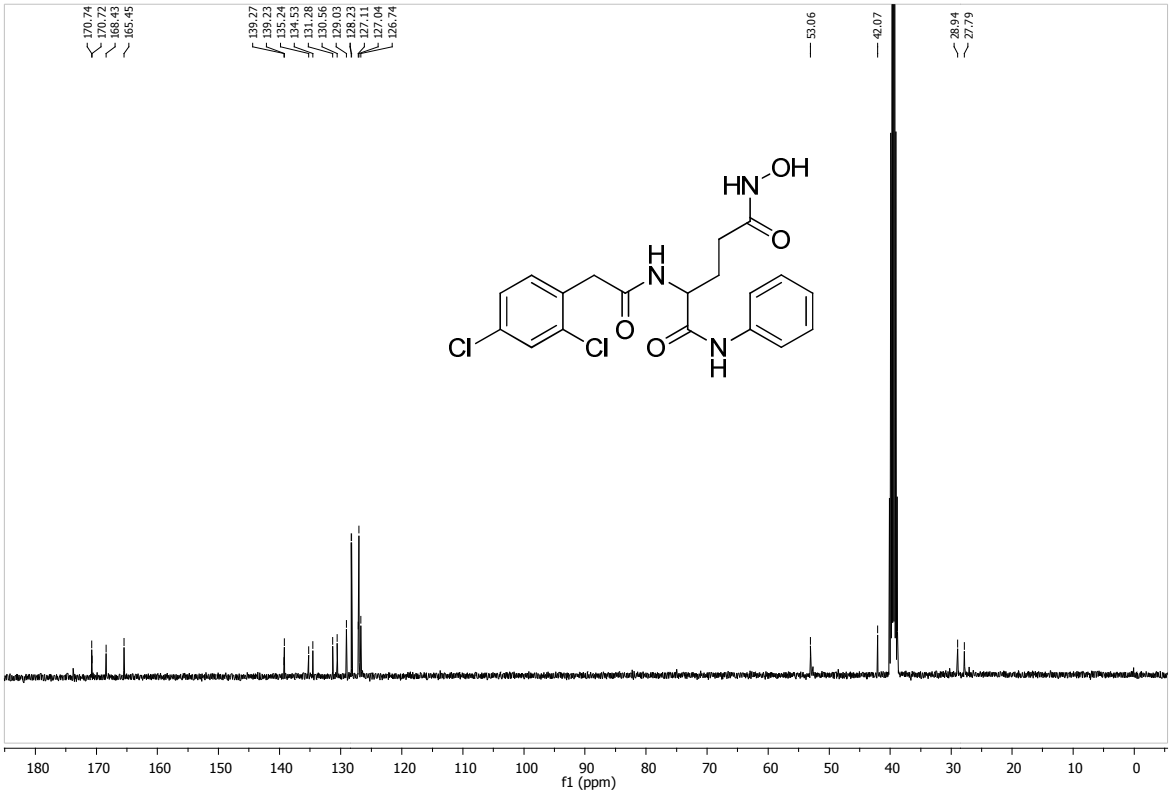

^{13}C NMR of **7j**

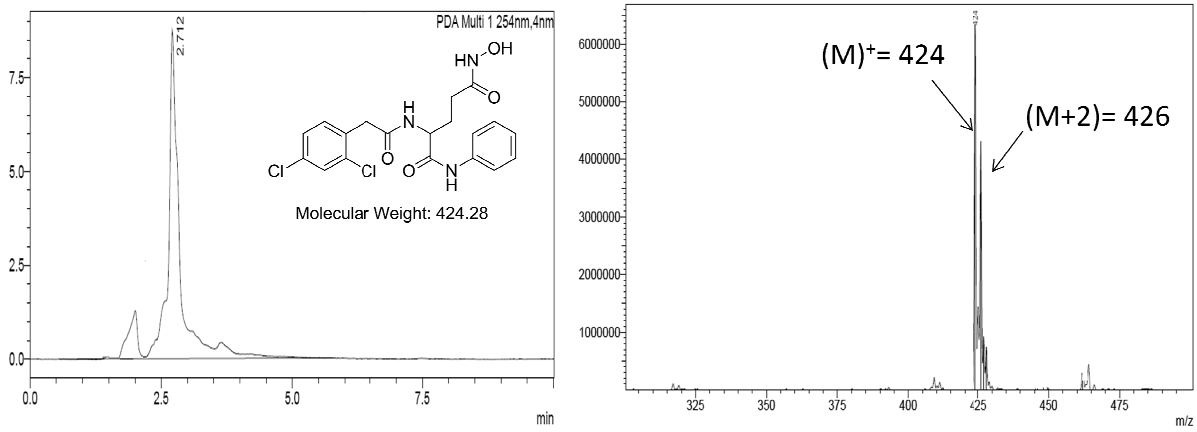

LC/MS of **7j**

N^5-hydroxy-2-(2-(naphthalen-2-yl)acetamido)-N^1-pentylpentanediamide (7k)

Yield 95.2%, white powder, ^{1}H NMR (400 MHz, DMSO-d_6) δ 8.39 (d, J = 8.2 Hz, 1H), 8.11 – 8.06 (m, 1H), 7.91 (m, 2H), 7.84 – 7.78 (m, 1H), 7.54 – 7.40 (m, 4H), 4.22 (m, 1H), 3.97 (d, J = 4.1 Hz, 1H), 3.09 – 2.95 (m, 2H), 2.01 – 1.69 (m, 4H), 1.41 – 1.15 (m, 7H), 0.84

(t, J = 7.1 Hz, 3H), ^{13}C NMR (101 MHz, DMSO-d_6) δ 170.79, 169.96, 168.48, 133.28, 132.80, 131.95, 128.28, 127.70, 126.96, 125.85, 125.56, 125.43, 124.29, 52.31, 38.39, 28.87, 28.61, 28.52, 28.45, 21.74, 13.85. HPLC Rt: 2.359, LC/MS calculated for expected $C_{22}H_{29}N_3O_4$ [M]: 399.48; $[M+H]^+$: 400, $[M+Na]^+$: 422.

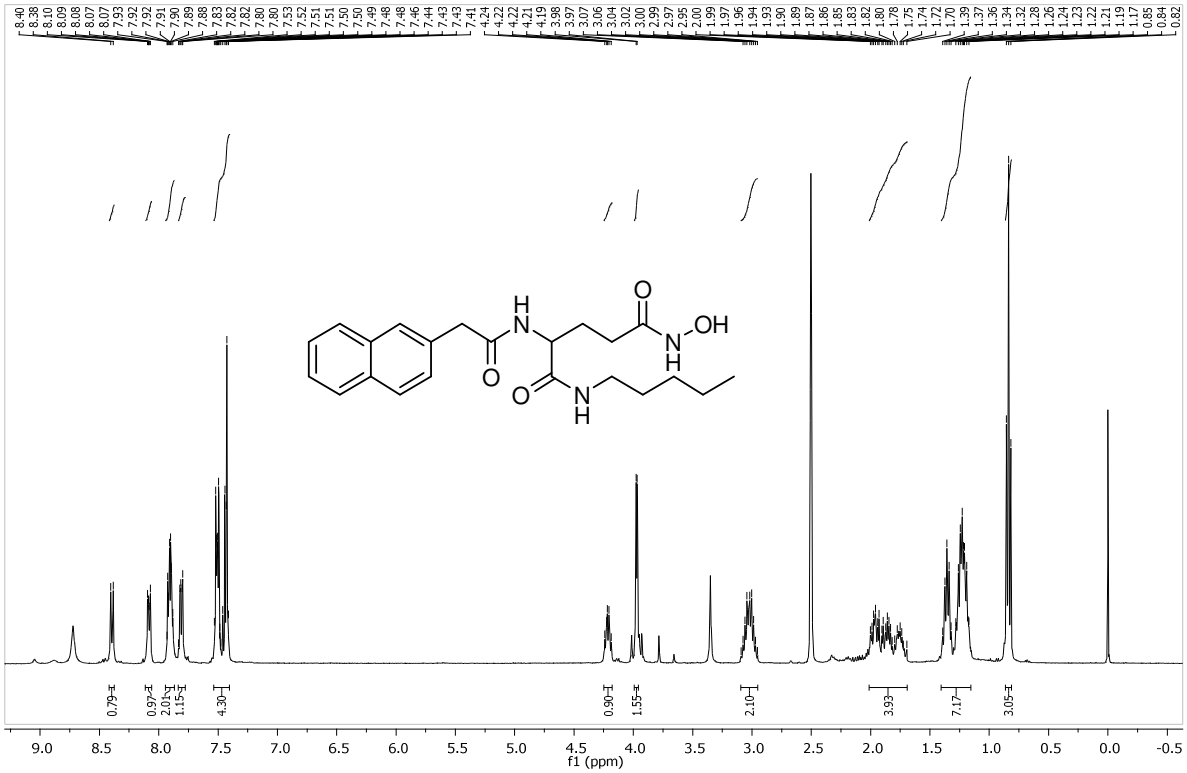

^{1}H NMR **7k**

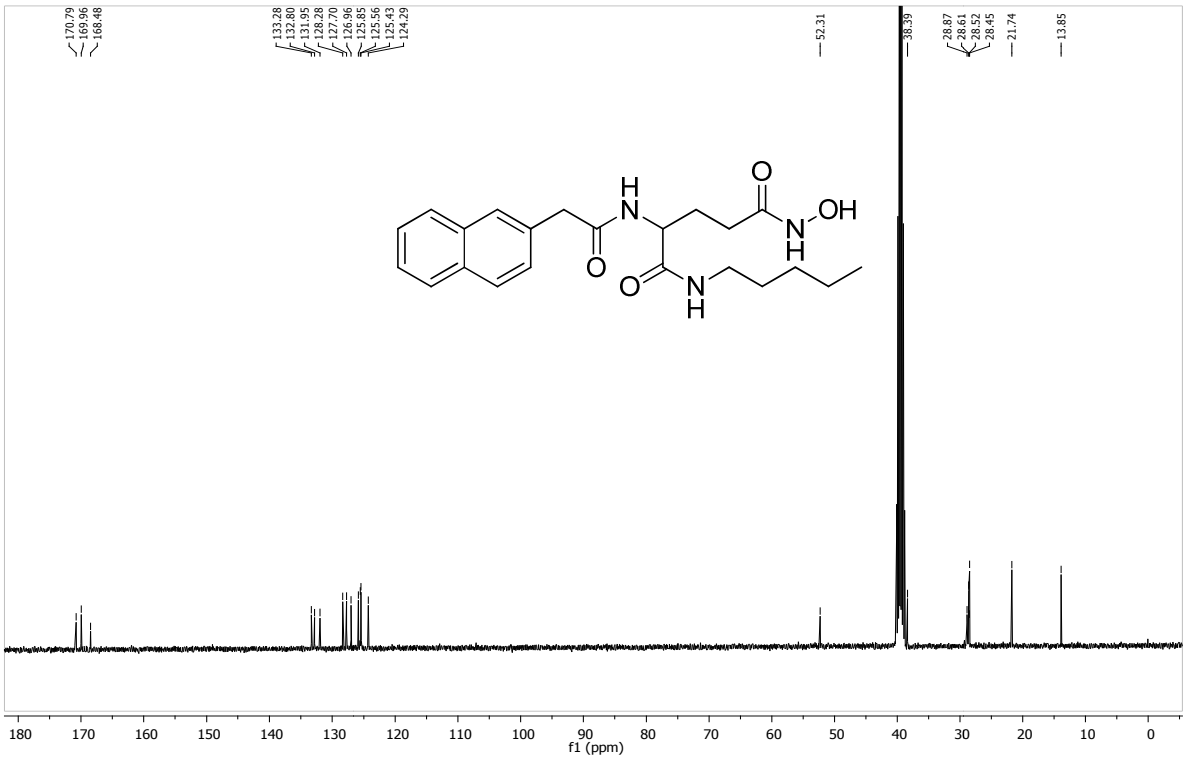

^{13}C NMR of **7k**

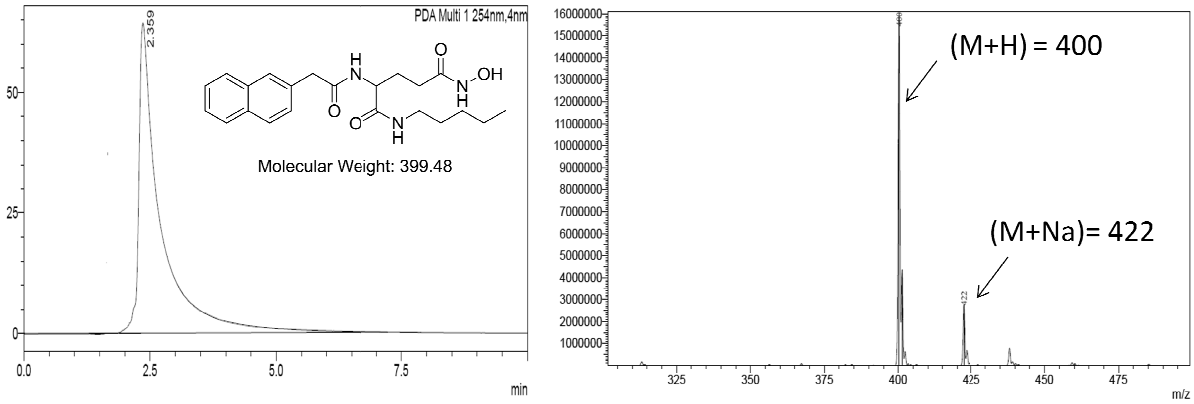

LC/MS of **7k**

***N*^{1}-hexyl-*N*^{5}-hydroxy-2-(2-(naphthalen-2-yl)acetamido)pentanediamide (7l):**

Yield=76.2%, white crystalline powder, ^{1}H NMR (400 MHz, DMSO-d_6) δ 10.43 (s, 1H), 8.42 (d, *J* = 8.1 Hz, 1H), 8.12 – 8.05 (m, 1H), 7.93 – 7.87 (m, 2H), 7.81 (dd, *J* = 6.3, 3.0 Hz, 1H), 7.53 – 7.41 (m, 4H), 4.24 – 4.17 (m, 1H), 3.98 (d, *J* = 2.8 Hz, 2H), 3.07 – 2.96 (m, 2H), 2.03 – 1.68 (m, 5H), 1.39 – 1.18 (m, 9H), 0.85 (t, *J* = 6.7 Hz, 3H). ^{13}C NMR (101 MHz, DMSO-d_6) δ 171.32, 170.49, 169.02, 133.77, 133.31, 132.45, 128.78, 128.22, 127.46,

126.35, 126.06, 125.93, 124.81, 52.87, 31.39, 29.40, 29.01, 26.30, 22.48, 21.54, 14.37. LC-MS calculated for expected $C_{23}H_{31}N_3O_4$ [M]: 413.51 and found $[M+H]^+$: 414.

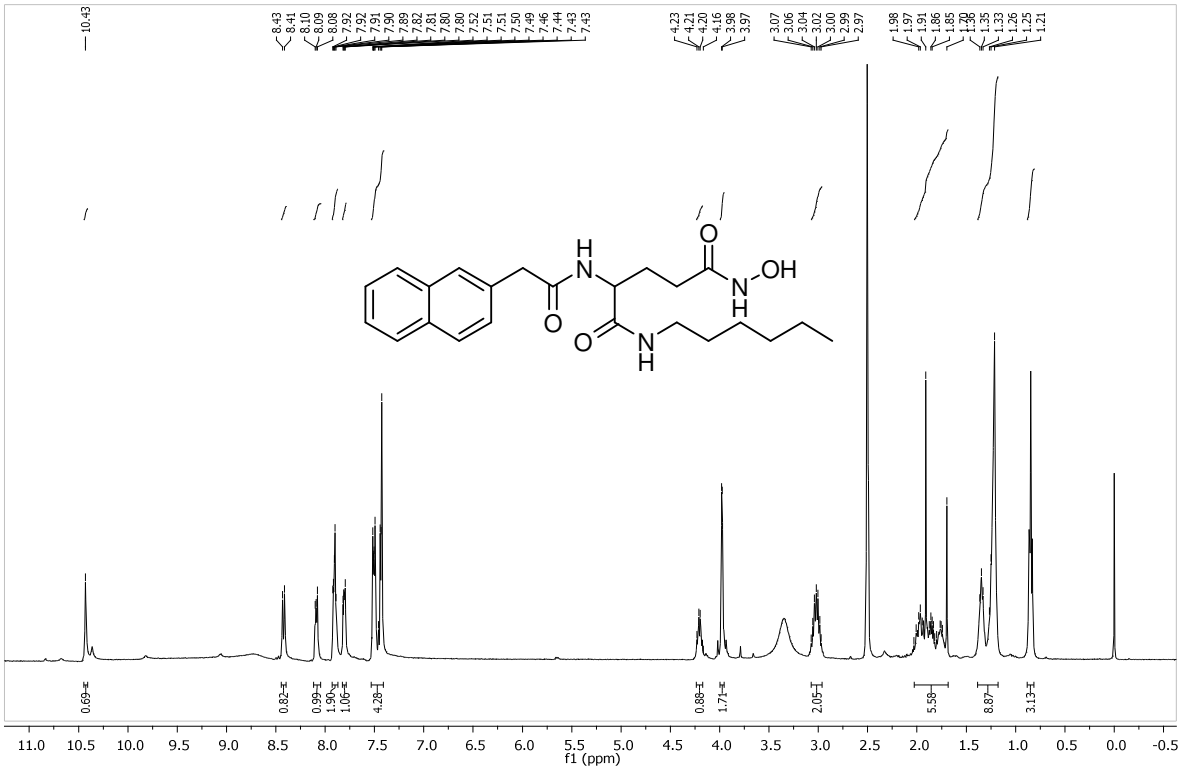

^{1}H NMR of **7l**

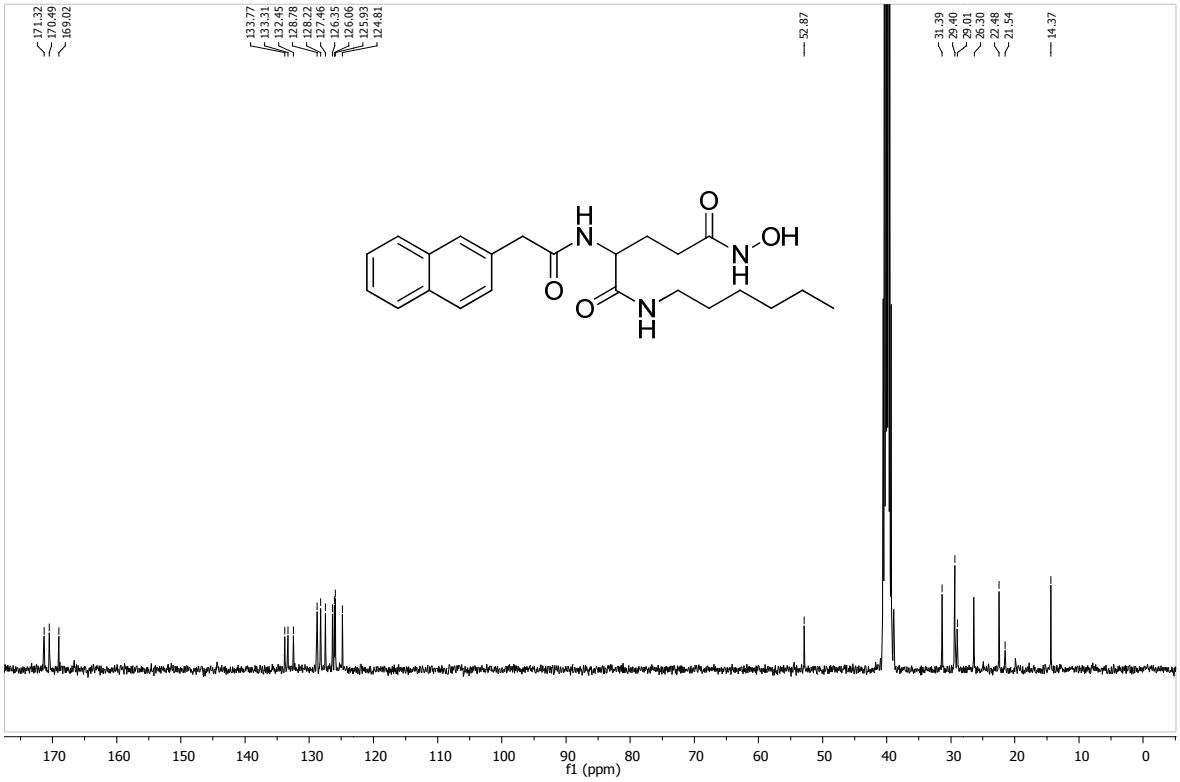

^{13}C NMR of **7l**

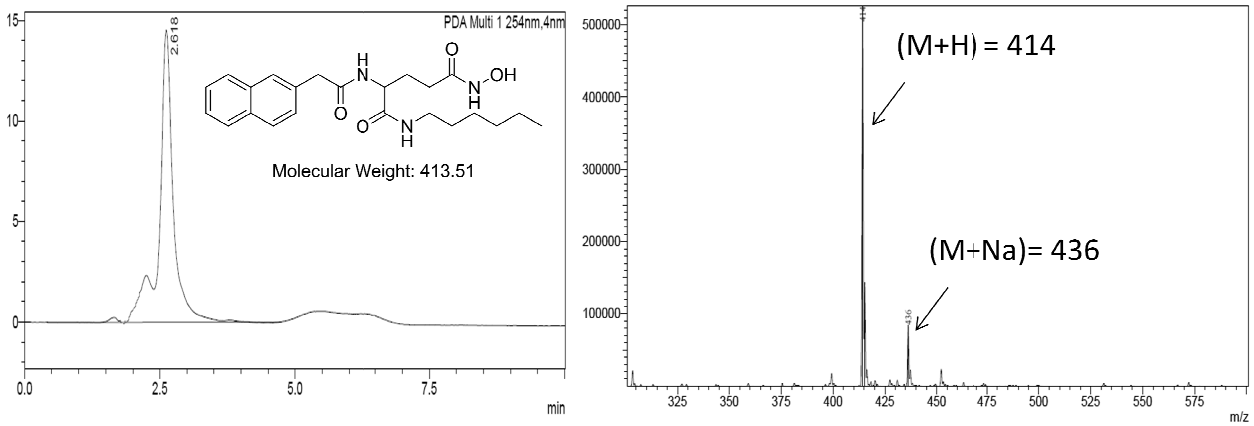

LC/MS of **7l**

4.3.2. HDAC inhibition assay using HeLa nuclear extract

The HDAC enzyme inhibition assay was performed using HDAC colorimetric assay kit (BML-AK501, ENZO life sciences) following vendor's protocol. Briefly, 5 µL of Hela nuclear extract (BML-KI137-0500), 10 µL of assay buffer (BML-KI143-0020), 10 µL of sample solution was added per well in a microtiter plate. 25 µL of *Color de Lys*® substrate (BML-KI138-0050) was added and plate was incubated in for 30 minutes at 37°C which was terminated by addition of a 50 µL mixture of developer plus stop solution. The plate was incubated for 15 minutes at 37°C and absorbance was measured at 405 nm. All synthesized compounds were screened at 10 µM concentration in duplicate.

4.3.3. HDAC3/NCOR1 assay

HDAC3 enzyme inhibition assay was performed using HDAC3/NCOR1 fluorimetric drug discovery kit (BML-AK531, ENZO life sciences) following vendor's protocol. Here, 10 µL of sample solution and 15 µL diluted HDAC3/NCOR1 complex solution (BML-KI574-0030) were added per well in microtiter plate. 25 µL Fluor de Lys® substrate solution (BML-KI177-0005) was added. The plate was incubated for 15 minutes at 37°C. Then, 50 µL of mixture of *Fluor de Lys*® developer II (BML-KI176-1250) and trichostatin A (BML-GR309-9090) was added per well and incubated for 45 minutes at 37°C. The fluorescence intensity was measured at excitation wavelength 360 nm, emission wavelength 460 nm using Spectramax M4 (Molecular Devices, USA). All synthesized compounds were screened at 10µM concentration in duplicate.

4.3.4. HDAC8 assay using human recombinant HDAC8

HDAC8 inhibition assay was performed using HDAC8 fluorimetric drug discovery kit (BML-AK518, Enzo life science) following vendor's protocol. Briefly, 15 µL of diluted

human recombinant HDAC8 enzyme (BML-SE145-0100) was incubated with 10 µL of test inhibitor (10 µM) and 25 µl of *Fluor de Lys*® HDAC8, deacetylase substrate (BML-KI178-0005). After 10 minutes incubation, reaction was terminated by adding 50 µL stop solution which contains *Fluor de Lys*®- Developer II (BML-KI176-1250) and trichostatin A. The plate was incubated for 45 minutes at 37°C and fluorescence intensity was measured at excitation wavelength 360 nm, emission wavelength 460 nm using Spectramax M4 (Molecular Devices, USA). All target compounds were screened at 10 µM concentration in duplicate.

4.3.5. Cell culture

The murine melanoma cell line (B16F10) was cultured in Dulbecco's Modified Eagle Medium (DMEM) (Himedia Laboratories Pvt. Ltd., Mumbai, India), Non-small cell lung cancer cells (A549) in Dulbecco's Modified Eagle Medium/ Nutrient Mixture F-12 Ham (DMEM/F12, 1:1 mixture, Himedia Laboratories Pvt. Ltd., Mumbai, India), and Jurkat E6 cells in Roswell Park Memorial Institute-1640 (RPMI-1640, Himedia Laboratories Pvt. Ltd., Mumbai, India), supplemented with 10% heat inactivated fetal bovine serum (Himedia Laboratories Pvt. Ltd., Mumbai, India) and 1 % of Antibiotic solution (10000 U Penicillin and 10 mg Streptomycin per ml, Himedia Laboratories Pvt. Ltd., Mumbai, India). Cells were cultured at 37°C in humidified atmosphere with 5% CO_2. Stock solutions of all synthesized compounds were prepared in DMSO-d_6 at a concentration of 100 mM and stored at -20°C.

4.3.5.1. MTT assay

Antiproliferative activity of the synthesized compounds was determined using MTT assay. 5×10^4 cells were seeded in 96 well plates and incubated overnight. Cells were treated with synthesized compounds at two concentrations (100 and 10µM) in triplicates and incubated for 72 hours. 50 µL of 5 mg/mL 3-(4,5-dimethylthiazol-2-yl)-2,5-diphenyltetrazolium bromide (MTT; Himedia Laboratories Pvt. Ltd., Mumbai, India) was added and incubated for 4 hours. Formazan crystals were dissolved using DMSO and evaluated spectrophotometrically at 570 nm and 650 nm using Spectramax M4 (Molecular Devices, USA).

For determination of IC_{50} values of promising compounds same procedure was followed as described above where five compounds (**7d, 7e, 7f, 7h** and **7i**) were tested at 10 different concentrations as 400, 200, 100, 50, 25, 12.5, 6.25, 3.125, 1.562 and 0.781µM.

For Jurkat E6 cells, 2×10^4 cells in 100 µL were seeded in 96 well plates and incubated overnight. Treatment concentrations were same for both experiments as described above for other cell lines. After 72 hour incubation with test compounds, cells were treated with 22 µL of Prestoblue™ (Invitrogen, life technologies, United States) reagent. Plate was incubated for 2 hours and fluorescence intensity was measured at excitation wavelength 560 nm, emission wavelength 590 nm using Spectramax M4 (Molecular Devices, USA).

4.3.5.2. Cell cycle Analysis

Briefly, $5x10^5$ B16F10 cells were seeded in 6 well plates and incubated overnight at 37°C. The next day, cells were treated with **7d** and **7i** and incubated for 72 hours. Cells were trypsinized, centrifuged and washed twice with PBS and fixed with 70% ice cold ethanol and stored at -20°C for 24 hours. The cells were centrifuged washed and resuspended in 500

μL PBS pH 7.4 containing RNAse (100 μg/mL) at room temperature for 20 minutes. Propidium iodide (PI) (50 μg/mL in PBS) was added to stain cellular DNA and kept in dark for 30 minutes. Flow cytometry analysis was performed and the percentage of cells in each phase of the cell cycle was estimated using the IDEAS Software (version 6.0).

4.4 CONCLUSION

Here, we have designed and synthesized a series of hydroxamates as selective HDAC8 inhibitors. All target compounds were evaluated for their HDAC enzyme inhibition efficiency with HeLa nuclear extract, human recombinant HDAC8 and human recombinant HDAC3 enzyme and these compounds were found to be effective HDAC inhibitors with preferential selectivity for HDAC8. It was found that five carbon side chain is most appropriate length. These compounds were also tested for their antiproliferative activity in three different cell lines (B16F10, HeLa and Jurkat E6). Promising compounds were also explored for their IC_{50} calculation in these cell lines. Compound **7f** and **7i** were found to possess efficient anticancer potential. Compound **7i** induced significant cell growth arrest in G2/M phase indicating its anticancer potential. These compounds can be further modified to improve their efficacy and selectivity.

Chapter 5

Summary and Conclusion

5. SUMMARY AND CONCLUSION

Cancer is one of the major causes of death worldwide. Even though progress has been made in prevention and treatment of cancer, still cancer burden is increasing globally. In past few years, deacetylation of histone has been considered as a promising target for anticancer therapy. HDAC inhibitors cause tumor cell death by inducing apoptosis, cell cycle arrest, senescence, differentiation, autophagy, etc. Therefore, HDAC inhibition has emerged as a potential anticancer target.

Since past few years, a number of HDAC inhibitors have been studied clinically and pre-clinically for various cancers. Most of these inhibitor are Pan HDAC inhibitors and but shows toxicity might be because of less selectivity towards HDAC isoforms as well as heir off target effects. Recent research focuses on development of HDAC inhibitors with increased specificity and selectivity.

The present investigation reported the development of three different series of HDAC inhibitors with preferential selectivity as well as promising anticancer activity.

In first objective, we have designed and synthesized a series of 2-aminobenzamide derivatives as selective HDAC3 inhibitors. All target compounds were evaluated for their HDAC enzyme inhibition efficiency with HeLa nuclear extract and human recombinant HDAC3 enzyme and these compounds were found to be effective HDAC inhibitors with preferential selectivity for HDAC3. These compounds were also tested for their antiproliferative activity in two different cell lines (B16F10 and HeLa). Compound **26c** (Ch.2) exhibited potent cell growth inhibition compared to both **CI-994** and **BG45**. One of the lead compound (compound **26c** (Ch.2)) showed appreciable selectivity (11.68-fold) in

HDAC3 inhibition over pan HDACs which is quite significant than **CI-994** (5.85-fold) and **BG45** (9.9-fold). Compound **26c** (Ch.2) induced significant cell growth arrest in G2/M phase and increased apoptosis level indicating improved anticancer potential compared to **CI-994** and **BG45**. Overall effort to make potent and selective HDAC inhibitors with different structural medication on the overlapping backbone of **BG45** and **CI-994** resulted in compound **26c** (Ch.2) as a potential HDAC3 inhibitor.

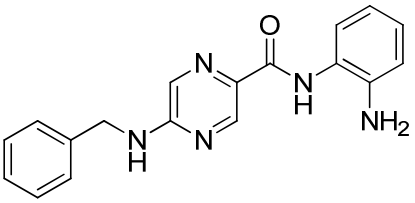

Compound **26c** (Ch.2)

Figure 5.1. Lead compound from the first series of 2-aminobenzamide derivatives

Additionally, all these biological evaluation studies indicated compound **26c** (Ch.2) can be further explored as a promising compound for anticancer therapy.

In second objective, we have designed and synthesized piperidine and piperazine derivatives containing hydroxamic acid as zinc binding group and different bulky cap groups. We successfully incorporated long chain methylene linker with piperidine and piperazine moiety. All target compounds were evaluated for their HDAC inhibition efficiency using HeLa nuclear extract, human recombinant HDAC3 and human recombinant HDAC8. These compounds were found to show effective HDAC inhibition with preferential selectivity towards HDAC8 over HDAC3. These newer analogues are more selective towards HDAC8 than prototype **SAHA**. Vorinostat (**SAHA**) inhibits HDAC3 and HDAC8 with almost similar potential while newer analogues showed remarkable difference between them.

These compounds were screened for their antiproliferative activity in various cell lines (B16F10, HeLa, A-549, MCF-7 and Jurkat E6). They displayed efficient activity on solid tumor cell lines as well as leukemia cell line. The more promising compounds (**5e, 16c** and **16d** from Ch.3) showed increased Caspase3/7 activity which provided the evidence of their anticancer potential by activation of apoptotic pathways.

From the series, compound **16d** (Ch.3) having alkyl piperazinyl urea in linker region and 4-aminoquinoline substituent in surface recognition site came out as lead compound, which can be further modified to design more efficacious and selective HDAC inhibitors.

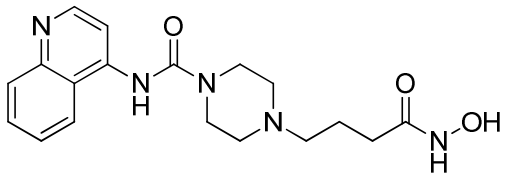

Compound **16d** (Ch.3)

Figure 5.2. Lead compound from the second series of hydroxamates with piperidine and piperazine linker derivatives

In third series, we have designed and synthesized a series of hydroxamates having aliphatic side chain as linker with a hanging aliphatic moiety between the ZBG and cap region as selective HDAC8 inhibitors. All target compounds were evaluated for their HDAC enzyme inhibition efficiency with HeLa nuclear extract, human recombinant HDAC8 and human recombinant HDAC3 enzyme and these compounds were found to be effective HDAC inhibitors with preferential selectivity for HDAC8. It was found that five carbon side chain is most appropriate length. These compounds were also tested for their antiproliferative activity in three different cell lines (B16F10, HeLa and Jurkat E6). Promising compounds were also explored for their IC_{50} calculation in these cell lines. Compound **7f** (Ch.4) and **7i** (Ch.4) were

found to possess efficient anticancer potential. Compound**7i** (Ch.4) induced significant cell growth arrest in G2/M phase indicating its anticancer potential. These compounds can be further modified to improve their efficacy and selectivity.

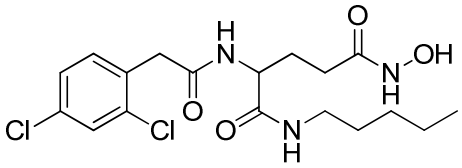

Compound **7i** (Ch.4)

Figure 5.3. Lead compound from the third series of novel hydroxamates

FUTURE PERSPECTIVES

Histone deacetylase inhibitors are widely studied as promising therapeutic agents in treatment of various cancers and other diseases. Over the last few years the HDAC inhibitors market has evolved with many drug molecules designed to treat a wide range of oncological and non-oncological disorders. With five commercialized products, the HDAC inhibitors' pipeline comprises of over 90 molecules under development. Over the last few years, the research focus has shifted from pan-HDAC to the development of class-specific HDAC inhibitors and isoform specific HDAC inhibitors. Few of the isoform selective HDAC inhibitors are under clinical trials.

In this work, we have developed molecules with preferential selectivity towards specific HDAC isoform. Structure and their biological activity data highlights can be helpful for further development of these molecules. These compounds possess efficient anticancer potential. They can be further studied for their pathway specific activity and can be modified to enhance their efficacy.

Currently, many HDAC inhibitors are studied in combination with DNMT inhibitors (e.g., 5-azacytidine), proteasome inhibitors (e.g., bortezomib) and agents acting on hormone therapy (e.g., tamoxifen). These molecules can also be explored as combination therapy for treatment of some diseases.

BIBLIOGRAPHY

Adams, Heiner, et al. (2010), 'Class I histone deacetylases 1, 2 and 3 are highly expressed in classical Hodgkin's lymphoma', *Expert opinion on therapeutic targets,* 14 (6), 577-84.

Adimoolam, Shanthi, et al. (2007), 'HDAC inhibitor PCI-24781 decreases RAD51 expression and inhibits homologous recombination', *Proceedings of the National Academy of Sciences,* 104 (49), 19482-87.

Alnemri, Emad S, et al. (1996), 'Human ICE/CED-3 protease nomenclature', *Cell,* 87 (2), 171.

Amin, Sk Abdul, Adhikari, Nilanjan, and Jha, Tarun (2017a), 'Is dual inhibition of metalloenzymes HDAC-8 and MMP-2 a potential pharmacological target to combat hematological malignancies?', *Pharmacological research,* 122, 8-19.

Amin, Sk Abdul, Adhikari, Nilanjan, and Jha, Tarun (2017b), 'Structure–activity relationships of hydroxamate-based histone deacetylase-8 inhibitors: reality behind anticancer drug discovery', *Future medicinal chemistry,* 9 (18), 2211-37.

Amin, Sk Abdul, Adhikari, Nilanjan, and Jha, Tarun (2018a), 'Structure-activity relationships of HDAC8 inhibitors: Non-hydroxamates as anticancer agents', *Pharmacological research*.

Amin, Sk Abdul, et al. (2018b), 'Designing potential HDAC3 inhibitors to improve memory and learning', *Journal of Biomolecular Structure and Dynamics,* (just-accepted), 1-25.

Ashraf, N, et al. (2006), 'Altered sirtuin expression is associated with node-positive breast cancer', *British journal of cancer,* 95 (8), 1056

Bala, Veenu, et al. (2015), 'Dithiocarbamate–thiourea hybrids useful as vaginal microbicides also show reverse transcriptase inhibition: design, synthesis, docking and pharmacokinetic studies', *Bioorganic & medicinal chemistry letters,* 25 (4), 881-86.

Bannister, Andrew J and Kouzarides, Tony (2011), 'Regulation of chromatin by histone modifications', *Cell research,* 21 (3), 381.

Baylin, Stephen B and Jones, Peter A (2011), 'A decade of exploring the cancer epigenome—biological and translational implications', *Nature Reviews Cancer,* 11 (10), 726.

Berger, Shelley L (2007), 'The complex language of chromatin regulation during transcription', *Nature,* 447 (7143), 407.

Bhaskara, Srividya, et al. (2008), 'Deletion of histone deacetylase 3 reveals critical roles in S phase progression and DNA damage control', *Molecular cell,* 30 (1), 61-72.

Bhaskara, Srividya, et al. (2010), 'Hdac3 is essential for the maintenance of chromatin structure and genome stability', *Cancer cell,* 18 (5), 436-47.

Bieliauskas, Anton V and Pflum, Mary Kay H (2008), 'Isoform-selective histone deacetylase inhibitors', *Chemical Society Reviews,* 37 (7), 1402-13.

Bishton, Mark J, et al. (2011), 'Deciphering the molecular and biological processes that mediate histone deacetylase inhibitor-induced thrombocytopenia', *Blood*, blood-2010-11-318055.

Bolden, JE, et al. (2013), 'HDAC inhibitors induce tumor-cell-selective pro-apoptotic transcriptional responses', *Cell death & disease,* 4 (2), e519.

Bolden, Jessica E, Peart, Melissa J, and Johnstone, Ricky W (2006), 'Anticancer activities of histone deacetylase inhibitors', *Nature reviews Drug discovery,* 5 (9), 769.

Bose, Prithviraj, Dai, Yun, and Grant, Steven (2014), 'Histone deacetylase inhibitor (HDACI) mechanisms of action: emerging insights', *Pharmacology & therapeutics,* 143 (3), 323-36.

Bradbury, CA, et al. (2005), 'Histone deacetylases in acute myeloid leukaemia show a distinctive pattern of expression that changes selectively in response to deacetylase inhibitors', *Leukemia,* 19 (10), 1751.

Buglio, Daniela, et al. (2011), 'HDAC11 plays an essential role in regulating OX40 ligand expression in Hodgkin lymphoma', *Blood*, blood-2010-08-303701.

Butler, Lisa M, et al. (2002), 'The histone deacetylase inhibitor SAHA arrests cancer cell growth, up-regulates thioredoxin-binding protein-2, and down-regulates thioredoxin', *Proceedings of the National Academy of Sciences,* 99 (18), 11700-05.

Campas-Moya, Clara (2009), 'Romidepsin for the treatment of cutaneous T-cell lymphoma', *Drugs of today (Barcelona, Spain: 1998),* 45 (11), 787-9

Campos, Eric I and Reinberg, Danny (2009), 'Histones: annotating chromatin', *Annual review of genetics,* 43.

Chen, Chang-Shi, et al. (2007), 'Histone deacetylase inhibitors sensitize prostate cancer cells to agents that produce DNA double-strand breaks by targeting Ku70 acetylation', *Cancer research,* 67 (11), 5318-27.

Chen, Chi-qi, et al. (2013), 'Histone deacetylases inhibitor trichostatin A increases the expression of Dleu2/miR-15a/16-1 via HDAC3 in non-small cell lung cancer', *Molecular and cellular biochemistry,* 383 (1-2), 137-48.

Choi, Jae-Hoon, et al. (2001), 'Expression profile of histone deacetylase 1 in gastric cancer tissues', *Japanese Journal of Cancer Research,* 92 (12), 1300-04.

Choi, Jung Hye, et al. (2010), 'Enhancer of zeste homolog 2 expression is associated with tumor cell proliferation and metastasis in gastric cancer', *Apmis,* 118 (3), 196-202.

CHOI, Y-W, et al. (2007), 'Gene expression profiles in squamous cell cervical carcinoma using array-based comparative genomic hybridization analysis', *International Journal of Gynecological Cancer,* 17 (3), 687-96.

Coiffier, Bertrand, et al. (2012), 'Results from a pivotal, open-label, phase II study of romidepsin in relapsed or refractory peripheral T-cell lymphoma after prior systemic therapy', *Journal of Clinical Oncology,* 30 (6), 631-36.

Dawson, Mark A and Kouzarides, Tony (2012), 'Cancer epigenetics: from mechanism to therapy', *Cell,* 150 (1), 12-27.

Egger, Gerda, et al. (2004), 'Epigenetics in human disease and prospects for epigenetic therapy', *Nature,* 429 (6990), 457.

Falkenberg, Katrina J and Johnstone, Ricky W (2014), 'Histone deacetylases and their inhibitors in cancer, neurological diseases and immune disorders', *Nature reviews Drug discovery,* 13 (9), 673.

Felsenfeld, Gary and Groudine, Mark (2003), 'Controlling the double helix', *Nature,* 421 (6921), 448.

Fenichel, Marilyn P (2015), 'FDA approves new agent for multiple myeloma', *JNCI: Journal of the National Cancer Institute,* 107 (6).

Finnin, Michael S, et al. (1999), 'Structures of a histone deacetylase homologue bound to the TSA and SAHA inhibitors', *Nature,* 401 (6749), 188.

Fitzmaurice, Christina, et al. (2015), 'The global burden of cancer 2013', *JAMA oncology,* 1 (4), 505-27.

Finnin, Michael S, et al. (1999), 'Structures of a histone deacetylase homologue bound to the TSA and SAHA inhibitors', *Nature,* 401 (6749), 188.

Fischer, André, et al. (2010), 'Targeting the correct HDAC (s) to treat cognitive disorders', *Trends in pharmacological sciences,* 31 (12), 605-17.

Food and Administration, Drug (2014), 'FDA approves Beleodaq to treat rare, aggressive form of non-Hodgkin lymphoma. July 3, 2014', *FDA Approves Beleodaq to Treat Rare, Aggressive Form of Non-Hodgkin Lymphoma*.

Fraga, Mario F, et al. (2005), 'Loss of acetylation at Lys16 and trimethylation at Lys20 of histone H4 is a common hallmark of human cancer', *Nature genetics,* 37 (4), 391.

Frew, Ailsa J, Johnstone, Ricky W, and Bolden, Jessica E (2009), 'Enhancing the apoptotic and therapeutic effects of HDAC inhibitors', *Cancer letters,* 280 (2), 125-33.

Fritzsche, Florian R, et al. (2008), 'Class I histone deacetylases 1, 2 and 3 are highly expressed in renal cell cancer', *BMC cancer,* 8 (1), 381.

Galli, Monica, et al. (2010), 'A phase II multiple dose clinical trial of histone deacetylase inhibitor ITF2357 in patients with relapsed or progressive multiple myeloma', *Annals of hematology,* 89 (2), 185.

Grant, Patrick A (2001), 'A tale of histone modifications', *Genome biology,* 2 (4), reviews0003. 1.

Gregoretti, IvanV, Lee, Yun-Mi, and Goodson, Holly V (2004), 'Molecular evolution of the histone deacetylase family: functional implications of phylogenetic analysis', *Journal of molecular biology,* 338 (1), 17-31.

Gupta, Praveer, et al. (2012), 'Towards isozyme-selective HDAC inhibitors for interrogating disease', *Current topics in medicinal chemistry,* 12 (14), 1479-99.

Haggarty, Stephen J, et al. (2003), 'Domain-selective small-molecule inhibitor of histone deacetylase 6 (HDAC6)-mediated tubulin deacetylation', *Proceedings of the National Academy of Sciences,* 100 (8), 4389-94.

Hammock, Bruce D, et al. (2016), 'Acyl piperidine inhibitors of soluble epoxide hydrolase', (Google Patents).

Hanigan, Thomas W, et al. (2017), 'Divergent JNK Phosphorylation of HDAC3 in Triple-Negative Breast Cancer Cells Determines HDAC Inhibitor Binding and Selectivity', *Cell chemical biology,* 24 (11), 1356-67. e8.

Harada, Takeshi, et al. (2017), 'HDAC3 regulates DNMT1 expression in multiple myeloma: therapeutic implications', *Leukemia,* 31 (12), 2670.

Hida, Yasutoshi, et al. (2007), 'Strong expression of a longevity-related protein, SIRT1, in Bowen's disease', *Archives of dermatological research,* 299 (2), 103-06.

Hiratsuka, Masaharu, et al. (2003), 'Proteomics-based identification of differentially expressed genes in human gliomas: down-regulation of SIRT2 gene', *Biochemical and biophysical research communications,* 309 (3), 558-66.

Holliday, Robin (2006), 'Epigenetics: a historical overview', *Epigenetics,* 1 (2), 76-80.

Hsieh, Hao-Yu, et al. (2017), 'Targeting breast cancer stem cells by novel HDAC3-selective inhibitors', *European journal of medicinal chemistry,* 140, 42-51.

Huang, Yen-Sung, et al. (2016), 'Xist reduction in breast cancer upregulates AKT phosphorylation via HDAC3-mediated repression of PHLPP1 expression', *Oncotarget,* 7 (28), 43256.

Huffman, Derek M, et al. (2007), 'SIRT1 is significantly elevated in mouse and human prostate cancer', *Cancer research,* 67 (14), 6612-18.

Jiang, Yanwen, et al. (2017), 'CREBBP inactivation promotes the development of HDAC3-dependent lymphomas', *Cancer discovery,* 7 (1), 38-53.

Jirtle, Randy L and Skinner, Michael K (2007), 'Environmental epigenomics and disease susceptibility', *Nature reviews genetics,* 8 (4), 253.

Johnstone, Ricky W, Ruefli, Astrid A, and Lowe, Scott W (2002), 'Apoptosis: a link between cancer genetics and chemotherapy', *Cell,* 108 (2), 153-64.

Jung, Kwang Hwa, et al. (2012), 'HDAC2 overexpression confers oncogenic potential to human lung cancer cells by deregulating expression of apoptosis and cell cycle proteins', *Journal of cellular biochemistry,* 113 (6), 2167-77.

Kandalkar, Sachin R, et al. (2013), 'Highly efficient one-pot amination of carboxylate-substituted nitrogen-containing heteroaryl chlorides via Staudinger reaction', *Tetrahedron Letters,* 54 (5), 414-18.

Keith, John M, et al. (2012), 'Aryl piperazinyl ureas as inhibitors of fatty acid amide hydrolase (FAAH) in rat, dog, and primate', *ACS medicinal chemistry letters,* 3 (10), 823-27.

Kelly, Wm Kevin, et al. (2003), 'Phase I clinical trial of histone deacetylase inhibitor: suberoylanilide hydroxamic acid administered intravenously', *Clinical Cancer Research,* 9 (10), 3578-88.

Khan, Shahper N and Khan, Asad U (2010), 'Role of histone acetylation in cell physiology and diseases: An update', *Clinica chimica acta,* 411 (19-20), 1401-11.

Kim, Hyun-Jung and Bae, Suk-Chul (2011), 'Histone deacetylase inhibitors: molecular mechanisms of action and clinical trials as anti-cancer drugs', *American journal of translational research,* 3 (2), 166.

Kouzarides, Tony (2007), 'Chromatin modifications and their function', *Cell,* 128 (4), 693-705.

Krusche, Claudia A, et al. (2005), 'Histone deacetylase-1 and-3 protein expression in human breast cancer: a tissue microarray analysis', *Breast cancer research and treatment,* 90 (1), 15-23.

Kumar, S and Lavin, MF (1996), 'The ICE family of cysteine proteases as effectors of cell death', *Cell death and differentiation,* 3 (3), 255-67.

Lee, J-H, et al. (2010), 'Histone deacetylase inhibitor induces DNA damage, which normal but not transformed cells can repair', *Proceedings of the National Academy of Sciences,* 107 (33), 14639-44.

Li, Junling, et al. (2004), 'Expression and functional characterization of recombinant human HDAC1 and HDAC3', *Life sciences,* 74 (22), 2693-705.

Li, Xiaoyang, et al. (2014), 'Discovery of the first N-hydroxycinnamamide-based histone deacetylase 1/3 dual inhibitors with potent oral antitumor activity', *Journal of medicinal chemistry,* 57 (8), 3324-41.

Libý, P, et al. (2006), 'Elevated and deregulated expression of HDAC3 in human astrocytic glial tumours', *Folia biologica,* 52 (1/2), 21.

Liu, Chungang, et al. (2013), 'Histone deacetylase 3 participates in self-renewal of liver cancer stem cells through histone modification', *Cancer letters,* 339 (1), 60-69.

Loprevite, Maura, et al. (2005), 'In vitro study of CI-994, a histone deacetylase inhibitor, in non-small cell lung cancer cell lines', *Oncology Research Featuring Preclinical and Clinical Cancer Therapeutics,* 15 (1), 39-48.

Lu, Duo (2013), 'Epigenetic modification enzymes: catalytic mechanisms and inhibitors', *Acta Pharmaceutica Sinica B,* 3 (3), 141-49.

Mackay, Helen J, et al. (2010), 'Phase II trial of the histone deacetylase inhibitor belinostat in women with platinum resistant epithelial ovarian cancer and micropapillary (LMP) ovarian tumours', *European Journal of Cancer,* 46 (9), 1573-79.

Maiso, Patricia, et al. (2006), 'The histone deacetylase inhibitor LBH589 is a potent antimyeloma agent that overcomes drug resistance', *Cancer research,* 66 (11), 5781-89.

Manal, Mohammed, et al. (2016), 'Inhibitors of histone deacetylase as antitumor agents: a critical review', *Bioorganic chemistry,* 67, 18-42.

Mann, Bhupinder S, et al. (2007), 'FDA approval summary: vorinostat for treatment of advanced primary cutaneous T-cell lymphoma', *The oncologist,* 12 (10), 1247-52.

Marson, Charles M, et al. (2013), 'Discovery of potent, isoform-selective inhibitors of histone deacetylase containing chiral heterocyclic capping groups and a N-(2-aminophenyl) benzamide binding unit', *Journal of medicinal chemistry,* 56 (15), 6156-74.

Marson, Charles M, et al. (2015), 'Potent and selective inhibitors of histone deacetylase-3 containing chiral oxazoline capping groups and a N-(2-aminophenyl)-benzamide binding unit', *Journal of medicinal chemistry,* 58 (17), 6803-18.

Marks, Paul A (2006), 'Thioredoxin in cancer—role of histone deacetylase inhibitors', *Seminars in cancer biology* (16: Elsevier), 436-43.

Mersfelder, Erica L and Parthun, Mark R (2006), 'The tale beyond the tail: histone core domain modifications and the regulation of chromatin structure', *Nucleic acids research,* 34 (9), 2653-62.

Milde, Till, et al. (2010), 'HDAC5 and HDAC9 in medulloblastoma: novel markers for risk stratification and role in tumor cell growth', *Clinical Cancer Research*, 1078-0432. CCR-10-395.

Miller, Thomas A, Witter, David J, and Belvedere, Sandro (2003), 'Histone deacetylase inhibitors', *Journal of medicinal chemistry,* 46 (24), 5097-116.

Minami, Jiro, et al. (2014), 'Histone deacetylase 3 (HDAC3) as a novel therapeutic target in multiple myeloma', *Leukemia,* 28 (3), 680.

Minamiya, Yoshihiro, et al. (2011), 'Expression of histone deacetylase 1 correlates with a poor prognosis in patients with adenocarcinoma of the lung', *Lung cancer,* 74 (2), 300-04.

Moreno, Daniel Antunes, et al. (2010), 'Differential expression of HDAC3, HDAC7 and HDAC9 is associated with prognosis and survival in childhood acute lymphoblastic leukaemia', *British journal of haematology,* 150 (6), 665-73.

Morita, Sachi, et al. (2012), 'Phase I dose-escalating study of panobinostat (LBH589) administered intravenously to Japanese patients with advanced solid tumors', *Investigational new drugs,* 30 (5), 1950-57.

Mottamal, Madhusoodanan, et al. (2015), 'Histone deacetylase inhibitors in clinical studies as templates for new anticancer agents', *Molecules,* 20 (3), 3898-941.

Munshi, Anupama, et al. (2005), 'Histone deacetylase inhibitors radiosensitize human melanoma cells by suppressing DNA repair activity', *Clinical Cancer Research,* 11 (13), 4912-22.

Nicholson, Donald W and Thornberry, Nancy A (1997), 'Caspases: killer proteases', *Trends in biochemical sciences,* 22 (8), 299-306.

Nimbarte, Vijaykumar D, et al. (2014), 'Design, synthesis and biological evaluation of 4-(1-(4 (sulphanilamide) phenyl)-3-(methyl)-1H-pyrazol-5-yl) dine urea and N-acyl derivatives as a soluble epoxide hydrolase inhibitors', *Medicinal Chemistry Research,* 23 (5), 2178-97.

O'Connor, Owen A, et al. (2015), 'Belinostat in patients with relapsed or refractory peripheral T-cell lymphoma: results of the pivotal phase II BELIEF (CLN-19) study', *Journal of Clinical Oncology,* 33 (23), 2492.

Oehme, Ina, et al. (2009), 'Histone deacetylase 8 in neuroblastoma tumorigenesis', *Clinical Cancer Research,* 15 (1), 91-99.

Ouaïssi, Mehdi, et al. (2008), 'High histone deacetylase 7 (HDAC7) expression is significantly associated with adenocarcinomas of the pancreas', *Annals of Surgical Oncology,* 15 (8), 2318-28.

Özdağ, Hilal, et al. (2006), 'Differential expression of selected histone modifier genes in human solid cancers', *BMC genomics,* 7 (1), 90.

Pacheco, Marina and Nielsen, Torsten O (2012), 'Histone deacetylase 1 and 2 in mesenchymal tumors', *Modern Pathology,* 25 (2), 222.

Peng, Lirong and Seto, Edward (2011), 'Deacetylation of nonhistone proteins by HDACs and the implications in cancer', *Histone Deacetylases: the Biology and Clinical Implication* (Springer), 39-56.

Pili, R, et al. (2012), 'Phase I study of the histone deacetylase inhibitor entinostat in combination with 13-cis retinoic acid in patients with solid tumours', *British journal of cancer,* 106 (1), 77.

Portela, Anna and Esteller, Manel (2010), 'Epigenetic modifications and human disease', *Nature biotechnology,* 28 (10), 1057.

Reis, Surya A, et al. (2016), 'Light-controlled modulation of gene expression by chemical optoepigenetic probes', *Nature chemical biology,* 12 (5), 317.

Rosato, Roberto R, Almenara, Jorge A, and Grant, Steven (2003), 'The histone deacetylase inhibitor MS-275 promotes differentiation or apoptosis in human leukemia cells through a process regulated by generation of reactive oxygen species and induction of p21CIP1/WAF1 1', *Cancer research,* 63 (13), 3637-45.

Rosato, Roberto R and Grant, Steven (2005), 'Histone deacetylase inhibitors: insights into mechanisms of lethality', *Expert opinion on therapeutic targets,* 9 (4), 809-24.

Rossi, Cristina, et al. (2011), 'Alkyl piperidine and piperazine hydroxamic acids as HDAC inhibitors', *Bioorganic & medicinal chemistry letters,* 21 (8), 2305-08.

Ryan, Qin C, et al. (2005), 'Phase I and pharmacokinetic study of MS-275, a histone deacetylase inhibitor, in patients with advanced and refractory solid tumors or lymphoma', *Journal of Clinical Oncology,* 23 (17), 3912-22.

Saji, Shigehira, et al. (2005), 'Significance of HDAC6 regulation via estrogen signaling for cell motility and prognosis in estrogen receptor-positive breast cancer', *Oncogene,* 24 (28), 4531.

Sakuma, Takumi, et al. (2006), 'Aberrant expression of histone deacetylase 6 in oral squamous cell carcinoma', *International journal of oncology,* 29 (1), 117-24.

Salisbury, Cleo M and Cravatt, Benjamin F (2007), 'Activity-based probes for proteomic profiling of histone deacetylase complexes', *Proceedings of the National Academy of Sciences,* 104 (4), 1171-76.

Schrump, David S, et al. (2008), 'Clinical and molecular responses in lung cancer patients receiving Romidepsin', *Clinical Cancer Research,* 14 (1), 188-98.

Serebryannyy, Leonid A, Cruz, Christina M, and De Lanerolle, Primal (2016), 'A role for nuclear actin in HDAC 1 and 2 regulation', *Scientific reports,* 6, 28460.

Shan, Xiu, et al. (2014), 'Ginsenoside Rg3 inhibits melanoma cell proliferation through down-regulation of histone deacetylase 3 (HDAC3) and increase of p53 acetylation', *PloS one,* 9 (12), e115401.

Silva, Gabriela, et al. (2013), 'Vorinostat induces apoptosis and differentiation in myeloid malignancies: genetic and molecular mechanisms', *PloS one,* 8 (1), e53766.

Siu, Lillian L, et al. (2008), 'Phase I study of MGCD0103 given as a three-times-per-week oral dose in patients with advanced solid tumors', *Journal of clinical oncology: official journal of the American Society of Clinical Oncology,* 26 (12), 1940.

Singh, Brahma N, et al. (2010), 'Nonhistone protein acetylation as cancer therapy targets', *Expert review of anticancer therapy,* 10 (6), 935-54.

Skov, Vibe, et al. (2012), 'Increased gene expression of histone deacetylases in patients with Philadelphia-negative chronic myeloproliferative neoplasms', *Leukemia & lymphoma,* 53 (1), 123-29.

Somoza, John R, et al. (2004), 'Structural snapshots of human HDAC8 provide insights into the class I histone deacetylases', *Structure,* 12 (7), 1325-34.

Staudinger, H and Meyer, Jules (1919), 'Über neue organische phosphorverbindungen III. Phosphinmethylenderivate und phosphinimine', *Helvetica Chimica Acta,* 2 (1), 635-46.

Sterner, David E and Berger, Shelley L (2000), 'Acetylation of histones and transcription-related factors', *Microbiology and Molecular Biology Reviews,* 64 (2), 435-59.

Sun, Jenny Y, et al. (2011), 'Histone deacetylase inhibitors demonstrate significant preclinical activity as single agents, and in combination with bortezomib in Waldenström's macroglobulinemia', *Clinical Lymphoma Myeloma and Leukemia,* 11 (1), 152-56.

Suresh, PS, et al. (2017), 'Review of bioanalytical assays for the quantitation of various HDAC inhibitors such as vorinostat, belinostat, panobinostat, romidepsin and chidamine', *Biomedical Chromatography,* 31 (1).

Ueda, Hirotsugu, et al. (1994), 'FR901228, a novel antitumor bicyclic depsipeptide produced by Chromobacterium violaceum no. 968', *The Journal of antibiotics,* 47 (3), 301-10.

Vannini, Alessandro, et al. (2004), 'Crystal structure of a eukaryotic zinc-dependent histone deacetylase, human HDAC8, complexed with a hydroxamic acid inhibitor', *Proceedings of the National Academy of Sciences,* 101 (42), 15064-69.

Vaux, D_L and Strasser, A (1996), 'The molecular biology of apoptosis', *Proceedings of the National Academy of Sciences,* 93 (6), 2239-44.

Wang, Difei, Helquist, Paul, and Wiest, Olaf (2007), 'Zinc binding in HDAC inhibitors: a DFT study', *The Journal of organic chemistry,* 72 (14), 5446-49.

Weichert, Wilko, et al. (2008), 'Class I histone deacetylase expression has independent prognostic impact in human colorectal cancer: specific role of class I histone deacetylases in vitro and in vivo', *Clinical Cancer Research,* 14 (6), 1669-77.

Weichert, Wilko (2009), 'HDAC expression and clinical prognosis in human malignancies', *Cancer letters,* 280 (2), 168-76.

Wilson, Andrew J, et al. (2006), 'Histone deacetylase 3 (HDAC3) and other class I HDACs regulate colon cell maturation and p21 expression and are deregulated in human colon cancer', *Journal of Biological Chemistry,* 281 (19), 13548-58.

Witt, Olaf, et al. (2009), 'HDAC family: What are the cancer relevant targets?', *Cancer letters,* 277 (1), 8-21.

Xie, Rui, et al. (2017), 'Design, synthesis and biological evaluation of novel hydroxamates and 2-aminobenzamides as potent histone deacetylase inhibitors and antitumor agents', *European journal of medicinal chemistry,* 134, 1-12.

Xu, WS, Parmigiani, RB, and Marks, PA (2007), 'Histone deacetylase inhibitors: molecular mechanisms of action', *Oncogene,* 26 (37), 5541.

Younes, Anas, et al. (2011), 'Mocetinostat for relapsed classical Hodgkin's lymphoma: an open-label, single-arm, phase 2 trial', *The lancet oncology,* 12 (13), 1222-28.

Zhang, Lei, et al. (2016), 'Bakkenolide A inhibits leukemia by regulation of HDAC3 and PI3K/Akt-related signaling pathways', *Biomedicine & Pharmacotherapy,* 83, 958-66.

Zhang, Zhenhuan, et al. (2004), 'HDAC6 expression is correlated with better survival in breast cancer', *Clinical Cancer Research,* 10 (20), 6962-68.

Zhang, Zhenhuan, et al. (2005), 'Quantitation of HDAC1 mRNA expression in invasive carcinoma of the breast', *Breast cancer research and treatment,* 94 (1), 11-16.

Zhang, Zhihua, et al. (2013), 'Inhibition of leukemic cells by valproic acid, an HDAC inhibitor, in xenograft tumors', *OncoTargets and therapy,* 6, 733.

Zorzi, Alexandra P, et al. (2013), 'A phase I study of histone deacetylase inhibitor, pracinostat (SB939), in pediatric patients with refractory solid tumors: IND203 a trial of the NCIC IND program/C17 pediatric phase I consortium', *Pediatric blood & cancer,* 60 (11), 1868-74.

APPENDIX

LIST OF PUBLICATIONS

From thesis work

1. **Prakruti Trivedi**, Nilanjan Adhikari, Sk. Abdul Amin, Tarun Jha, Balaram Ghosh. Design, synthesis and biological screening of 2-aminobenzamides as selective HDAC3 inhibitors with promising anticancer effects, ***European Journal of Pharmaceutical Science***, 124 :2018, 165-181
2. **Prakruti Trivedi,** Ganesh Routholla, Yamini Bobde, Balaram Ghosh. Design, synthesis and biological activity of novel hydroxamates with piperidine and piperazine linker as HDAC8 inhibitors and potential anticancer agents, manuscript under revision
3. **Prakruti Trivedi,** Ganesh Routholla, Dhanya Vijay, Balaram Ghosh. Development of HDAC8 inhibitors with promising anticancer effects, manuscript under preparation

Other publications

1. Nilanjan Adhikari, Sk. Abdul Amin, **Prakruti Trivedi**, Tarun Jha, Balaram Ghosh. HDAC3 is a potential validated target for cancer: An overview on the benzamide-based selective HDAC3 inhibitors through comparative SAR/QSAR/QAAR approaches. ***European Journal of Medicinal Chemistry***, 157:2018, 1127-1142
2. Sri Vishnu Kiran Rompicharla[#], **Prakruti Trivedi[#]**, Preeti Kumari, Prathyusha Ghanta, Balaram Ghosh, and Swati Biswas.Polymeric micelles of suberoylanilide hydroxamic acid to enhance the anticancer potential *in vitro* and *in vivo*: ***Nanomedicine***. 2017 Jan; 12(1):43-58.
3. Sri Vishnu Kiran Rompicharla, Prakruti Trivedi, Preeti Kumari, Omkara Swami Muddineti, Sowmya Theegalapalli, Balaram Ghosh, Swati Biswas: Evaluation of Anti-tumor Efficacy of Vorinostat Encapsulated Self Assembled Polymeric Micelles in solid tumors, AAPSPharmaSciTech, 2018 Aug 21. doi: 10.1208/s12249-018-1149-2. [Epub ahead of print] PMID:30132129

4. Shweta Pawar, T. Uday Kumar, **Prakruti Trivedi**, Balaram Ghosh, Anupam Bhattacharya, Amit Nag. FRET Mediated Zn2+ Sensing in Aqueous Micellar Solution and its Application in Cellular Imaging: ***ChemistrySelect*** 2017, 2, 8731– 8737.

5. Amit K Keshari, Ashok K Singh, Vinit Raj, Amit Rai, **Prakruti Trivedi**, Balaram Ghosh, Umesh Kumar, Atul Rawat, Dinesh Kumar, Sudipta Saha.p-TSA promoted syntheses of 5H-benzo[h]thiazolo[2,3-b]quinazoline and indeno[1,2-d]thiazolo[3,2-a]pyrimidine analogues: Molecular modeling, *in-vitro* antitumor activity against hepatocellular carcinoma: ***Drug Des Devel Ther***. 2017 May;11:1623-1642

6. Raj V, Rai A, Singh AK, Keshari AK, **Trivedi PH**, Ghosh B, Kumar U, Kumar D, Saha S.Discovery of Novel 2-Amino-5-(Substituted)-1,3,4-Thiadiazole Derivatives: New Utilities for Colon Cancer Treatment: ***Anticancer Agents Med Chem***. 2017 Apr .

7. Yadagiri Thigulla, T. Uday Kumar, **Prakruti Trivedi**, Balaram Ghosh, Anupam Bhattacharya: One-Step Synthesis of Fused Chromeno[4,3-b]pyrrolo [3,2-h]quinolin-7(1H)-One Compounds and their Anticancer Activity Evaluation. ***ChemistrySelect*** 2017, 2, 2721 – 2724.

8. M. Zubair K. Baig, Gangaram Pallikonda, **Prakruti Trivedi**, R.N. Prasad, Balaram Ghosh**,** Manab Chakravarty. Metal-free arylation to access distinct anthracenylphosphonates and anticancer activities for these and allied phosphonates. ***ChemistrySelect*** 2016, 1, 4332 – 4339.

9. Yadagiri Thigulla, Mahesh Akula, **Prakruti Trivedi,**Balaram Ghosh, Mukund Jha, Anupam Bhattacharya; Synthesis and anti-cancer activity of 1, 4-disubstituted imidazo[4,5-c]quinolines; ***Organic & Biomolecular Chemistry*** 2015, 14, 876-883

10. Singireddi Srinivasarao; Shashidhar Nizalapur; Tsz Tin Yu; Daniel Stanley Wenholz; **Prakruti Trivedi**; Balaram Ghosh; Krishnan Rangan; Naresh Kumar; Chandra Sekhar Venkata Gowri Kondapalli. Design, Synthesis and Biological Evaluation of Triazole-containing 2-Phenylindole and Salicylic Acid as Quorum Sensing Inhibitors against Pseudomonas aeruginosa, ***Chemistry select***, 24 Aug 2018, 3, 32.

Patents:

1. Swati Biswas, Balaram Ghosh, Rompicharla Sri Vishnu Kiran, **Trivedi Prakruti**. Chemotherapeutic composition for treating malignant tumors and method for preparing the same: Indian Patent Application number 201711028012; Filed on August 7, 2017

Papers accepted/presented in conference

From thesis

1. **Prakruti Trivedi**, Swati Biswas, Balaram Ghosh: Benzamide Derivatives as Histone Deacetylase (HDAC) Inhibitors and Potential Anticancer Agents: 21st National Symposium in Chemistry (NSC-21) under the auspices of the Chemical Research Society of India (CRSI) at the CSIR-Indian Institute of Chemical Technology, Hyderabad (IICT-Hyderabad), 13-16 July, 2017.
2. **Prakruti Trivedi**, Swati Biswas, Balaram Ghosh: Histone Deacetylase Inhibitors as potential Anticancer agents: International conference on "Pharmaceutical Education-Academia Relation to Industry-Current Scenario: Organized by Centre for Pharmaceutical Sciences Institute of Science and Technology, JNTUH, Kukatpally, Hyderabad, 17th & 18th March 2017
3. **Prakruti Trivedi**, Swati Biswas, Balaram Ghosh: Design, Synthesis and Biological Activity of Histone Deacetylase (HDAC) Inhibitors as Anticancer Agents: The Ramanbhai Foundation 8th International Symposium on Current Trends in Healthcare: Advances in New Drug Discovery and Development: Ahmadabad, Feb 2-4, 2017
4. **Prakruti Trivedi**, Swati Biswas, Balaram Ghosh: Development of Histone Deacetylase (HDAC) Inhibitors as Anticancer Agents: National Conference on Advanced Cancer Therapeutics-2016 (ACT-2016; CSIR-Chemical Institute of Chemical Technology, Hyderabad, India. 4-5 April, 2016. [**Awarded as Best Poster**]
5. **Prakruti Trivedi**, Swati Biswas, Balaram Ghosh: Development of Isoform Selective HDAC3 inhibitors as Long-Term Memory Enhancers: 66th Indian Pharmaceutical Congress at Hyderabad, 23rd to 25th January 2015.

BIOGRAPHY OF PRAKRUTI TRIVEDI

Ms. Prakruti Trivedi completed her Bachelor of Pharmacy in the year 2009 from Saurashtra University, Gujarat, India. She completed her Master of Pharmacy in the year 2011 from Ganpat University, Mehsana, Gujarat, India. She has received institution fellowship from Birla Institute of Technology and Science-Pilani, Hyderabad to carry out her doctoral research work under the supervision of Dr. Balaram Ghosh in 2014. She has been awarded Senior Research Fellowship (SRF) by Council of Scientific and Industrial Research (CSIR), India for a period of two years (2017-2019) for her PhD work. She has published 13 scientific papers in peer reviewed international journals and she is one of the inventors of one Indian patent filed in 2017. She has presented 5 papers in various scientific conferences and one of her poster has been awarded as the best poster in the conference.

BIOGRAPHY OF Dr. BALARAM GHOSH

Dr. Balaram Ghosh is presently working as an Assistant Professor, in the Department of Pharmacy, Birla Institute of Technology and Science, Pilani, Hyderabad Campus. He received his B. Pharm degree (1998) and M.Pharm (2000) from Jadavpur University, India. He was awarded his Ph.D. in Pharmaceutical Sciencesin the year 2009 from Wayne State University, Michigan, USA. After completion of doctoral studies, he pursued his postdoctoral studies at the Centre for Human Genetic Research (CHGR), Harvard Medical School, Harvard University, USA (2013). He has been involved in research for the last 15 years. He has published more than 54 research publications, three US patents and three Indian Patents. He has authored 4 book chapters. One of the research molecule (BG45) developed by him at Harvard Medical School has been commercialized with Sigma-Aldrich. He has successfully completed many sponsored projects and currently handling projects sponsored by SERB, Government of India and Sun Pharma Advanced Research Company Ltd. (SPARC), India. Currently three students are pursuing their Ph.D. work under his guidance.